JOINT TRANSPORTATION
RESEARCH PROGRAM
INDIANA DEPARTMENT OF TRANSPORTATION
AND PURDUE UNIVERSITY

Improved Reliability of FWD Test Results and Correlations with Resilient Modulus

Kanika Gupta, Sung Soo Park, Antonio Bobet, Tommy Nantung

SPR-4334 • Report Number: FHWA/IN/JTRP-2022/07 • DOI: 10.5703/1288284317370

RECOMMENDED CITATION

Gupta, K., Park, S. S., Bobet, A., & Nantung, T. (2022). *Improved reliability of FWD test results and correlations with resilient modulus* (Joint Transportation Research Program Publication No. FHWA/IN/JTRP-2022/07). West Lafayette, IN: Purdue University. https://doi.org/10.5703/1288284317370

AUTHORS

Kanika Gupta
Graduate Research Assistant
Lyles School of Civil Engineering
Purdue University
(765) 775-9328
gupta584@purdue.edu
Corresponding Author

Sung Soo Park
Graduate Research Assistant
Lyles School of Civil Engineering
Purdue University

Antonio Bobet Sc.D, PhD
Professor of Civil Engineering
Lyles School of Civil Engineering
Purdue University

Tommy Nantung, PhD, PE
Section Manager
Division of Research and Development
Indiana Department of Transportation

JOINT TRANSPORTATION RESEARCH PROGRAM

The Joint Transportation Research Program serves as a vehicle for INDOT collaboration with higher education institutions and industry in Indiana to facilitate innovation that results in continuous improvement in the planning, design, construction, operation, management and economic efficiency of the Indiana transportation infrastructure. https://engineering.purdue.edu/JTRP/index_html

Published reports of the Joint Transportation Research Program are available at http://docs.lib.purdue.edu/jtrp/.

NOTICE

TECHNICAL REPORT DOCUMENTATION PAGE

1. Report No. FHWA/IN/JTRP-2022/07	**2. Government Accession No.**	**3. Recipient's Catalog No.**
4. Title and Subtitle Improved Reliability of FWD Test Results and Correlations with Resilient Modulus		**5. Report Date** January 2022 **6. Performing Organization Code**
7. Author(s) Kanika Gupta, Sung Soo Park, Antonio Bobet, and Tommy Nantung		**8. Performing Organization Report No.** FHWA/IN/JTRP-2022/07
9. Performing Organization Name and Address Joint Transportation Research Program Hall for Discovery and Learning Research (DLR), Suite 204 207 S. Martin Jischke Drive West Lafayette, IN 47907		**10. Work Unit No.** **11. Contract or Grant No.** SPR-4334
12. Sponsoring Agency Name and Address Indiana Department of Transportation (SPR) State Office Building 100 North Senate Avenue Indianapolis, IN 46204		**13. Type of Report and Period Covered** Final Report **14. Sponsoring Agency Code**

15. Supplementary Notes
Conducted in cooperation with the U.S. Department of Transportation, Federal Highway Administration.

16. Abstract
Resilient modulus (M_R) is a key factor in the *Mechanistic Empirical Pavement Design Guide* (MEPDG) which was adopted by INDOT in January 2009. The resilient modulus can be determined in new pavement projects from subgrade soil samples collected at the site. However, for a pavement rehabilitation project, it becomes difficult to obtain soil information, and coring for samples may not be feasible because of traffic. The literature is rich with correlations between the M_R of the subgrade obtained in the laboratory with that estimated from FWD tests in the field. However, the review conducted shows very contradictory and inconsistent findings, thus existing correlations seem to apply only to the cases investigated, i.e., they are ad hoc correlations and cannot be generalized. To improve the interpretation of the FWD data and enhance the reliability of the results in Indiana, FWD and GPR tests were performed at five different road construction projects at the same locations where soil samples were collected and tested in the laboratory for resilient modulus. The selected sites included roads with rigid pavement and treated subgrade and flexible pavement with untreated subgrade. The study showed that (1) FWD backcalculation is greatly affected by pavement thickness; (2) GPR can provide actual thicknesses and can identify discrepancies between as-built and design pavement thickness; (3) for flexible pavements, a one-to-one correlation exists between FWD modulus and laboratory resilient modulus values for untreated subgrade soils; (4) MODTAG or ELMOD codes can both be used to estimate the resilient modulus of the subgrade in flexible pavements; (5) for rigid pavements, results of FWD backcalculation analysis using ELMOD or MODTAG greatly overestimate the resilient modulus of the soil, with backcalculated moduli 1.3 to 6 times higher than laboratory results; (6) ELMOD is recommended for routine analysis of FWD data, while MODTAG is recommended for research or to evaluate the quality of the data, when needed.

17. Key Words resilient modulus, FWD, ELMOD, MODTAG, subgrade	**18. Distribution Statement** No restrictions. This document is available through the National Technical Information Service, Springfield, VA 22161.

19. Security Classif. (of this report) Unclassified	**20. Security Classif. (of this page)** Unclassified	**21. No. of Pages** 159 including appendices	**22. Price**

Form DOT F 1700.7 (8-72) Reproduction of completed page authorized

EXECUTIVE SUMMARY

Introduction

The resilient modulus (M_R) is an important parameter to assess the performance of subgrade soils subjected to traffic loading. It is widely used for the analysis and design of pavements and is also a key factor in the *Mechanistic-Empirical Pavement Design Guide* (MEPDG), which was adopted by INDOT in January 2009. Accurate determination of the resilient modulus is important for the pavement design of new road projects, for pavement rehabilitation, and for making predictions on the life-span of existing pavements. The available literature is rich with attempts at estimating the M_R of the subgrade obtained in the laboratory using estimates from FWD tests in the field. However, the review conducted on the work finished thus far shows very contradictory and inconsistent findings and clearly indicates that the issue is far from being resolved. Thus, there is need and opportunity to improve the interpretation of the FWD data and enhance the reliability of the FWD results by decreasing the sources of uncertainty, including the performance of the field tests and the quality and interpretation of the data. This project addresses these issues and aims at improving the reliability and the interpretation of FWD tests by (1) performing a comprehensive literature review of available FWD protocols and back calculation tools; (2) evaluating non-destructive testing methods for pavement thickness determination; and (3) expanding the existing database of high-quality data pairs of FWD and M_R. A total of six sites (I-865, SR-46, US-31, S-BRITE, SR-37, and I-65) across Indiana were selected for this project to perform field tests (FWD and GPR) and to collect subgrade soil samples for laboratory testing.

Findings

Six sites were selected to collect subgrade soil samples: (1) I-865 (PCCP over a cement stabilized subgrade layer), (2) SR-46 (asphalt pavement over an untreated subgrade), (3) US-31 (PCCP pavement over a cement treated subgrade), (4) S-BRITE (compacted base over a cement treated subgrade layer), (5) SR-37 (PCCP over a cement treated subgrade), and (6) I-65 (PCCP over a cement treated subgrade). FWD and GPR tests were performed on four sites—I-865, SR-46, US-31, and SR-37. FWD data was analyzed using MODTAG and ELMOD. To establish correlations between the two tests, the backcalculated moduli for the subgrade layer was then compared with the laboratory resilient modulus results for both treated and untreated soil specimens. The following key conclusions were derived from the work.

- GPR is a useful tool to determine the thickness of pavement layers and to identify discrepancies between as-built and design pavement thickness. For flexible pavements, GPR is able to distinguish between the HMA and base course layer. For rigid pavements, GPR was able to identify the top two layers of the pavement—PCCP and the base/subbase layer.
- For rigid pavements, results of FWD backcalculation analysis using both ELMOD and MODTAG greatly overestimate the resilient modulus of the soil. The backcalculated results for the subgrade are 1.3 to 6 times higher than the laboratory results.
- For flexible pavements, results of the FWD backcalculation analysis suggests that a one-to-one correlation exists between FWD modulus and laboratory resilient modulus values for untreated subgrade soils. That is, $E_{FWD} \sim M_{R,UNTREATED}$.
- The code ELMOD is recommended for routine calculations because it is easy to use and provides accurate results for the resilient modulus. MODTAG can be used for research or to provide an in-depth analysis of the results at any given location.

Implementation

1. When good quality FWD data are available, the resilient modulus of untreated subgrade soils under flexible pavements can be estimated from FWD tests using ELMOD or MODTAG. The recommended relation is that resilient modulus backcalculated from FWD is equal to the resilient modulus obtained in the laboratory.
2. The resilient modulus obtained from FWD data performed on rigid (PCCP) pavements overestimates the resilient modulus obtained in the laboratory. The backcalculated modulus for the subgrade is 1.3 to 6 times higher than the laboratory results. An initial estimate of the resilient modulus of the subgrade on rigid pavements could be obtained by dividing the backcalculated moduli from the FWD by a factor of three. However, this estimate should not be used for design but only as a reference.
3. It is hypothesized that the errors in the resilient modulus on PCCP pavements are due to a number of factors—magnitude of the load and/or small deflections obtained, position of the sensors relative to pavement joints, and rigid movements of the pavement slabs that mask the "basin" deflection expected for the calculations. Further research is recommended to bring the level of interpretation of FWD test results to that of flexible pavements.
4. It is recommended to run, concurrently with FWD tests, GPR tests to determine the actual thickness of the pavement layers, and more specifically of the asphalt and concrete layers (layers with high stiffness). The study conducted suggests that errors on pavement layer thickness of $\pm 1''$ result in approximately a 45% difference in the moduli of the subbase and subgrade layers.
5. Most of the DOTs surveyed perform FWD tests using a drop sequence comprised of a seating load and repetitive drops for the same load. Repetitive loading seems to improve the accuracy of the results and allows for better interpretation of FWD data. It would be interesting to set up a test program that compares the results of FWD tests conducted at the same location following current INDOT protocol with the "drop sequence" used by other DOTs to see if there is a performance improvement. This may be particularly interesting in PCCP pavements, where the results are not satisfactory. The current protocol that INDOT uses provides satisfactory results on asphalt pavements.
6. Based on the analysis performed for both flexible and rigid pavements, the software ELMOD is preferred for routine calculations based on its simplicity and accuracy. MODTAG could be used for research or for detailed analysis of results, as it offers tools to analyze the quality of data and include a larger number of pavement layers.
7. It is recommended to continue the collection of data from road construction projects, particularly from sites comprised of flexible pavements with treated subgrades, which have not been investigated to improve these correlations.

CONTENTS

LIST OF TABLES

LIST OF FIGURES

1. INTRODUCTION

The resilient modulus (M_R) is an important parameter to assess the performance of subgrade soils subjected to traffic loading. It is widely used for the analysis and design of pavements and is also a key factor in the *Mechanistic-Empirical Pavement Design Guide* (MEPDG), which was adopted by INDOT in January 2009. Accurate determination of the resilient modulus is thus important to ensure efficiency of pavement design for new road projects, for pavement rehabilitation and for making predictions for the life of existing pavements.

M_R values used for design are obtained by performing repeated load triaxial tests according to AASHTO T 307-99 (2007) *Standard Method of Test for Determining the Resilient Modulus of Soils and Aggregate Materials*. The test method requires specialized and expensive equipment and skilled labor. The resilient modulus can be determined in new pavement projects from subgrade soil samples collected at the site. However, for a pavement rehabilitation project, it becomes difficult to obtain soil information and coring for samples is not a feasible option because of traffic. The large length of pavement rehabilitation projects and the added spatial variability of the soil along even short stretches of the pavement make the process of soil subgrade exploration very expensive and time consuming. Thus, it becomes crucial to identify non-destructive methods that can accurately determine resilient modulus values and provide a good understanding of the field conditions.

The Falling Weight Deflectometer (FWD) is a non-destructive testing method used to evaluate the structural condition of pavements. An impulse load is applied to the pavement surface and deflections are recorded which are then used to estimate in-situ moduli (E_{FWD}) of the pavement layers, including the subgrade. Many researchers have tried to establish correlations between the laboratory measured resilient modulus (M_R) values and FWD back-calculated modulus (E_{FWD}). Von Quintus and Killingsworth (1998) reported that the back-calculated moduli are consistently higher than the laboratory measured values for unbound pavement materials and subgrade soils, with the M_R/E_{FWD} ratio up to 3.5, depending on the type of pavement and subgrade soil. Siekmeier et al. (1999) investigated granular subgrades and found that the FWD back-calculated moduli compared well with laboratory resilient moduli at lower deviatoric stresses (0.06 MPa). In addition to performing the FWD test, the Loadman portable falling weight deflectometer (PFWD) and Humboldt soil stiffness gage (SSG) have been also used to evaluate subgrade stiffness values. The results from PFWD and SSG indicate higher stiffness under the wheel path than the M_R. It seems that the FWD backcalculated moduli is higher than the moduli from PFWD and SSG tests. The differences in moduli and discrepancies from different tests has been attributed to the confinement provided by the asphalt concrete pavement. Siekmeier et al. (1999) thus suggested that the accuracy of back-calculated moduli is affected by the confinement provided by the pavement layers and also by pavement edge effects.

Ping et al. (2002) performed laboratory resilient modulus tests on specimens prepared at in-situ water content and density and compared the results with field FWD moduli. The state of stress of a point in the middle of the subgrade layer, experiencing 40 kN FWD impact load and located vertically below the point of application, was used for the M_R test in the laboratory. The authors found a ratio of $M_R/E_{FWD} = 1.6$ for A-3 and A-2-4 soils.

Rahim and George (2003) found that the backcalculated FWD moduli compared well with the laboratory resilient modulus. The moduli measured from FWD tests performed directly on the subgrade was smaller but closer to the laboratory M_R than the back-calculated FWD moduli conducted on the pavement surface. However, Park et al. (2018) findings pointed to the opposite; that is, FWD test results conducted on the top of the subgrade were much lower than the M_R in the laboratory and hypothesized that this was because of the lack of confinement of the subgrade.

The difference between the laboratory M_R and FWD back-calculated values could arise from the linear elastic theory approach used in most FWD back-calculation programs. Nazzal and Mohammad (2010) performed laboratory resilient modulus tests on different Louisiana subgrade soils ranging from A-4 to A-7-6. The results were compared with FWD backcalculated moduli obtained from EVERCALC, MODULUS, and ELMOD software packages. The E_{FWD}/M_R ratio ranged between 0.51 and 8.1, with the higher ratios corresponding to weaker subgrade soils. They also found that the backcalculation approach had a significant impact on the E_{FWD}/M_R ratio and ELMOD provided the best correlation results.

As one can see, the literature is rich on attempts at estimating the M_R of the subgrade obtained in the laboratory with that estimated from FWD tests in the field. However, the review conducted on the work done so far shows very contradictory and inconsistent findings and clearly indicates that the issue is far from being resolved. In addition, very few correlation studies have been performed on Indiana soils. Kim et al. (2010) performed FWD tests under different weather conditions throughout the year and compared the results with laboratory resilient modulus values performed on specimens compacted at Optimum Moisture Content (OMC). They found that backcalculated subgrade moduli showed great seasonal variations, with moduli in winter months being 40% higher than in summer months. They also reported that the average FWD modulus was twice the laboratory M_R. Park et al. (2018) collected subgrade soil samples from various Indiana road projects and conducted FWD tests on top of the subgrade as well as on top of the pavement approximately 1 year after operation. The location of the FWD tests was exactly the same as the location where soil samples were taken to obtain the resilient

modulus in the laboratory. They found that moduli obtained from FWD tests performed on top of the pavement surface compared very well with the laboratory obtained resilient modulus, i.e., $M_R = E_{FWD}$. While the results are encouraging and suggest that a better correlation can be obtained when soil variability is not an issue, the findings are supported by limited data, and only for untreated subgrades. Thus, there is the need, and the opportunity, to improve the interpretation of the FWD data and enhance the reliability of the results by decreasing the sources of uncertainty identified: performance of field tests, and quality and interpretation of the field data. The current research work aims at addressing these issues and builds on the work and findings from those of Park et al. (2018).

This research has the following major objectives.

1. Improve the reliability of FWD field experiments. The reliability of the FWD data is based on the quality of the tests and on the pavement data. The objective is the development of testing and QA/QC protocols that provide high confidence in the results obtained.
2. Improve the interpretation of the FWD results. Interpretation of the results is done in Indiana with the code ELMOD. While the software can be successfully used for most routine cases, it has important limitations that may impact the accuracy of the results obtained, in particular the stiffness of the subgrade. Two such limitations are the maximum number of pavement layers that the code considers, and the assumption that the stiffness of the pavement layers decreases with depth. This assumption can be violated when there is a shallow stiff layer such as bedrock or high water table near the surface. Other software may provide more flexibility in considering the geometry and characteristics of the pavement, e.g., larger number of layers such that a distinction can be made between the subgrade and the natural soil; potential for defects in the pavement such as weak pavement or subgrade or slip between pavement layers. The objective is the evaluation of other codes that can be used, as replacement or complementary to ELMOD. Another major parameter affecting the backcalculated moduli is the pavement thickness values used as input. These pavement thicknesses are mostly based on design values. Thus, the project also aims at identifying potential non-destructive methods that could be used to assess the thickness of the pavement layers at the location of the FWD tests and that can be implemented in conjunction with the FWD equipment.
3. Increase the number of high-quality data for FWD-M_R correlations. As mentioned, the number of data points used to provide the one-to-one correlation between the subgrade resilient modulus and FWD interpretation is limited due to the high quality of the data required. The objective is to expand the database with additional cases.

The objectives have been accomplished through a number of tasks which include a comprehensive literature review of current FWD testing protocols, back calculation programs, non-destructive testing methods and existing correlations for resilient modulus, as well as field and laboratory testing.

The following chapters provide a summary of the work done and major conclusions drawn. The appendices, attached to this report, include all the results from the tests performed.

2. LITERATURE REVIEW

2.1 Correlations Between Resilient Modulus and Soil Properties

The resilient modulus is an important parameter for the design of pavements according to the *Mechanistic Empirical Pavement Design Guide* (MEPDG). The laboratory determination of resilient modulus is time consuming and requires expensive equipment and expertise. Many researchers have developed empirical relationships by establishing correlations between resilient modulus and soil properties. The soil properties influencing the resilient modulus response have been found to be different for fine- and coarse-grained soils; thus, many correlations have been proposed based on the type of soil.

Carmichael III and Stuart (1985) performed tests on over 250 different soils and developed correlations for predicting resilient modulus based on their gradation. They found that the resilient modulus values for cohesive soils correlated well with plasticity index, water content, fines content as well as deviatoric stress and confining stresses, whereas the M_R values of granular soils were found to depend on water content and bulk stress.

Group 1: Fine grained soils (CH, MH, Cl, ML) (see Equation 2.1)

$$M_R = 37.431 - 0.4566PI - 0.6179\%W - 0.1424S200 + 0.1791CS - 0.3248DS + 36.422CH + 17.097MH$$

$$R^2 = 0.759$$

(Equation 2.1)

where, CH = 1 for CH type soil, otherwise, CH = 0
MH = 1 for MH type soil, otherwise, MH = 0

Group 2: Coarse grained soils (GW, GP, GC, SW, SP, SM, or SC) (see Equation 2.2)

$$\log M_R = 0.523 - 0.0225\%W + 0.544\log T + 0.173SM + 0.197GR$$

$$R^2 = 0.759$$

(Equation 2.2)

where, SM = 1 for SM type soil, otherwise, SM = 0
GR = 1 for GM, GW, GC, or GP soils; otherwise, GR = 0
where, M_R = resilient modulus, in ksi,
PI = plasticity index,
%W = water content,
S200 = percentage passing No. 200 sieve,
CS = confining stress, in psi,
DS = deviator stress, in psi, and
T = bulk stress, in psi (DS + 3CS).

Drumm et al. (1990) related M_R with soil index properties and modulus obtained from unconfined

compression (UC) tests, based on data obtained from 11 different Tennessee soils. The UC tests were performed on specimens that had undergone M_R tests. They reported an increase in M_R with increasing confining stress for granular soils and a decrease in M_R with increasing amplitude of deviatoric stress for fine grained soils. They proposed two different correlations, included below as Model 1 and Model 2 (see Equations 2.3 and 2.4).

Model 1:

$$E_{ri} = 45.8 + 0.00052\frac{1}{a} + 0.188\,q_u + 0.45PI - 0.216\gamma - 0.25S - 0.15\%\#200 \quad (R^2 = 0.83) \qquad \text{(Equation 2.3)}$$

where, E_{ri} = resilient modulus, in ksi, at deviatoric stress = 6 psi,
= initial tangent modulus, in psi, obtained from unconfined compression tests,
q_u = unconfined compressive strength, in psi,
PI = plasticity index,
γ = dry unit weight, in pcf,
S = degree of saturation,
and % #200 = percent passing #200 sieve.

Model 2:

$$E_r = \frac{a' + b'\sigma_d}{\sigma_d} \text{ for } \sigma_d > 0 \qquad \text{(Equation 2.4)}$$

where, $\alpha' = 318.2 + 0.337\ q_u + 0.73\ \%\ clay + 2.26\ PI - 0.915\ \gamma - 2.19\ S - 0.304\ \%\ \#200 \quad (R^2 = 0.81)$

$$b' = 2.1 + 0.00039\frac{1}{a} + 0.104 q_u + 0.09\ LL - 0.1\%finer\#200 \quad (R^2 = 0.73)$$

Er = resilient modulus, in ksi,
σ_d = deviatoric stress, in psi,
LL = liquid limit, and
% clay = percent finer than 0.002 mm.

Lee et al. (1997) prepared soil specimens at different moisture contents and compaction energy using soil samples collected from three different sites in Indiana. They found unique relationships between stress causing 1% strain in unconfined compressive strength tests ($S_{u1\%}$) and moisture content (Equation 2.5). Resilient modulus tests were performed on specimens already subjected to UC tests. The compressive strength and resilient modulus values reduced with increase in moisture content. They reported that $S_{u1\%}$ was a good indicator of resilient modulus and proposed non-linear correlations for predicting resilient modulus based on $S_{u1\%}$.

$$M_R = 695.4 S_{u1\%} - 5.93 S_{u1\%}^2 \quad (R^2 = 0.97) \qquad \text{(Equation 2.5)}$$

Various stress independent models have also been developed where soil properties such as percentage of fines, Atterberg limits, dry density, moisture content, unconfined compressive strength, etc. are related with M_R. Resilient modulus is treated as a dependent variable and soil properties act as independent or explanatory variables.

Rahim (2005) conducted resilient modulus tests on undisturbed subgrade soil samples collected from 12 test sections in Mississippi. They reported that the deviatoric stress had a significant effect on M_R values of fine-grained soils. Two different equations were proposed for predicting resilient modulus of subgrade soils, both based on soil index properties from soil gradation (Equation 2.6 and 2.7). A linear multiple regression analysis was performed to determine the significance of various soil parameters. Independent variables such as liquid limit, moisture content and dry density showed high correlations among themselves and thus were combined to form a separate variable for predicting resilient modulus of fine-grained soils. Similarly, based on high correlation values obtained between percentage fines and coefficient of uniformity, these were combined for predicting resilient modulus of coarse-grained soils.

Fine Grained Soil:

$$M_R = 17.29\left[\left(\frac{LL}{w_c + 1}\gamma_d\right)^{2.18} + \left(\frac{\#200}{100}\right)^{-0.609}\right] \quad (R^2 = 0.70) \qquad \text{(Equation 2.6)}$$

Coarse Grained Soil:

$$M_R = 324.14\left[\left(\frac{\gamma_d}{w_c + 1}\right)^{0.8998} + \left(\frac{\#200}{\log c_u}\right)^{-0.4652}\right] \quad (R^2 = 0.75) \qquad \text{(Equation 2.7)}$$

where, M_R = resilient modulus, MPa
w_c = moisture content, %,
c_u = uniformity coefficient,
LL = liquid limit,
γ_d = dry density (kN/m^3), and
#200 = percent passing #200 sieve.

Hossain and Kim (2015) collected 29 different soil samples from ongoing construction projects in Virginia and developed stress-independent correlations for estimating resilient modulus. The proposed models were based on unconfined compressive strength (q_u) obtained from UC tests. The model was judged based on R^2 values obtained for predicted versus measured resilient modulus data corresponding to a confining pressure of 2 psi and a deviator stress of 6 psi. They found better correlations when the compressive strength was used along with basic soil properties such as plasticity index (PI) and percent passing No. 200 sieve (P_{200}). They also explored the impact of different sample preparation techniques on UC tests. Specimens prepared with impact compaction resulted in better correlations than those prepared with static compaction

techniques (see Equations 2.8 and 2.9).

$$\text{Static Compaction: } M_R = 7{,}884.2 + 99.7\ q_u + 193.1PI - 47.9P_{200}\ \left(R^2 = 0.86\right) \quad \text{(Equation 2.8)}$$

$$\text{Impact Compaction: } M_R = 6{,}113.0 + 95.1\ q_u + 173.7PI - 27.8P_{200}\ \left(R^2 = 0.91\right) \quad \text{(Equation 2.9)}$$

Many models have been proposed that rely on constitutive relations developed for resilient modulus. Hicks and Monismith (1971) characterized the resilient response of granular materials as a function of bulk stress, as expressed in Equation 2.10.

$$M_R = k_1 \sigma_b^{k_2} \quad \text{(Equation 2.10)}$$

where, k_1 and k_2 = material parameters, and
σ_b = bulk stress.

Moossazadeh and Witczak (1981) proposed a simple model based on deviatoric stress to approximate the non-linear behavior of fine-grained soils (Equation 2.11). The model did not consider the effects of confining stresses. Confining stresses greatly influence the behavior of cohesive soils at greater depths; thus, this method was found to be useful for soils at shallow depths.

$$M_R = k_1 \sigma_d^{k_2} \quad \text{(Equation 2.11)}$$

where, k_1 and k_2 = constants dependent on soil properties, and
σ_d = deviatoric stress.

Uzan (1985) proposed the following three-parameter model which could be used for all soil types, expressed in Equation 2.12.

$$M_R = k_1 \sigma_b^{k_2} \sigma_d^{k_3} \quad \text{(Equation 2.12)}$$

where, k_1, k_2, and k_3 = material constants dependent on soil properties,
σ_b = bulk stress, and
σ_d = deviatoric stress.

Witczak and Uzan (1988) modified the Uzan model by replacing deviatoric stress with octahedral stress to incorporate the effects of shear stress along with confining stresses. This model is also known as the Universal model and is expressed by Equation 2.13.

$$M_R = k_1 \sigma_b^{k_2} \tau_{oct}^{k_3} \quad \text{(Equation 2.13)}$$

where, k_1, k_2, and k_3 = material constants dependent on soil properties,
σ_b = bulk stress, and
τ_{oct} = octahedral stress.

NCHRP (2004) recommended the following changes to the Witczak and Uzan (1988) model. This model is used in the level 1 analysis in the MEPDG (*Mechanistic Empirical Pavement Design Guide*) and is also called the octahedral stress model (Equation 2.14).

$$M_R = k_1 p_a \left(\frac{\sigma_b}{p_a}\right)^{k_2} \left(\frac{\tau_{oct}}{p_a} + 1\right)^{k_3} \quad \text{(Equation 2.14)}$$

where, k_1, k_2, and k_3 = material constants dependent on soil properties,
σ_b = bulk stress,
τ_{oct} = octahedral stress, and
p_a = atmospheric pressure.

Mohammad et al. (1999) developed models for the resilient modulus including the octahedral shear stress, soil properties, California bearing ratio and unconfined compressive strength. They proposed three different models. The models were validated with data from eight different Louisiana soils. Resilient modulus tests were performed on specimens having different moisture contents and dry densities. They found that models relating material coefficients (k_1, k_2, and k_3 coefficients, as expressed by Equation 2.15) with soil properties produced most accurate correlations (R^2 = 0.48 to 0.8). They also found that M_R values were greatly influenced by moisture content, liquid limit, and plastic limit.

Octahedral stress state model:

$$\frac{M_R}{\sigma_{atm}} = k_1 \left(\frac{\sigma_{oct}}{\sigma_{atm}}\right)^{k_2} \left(\frac{\tau_{oct}}{\sigma_{atm}}\right)^{k_3} \quad \text{(Equation 2.15)}$$

$$\log k_1 = -0.679 + 0.0922w + 0.00559\ \gamma_d + 3.54D_c + 2.4D_m + 0.00676\ LL + 0.0116PL + 0.022\%\ sand + 0.0182\%silt \quad \left(R^2 = 0.80\right)$$

$$\log\ k_2 = -0.887 + 0.0044w + 0.00934\ \gamma_d + 0.264D_c + 0.305D_m + 0.00877\ LL + 0.00665PL + 0.0116\%\ sand + 0.00429\%silt \quad \left(R^2 = 0.86\right)$$

$$\log k_3 = -0.638 + 0.00252w + 0.00207\ \gamma_d + 0.61D_c + 0.152D_m + 0.000497\ LL + 0.00416PL + 0.00311\%\ sand + 0.00413\%silt \quad \left(R^2 = 0.48\right)$$

where, σ_{oct}, τ_{oct} = octahedral normal and shear stresses, respectively,
σ_{atm} = atmospheric pressure = 100 kPa,
k_1, k_2, and k_3 = model constants,
w = moisture content,

σ_d = dry density (kN/m^3),
D_c = degree of compaction or relative compaction which is the ratio of dry density of the specimen to MDD,
D_m = degree of moisture which is the ratio of moisture content of the specimen to OMC, and
LL, PL = liquid limit and plastic limit, respectively.

Dai and Zollars (2002) analyzed subgrade soils from six different Minnesota road projects where undisturbed soil samples were collected. Stress-dependent models were used to predict M_R values using soil properties (Equation 2.16 and 2.17). They found that plasticity index, liquid limit, fines percentage, and dry density were the major influencing parameters.

$$\text{Deviator stress model: } M_R = A\sigma_d^N \quad \text{(Equation 2.16)}$$

where, σ_d = deviator stress,
A and N = regression constants,

$$A = 2{,}866.1 - 38.1\left(\frac{D_{en}}{PI}\right)^3 - 4{,}382.9w + 4.49PI - 24.35\ \lambda - 13.82LL \quad (R^2 = 0.924)$$

$$N = 62.68 - 15.68D_{en}^{0.5} - 113.3\ w^{1.5} - 0.006PI + 0.118S \quad (R^2 = 0.711)$$

$$\text{Stress model: } M_R = k_1\theta^{k_2}\tau_{oct}^{k_3} = k_4\theta^{k_2}\sigma_d^{k_3} \quad \text{(Equation 2.17)}$$

where, θ = bulk stress (MPa),
τ_{oct} = octahedral shear stress (MPa),
k_1, k_2, k_3, and k_4 = regression constants,

$$k_4 = 5{,}770.8 - 520.98D_{en}^{0.5} - 3{,}941.8\ w^{0.5} + 33.1PI - 36.62LL - 17.93\lambda \quad (R^2 = 0.920)$$

$$k_3 = 409.9 - 306.18D_{en}^{0.1} - 82.63\ w + 0.033PI - 0.138S - 0.041LL \quad (R^2 = 0.701)$$

$$k_2 = -5.334 - 0.000316D_{en}^3 + 9.686\ w - 0.054PI + 0.046LL + 0.022\lambda \quad (R^2 = 0.711)$$

D_{en} = dry density of soil (kN/m^3),
w = moisture content (%),
PI = plasticity index (%),
LL = liquid limit (%),
S = saturation (%), and
λ = % passing #200 sieve.

Nazzal and Mohammad (2010) examined the validity of the correlation equations developed by the long-term pavement performance (LTPP), to predict the M_R. The model parameters in the NCHRP 2004 model were correlated with liquid limit, moisture content and dry density (Equation 2.18). The effect of moisture content on the regression coefficients was analyzed and an extensive catalog containing a range of coefficients based on soil type and moisture content was developed. They emphasized that a particular model could not be applied to all locations and thus calibration of the models with regional soil data was required.

$$\text{NCHRP model: } M_R = k_1 p_a\left(\frac{\sigma_b}{p_a}\right)^{k_2}\left(\frac{\tau_{oct}}{p_a} + 1\right)^{k_3} \quad \text{(Equation 2.18)}$$

$$\ln k_1 = 1.334 + 0.0127P200 + 0.016\ LL - 0.036\gamma_{dmax} - 0.011MCCL + 0.001\ MCDD\max P \quad (R^2 = 0.61)$$

$$k_2 = 0.722 + 0.0057LL - 0.00454\ (MCDDmaxPI)^{0.641} + 0.00324\ (MCDDP)^{1.28} - 0.875P200 \quad (R^2 = 0.74)$$

$$k_3 = -7.48 + 0.235\frac{\gamma_d}{mc} + 0.038\ LL - 0.0008MCPI + 0.033\ \gamma_{dmax} - 0.016MCDDP \quad (R^2 = 0.66)$$

where, p_a = atmospheric pressure,
k_1, k_2, and k_3 = model constants,
σ_b = bulk stress, and
τ_{oct} = octahedral stress.

$$MCCL = (mc - mc_{opt})^{*}clay\%$$

$$MCDDmaxP = P200 * \left(\frac{mc - mc_{opt}}{mc_{opt}}\right) * \left(\frac{\gamma_d}{\gamma_{dmax}}\right)$$

$$MCDDmaxPI = PI * \left(\frac{mc - mc_{opt}}{mc_{opt}}\right) * \left(\frac{\gamma_d}{\gamma_{dmax}}\right)$$

$$MCDDP = \left(\frac{P200 * \gamma_d}{mc}\right)$$

$$MCPI = PI * \left(\frac{mc - mc_{opt}}{mc_{opt}}\right)$$

P200 = % passing sieve No. 200,
clay % = % of clay in soil,
LL and PI = liquid limit and plasticity index (%),
mc = moisture content (%),
mc_{opt} = OMC (%),
γ_d = dry unit weight (pcf), and
γ_{dmax} = MDD (pcf).

Correlations have also been developed for resilient modulus and soil properties of treated subgrade soils. Puppala et al. (2011) examined the effects of different cement dosages and various confining and deviatoric stress levels on the resilient modulus response of treated reclaimed asphalt pavement (RAP) materials. The three parameter model expressed in Equation 2.19 was proposed.

$$\frac{M_R}{\sigma_{atm}} = k_3 \left(\frac{\sigma_3}{\sigma_{atm}}\right)^{k_4} \left(\frac{\sigma_d}{\sigma_{atm}}\right)^{k_5} \qquad \text{(Equation 2.19)}$$

M_R test results showed that stress-dependent constitutive models were reasonably capable of capturing the effects of stress levels on treated RAP resilient modulus. Table 2.1 shows the results of their regression analysis. The resilient modulus was reported to increase with confining pressure and treatment, and higher values of material constants were associated with high confining pressure and treatment. The change in M_R with deviatoric stress was found to be more pronounced in treated specimens.

Rout et al. (2012) studied the effect of lime-cement stabilization on the resilient modulus of three high plasticity clayey soils (CH) from different sites in Texas and reported a significant increase of resilient modulus with treatment. They observed that for untreated subgrade soils, at all three confining pressures, an increase in deviatoric stress resulted in a decrease of the resilient modulus. However, treated soils exhibited strain hardening behavior—an increase in resilient modulus with an increase in the deviatoric stress. Their findings were similar to those of Puppala et al. (2011): stabilization resulted in an increase in material constants. The regression coefficients of untreated and treated soils for the octahedral stress model were also determined (Table 2.2).

Octahedral stress model:

$$M_R = k_1 p_a \left(\frac{\sigma_b}{p_a}\right)^{k_2} \left(\frac{\tau_{oct}}{p_a} + 1\right)^{k_3}$$

Even though the relationships and models proposed by different researchers are statistically significant and show high correlation values, there is a lack of understanding of the significance of coefficients in terms of the effect that each individual soil property has on the resilient modulus. In the current study, subgrade soils were collected from six different road construction projects in Indiana. These soils were then tested in the laboratory and attempts were made to establish correlations between various soil properties and resilient modulus. The results of this analysis are discussed in detail in Chapter 4.

TABLE 2.1
Results of Regression Analysis (Puppala et al., 2011)

	Log k_3	k_4	k_5	R^2
Untreated RAP	3.47	0.20	0.09	0.98
2% Cement-Treated RAP	3.55	0.19	0.15	0.97
4% Cement-Treated RAP	3.62	0.19	0.14	0.96

TABLE 2.2
Results of Regression Analysis of Treated and Untreated Soil Specimens (Rout et al., 2012)

Site	Treatment	k_1	k_2	k_3	R^2
A	Untreated	763.5	0.26	-2.00	0.99
	Treated	1,201.7	0.42	-0.27	0.86
B	Untreated	571.8	0.31	-2.53	0.98
	Treated	1,015.5	0.58	-0.27	0.97
C	Untreated	577.4	0.23	-2.14	0.97
	Treated	1,126.6	0.56	-0.27	0.97

2.2 Current FWD Test Protocols and Backcalculation Programs

The reliability of the FWD data is based on the quality of the tests and thus it is imperative that the deflection testing is conducted consistently, ensuring good quality assurance and quality control (QA/QC) measures. FWD protocols of various DOTs are summarized in Table 2.3 (Abdelnaby et al., 2018; Alland et al., 2018, Bryce et al., 2016, Guccunksi et al., 2009, FHWA-LTPP Technical Support Services Contractor LAW PCS, 2000; Schmalzer, 2006; Titi et al., 2018, Zhou & Scullion, 2007). The table shows that the typical testing pattern for FWD varies depending on the project type (research or project level) and on the type of pavement (flexible, rigid) under consideration. Test frequency also changes depending on project size, and it ranges from 25 ft for a small project (<500 ft) to 1,500 ft for large scale projects. The loading used for FWD tests is mostly 9,000 lbs as it corresponds to the load of each tire under an 18,000 lbs axle, which is the standard load used in structural pavement design. Backcalculation of the tests is typically performed using ELMOD or DARWin.

INDOT testing protocol follows the recommendations in the FHWA-HRT-16 report published in 2017. A total of nine sensors placed at increasing radial offsets from the center of the loading plate are recommended and includes one sensor placed under the plate. The FHWA report also recommends to account for the temperature of the ambient air, of the pavement surface and under the pavement. INDOT protocol mentions the measurement of air and surface temperature; however, the temperature within the pavement is not measured. The testing locations for PCC pavements must include transverse joint location along with the midlane and outer wheel paths. As per INDOT protocol, FWD tests

TABLE 2.3
DOT's FWD Protocols

Agency	Frequency	Drop Levels	Backcalculation
INDOT	Every 300 ft	3 (7,000, 9,000, and 11,000 lb)	ELMOD
FHWA (*LTPP Manual for FWD Measurements*, Version 4.1)	25~1,000 ft (various test plans exist depending on lane specification)	4 (6,000, 9,000, 12,000, 16,000 lb) Repetitive loading per drop	–
Penn DOT (Pennsylvania)		3 (9,000, 12,000, 16,000 lb) Repetitive loading per drop	DARWin
VDOT (Virginia)	25~200 ft Depends on project size	4 (6,000~16,000lb) Repetitive loading per drop	ELMOD
NJ DOT (New Jersey) (Gucunski et al., 2009)	Project Level–250 ft Network Level–530 ft	3 (6,500, 9,000, 12,000 lb)	
WisDOT (Wisconsin)	20~530 ft	3 (5,000, 9,000, 12,000 lb) Repetitive loading per drop	DARWin or ME Design Backcalculation tool
TxDOT (Texas)	<530 ft	Load may vary from 2,500~27,000 lb)	MODULUS
TNDOT (Tennessee)		3	ELMOD
CDOT (Colorado)	<530 ft	9,000 lb	DARWin

TABLE 2.4
Summary of Deflection Sensor Locations

Deflection Sensor	FHWA (LTTP) Nine Sensors (in.)	INDOT Nine Sensors (in.)
D1	0	0
D2	8	-12
D3	12	8
D4	18	12
D5	24	18
D6	36	24
D7	48	36
D8	60	48
D9	-12	60

are performed either on the midlane or under the outer wheel path for both HMA and PCC pavements. Table 2.4 and 2.5 provide a comparison of deflection sensor location and load level and drop sequence between FHWA recommendations and INDOT protocol, respectively. Additionally, annual calibration of deflection sensors and load cell is essential to ensure accuracy of deflection and loading measurements. The ASTM standards (ASTM D 4695-03, 2003; ASTM D4694-09, 2009) describes the calibration of the equipment, test frequency, and general FWD procedures.

In addition to test protocols, FWD data backcalculation methods have also been reviewed. Figure 2.1 describes the concept of backcalculation for flexible pavements. The figure shows a three-layered pavement system with surface deflections measured by five sensors at different locations. The load is assumed to be distributed through the pavement layers, as shown with the dashed line. Sensor 4 and sensor 5, which are located outside the stress zone of the HMA and base layers, measure the deflection due to the subgrade only. The deflection measured by sensor 3 is independent of the modulus of the HMA layer. The deflections on sensors 1 and 2 depend on the properties of all three layers. This approach based on layered elastic theory is commonly used for the backcalculation analysis of rigid pavements as well.

Backcalculation of FWD tests on pavements are based on either Boussinesq's solution, multi-layer elastic theory, finite element method or plate theory. The approach based on multi-layer elastic theory applies to both flexible and rigid pavements, while the plate load theory approach is specifically used for rigid pavements. Depending on the pavement type, iteration procedure, and forward/backcalculation method used, they can be classified into following categories: Regression Equations, the *1993 AASHTO Design Guide*, Method of Equivalent Thickness (MET), Optimization Method, Iterative Method, Dynamic Backcalculation Methods, Artificial Neural Network (ANN) Analysis, Area Method, and Best-Fit method (Smith et al., 2017).

2.2.1 Regression Equations

Rohlf and Rogness (1985) suggested that deflection measurement recorded by sensor placed about 48 in. from the loading plate could be used to predict subgrade modulus. Several researchers have attempted to develop regression equations using deflection data to predict modulus values. Newcomb (1986) used ELSYM5 to generate data covering range of pavement input parameters (such as load values, layer thicknesses, and moduli values) to develop regression equations predicting layer moduli for 2-layer and 3-layer systems. Badu-Tweneboah (1989) generated deflection data using BISAR to develop layer moduli prediction equations.

TABLE 2.5
Summary of Load Levels and Drop Sequence

Height Designation	FHWA (LTTP)			INDOT	
	Target Load (lbf)	No. of HMA Drops	No. of PCC Drops	Target Load (lbf)	No. of Drops
Seating	NA	3	3	NA	NA
1	6,000	4	NA	7,000	1
2	9,000	4	4	9,000	1
3	12,000	4	4	11,000	1
4	16,000	4	4	–	–

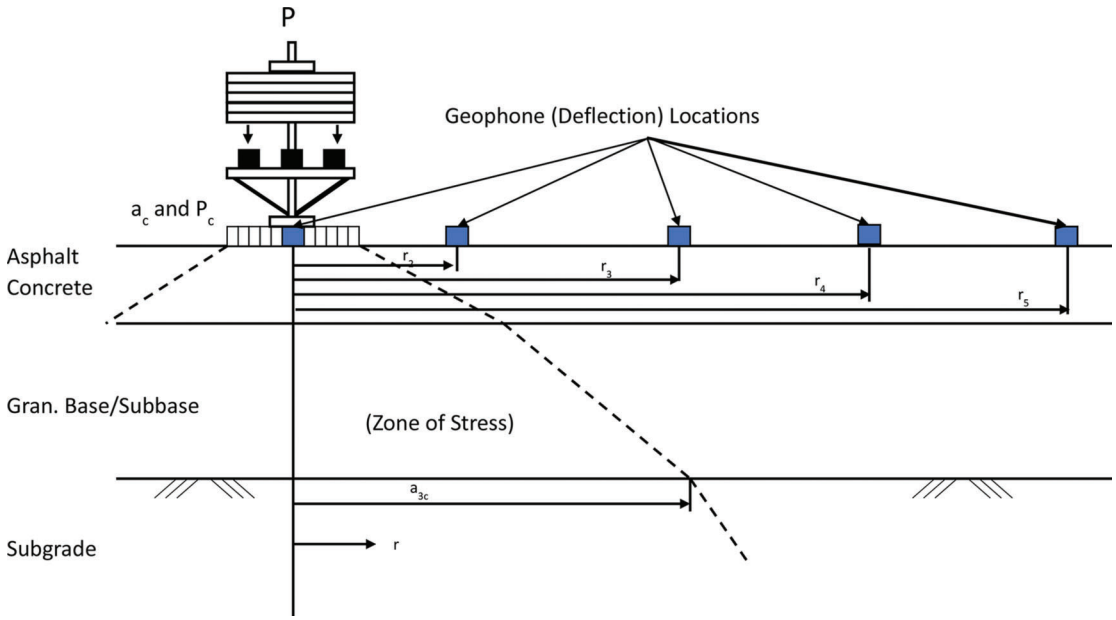

Figure 2.1 Diagram of stress zone under the FWD load.

2.2.2 1993 AASHTO Design Guide

The *1993 AASHTO Design Guide* describes the most widely accepted method for estimating subgrade modulus (Equation 2.20). The method uses a single deflection measurement and radial distance between loading plate and deflection sensor.

$$M_R = \frac{0.24P}{d_r r} \qquad \text{(Equation 2.20)}$$

Where,

M_R = Backcalculated subgrade resilient modulus, MPa (lbf/inch^2),

P = Load, kN (lbf),

d_r = Measured deflection at distance r from applied load, mm (in.), and

r = Radial distance at which the deflection is measured, mm (in.).

The obtained value for M_R must also be multiplied by a reduction factor equal or greater than 0.33 for fine-grained, stress-dependent soils.

2.2.3 Method of Equivalent Thickness (MET)

The MET is based on Odemark's assumption which approximately converts a multilayered pavement system with moduli E_i and layer thicknesses h_i into a single layer having an equivalent thickness H and modulus E using Equation 2.21.

$$H = \sum_i^n Ch_i \left(\frac{E_i}{E}\right)^{\frac{1}{3}} \qquad \text{(Equation 2.21)}$$

C = layer coefficient (0.8 ~ 0.9).

This approach uses Boussinesq's original closed-form relationships between vertical deflection (d_r) and elastic modulus E (Equation 2.22 and 2.23). These equations were formed with the assumption that deflection is measured on the surface of an isotropic, linearly elastic and homogeneous material.

$$d_r = \frac{2(1-\upsilon^2)P}{\pi \times a \times E} \text{ (vertical deflection under a uniformly distributed load)} \qquad \text{(Equation 2.22)}$$

$$d_r = \frac{(1-\upsilon^2)P}{\pi \times r \times E} \text{ (vertical deflection under a point load)}$$

(Equation 2.23)

Where:
P = Surface load, kN (lbf).
r = Radial distance from center of load, mm (in.).
a = Radius of loaded area, mm (in.).
υ = Poisson's ratio.

The MET approach allows for faster computation times and also considers the effects of material nonlinearity.

2.2.4 Optimization Method

Optimization method approach uses forward calculation programs, such as WESLEA, to produce a database of deflection basins. A range of expected pavement parameter values (layer moduli, layer thicknesses, material properties, pavement types, and loading conditions) are selected to create this database. Basin search pattern technique is then used to find the best fit for the FWD measured deflection basin in the generated database. WESDEF and MODULUS software programs use this approach.

2.2.5 Iterative Method

The iterative method approach assumes that dynamic deflections relate to moduli predicted using elastic layer theory. Measured deflection values along with initial seed moduli and pavement layer information is used to calculate a deflection basin. A convergence criterion or a tolerance limit is set, and the layer moduli is iterated till a best fit between the calculated and measured basins is obtained. MODCOMP, MICHBACK, and EVERCALC, are few of the softwares that use iterative method.

2.2.6 Dynamic Backcalculation Methods

Dynamic backcalculation methods are based on applied load and deflection time history in either frequency domain or time domain. The approach methods discussed so far consider load to be static and use layered linear elastic theory. This approach however uses finite element modeling techniques and thus can incorporate different geometric shape, load type, and material properties including elasto plastic material behavior. In the dynamic deflection analysis, the vertical profile is divided into a number of thin computational layers, and the difference between the computed response and FWD sensor response over time is minimized. The dynamic analysis results in higher subgrade moduli as compared to results of static analysis (Ling et al. 1991).

2.2.7 Artificial Neural Network (ANN) Analysis

ANNs are simplified computations models inspired by the way a biological nervous system functions. These individual processing elements are referred to as neurons (Pekcan et al., 2008). These methods are capable of producing less errors compared to the static analysis approaches and have a faster computation time as well. Pekcan et al. (2008), Sharma and Das (2008), and Saltan et al. (2013) developed ANN models for backcalculation of flexible pavement layer systems and found ANN results to be satisfactory in terms of accuracy as well as computation times.

2.2.8 AREA Method

The AREA Method is a graphical backcalculation process used specifically for rigid pavement systems. The approach is based on plate theory and utilizes Westergaard's closed form solution for a horizontally infinite plate on dense liquid foundation. It involves measurement of normalized area of the deflection basin followed by the determination of the radius of relative stiffness, l. These are then used to backcalculate subgrade support parameters, modulus of subgrade reaction, k and subgrade constant, C. Subgrade modulus (E_s) for a known Poisson's ratio (μ_s) can then be calculated as per Equation 2.24.

$$E_s = C * (1 - \mu_s^2) \quad \text{(Equation 2.24)}$$

2.2.9 Best Fit Method

Best Fit method is another approach commonly used to backcalculate layer moduli for rigid pavements. It is similar to optimization approach discussed earlier in terms of finding the best fit between the measured and calculated deflection profiles. This approach offers a less stringent criteria to match deflection basin as compared to the AREA method and is good for 2-layer rigid pavement systems.

Table 2.6 shows comparisons between ELMOD, MODCOMP, MODULUS, and EVECALC, which are backcalculation software commonly used. ELMOD uses the method of equivalent thickness (MET) and an iterative method for backcalculation, while MOD COMP, MODULUS, and EVERCALC use an iterative method with multilayer elastic theory.

2.3 Surface Wave Methods

Seismic surface waves are stress waves traveling along the free surface of a medium and usually are the predominant portion (over body waves: compressive and shear waves) in a wave train. In a homogeneous isotropic full-space, only body waves exist and are transmitted as compressive waves and as shear waves. If the medium is bounded by a stress-free surface,

TABLE 2.6
Comparison of Backcalculation Software

Program	Pavement Type	Forward Calculation Method	Forward Calculation Subroutine	Backcalculation Method	Non-Linear Analysis	Maximum No. of Layers
ELMOD	Flexible/Rigid	Equivalent thickness/ Finite element	MET	Iterative	Yes (subgrade only)	4 (exclude bedrock layer)
MODCOMP	Flexible	Multilayer elastic theory	CHEVRON	Iterative	Yes	2~15
MODULUS	Flexible	Multilayer elastic theory	WESLEA	Database (optimization)	No	4 plus rigid layer
EVERCALC	Flexible	Multilayer elastic theory	WESLEA	Optimization	Yes	4 (exclude bedrock layer)

different types of surface waves (e.g., Rayleigh, Love, Lamb waves) may also be present. Surface waves are characterized by low velocity, low frequency, and large amplitude. They propagate directly from source to receiver, are confined to the interface and, their amplitude decreases with depth. At receiver stations, close to the source location, they tend to obscure the events of reflected waves because of their often very large amplitudes. In conventional seismic, they are regarded as coherent noise. For the investigation of near-surface layers, however, they are an important source of information (e.g., Hering et al., 1995; Socco & Strobbia, 2004). The Spectral Analysis of Surface Waves (SASW) allows for rapid determination of elastic moduli as well as pavement layer thicknesses in a non-destructive manner. The velocity of propagation is a direct indicator of material stiffness. The true shear wave velocity profile is obtained by inversion, which is an iterative process that requires the phase velocity-wavelength relationships to determine thickness and stiffness of different layers (Ismail et al., 2009; Nazarian & Stokoe, 1986). Roesset et al. (1990) conducted a number of studies to optimize the spacing between source and receiver by simulating pavement systems (both AC and PCCP). They found the results to be very promising when the ratio of distance of the receivers from the source was maintained between 1.5 to 2. The asphalt concrete layer thicknesses were found to compare well with core data while the modulus was found to be higher than laboratory results due to the small strains and high frequencies involved. The error in the estimated pavement thickness was found to vary from 0.5% to 12%. Ismail et al. (2009) used SASW to determine the near surface profiles of two asphalt pavement sites. The abrupt changes measured in the shear wave velocities were found to correlate well with the different layers of the pavement under consideration. The results of their case studies are shown in Figure 2.2. They also reported that SASW was accurate in detecting sandwiched low modulus pavement layers.

Olson and Miller (2009) performed Spectral Analysis of Surface Waves (SASW) and Multiple Impact of Surface Waves (MISW) tests to evaluate thickness of pavements. The study concluded that the MISW method, which utilized the phase velocity spectrum, provided better results for both asphalt and concrete pavements (especially for those with a softer base under rigid pavements) and thus could estimate more accurate moduli and pavement thickness data (within 4–5 mm).

2.4 Ground Penetrating Radar

Ground penetrating radar (GPR) is a high-resolution geophysical technique that utilizes electromagnetic radar waves to locate and map subsurface targets, including buried drainage systems (Daniels, 2000). GPR operates by transmitting short pulses of electromagnetic energy into the pavement. These pulses are reflected back to the radar antenna. The amplitude and arrival time are related to the depth of the target and surrounding material properties. GPR has been also used to ascertain the nature of the subgrade soil and stratigraphy underlying roadways (Saarenketo & Scullion, 2000). Because of the fast processing and nondestructive nature of GPR, it is also widely used in transportation, especially for road evaluation. Various researchers have used GPR to evaluate pavement thickness and assess pavement quality. Scullion et al. (1994) presented several case studies to illustrate various applications of GPR in the analysis of subsurface pavement conditions. GPR was found to predict asphalt layer thickness with an accuracy greater than 95%. However, for concrete pavement, the accuracy decreases because of the similarity in dielectric properties of concrete pavement and granular subbase materials. In addition, GPR can also be used to assess frost susceptibility of subgrade soils, estimate pavement thickness, and detect defects such as voids larger than half inch and stripping and rutting (Saarenketo & Scullion, 2000). The estimation of pavement thickness layers relies greatly on the difference in their dielectric properties.

GPR systems either use air coupled (horn antennas) or ground coupled antenna systems to transmit signals. The air coupled systems are employed 150–500 mm above the pavement surface which allows for faster data accumulation. These however have a limited penetration depth due to partial reflection of the electromagnetic waves on the pavement surface. Ground coupled antennas are placed in contact with the pavement surface. This makes the data accumulation process slow but provides greater penetration depths for the same frequency. Thus, the choice of antenna used also plays a crucial role in accurately determining pavement thicknesses. Few researchers have tried to improve the

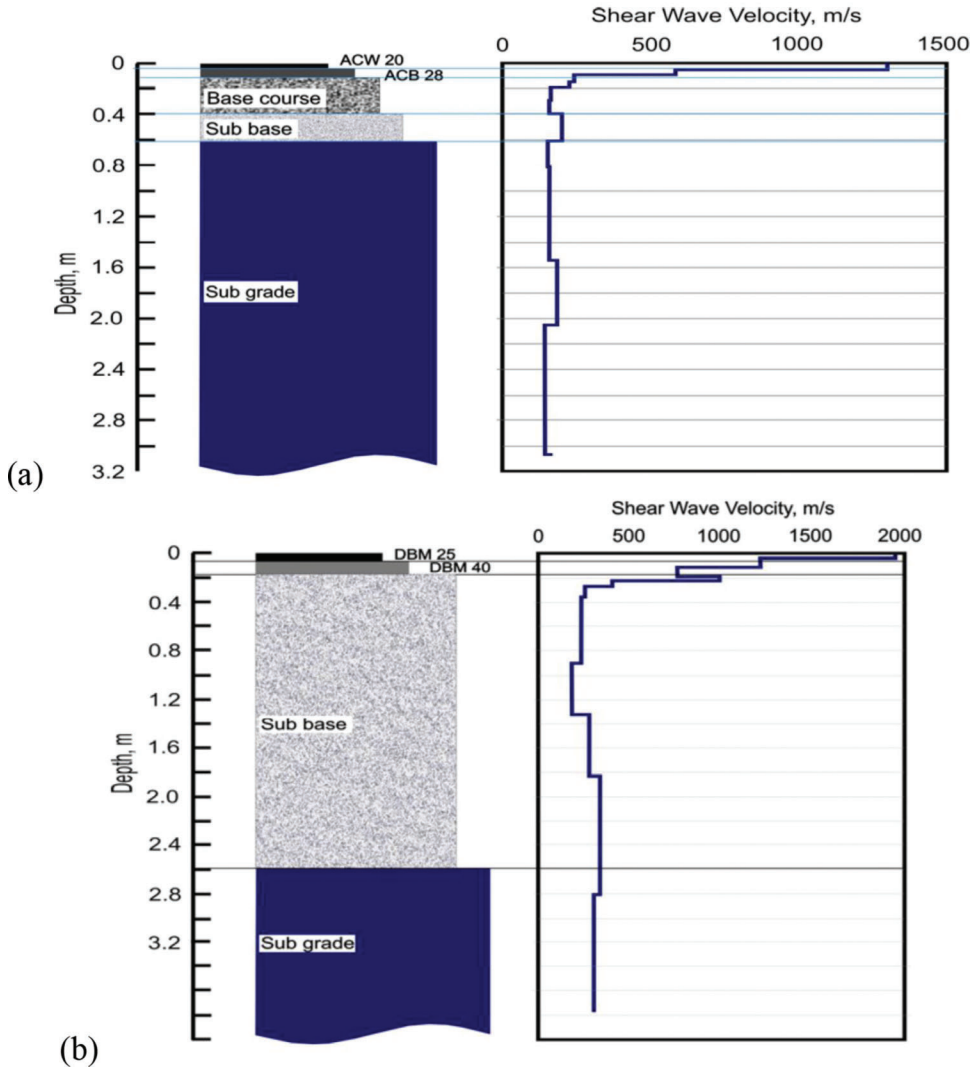

Figure 2.2 Designated pavement profile and final shear wave velocity plots (a) Case study 1 (b) Case study 2 (Ismail et al., 2009).

accuracy of estimates of pavement thickness results obtained from GPR by studying signal processing techniques and the effect of the initial seed value used for the analysis. These effects are discussed in detail in the following.

Al-Qadi and Lahouar (2005) performed GPR tests over a flexible pavement comprising a wearing surface (38 mm), hot mix asphalt (HMA) base layer (150 mm), an asphalt treated drainage layer (75 mm), cement stabilized limestone base layer, a limestone aggregate base layer and subgrade layer, at the Virginia Smart Road pavement test facility. The air coupled GPR antennas used could only identify two reflections: surface reflection and the HMA-based interface. The inability to detect different base and subgrade interfaces was attributed to their similar dielectric properties. GPR could also not identify the HMA layer composition as the reflections within the HMA layers were masked by surface reflections. This overlap between reflections from wearing surface and HMA layers exists due to their relatively small thicknesses. The depth resolution of GPR is governed by the transmitted pulse width and the dielectric constant of the layer targeted. Pavement layers with thickness lower than the GPR depth resolution are considered thin and affect the accuracy of measurements. Thus, the researchers proposed considering different HMA layers as a single entity, with an average dielectric constant value, collecting the GPR data simultaneously from air coupled and ground coupled antennas, and applying signal processing techniques such as deconvolution. Deconvolution is the process of signal filtration needed to get rid of undesired signal mixing. This method reduced the errors in thickness estimation from 12% (before deconvolution) to 3% (after deconvolution).

To accurately determine pavement layer thicknesses using GPR, the instrument needs to be calibrated well. The calibration process is carried out with the help of metal plates. The plates are placed on top of the pavement surface and data generated by reflections with and without the plates are analyzed. The use of actual pavement core data in the post processing of

GPR data increases the accuracy of GPR. Willett et al. (2006) determined pavement surface thicknesses for both asphalt and Portland cement concrete pavements using GPR and observed that the accuracy of GPR estimates depended on the number of pavement core data used for calibration. GPR tests and core information was collected from seven different projects in Kentucky. GPR results were analyzed and compared with the average core thicknesses to assess the accuracy of the GPR. The researchers observed that errors in pavement thickness decreased when core information was used in conjunction with GPR data. Information from four pavement cores for every 2-mile stretch was reported as the optimum number to improve the reliability of pavement thickness using GPR.

Information from a number of DOTs was also gathered to learn about the use of GPR for pavement thickness evaluation. The following states were reviewed: Iowa, Kentucky, Minnesota, and Texas.

2.4.1 Iowa Department of Transportation

Hu et al. (2016) evaluated the thickness of pavement and stabilized foundation layers using a ground coupled GPR. GPR specifications: ground-coupled 900 MHz antenna setup with SIR-20 data acquisition system. A dielectric probe GS3 sensor manufactured by Decagon Devices, Inc. was also used to measure dielectric properties of asphalt and foundation layer materials.

Pavement thickness was measured using three different methods: Method 1 used GS3 to measure dielectric and two-way travel time data obtained from GPR; Method 2 used two-way travel time data obtained from all core locations to determine the dielectric constants; and Method 3 used two-way travel time data obtained from one core location to determine dielectric constants. The pavement thickness prediction using Method 2 reported the least errors. The comparison of thickness measurements is presented in Table 2.7. GPR was also used to study the effects of freezing and thawing, and to detect moisture variations in the subbase and subgrade layers. GPR was unable to provide useful data on frozen layers because of similar dielectric constants of materials when frozen.

2.4.2 Kentucky Transportation Center Report GPR Specifications

SIR 10B GPR system manufactured by Geophysical Survey Systems Inc. (G.S.S.I.), model 4108 (1 GHz) air launched horn antenna (Willet & Rister, 2002; Willet et al., 2006).

GPR was used for the following purposes:

1. to measure the pavement surface thicknesses for both asphalt and Portland cement concrete pavements, and
2. to check repeatability of GPR test data in wet and dry conditions.

GPR was run on the same stretch of pavement under different cycles of drying and wetting. GPR results were found to be indifferent to the surface conditions, i.e., wet, or dry. Surface water was found to have negligible effect on GPR thickness measurements. Post processing of GPR data utilized actual field core data for accuracy. Cores were extracted at intervals ranging from 500 m to 2,000 m depending on data requirement. Table 2.8 presents the error reported in the pavement thickness estimation.

2.4.3 Minnesota Road Research Test Facility

Various projects have been carried out by the Minnesota Road Research test facility to assess the quality of pavement using GPR. GPR has been used for the following purposes:

1. to measure the asphalt layer thickness,
2. to detect areas of potential stripping, and
3. to estimate the aggregate base thickness.

Table 2.9 provides a summary of their projects and results.

2.4.4 Texas Transportation Institute

Implementation of the Texas GPR system (Scullion et al., 1994). GPR specifications: Penetradar Model PS-24 with 5 MHz air launched antenna.

Case studies were presented for various GPR applications such as layer thickness determination, void

TABLE 2.7
Comparison of Thickness Measurements from Cores and GPR Scans

Asphalt Layer Description	Core Thickness (mm)	Method 1 Error (%)	Method 2 Error (%)	Method 3 Error (%)
50-mm HMA surface with LAA and 102-mm HMA base with LAA	163.3	10.3	3.6	3.9–8.5
50-mm WMA surface with LAA and 102-mm WMA base with LAA	165.5	11.3	2.7	2.7–5.1
50-mm HMA surface with HAA and 102-mm HMA base with LAA	165.4	11.1	5.3	5.3–8.6
50-mm WMA surface with HAA and 102-mm HMA base with LAA	160.1	9.5	3.8	4.8–7.2
50-mm WMA surface with HAA and 102-mm WMA base with LAA	163.8	11.4	3.1	3.4–6.3

TABLE 2.8
Kentucky Transportation Center Report–Pavement Thickness Error

Type of Pavement	% Difference from Core Value (no. of cores performed)
Asphalt (I-75) 2-mile stretch	8.63 (3) 10.32 (2) 16.29 (1) 23.44 (0)
Asphalt (I-64) 2.6-mile stretch	0.40 (3) 8.87 (2) 33.82 (1) 5.82 (0)
Asphalt (KY-17) 1.8 mile	1.34 (3) 53.28 (0)
Asphalt (University of Kentucky parking lot)	2.54 (4) 165.04 (0)
Asphalt (US 27 Paris Pike) 2 mile	5.13 (3) 1.36 (2)
Concrete (Interstate I-275 east 1) 1.85 mile	0.84 (3) 29.24 (0)
Concrete (Interstate I-275 east 2) 1.7 mile	5.83 (4) 43.93 (0)
Concrete (Interstate I-275 west) 1.94 mile	1.21 (4) 31.02 (0)

TABLE 2.9
Minnesota Road Research Test Facility Projects

Project	GPR Specifications	Type of Pavement	Result
Minnesota Road Research (Dai & Yan, 2014)	SIR 2000 data acquisition system with 5 antennae	Asphalt (Cell 33) Pavement design: Asphalt- 4.5″ Road mix- 2″ Aggregate base-4–7″ concrete	Pavement thickness from GPR is within 5% of traditional field test coring result Asphalt-4″ (102 mm) Road mix-3″ (76 mm) Aggregate base-5″ (127 mm)
Minnesota Road Research (Loken, 2005)	SIR 020 and SIR 2000 data acquisition system 3 ground-coupled antennas (100 MHz, 400 MHz, 1.5 GHz), and 2 air-coupled antennas (1.0 GHz and 2.0 GHz)	Asphalt (CSAH 61 in Pine County) Asphalt over concrete (TH 8)	Identified asphalt, road-mix, and aggregate base layer thicknesses along 10 mile stretch and concrete base in spot locations Mean thickness = 5.1″ in. with S.D. = 2.3″
Minnesota Road Research (Saarenketo et al., 2000)	SIR-10H data acquisition system 1 GHz horn antenna, 1.5 GHz and 400 MHz ground coupled antennas	Asphalt (TH-23 and TH-71 Willmar)	GPR along with FWD data was used to identify stripping

detection, base course evaluation and locating areas of asphalt stripping. Results for the layer thickness measurements are listed in Table 2.10.

Liu and Scullion (2006) developed the integrated software package PAVECHECK to provide accurate FWD data analysis using pavement data from GPR. The program automatically finds the GPR thicknesses for the FWD drop locations when the FWD back-calculations are performed. The PAVECHECK program also allows the user to input other data types such as right-of-way (R-O-W) digital images, pavement core information, GPS coordinates, and test location distances.

Walubita et al. (2009) analyzed GPR measurements to determine defects such as segregation, moisture entrapment, low density areas, air void variation, non-uniform layer thickness, etc. and were compared with cores to validate findings. Table 2.11 summarizes their observations.

TABLE 2.10
Pavement Thickness Error Estimates (Scullion et al., 1994)

Type of Pavement	Result
Asphalt (US-82)	Error: 1.4%
Core Hole 5 (10.75″)	Surface thickness = 10.6″
Asphalt (US-82)	Error: 3.1%
Core Hole 4 (17.75″)	2 Layers = 5.9″ + 11.3″ = 17.2″
Asphalt (US-82)	Error: 3%
Core Hole 3 (14.75″)	2 Layers = 4.3″ + 10.9″ = 15.2″

TABLE 2.11
Comparison of GPR and Core Data (Walubita et al., 2009)

Case Study Location	Result–GPR Data	Result–Core Data
IH-35 Laredo (Gilbert)	No subsurface anomalies or color signature from intermediate layer interfaces were found.	Solid cores; no visual evidence of major defects.
IH-35 Waco (McLennan)	GPR trace showed negative reflections indicating low density spots.	Core obtained from location was debonded at the bottom.
	COLORMAP data showed patterns of red reflection underlain with blue reflections, indicating trapped moisture and high air voids.	Core showed problems of compaction in the bottom layers.

GPR specifications: 1 GHz air-launched GPR unit.

A number of researchers have combined GPR and FWD test results to improve the reliability of estimates of subgrade stiffness. Uzarowski et al. (2005) conducted GPR and FWD tests on three different projects in Ontario. Deflection profiles from FWD and GPR data were analyzed together to detect the size and location of voids. The GPR data was used to obtain the pavement thickness profile which was then used for FWD modulus back calculations using the ELMOD software. The deflection peaks observed in FWD tests were found to correlate well with void locations observed in the GPR data. The combined use of GPR and FWD was reported to be useful for repair and rehabilitation works. Ahmed and Tarefdar (2017) developed a mechanistic-empirical pavement design methodology that utilized GPR and FWD data to evaluate pavement thickness and stiffness, respectively. The methodology was used to assess the quality and performance of three pavement sites in New Mexico. GPR estimates of asphalt and base layer thicknesses were found to be at least 90% accurate, while the reliability of the stiffness backcalculated from FWD tests, incorporating GPR thicknesses, ranged from 66% to 96%.

The integrated use of non-destructive testing methods such as FWD and GPR data has the potential to increase the accuracy of the subgrade stiffness, which in turn could further improve the reliability of correlations between FWD and laboratory resilient modulus.

3. LABORATORY AND FIELD TESTS

A key objective of this research is to increase the number of high-quality data sets for FWD-M_R correlations. This objective was achieved by targeting a wide variety of subgrades. Site locations include untreated and treated subgrade soils ranging from A-1 to A-6. Soil samples were collected during the construction of new roads and road reconstruction projects, when the subgrade soils were accessible. A representative 90 m (300 ft) long section at each site was chosen and eleven points at 9 m (30 ft) intervals were identified (Figure 3.1a). Disturbed representative samples were collected from each point for laboratory testing. At the same location of soil collection, measurements of the pavement thickness using GPR and FWD tests will be performed to obtain meaningful comparisons between M_R and FWD tests. Soil samples were also collected from S-BRITE, a Purdue research facility. Three samples over a 60-ft stretch were collected from the test strip prior to cement treatment (Figure 3.1b).

3.1 Sample Location

Soil samples were collected from the following sites: I-865, SR-46, US-31, S-BRITE, SR-37, and I-65. The location of the sites is displayed in Figure 3.2.

Site 1: Interstate 865

This site is located on Interstate 865 (I-865) in Marion County around Indianapolis and comprised station 297+00 to station 300+00. It has a Portland cement concrete pavement (PCCP) over a cement stabilized subgrade layer, which had a cement content of 6% to achieve a target design strength of 300 psi. Untreated subgrade soil was collected at each point in August 2019. The moisture content of the in-situ soil ranged between 7.0% and 11.5% (average 8.2%).

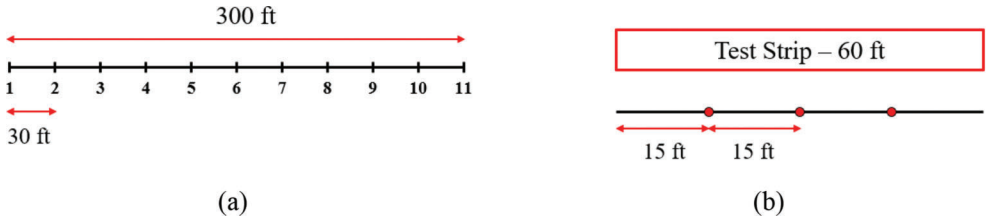

Figure 3.1 Selected points for sample collection and future FWD tests on (a) Sites 1, 2, 3, 5, and 6 (b) Site 4.

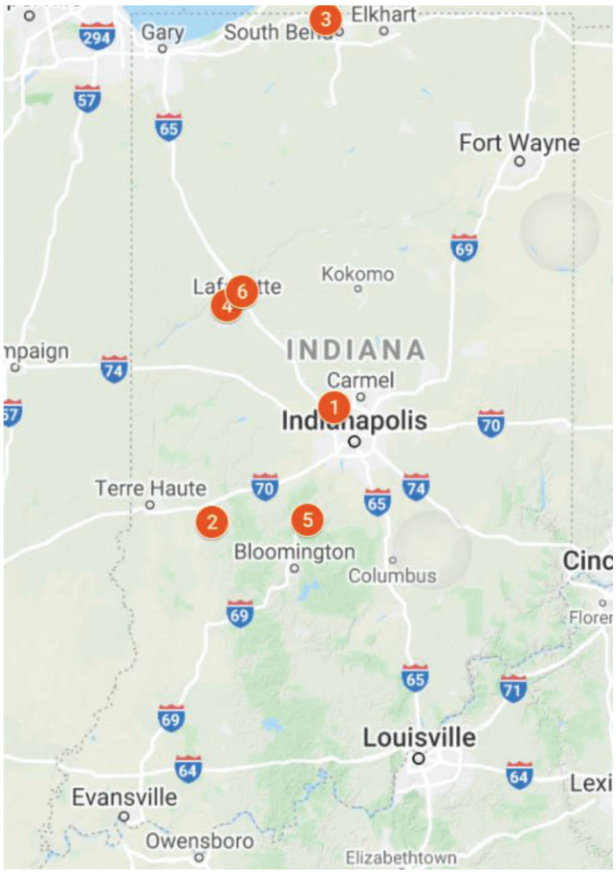

Figure 3.2 Selected sites for field testing.

Site 2: State Road 46

This site is located on State Road 46 (SR-46) in Clay County, near Terre Haute, around station 576+50 and had asphalt pavement. The sample collection was done in October 2019 during the construction phase. The water content of the in-situ soil was between 6.0% and 10.0% (average 7.9%). The in-situ soil unit weight was 2.05 g/cc (128.0 lb/ft^3).

Site 3: US-31

This site is located on US-31 in St. Joe County, near South Bend, from station 170+00 to 173+00. Untreated soil samples were collected in July 2020 during road construction. This site comprises PCCP pavement over a cement stabilized subgrade (4%). Water content of the in-situ soil was between 6.0% and 13.1% (average 8.6%).

Site 4: S-BRITE

Two test strips were constructed at the site, each having either a treated or untreated subgrade, under a compacted aggregate layer. For the subgrade-treated strip, subgrade soil was mixed with a cement slurry to achieve a cement percentage of 4%. The average in-situ water content was 12.7%. Two sand cone tests were performed on the untreated and treated sections, and the in-situ unit weight was found to be 1.97 g/cc (123.0 lb/ft^3) and 1.83 g/cc (114.2 lb/ft^3), respectively. The sand cone tests were performed per ASTM D 1556-07.

Site 5: State Road 37

This site is located on State Road 37 in Martinsville. Soil samples were collected from RP 349+08 to 346+08 during construction, in July 2020. The road has PCCP pavement over a cement stabilized subgrade (5%). The water content of the in-situ soil was between 9.8% and 13.9%. A sand cone test was performed near station 6 and the in-situ soil unit weight was determined to be 1.98 g/cc (123.3 lb/ft^3).

Site 6: Interstate 65

This site is located on I-65 in West Lafayette, Tippecanoe County. Untreated soil samples were collected in August 2020 on the south-bound section near exit 178 (RP 815+00). It has a PCCP-type pavement over a cement stabilized subgrade (5% cement content). Water content of the in-situ soil was between 6.0% and 13.1% (average 8.6%).

3.2 Laboratory Tests

The soil samples collected from the sites were tested in the laboratory. Atterberg limit tests and grain size analysis were performed following the AASHTO T-89-10/T-90 (2011, 2020) and ASTM C 136-14 (2015) standards, respectively. Moist samples were washed through the #200 sieve prior to the sieve analysis to determine the grain size distribution. These tests were used to classify the soils per AASHTO M 145-91 (2012). The Standard Proctor test, following AASHTO T-99 (2019), was also performed on all soil samples. Remolded specimens of untreated soil compacted at 95% of the Standard Proctor energy were prepared to conduct resilient modulus tests, following AASHTO T 307-99 (2007) for Type 2 material, i.e., for fine-grained soils.

3.2.1 Atterberg Limits, Grain Size Distribution, and Compaction Test Results

The I-865 samples were found to exhibit little variability, and nine of the eleven samples were classified as A-4. The average liquid limit and plastic limit of the samples were 20% and 12%, respectively. The percentage of fines ranged from 45% to 65%. Figure 3.3a shows the grain size distribution curves and the Proctor test results of the I-865 samples. The average maximum dry density and optimum moisture content were 2.05 g/cc (128 lb/ft^3) and 9.7%, respectively. The soil properties such as Atterberg limits, percentage fines, optimum moisture content and maximum dry density of the I-865 samples are provided in Table A.1 in Appendix A.

The SR-46 samples showed variability with location and could be grouped into two categories, AASHTO classification type A-6 and A-4, based on their soil properties. Samples 1 to 5 had a higher liquid limit, plastic limit, and optimum moisture content, when compared to the remaining samples. The average liquid limit, plastic limit, and OMC values for samples 1–5 were 32%, 21%, and 15%, and for samples 6–11, 26%, 15%, and 10%, respectively. The maximum dry density for samples 1–5 was about 1.78 g/cc (110.9 lb/ft^3), which was significantly lower than for samples 6–11 (1.98 g/cc or 123.6 lb/ft^3). The two different soils can also be distinguished from the grain size distribution and compaction curves (Figure 3.3b). The results of the tests are presented in Table A.2 in Appendix A.

The laboratory test results of subgrade soil samples collected from Site 3, US-31, indicate quite a bit of variability. Two of the soil samples, samples 4 and 7, are gap-graded with a high percentage of sand particles. The soils exhibited low to no plasticity. The results obtained from classification and compaction tests performed on all eleven samples are tabulated in Table A.3 (Appendix A). Figures 3.3c shows the grain size distribution and compaction curves, respectively. The soils also exhibited a wide range of MDD values, ranging from 1.83 to 1.99 g/cc (114 to 124 lb/ft^3). The soils were classified as coarse-grained A-1.

The three samples collected from the S-BRITE site, Site 4, were found to be very uniform. This was observed in the grain size distribution and compaction test results (Figure 3.4a). The soils were classified as low plasticity clays (CL) as per ASTM classification or A-6 as per AASHTO classification. The OMC and MDD values were 12% and 1.88 g/cc (117.5 lb/ft^3), respectively.

Little variability was observed across the samples collected from Site 5, SR-37. The results obtained from classification and compaction tests performed on all eleven samples are tabulated in Table A.5 in Appendix A. All soil samples had high percentage of sand (on average 60%) with low liquid limit and plastic limit values. The gradation and compaction curves also showed uniform results (Figures 3.4b). The average OMC and MDD values were found to be 10% and 2.02 g/cc (126.1 lb/ft^3), respectively. The soils were classified as A-2-4, per the AASHTO classification.

Classification tests performed on samples collected from Site 6, I-65, indicated that the soils were low plasticity clays and were classified mostly as A-6 (Table A.6 in Appendix A). A few of the samples had a lower percentage of fines (~50%) compared to the rest (70%–80%). The results from compaction tests gave a range of OMC and MDD values (~ 16% and 1.70–1.85 g/cc) except for sample 1 that exhibited a low OMC (9%) and high MDD (2.07 g/cc) (Figure 3.4c).

3.2.2 Resilient Modulus Test

The resilient modulus tests were performed as per AASHTO T 307-99 (2007). Remolded specimens were compacted in 5 layers using spacers of different thickness to ensure all layers had equal volume (the double plunger method was used). After compaction, three measurements of height and diameter were taken to obtain the average volume of the sample. The specimens were approximately 71 mm in diameter and 142 mm in height. The mass and density of the specimens were also obtained. The M_R test comprised 16 loading sequences with a combination of five deviatoric (2, 4, 6, 8, and 10 psi) and three confining stresses (2, 4, and 6 psi), including a conditioning sequence. The first sequence consisted of a conditioning cycle of 750 repetitions to ensure proper contact between specimen and loading cap and to remove any effects of initial loading versus reloading. All other sequences had 100 cycles of loading and reloading. The average resilient modulus obtained for the last five cycles was reported for each sequence. Each test resulted in 15 resilient modulus values corresponding to each deviatoric and confining stress.

The I-865 specimens did not show any clear dependency on the deviatoric stress or the confining stress. The resilient modulus values were found to be in the range of 5,000 to 26,000 psi (33 to 180 MPa), with lower values corresponding to low confining stresses and high deviatoric stresses. M_R tests were also performed on cement-treated specimens of the I-865 subgrade soil. The natural soil was mixed with 6% cement and water. The treated specimens were carefully wrapped with clingfilm and stored in a water cooler for 28 days. Control specimens were also prepared for cement treated and untreated specimens to determine changes in water content during the curing period. The water content of treated specimens was measured just after specimen preparation as well as after performing the resilient modulus test. The loss of water content of the treated samples after curing was about 10%, whereas the untreated specimen showed negligible change in water content. The decrease in water content for treated specimens could thus be attributed to the chemical reaction between soil and cement. All M_R test specimens (treated as well as untreated) were prepared at OMC and MDD values corresponding to Standard Proctor test results on untreated samples. The resilient modulus

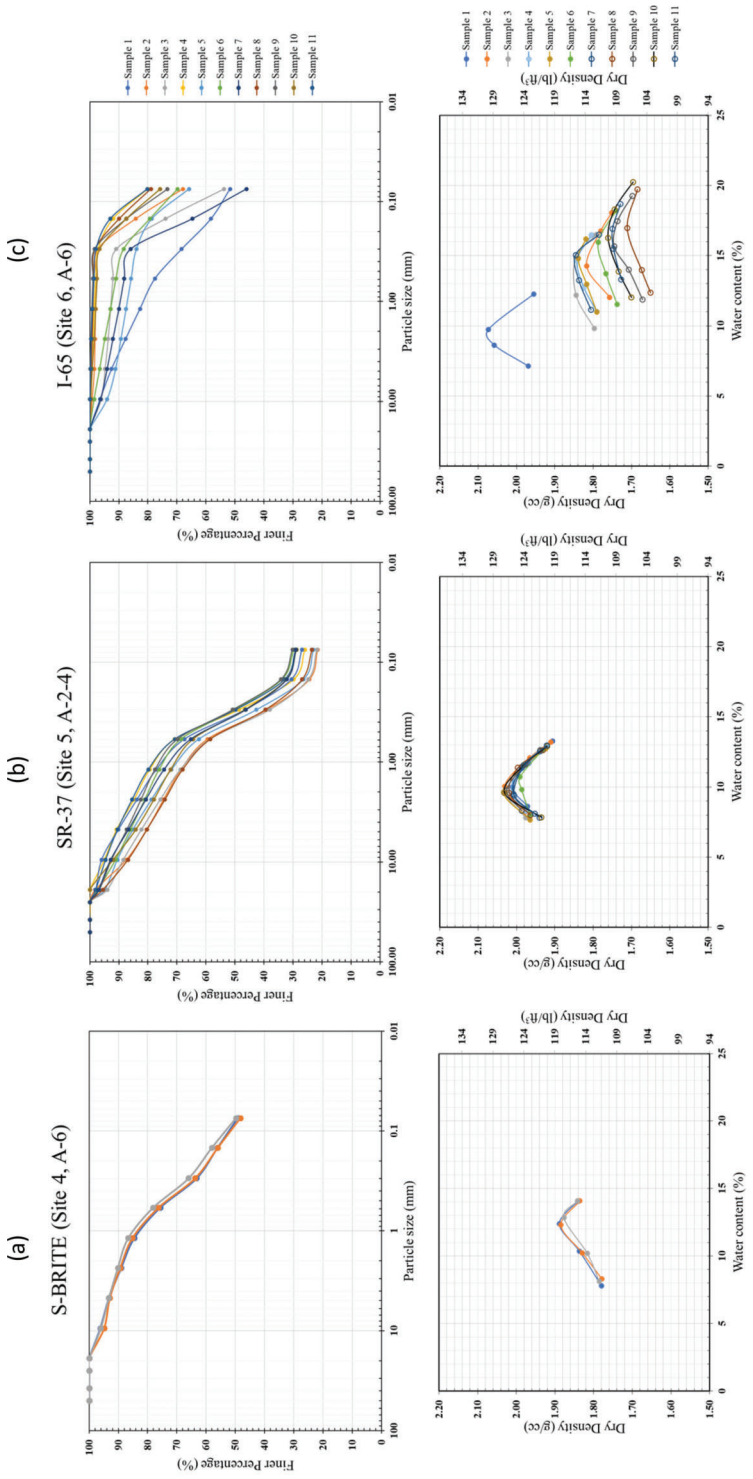

Figure 3.3 Grain size distribution and compaction results for Sites 1, 2, and 3 (a) I-865, (b) SR-46, (c) US-31.

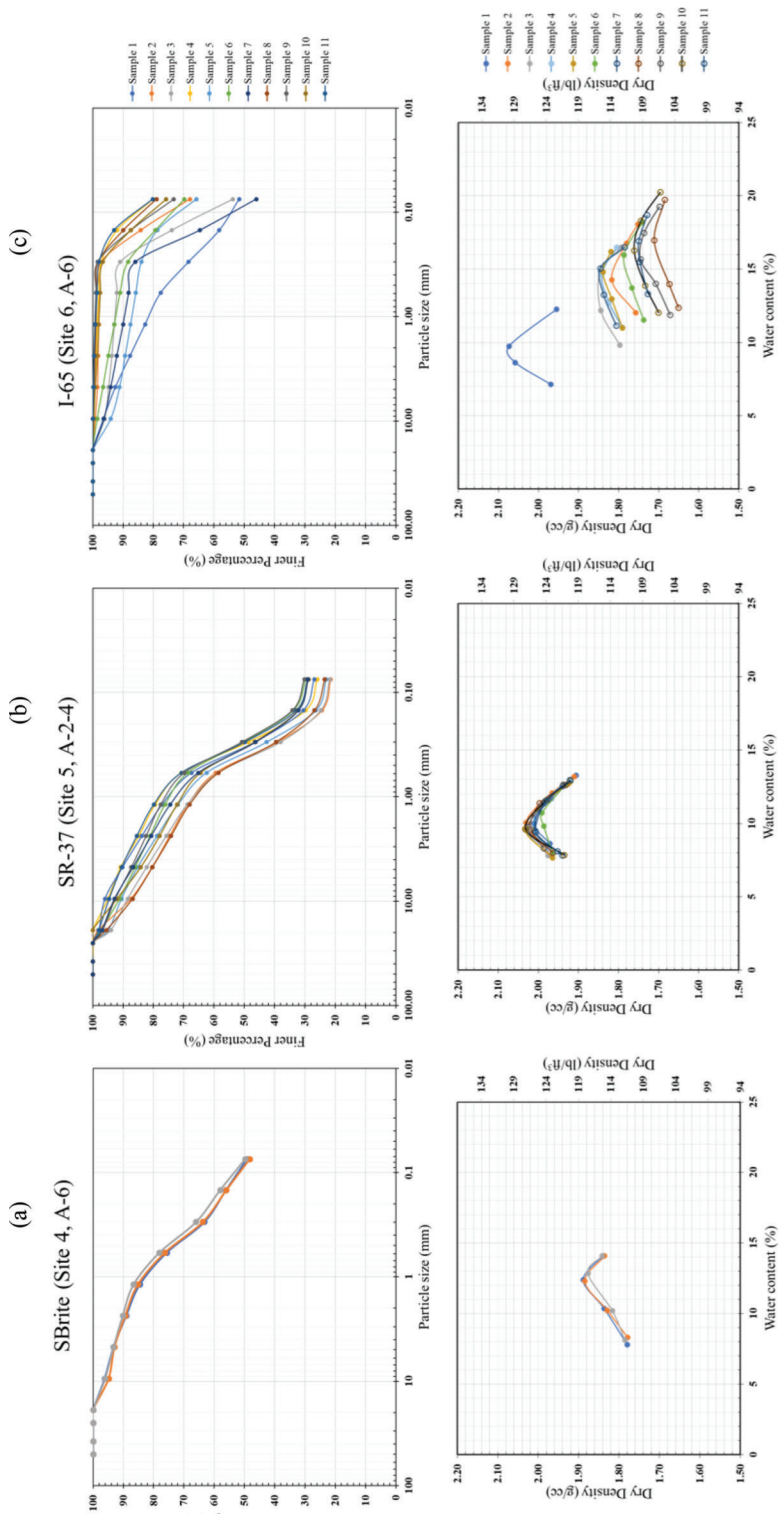

Figure 3.4 Grain size distribution and compaction results for Sites 4, 5, and 6 (a) S-BRITE, (b) SR-37, (c) I-65.

values of the cement treated specimens was almost three times higher than the untreated soil, with values in the range of 15,000 to 80,000 psi (100 to 550 MPa). Resilient modulus values of treated specimens showed a slight increase with increasing confining stresses. Samples 3, 6, 8, and 10 also exhibited a slight increase in M_R with increase in deviatoric stresses. The resilient modulus values corresponding to a deviatoric stress of 6 psi are presented in Figure 3.5, for comparison.

The resilient modulus for SR-46 subgrade soil was performed only for untreated soil samples as the design cross-section for the site consisted of an untreated subgrade. The M_R test results for this site also showed little variation with change in deviatoric and confining stresses. The resilient modulus results corresponding to a deviatoric stress of 6 psi for SR-46 samples are presented in Figure 3.6. The M_R values for samples 1–5 were in the range of 6,600 to 20,000 psi (45 to 140 MPa), significantly lower than samples 6–11 (11,300 to 38,000 psi or 78 to 268 MPa). The difference seems to be due to the higher dry densities and lower moisture contents of samples 6–11, compared to samples 1–5.

Resilient modulus tests were performed on treated as well as untreated soils for Site 3 (US-31). The soil specimens were compacted at MDD values obtained from results of Standard Proctor tests on untreated samples. The relative compaction for all samples was found to be greater than 95%. The treated specimens were prepared with 4% cement mixed with the natural soil and cured for 28 days. The water content was recorded at the time of sample preparation and after performing the resilient modulus test. The water content was found to decrease by 10%, on average, among all eleven samples after the test. Small differences in M_R values, for untreated specimens, were found for all the soils at the site; however, treated specimens exhibited larger differences. For untreated specimens, the M_R, ranged from 5,800–20,200 psi (40–140 MPa), while for treated specimens, the resilient modulus was three times higher, on average, than that of untreated specimens (18,000–68,000 psi or 120–470 MPa). Figure 3.7 shows the resilient modulus results corresponding to a deviatoric stress of 6 psi, for comparison. The variability observed in treated specimens could be due to the differences in gradation and plasticity of the soils. The resilient modulus of treated specimens showed a slight dependency on confining stress, but little to no effect with the deviatoric stresses.

The results for resilient modulus tests for samples collected from S-BRITE site is presented in Figure 3.8. The M_R values for the untreated soil was between 8,000 to 14,500 psi (55 to 100 MPa). Soil specimens for the treated resilient modulus tests were prepared with 4% cement and compacted at OMC and MDD values obtained from tests performed with untreated soil. These specimens were then cured for 28 days which resulted in 4% reduction of moisture content. For treated samples, even though the relative compaction (0.99), water content variation (-3%) and water content loss during curing (4%) across all three samples was almost same, the values for resilient modulus were quite widespread 21,000 to 75,000 psi (145 to 500 MPa). The treated specimens also showed significant dependence on deviatoric stress, with high resilient modulus values corresponding to high deviatoric stress, as is expected for fine grained soils.

For SR-37 site, as with the other sites, resilient modulus tests were performed on treated and untreated

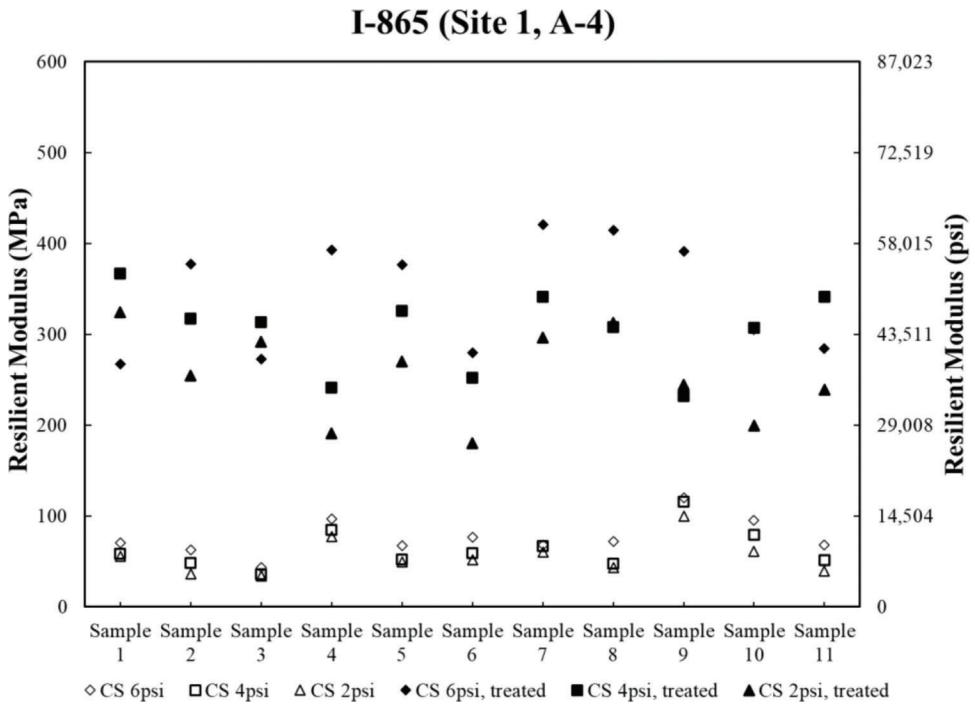

Figure 3.5 Resilient modulus test results corresponding to 6 psi deviatoric stress for I-865.

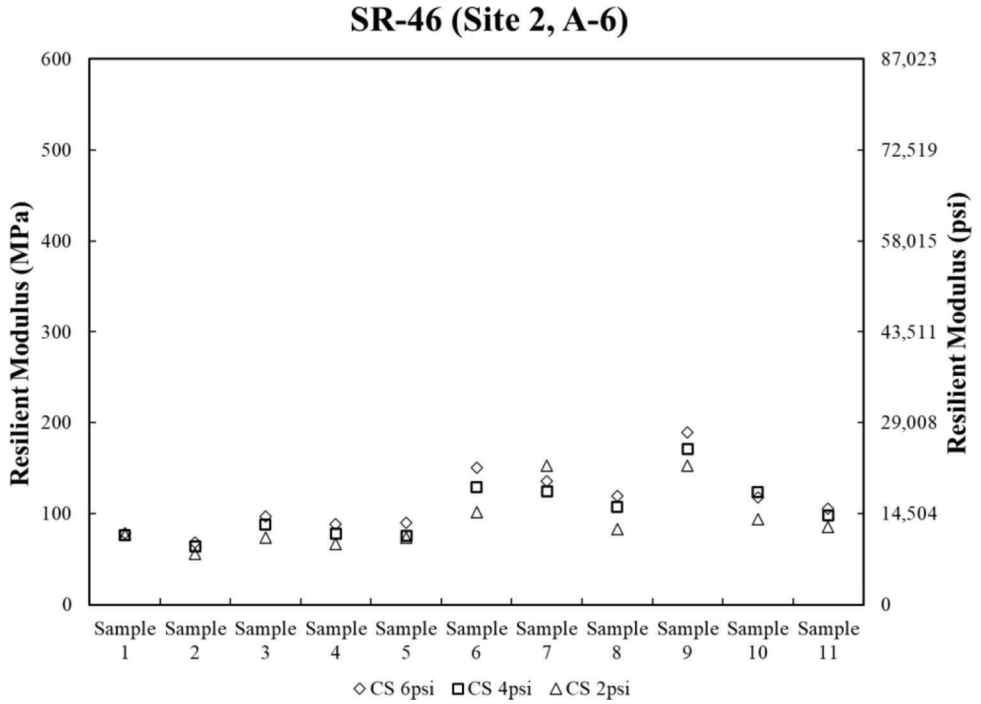

Figure 3.6 Resilient modulus test results corresponding to 6 psi deviatoric stress for SR-46.

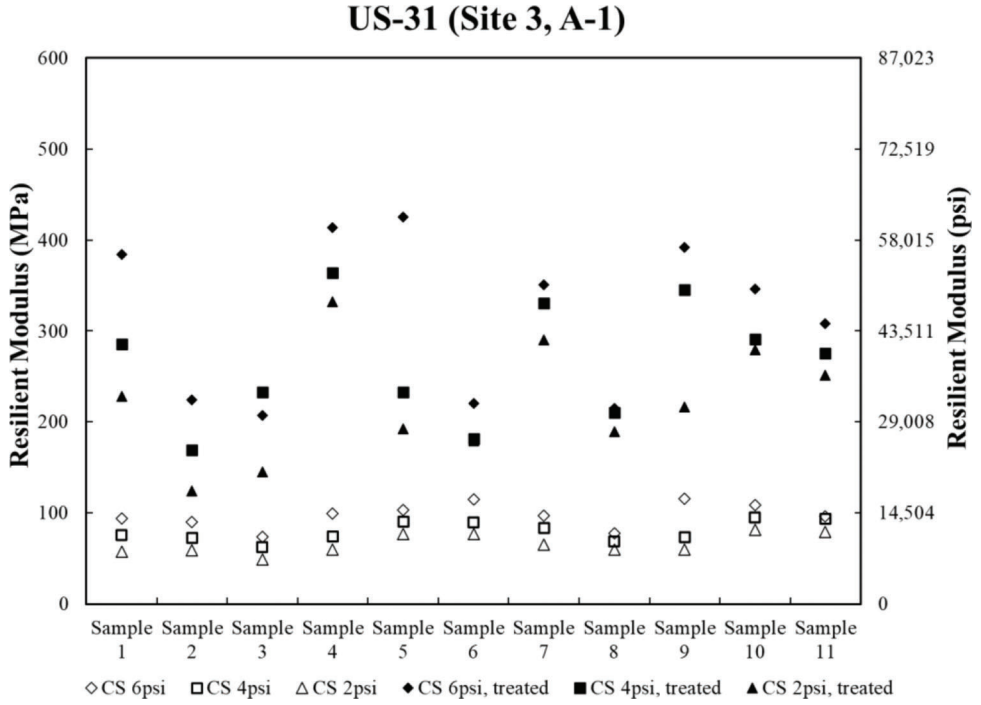

Figure 3.7 Resilient modulus test results corresponding to 6 psi deviatoric stress for US-31.

specimens, which were compacted at MDD and OMC values from Standard Proctor tests on untreated soil. The relative compaction for all samples was found to be greater than 95%. The treated specimens were prepared with 5% cement mixed with natural soil and cured for 28 days. The values for the untreated specimens are between 7,000 to 28,000 psi (48 and 190 MPa) and for treated specimens they are in the range of 25,000 to 75,000 psi (170 to 520 MPa). The effect of confining stress was observed in treated as well as in untreated specimens, with treated specimens exhibiting a greater increase with increasing confining stress. This can be seen in Figure 3.9 which depicts the M_R values at a deviatoric stress of 6 psi. The resilient modulus results also indicate

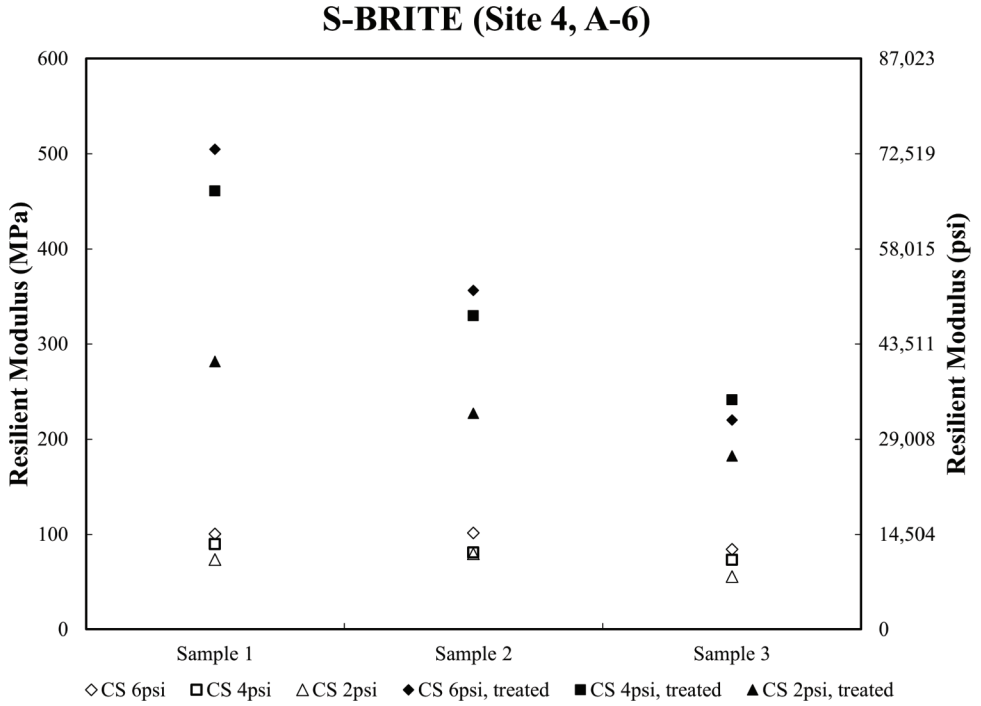

Figure 3.8 Resilient modulus test results corresponding to 6 psi deviatoric stress for S-BRITE.

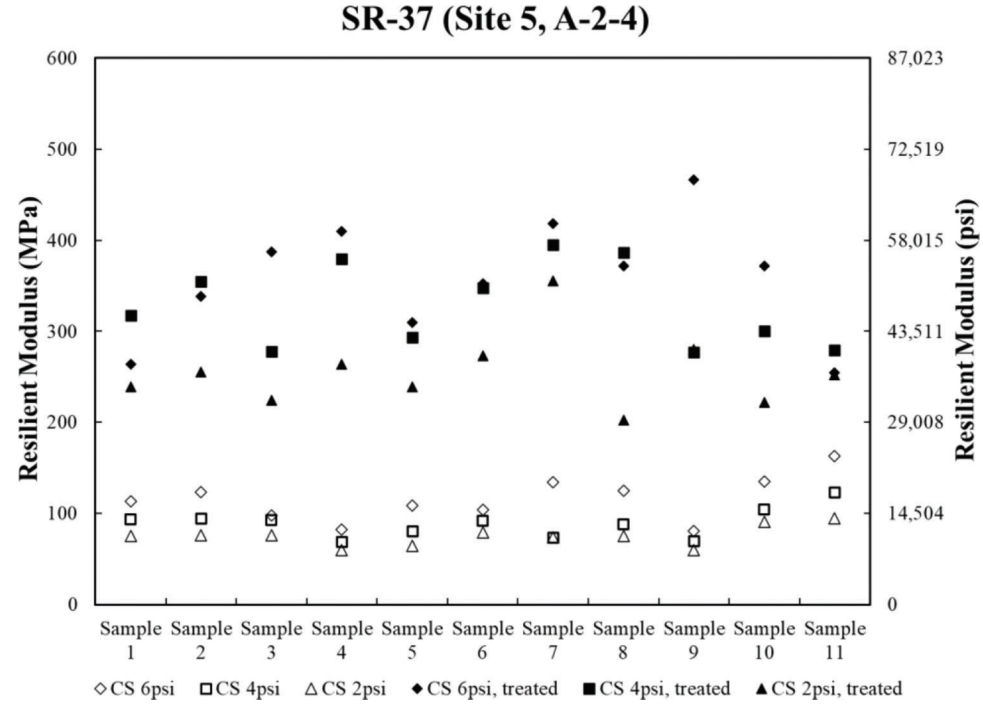

Figure 3.9 Resilient modulus test results corresponding to 6 psi deviatoric stress for SR-37.

uniformity across all stations, which was expected due to the small variation in soil properties. Few untreated specimens showed a slight decrease in M_R values with increasing deviatoric stresses (Figure B.5).

The resilient modulus test results for I-65 samples were performed for treated as well as untreated specimens. The treated specimens were prepared with 5% cement and cured for 28 days. All the resilient modulus test specimens were compacted at OMC and MDD obtained from tests on untreated soil samples. The relative compaction was obtained to be in the range of 0.97 to 1.00. The values for untreated resilient modulus ranged from 5,000 to 19,000 psi (35 to 135 MPa), with the lowest values corresponding to sample 7 which had

lowest percentage of fines and was gap graded. None of the untreated specimens showed any dependence on confining stress or deviatoric stress, but few treated specimens showed a gradual increase in moduli with increasing deviatoric stress. The treated M_R varied from 11,000 to 70,000 psi (80 to 500 MPa). Figure 3.10 shows the variation in resilient modulus for treated and untreated specimen across the eleven locations, for deviatoric stress of 6 psi.

3.3 Field Tests

FWD and GPR tests were performed at Site 1 (I-865) and Site 2 (SR-46) in July 2020 and on Site 3 (US-31) and Site 5 (SR-37) in September 2021. The tests were conducted on top of the pavement surface. The locations where soil samples were collected for the laboratory tests were identified and FWD tests were conducted at the same locations at Sites 1, 2, and 3. However, due to traffic control issues and ongoing construction activities, the FWD and GPR tests at Site 5 were performed on the northbound road, while the samples were collected on the southbound road. An extra set of FWD tests was also conducted on Site 3, US-31, on the southbound road to compare differences in the two directions (northbound, where the samples for the laboratory were collected and southbound). FWD test locations on SR-37 northbound road and US-31 southbound road were marked such that they have the same RP as the points where soil samples were collected (on the SR-37 southbound and US-31 northbound). The GPR test was performed for the complete stretch of 300 ft on all the sites.

The Dynatest 8000 FWD Test System was used for the FWD tests. The radius of the loading plate was 15 cm, and nine sensors were used to measure deflection. The forces generated by the FWD were 7,500 to 12,000 lb. The FWD sensor spacing used for the test was 0, -12, 8, 12, 18, 24, 36, 48, and 60 inches. The GPR data was collected using an SIR-30 control unit along with a 2 GHz horn antenna, a 900 MHz ground coupled antenna, and a 400 MHz ground coupled antenna. The data from the horn antenna was utilized to calculate the velocity of the radar wave. The wave travel times were then found by extracting the suspected interface at the base of the pavement. The results of the GPR tests were compared with the available pavement design cross-sections to determine any differences between the design and as-built profiles. FWD back calculations were carried out using the design and GPR measured thicknesses using the MODTAG (Clark et al., 2016) and ELMOD (Dynatest, 2013) software.

Site 1, I-865, is a PCCP type pavement. The GPR data from the 900 MHz and 400 MHz ground coupled antenna was used to measure the thickness of the pavement. The GPR data identified two of the five layers in the design cross-section: layer 1 with an average thickness of 12.3 in. and layer 2 having an average thickness of 5.5 in. (Figure 3.11). The designed subbase consisted of a 3 inch intermediate OG 19 mm, over 6-inch Coarse Aggregate No. 53; however, the GPR data suggested a subbase layer of 5.5-in. thickness only. The GPR data could not be analyzed at joint locations due to the presence of the dowel bars. Table 3.1 shows the FWD applied load and the measured deflections for the second drop. Peak deflections under the loading

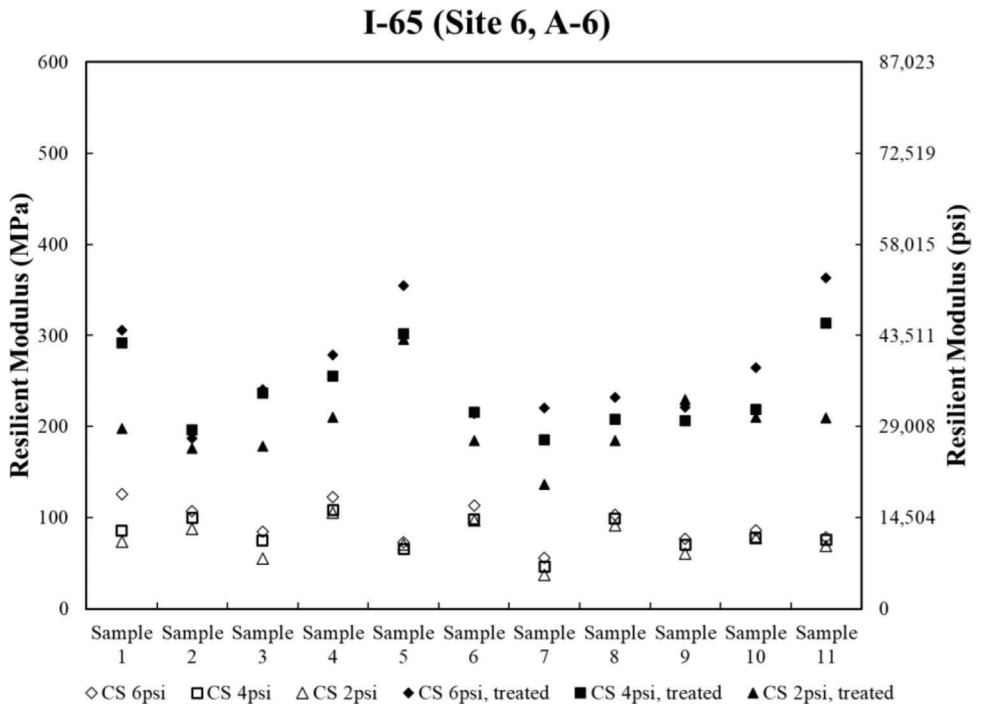

Figure 3.10 Resilient modulus test results corresponding to 6 psi deviatoric stress for I-65.

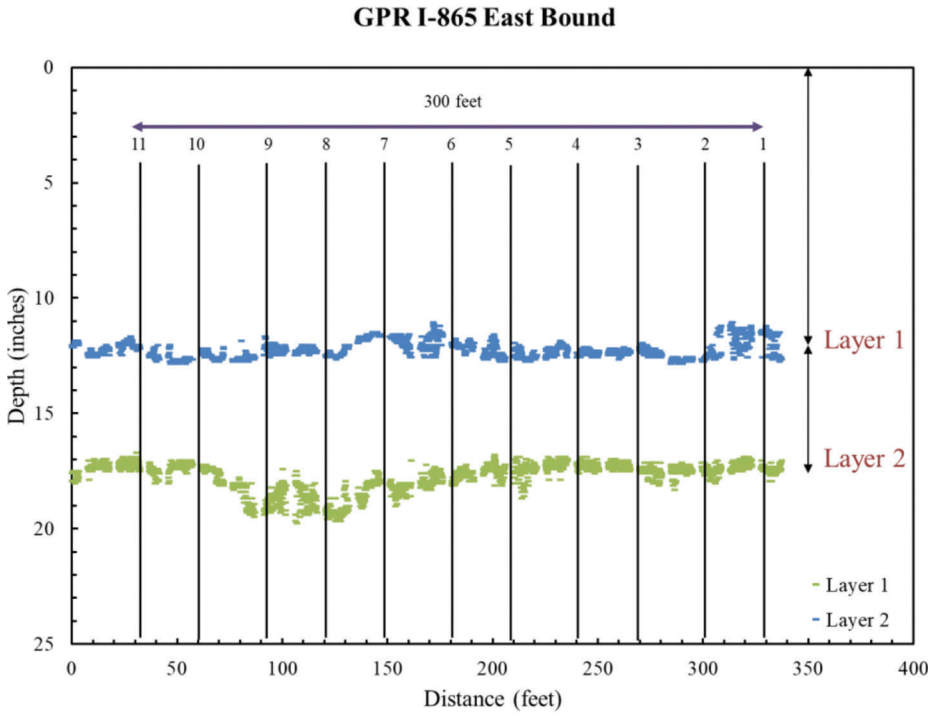

Figure 3.11 GPR pavement thickness results for I-865.

TABLE 3.1
FWD Deflection Data for I-865

Station	11	10	9	8	7	6	5	4	3	2	1
Applied Load (lbs)	9,274	9,252	9,121	9,121	9,056	8,924	8,837	8,968	8,881	8,727	8,684
Deflection Under Load (mil or 10^{-3} in.)	4.26	3.05	3.64	3.36	4.46	3.62	3.78	2.25	2.4	2.75	2.31

plate for a load drop of 9,000 lb vary from 2.3 to 4.5 milli in. (mil or 10^{-3} in.).

Site 2, SR-46, has asphalt pavement. The GPR data from 2 GHz horn antenna along with the 900 MHz and 400 MHz ground coupled antennas was used to measure the thickness of the pavement layers. The GPR identified two layers below the pavement surface: layer 1 with an average thickness of 9.9 in. and layer 2 having an average thickness of 12.7 in. (Figure 3.12). The design pavement cross section was compared with the GPR results. The GPR was unable to distinguish between the different asphalt layers because they have similar dielectric properties. The FWD applied load and the measured deflections at the center of the loading plate are tabulated in Table 3.2. The FWD deflection data corresponding to all three drop loads is provided in Appendix C. The peak deflections measured by the sensors at this site are 1.5 to 2 times higher than those experienced by PCCP pavements.

The GPR data was collected with 400 MHz antennas in the right and left wheel paths (RWP and LWP) and a 900 MHz antenna in the RWP for the northbound, US-31 southbound and SR-37 northbound roads. The dielectric constant and therefore the velocity was estimated using data from the horn antenna, while the ground coupled antennas were used to compute travel time information.

Site 3, US-31, has a PCCP pavement. Two layers were identified in the northbound road, while three layers were present in the southbound road (Figure 3.13 and Figure 3.14). Layer 1 is the PCCP, while layer 2 is the subbase for PCCP pavement. As per section 302 of INDOT standard specifications, the subbase for PCCP pavement comprises 3-inch Coarse Aggregate No. 8, which acts as a drainage layer, placed over 6-inch Coarse Aggregate No. 53, as the separation layer. The average thickness of layer 1 on the northbound road was 11.3 in., while that of layer 2 was 8.5 in. The thickness of layer 1 was not uniform through the 300 ft section and ranged from 9.5 to 13 in. For the southbound road, the average thicknesses measured with GPR are layer 1=10.9 inch, layer 2=4.7 inch, and layer 3=6.5 inch. The FWD measured deflection corresponding to the second drop for the northbound and southound are tabulated in Tables 3.3 and 3.4, respectively. The peak deflection varies from 3.7 to 2.1 mil, while the range of the deflection basin ranges from 3.7 to 1.0 mil.

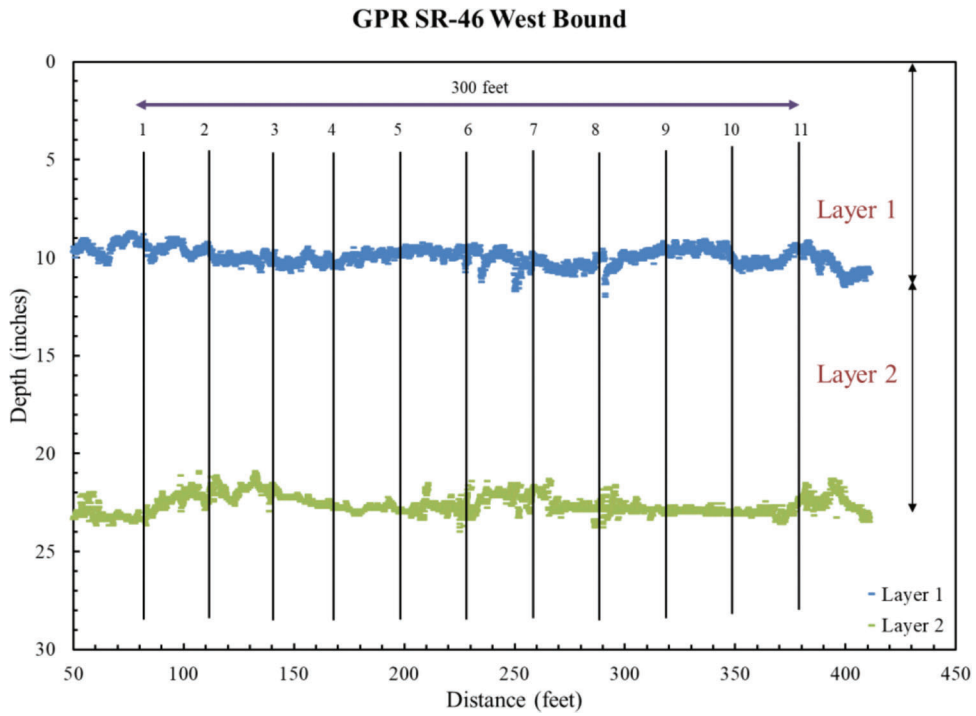

Figure 3.12 **GPR** pavement thickness results for SR-46.

TABLE 3.2
FWD Deflection Data for SR-46

Station	1	2	3	4	5	6	7	8	9	10	11
Applied Load (lbs)	9,646	9,548	9,570	9,559	9,591	9,624	9,580	9,613	9,646	9,570	9,559
Deflection Under Load (mil or 10^{-3} in.)	6.56	6.76	6.83	7.48	6.95	6.66	7.84	7.03	7.15	9.87	10.2

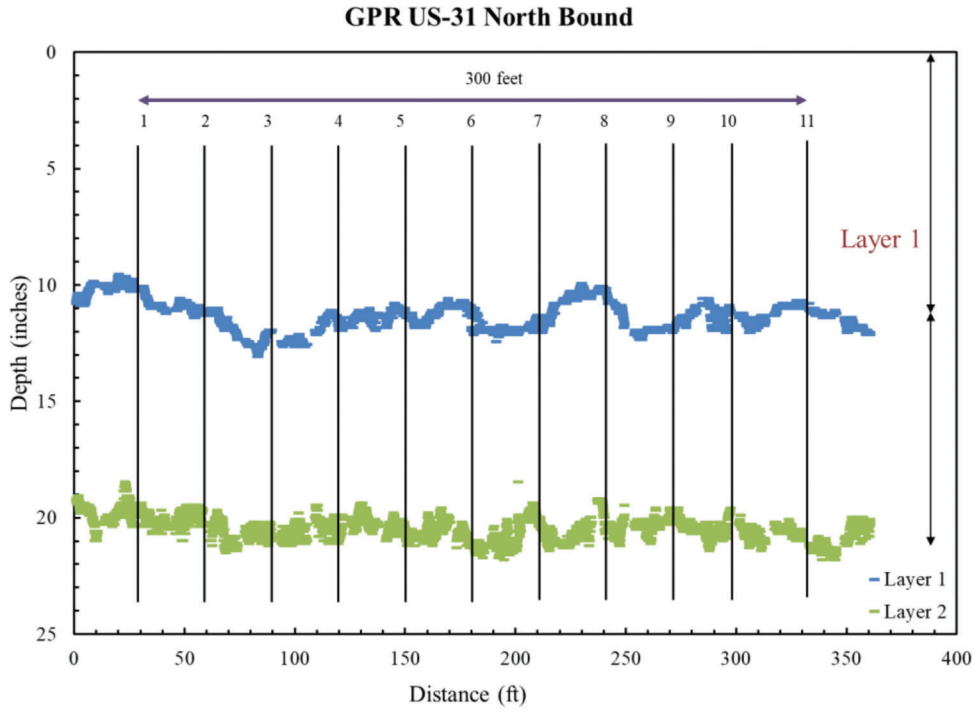

Figure 3.13 GPR pavement thickness results for US-31 northbound.

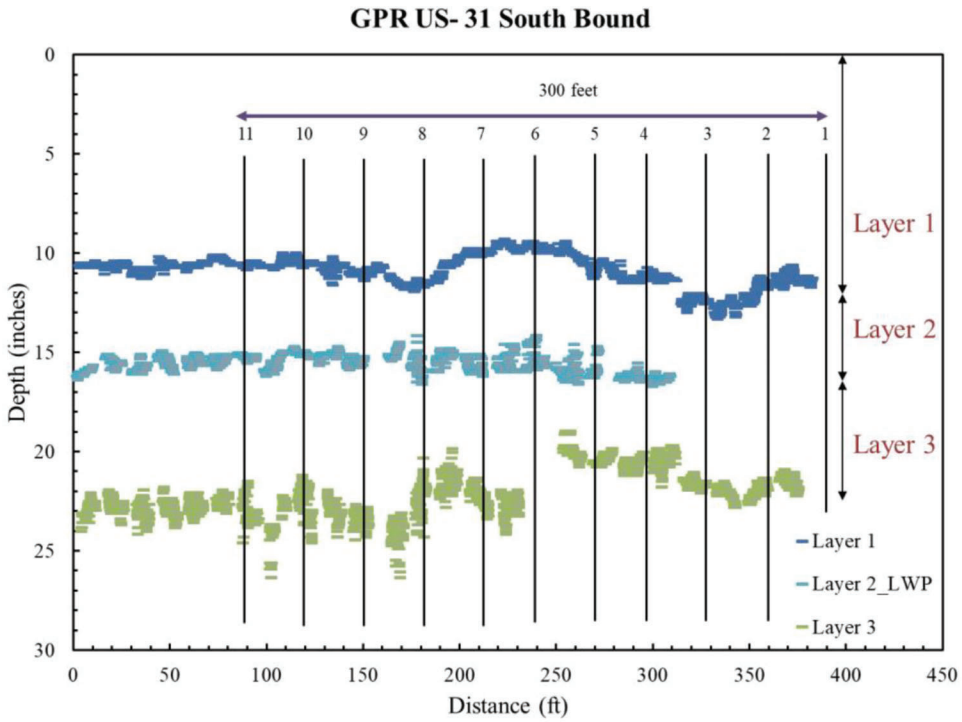

Figure 3.14 GPR pavement thickness results for US-31 southbound.

TABLE 3.3
FWD Deflection Data for US-31 Northbound

Station	1	2	3	4	5	6	7	8	9	10	11
Applied Load (lbs)	8,771	8,804	8,870	8,848	8,673	8,443	8,542	8,651	8,640	8,760	8,640
Deflection Under Load (mil or 10^{-3} in.)	3.65	3.38	2.65	2.1	2.31	2.07	2.2	2.25	2.15	2.12	2.72

TABLE 3.4
FWD Deflection Data for US-31 Southbound

Station	11	10	9	8	7	6	5	4	3	2	1
Applied Load (lbs)	9,209	9,362	9,296	9,395	8,749	8,662	9,318	9,263	9,176	8,804	9,121
Deflection Under Load (mil or 10^{-3} in.)	2.31	2.49	2.69	2.6	2.63	2.72	2.67	2.65	2.57	2.93	2.96

The design pavement cross-section for Site 5, SR-37 consisted of three layers: 10 inch of PCCP over a subbase for PCCP, which was overlying a 14 inch of cement-treated subgrade. Two of the layers were identified with the GPR, the average thickness for layer 1 and layer 2 were estimated to be 11.1 and 8.3 in., respectively (Figure 3.15). The peak deflections measured under the loading plate by the FWD corresponding to drop 2 (~9,000 lb) are included in Table 3.5.

The continuous thickness output from the GPR provides the pavement thickness information at each point of sample collection. Backcalculation of the pavement moduli is done for two scenarios: using the design cross-sections; and the actual thickness of the pavement layers obtained from the GPR tests. All cases are analyzed using ELMOD and MODTAG. In addition, for US-31 southbound, based on the GPR data shown in Figure 3.14, the 300-ft section was divided into two segments to capture the effect of pavement layer thickness in the backcalculated moduli. The software MODTAG was used for the calculations. The analysis of the results is included in Chapter 4.

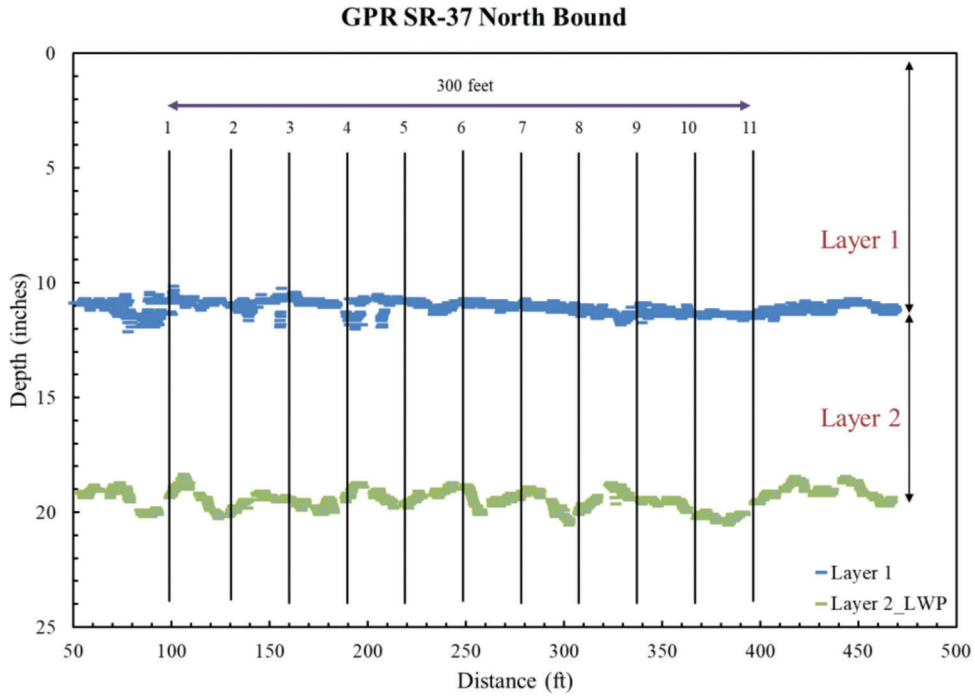

Figure 3.15 GPR pavement thickness results for SR-37 northbound.

TABLE 3.5
FWD Deflection Data for SR-37 Northbound

Station	1	2	3	4	5	6	7	8	9	10	11
Applied Load (lbs)	9,001	8,990	9,034	8,990	8,957	8,979	8,979	8,957	8,946	8,979	8,968
Deflection Under Load (mil or 10^{-3} in.)	1.72	1.72	1.8	1.76	1.83	1.74	1.68	1.69	1.69	1.75	1.79

4. ANALYSIS OF RESULTS

Six different site projects (I-865, SR-46, US-31, S-BRITE, SR-37, and I-65) were identified for subgrade soil sample collection and to run FWD and GPR tests. The results obtained from the laboratory tests and field tests were analyzed to determine if good correlation models exist for resilient modulus determination. This chapter comprises of two sections, the first section attempts at using regression analysis to find correlation between M_R and soil properties. In the second section, the results from FWD test are analyzed using MODTAG and ELMOD and the backcalculated moduli thus obtained for the subgrade soil are compared with laboratory resilient modulus.

4.1 Regression Analysis

Several researchers (Carmichael III & Stuart, 1985; Drumm et al., 1990; Hossain & Kim, 2015; Lee et al., 1997; Rahim, 2005) have correlated soil properties such as Atterberg limits, percentage of fines, undrained compressive strength, compaction parameters, etc. with the resilient modulus to establish stress-independent correlations. In this research, a comprehensive statistical analysis was performed to relate the laboratory resilient modulus data in Chapter 3 with soil properties such as dry density, moisture content, Atterberg limits, and fines percentage using the SPSS software.

The following three types of regression analysis were performed:

1. linear regression analysis for all input variables,
2. stepwise linear regression, which chooses only the parameters having the highest significance; and,
3. non-linear regression analysis, to evaluate coefficient parameters for the Uzan and octahedral stress models (discussed in Chapter 2).

The first two types of regression analysis were performed to obtain stress-independent relationships. The soil properties were treated as independent variables in the regression analysis. Plastic limit and percentage of fines, liquid limit and plasticity index, water content and optimum moisture content were found to have high Pearson correlation values. When building any regression model, it is important to identify any relationship

between independent variables, given that multicollinearity issues arise when there exists a high correlation among independent variables. The variance inflation factor (VIF) values greater than 10 give an indication of codependency among independent variables.

The load resilient modulus tests give fifteen different moduli depending on confining stress and deviatoric stresses. For the regression analysis, different sets of resilient moduli values were considered: average M_R values, M_R values corresponding to 6 psi deviatoric stress, and 4 psi confining stress, M_R values corresponding to 6 psi deviatoric stress, and 2 psi confining stress and M_R values corresponding to 6 psi deviatoric stress, and 6 psi confining stress. The regression analysis was carried out by grouping soils having the same AASHTO classification. It was observed that the stress-independent models did not provide any statistically significant relationship. Even the models obtained using the linear regression analysis in SPSS did not provide insight into the dependence of a soil property and resilient modulus. It was thus concluded that no meaningful stress-independent relationship existed for the current sample database.

A number of researchers (e.g., Dai & Zollars, 2002; Nazzal & Mohammad, 2010; Puppala et al., 2011; Rout et al., 2012) have used the constitutive relationships discussed in Chapter 2 to estimate the resilient modulus. This was the basis for the third type of regression analysis performed in this study. The following two models were used.

Model 1: Uzan Model

$$log\left(\frac{M_R}{P_a}\right) = logk_1 + k_2 \; log\frac{\sigma_{bulk}}{P_a} + k_3 log\frac{\sigma_{dev}}{P_a}$$

Model 2: Octahedral Stress Model

$$log\left(\frac{M_R}{P_a}\right) = logk_1 + k_2 \; log\frac{\sigma_{bulk}}{P_a} + k_3 log\left(\frac{\tau_{oct}}{P_a} + 1\right)$$

A non-linear regression analysis was performed in SPSS to obtain the regression coefficients k_1, k_2, and k_3 for the two models. Regression analyses were performed on both untreated and cement-treated specimens. The results obtained for Uzan model analysis are presented in Appendix D, while octahedral model results are in Appendix E. It was observed that the regression coefficient k_1 was significantly higher for treated specimens than for untreated specimens, for both the Uzan and octahedral stress models. This is expected because of the increase in resilient modulus due to the chemical reactions with cement. It was also observed that the parameter k_2, which is a coefficient for the bulk stress in both models, increased slightly for coarse grained soils (US-31 and SR-37), while the increase was more substantial for fine grained A-6 type soils (S-BRITE and I-65). The values of k_2 for both treated and untreated specimens ranged from 0.25 to 0.56, somewhat consistent with the expectation that the soil stiffness is proportional to the square root of the mean effective stress (confinement). The parameter k_3 was found to have negative values for both treated and untreated specimens, which suggests that the resilient modulus decreases with the deviatoric or octahedral stresses (Hossain et al., 2009; Nazzal & Mohammad, 2010; Titi et al., 2018). It was also observed that the values of k_3 increased with treatment, which is expected based on previous observations where the effect of the deviatoric stress decreases for treated specimens with high stiffness (Puppala et al., 2011; Rout et al., 2012). The stress-dependent model parameters showed significant variability across the eleven samples collected from a single site. This was expected since the soil samples collected from the same site were quite variable, as discussed in Chapter 3. However, the stress-dependent model parameters determined for an individual specimen were found to give a strong correlation. Figures D.1 and D.2 in Appendix D and Figures E.1 and E.2 in Appendix E show the relationship between the measured and the calculated M_R of treated as well as untreated soil samples collected from I-865, US-31, S-BRITE, SR-37, I-65, and SR-46 using the Uzan and octahedral stress models. The predicted M_R values were calculated based on individual regression analysis results. Each plot thus represents data obtained from eleven samples collected from a site and eleven sets of regression parameters (k_1, k_2, and k_3). The coefficient of regression (R^2) was greater than 0.8 for untreated samples and greater than 0.66 for treated specimens. The average values for the regression parameters: k_1, k_2, and k_3 for the Uzan and the octahedral stress models are listed in Tables 4.1 and 4.2, respectively. The k_1, k_2, and k_3 parameters along with the R^2 obtained from the regression analysis are provided in Appendices D and E. Please note that the results are obtained and are applicable to each particular site. In other words, no generalization can be done.

TABLE 4.1
Results of Regression Analysis of Treated and Untreated Soil Specimens–Uzan Model

Site	Treatment	k_1	k_2	k_3
I-865	Untreated	482	0.45	-0.30
	Treated	2,765	0.37	-0.07
US-31	Untreated	622	0.46	-0.20
	Treated	2,219	0.48	-0.12
S-BRITE	Untreated	741	0.28	-0.03
	Treated	3,266	0.56	0.19
SR-37	Untreated	701	0.44	-0.21
	Treated	2,565	0.50	-0.14
I-65	Untreated	762	0.25	-0.05
	Treated	2,373	0.38	0.06
SR-46	Untreated	747	0.29	-0.28

TABLE 4.2
Results of Regression Analysis of Treated and Untreated Soil Specimens–Octahedral Stress Model

Site	Treatment	k_1	k_2	k_3
I-865	Untreated	966	0.44	-2.13
	Treated	3,369	0.36	-0.42
US-31	Untreated	986	0.45	-1.39
	Treated	2,840	0.47	-0.79
S-BRITE	Untreated	792	0.29	-0.32
	Treated	2,185	0.56	1.32
SR-37	Untreated	1,147	0.43	-1.45
	Treated	3,500	0.49	-0.95
I-65	Untreated	845	0.26	-0.40
	Treated	2,184	0.37	0.55
SR-46	Untreated	1,426	0.29	-2.09

4.2 Analysis of FWD Results

Pavement deflection obtained from FWD tests is widely used to measure the structural condition of different pavement layers including the subgrade layer. The backcalculation approaches used in practice are discussed in Chapter 2. The following section contains backcalculation analyses of FWD data using ELMOD and MODTAG, as well as comparison of backcalculated moduli with resilient moduli obtained from the laboratory tests.

ELMOD is a frequently used software package that uses an iterative backcalculation method. It is also the code preferred by INDOT to interpret FWD results. The software uses the equivalent thickness forward backcalculation scheme to estimate moduli for flexible pavement, while a finite element method is used for rigid pavements. There are certain limitations associated with ELMOD—(1) the maximum number of layers that can be used as input (including the rigid layer) is limited to 4; (2) the code assumes that layer stiffness decreases with depth. Since the software is not available in the public domain, all the analyses with ELMOD were performed with the help of Dr. Boonam Shin from INDOT.

MODTAG is a combination of TAG (test and guess) and MODCOMP (modulus computation) and was developed by VDOT (Virginia Department of Transportation) and Cornell University. The software utilizes optimization techniques to backcalculate the layer moduli. It uses multilayer elastic theory for forward backcalculation and compares and adjusts the calculated deflection basin to the measured deflection basin. MODTAG also helps to judge the quality of the data by performing a series of checks, such as SLIC analysis and cumulative difference. SLIC analysis is helpful in identifying errors that could arise due to surface defects in the pavement or improper sensor location, while cumulative difference plots are indicative of changes in pavement layer thicknesses and could be used to identify locations for coring. The MODTAG software was provided by Dr. David Orr from Cornell University. He also assisted in the analysis of FWD data and in the interpretation of the results.

Previous research by Uzarowski et al. (2005), Ahmed et al. (2014), and Ahmed and Tarefdar (2017) has shown that the use of GPR data in conjunction with FWD test helps improve the reliability of the results. FWD backcalculation results are affected by pavement thickness and sometimes there exists discrepancies in the design data available and the as-built profile. For the analyses, the GPR data was compared with the available design cross-section, and backcalculation was performed using the thickness of the pavement layers obtained from GPR data and from the design cross-sections provided by INDOT. The FWD tests were all performed during the day and the effects of concrete slab curling were not considered in the analysis.

4.2.1 Rigid Pavements

4.2.1.1 Site 1: I-865. This site was located in Marion County, Indiana. Figure 4.1a shows the exposed subgrade layer, where the soil samples were collected in August 2019, and Figures 4.1b and 4.1c show the FWD and GPR tests performed in July 2020 during daytime. The pavement was slightly wet due to light rains the day prior to the FWD and GPR tests. The pavement design cross-section, as shared by INDOT, along with the GPR-interpreted thicknesses are provided in Table 4.3.

MODTAG Analysis

The pavement cross-section was designed as a 4-layer system (excluding the hard bottom). Layer 1 was the PCCP layer. The intermediate OG layer and compacted aggregate layer were considered as a single subbase layer (layer 2: SB) with 9-in. thickness. The 12-in. cement-stabilized subgrade layer and 14-in. foundation improvement layer which also had cement stabilization were treated as a single layer (layer 3: treated subgrade–TSG). Layer 4 comprised of the unbound soil below the treated subgrade and its thickness was determined by MODTAG based on the computed hard bottom (unbound subgrade–UBSG). The effect of pavement thickness was evaluated by considering the following cases.

Case 1: pavement layer thickness based on design cross-section. Results are denoted as "D."

Case 2: pavement layer thickness based on GPR measurements for layer 1 and layer 2, with results denoted as "GPR."

Due to inconsistencies observed in the design and GPR measurements, a third case was identified for this site which considered a 6-in. thick layer 2. This case was denoted as "DGPR."

The different cases analyzed to study the influence of pavement thickness, hard bottom and seed moduli on the backcalculated moduli are tabulated in Table 4.4 and Table 4.5. The results from all the analysis performed using MODTAG are included in Appendix F.

MODTAG allows multiple preliminary checks to analyze the FWD data prior to performing back

Figure 4.1 Photographs at Site 1, I-865: (a) subgrade sample collection, (b) GPR test, (c) FWD test.

TABLE 4.3
I-865 Pavement Design Cross-Section, as Provided by INDOT, and from GPR Data

Layer	Design Thickness (in.)	GPR Measured Thickness (in.)
Plain jointed QC/QA PCCP	12.0	12.3
QC/QA-HMA, 4, 76, Intermediate OG19.0 mm	3.0	5.5
Compacted Aggregate No. 53 on Geotextile Type 1A	6.0	ND
Cement Stabilized Subgrade	12.0	ND
Foundation Improvement (chemical stabilization with cement)	14.0	ND

Note: ND = Not Detected.

TABLE 4.4
Cases for MODTAG Analysis for Site 1: I-865 Based on Pavement Thickness and Hard Bottom

		Design	GPR	Design GPR	Design	GPR	Design GPR
Layer	**Seed Moduli (ksi)[1]**	**D**	**GPR**	**DGPR**	**D_HB**	**GPR_HB**	**DGPR_HB**
PCCP	2,000	12.0	12.3	12.0	12.0	12.3	12.0
SB	40	9.0	5.5	6.0	9.0	5.5	6.0
TSG	100	26.0	26.0	26.0	26.0	26.0	26.0
UBSG	10	–	–	–	–	–	–
Hard Bottom	500		Ignored			Considered	

Note: All thicknesses in inches.
[1]1 ksi = 1,000 psi.

TABLE 4.5
Cases for MODTAG Analysis for Site 1: I-865 Based on Seed Moduli

	Thickness (in.)	Seed Moduli (ksi = 1,000 psi)					
Layer	**GPR**	**Case 1**	**Case 2**	**Case 3**	**Case 4**	**Case 5**	**Case 6**
PCCP	12.3	4,500	2,000	4,500	2,000	2,000	4,500
SB	5.5	50	50	40	40	40	40
TSG	26	100	100	100	100	100	100
UBSG	–	5	5	5	5	10	10

calculation analysis. After uploading the FWD file in MODTAG, SLIC transformation, cumulative differences of deflection and surface modulus plots were analyzed to check for pavement homogeneity, sensor effectiveness and to assess the pavement structure. The hard bottom was located at 300 in. or deeper for most of the station locations. It was noticed that when sensor 2 (at -12 in.) was used in the analysis, the preliminary checks (SLIC transformation, cumulative differences, surface modulus) could not be performed and high root mean square (RMS) error values were obtained. This was due to the presence of another sensor at the 12-in. location. Sensors spaced at repeated distances result in skewed results, thus for the analysis with MODTAG, only 8 sensors (located at 0, 8, 12, 18, 24, 36, 48, and 60 in.) were considered.

Figure 4.2 shows the backcalculated moduli for the 4-Layer system which considers GPR measured thickness for the PCCP and subbase layers. The subbase layer, which is a comparatively thin layer is sandwiched between the stiffer PCCP and thick cement stabilized subgrade layer. This has led to underestimating the backcalculated modulus for the subbase and overestimating the moduli for the treated subgrade. It was also observed that the backcalculated moduli for the cement-treated layer 3, TSG (treated subgrade), was abnormally high (5×10^6 psi) at a number of locations. The number of stations with high moduli increased when the hard bottom was considered in the analysis or when a higher seed modulus value was chosen for the PCCP layer (4,500 ksi as compared to 2,000 ksi).

MODTAG considers the influence of hard bottom if its depth is less than 300 in. The average depth of the hard bottom at I-865 was estimated to be 270 in. with MODTAG. Figure 4.3 shows the effect of the hard bottom on the treated subgrade and the underlying unbound soil layer. The results are displayed with dashed lines. It can be seen that when hard bottom is considered, MODTAG further overestimates the modulus for the TSG (treated subgrade) layer and underestimates the stiffness of the unbound soil layer. If we eliminate the outliers (back-calculated moduli higher than 5×10^6 psi) for the treated subgrade layer, the TSG modulus is overestimated by approximately 20%, while the unbound soil layer is underestimated by 50%.

The results of back calculation for the subgrade layer moduli are greatly affected by pavement layer thicknesses. Figure 4.4 shows the effect of varying pavement thickness and also the need to use GPR in conjunction with the FWD test to get more accurate pavement thickness information. The TSG (treated subgrade) layer moduli using the design pavement cross section are found to be too high (8 out of 11 locations are greater than 5×10^6 psi). When GPR measurements are used, the number of locations with high moduli are reduced and a reasonable average moduli value of 118,000 psi (average excluding the 2 outliers) is obtained.

In addition to this, MODTAG was also used to study the effect of change in seed moduli values. It was observed that the results obtained from MODTAG were sensitive to the seed moduli value chosen for the PCCP layer. Figure 4.5 shows the effect of seed moduli on the modulus of treated subgrade layer for Site 1. The blue plots (Cases 1, 3, and 6), corresponding to a seed value of 4,500 ksi for PCCP, yield higher moduli than the orange plots (Case 2, 4, and 5) with a PCCP seed modulus of 2,000 ksi. This shows that when the seed moduli for PCCP was increased by 2.25 times, the average moduli for the treated subgrade increased by more than 200%. It was also seen that changes in seed modulus for the subbase (SB) or unbound soil layer did not affect the results. A 10,000 psi reduction in SB seed moduli resulted in an average difference of less than 12%; however, when the seed modulus of the unbound soil was doubled, the average difference was less than 7%. The RMS error for all cases considered was less than 5%. The MODTAG analysis results are presented in Appendix G.

ELMOD Analysis

FWD backcalculation analysis was performed with the ELMOD software with the help of Dr. Boonam Shin, research engineer at INDOT. The protocol followed by INDOT to backcalculate moduli using ELMOD does not consider a hard bottom in the analysis and requires data from only 8 sensors (-ve sensor location is not considered for backcalculation). Table 4.6. presents the two pavement structures considered. It was observed that the results obtained from ELMOD were not highly sensitive to the pavement thickness measurements and yielded reasonable modulus for all pavement layers (Figure 4.6). The change in thickness of the subbase layer resulted in up to 30% variation in the moduli of treated subgrade layer. ELMOD results also did not exhibit any compensating

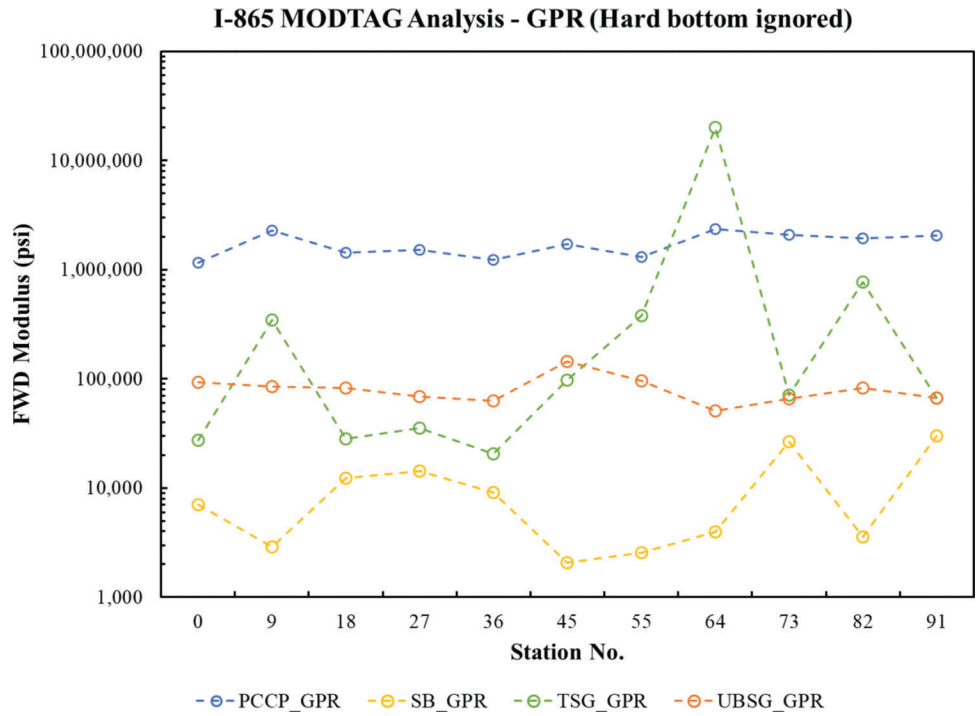

Figure 4.2 I-865 MODTAG analysis–4 layer model.

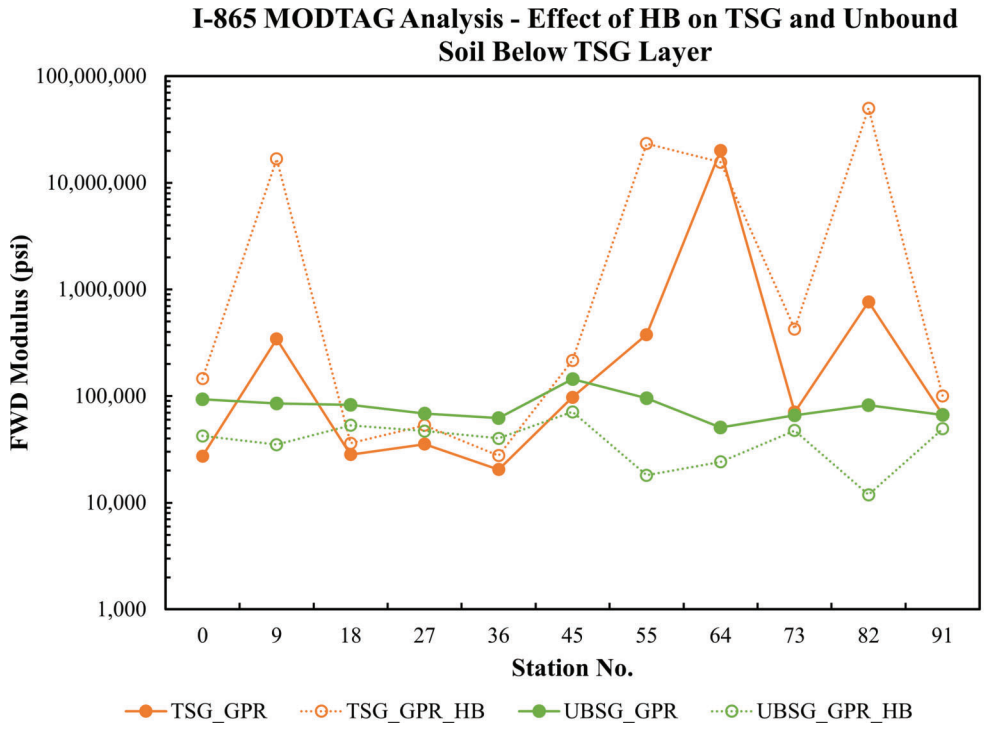

Figure 4.3 I-865 MODTAG analysis–effect of hard bottom.

layer effect and were accompanied with very low RMS error values (0.02%–0.03%).

The results obtained from the FWD back calculation analysis with ELMOD and MODTAG were compared with the laboratory resilient modulus data. The moduli of the unbound subgrade layer were compared with the average resilient moduli from the untreated subgrade soil samples collected at the site (Figure 4.7a), and the FWD modulus for the treated subgrade layer was compared with the average laboratory resilient modulus from tests performed on the cement treated specimens cured for 28 days (Figure 4.7b). The backcalculated

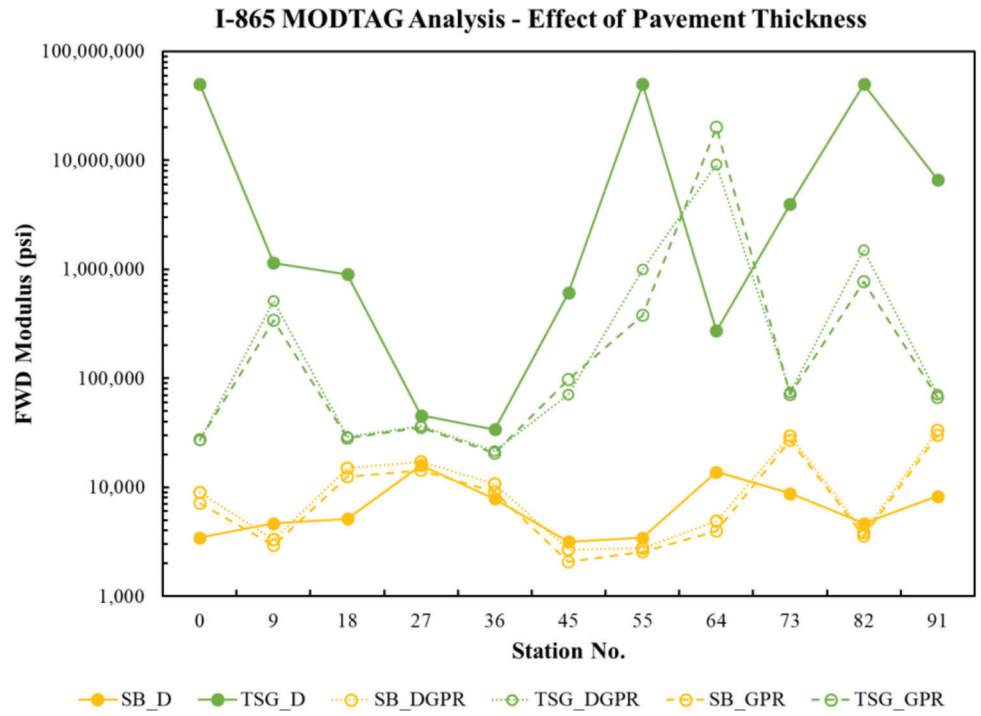

Figure 4.4 I-865 MODTAG analysis–effect of pavement thickness.

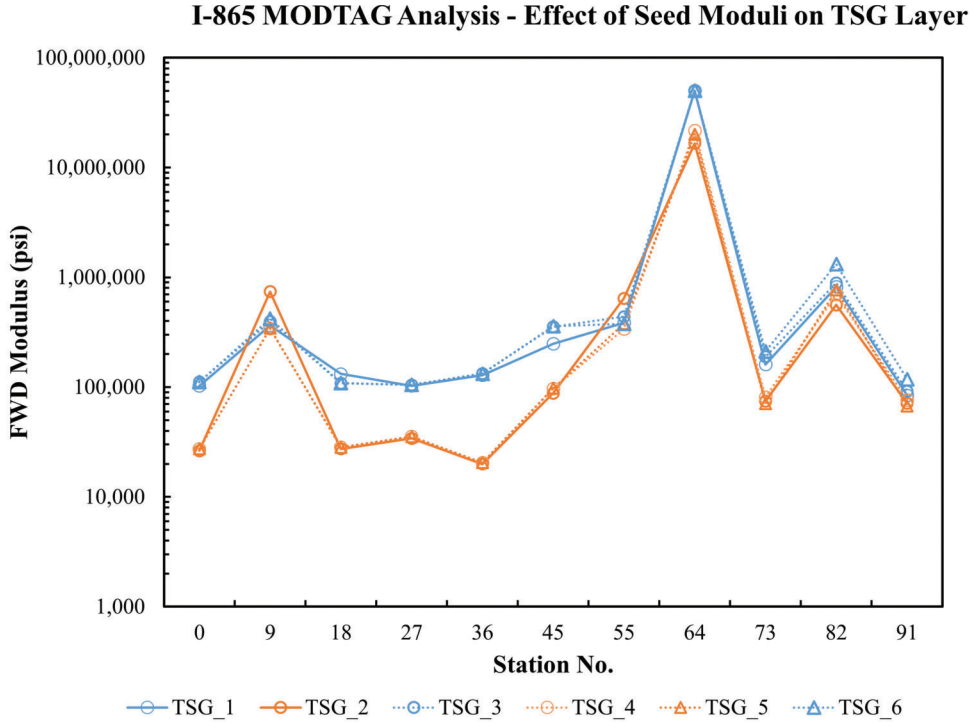

Figure 4.5 I-865 MODTAG analysis–effect of seed moduli.

unbound subgrade moduli were spread over a wide range: 50,000–100,000 psi using MODTAG and GPR-measured thickness, and 30,000–80,000 psi using MODTAG with the design thicknesses. The untreated laboratory M_R ranged from 6,000–19,000 psi. Both ELMOD and MODTAG overestimated the modulus values by: E_{ELMOD_D} = 2.8 $M_{R,UNTREATED}$ and E_{ELMOD_GPR} = 2.8 $M_{R,UNTREATED}$; and E_{MODTAG_D} = 6.2 $M_{R,UNTREATED}$ and E_{MODTAG_GPR} = 8.6 $M_{R,UNTREATED}$. The results for the treated subgrade

TABLE 4.6
Cases for ELMOD Analysis for Site 1: I-865 Based on Pavement Thickness

		Design	GPR
Layer	**Seed Moduli (ksi)[1]**	**D**	**GPR**
PCCP	2,000	12.0	12.3
SB	40	9.0	5.5
TSG	100	26.0	26.0
UBSG	10	–	–
Hard Bottom	500	Ignored	

Note: All thicknesses in inches.
[1]1 ksi = 1,000 psi.

resulted in better correlations using ELMOD than using MODTAG. The ELMOD estimates using GPR or design pavement thicknesses were too high, while MODTAG results considering GPR data were reasonable but for only few locations. The following correlations were obtained: $E_{ELMOD\_D} = 2.6\ M_{R,TREATED}$, $E_{ELMOD\_GPR} = 2.2\ M_{R,TREATED}$ and $E_{MODTAG\_GPR} = 1.3\ M_{R,TREATED}$. The results from the backcalculation analysis are presented in Appendix G, Table F.1, and F.2.

4.2.1.2 Site 3: US-31. This site was in St. Joe County, Indiana. Figure 4.8 shows photographs taken at the site during subgrade sample collection in July 2020, and during FWD and GPR testing in September 2021. The FWD and GPR tests were performed during the day. The soil samples were collected from the northbound road, while FWD and GPR tests were performed on both the northbound and southbound lanes. The pavement design cross-section, as shared by INDOT, along with GPR measured thicknesses are provided in Table 4.7.

MODTAG and ELMOD Analysis

The pavement cross-section was designed as a 4-layer system (excluding the hard bottom). The pavement layers and cases considered are tabulated in Table 4.8. The hard bottom depth was computed to be greater than 300 in., thus its influence was not considered. During the preliminary checks performed in MOD TAG, 5 SLIC warnings were recorded. SLIC transformation checks are computed from deflection data and radial offset location, and they help identify errors due to sensor location. This also suggests that the quality of data for the site was not very good. The actual GPR thickness measured for the PCCP layer was approximately an inch thicker than the designed value. It was observed that MODTAG backcalculated values for the TSG (treated subgrade) layer were unrealistically high for most locations, while ELMOD results were within reason (average 130,000 psi). The RMS error values were less than 3.1% for all data points except at Station 37 (RMS_{MODTAG} = 7.2%). MODTAG manual suggests that RMS errors greater than 3% suggest that the backcalculation results are questionable and the FWD data should be examined. Furthermore, even with ELMOD, the backcalculated TSG modulus at Station 37 was approximately 10 times lower than at other station locations. While marking the points that correspond to locations where the subgrade soil samples were collected, it was observed that few locations were very close to slab joints. Due to this, the FWD sensors were spread over two different slabs which in turn could have

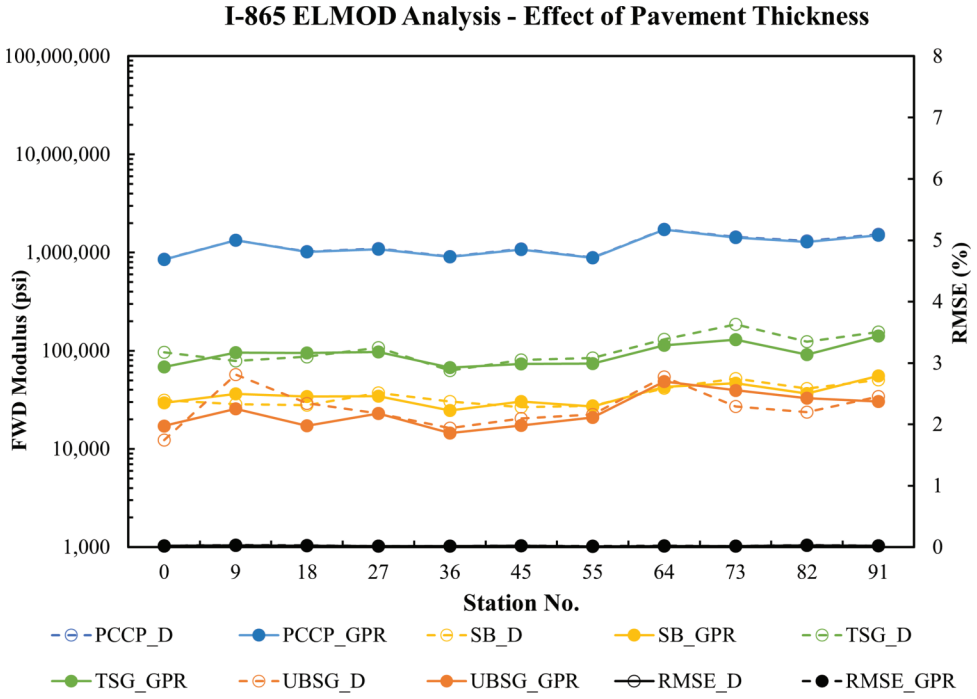

Figure 4.6 I-865 ELMOD analysis–effect of pavement thickness.

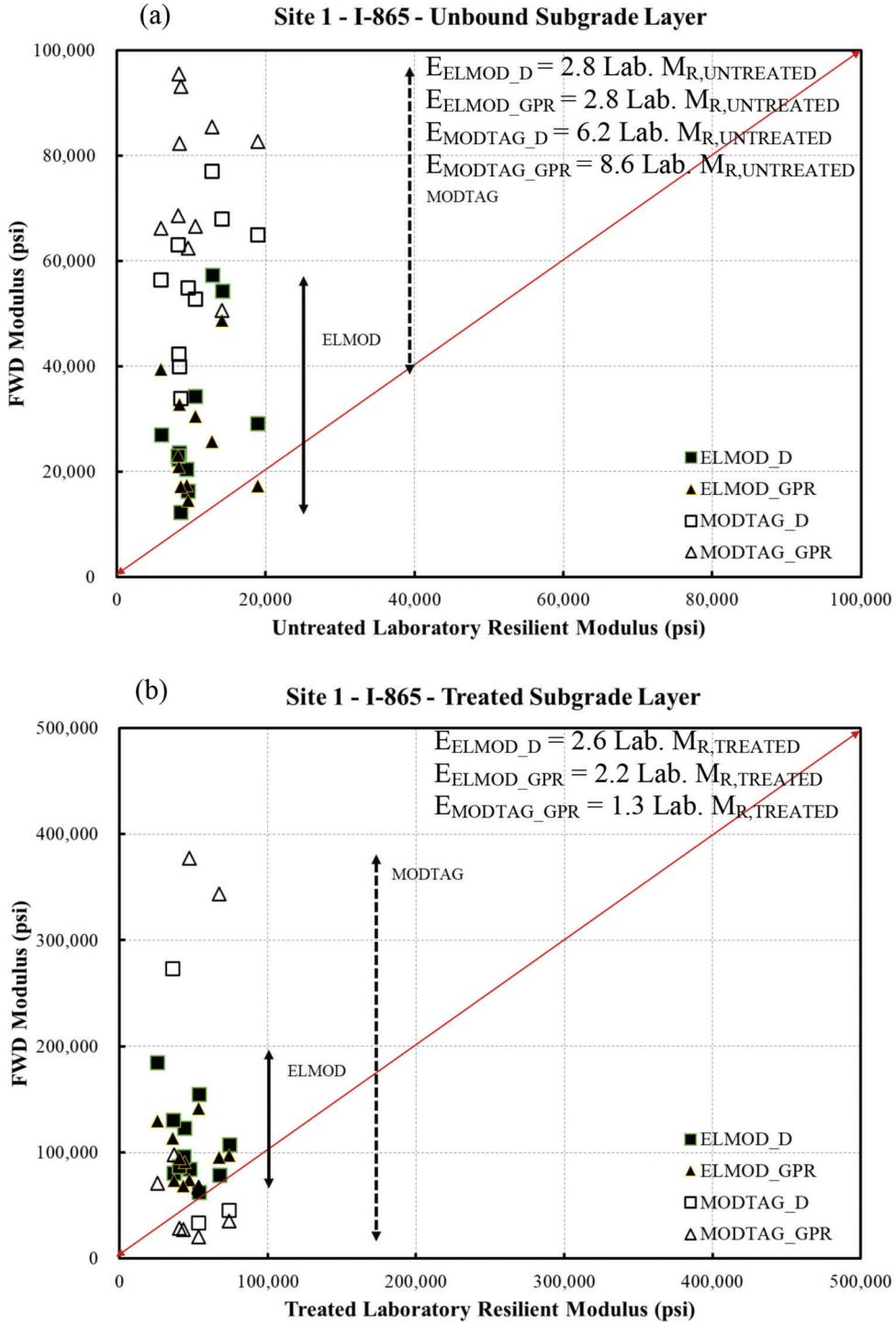

Figure 4.7 Comparison between laboratory M_R and FWD modulus for Site 1, I-865: (a) unbound subgrade layer (UBSG) (b) treated subgrade layer (TSG).

affected the deflection basin under the load. The backcalculated ELMOD moduli for the subbase layer yielded a wide range of values, from 40,000 to 500,000 psi, all overestimating the material stiffness. Table 4.9 shows the percentage difference between MODTAG and ELMOD results (the percentage was calculated as the difference between the moduli obtained from ELMOD and MODTAG, divided by the ELMOD moduli). The cells marked "high" correspond to unreasonably high moduli from MODTAG. The PCCP moduli obtained with MODTAG were consistently higher, and the subbase (SB) moduli were lower compared with ELMOD values. To study the effect of seed moduli in MODTAG, two sets of seed moduli values were considered: Set 1 (S1) had seed moduli values used as default in ELMOD, while Set 2 (S2) is

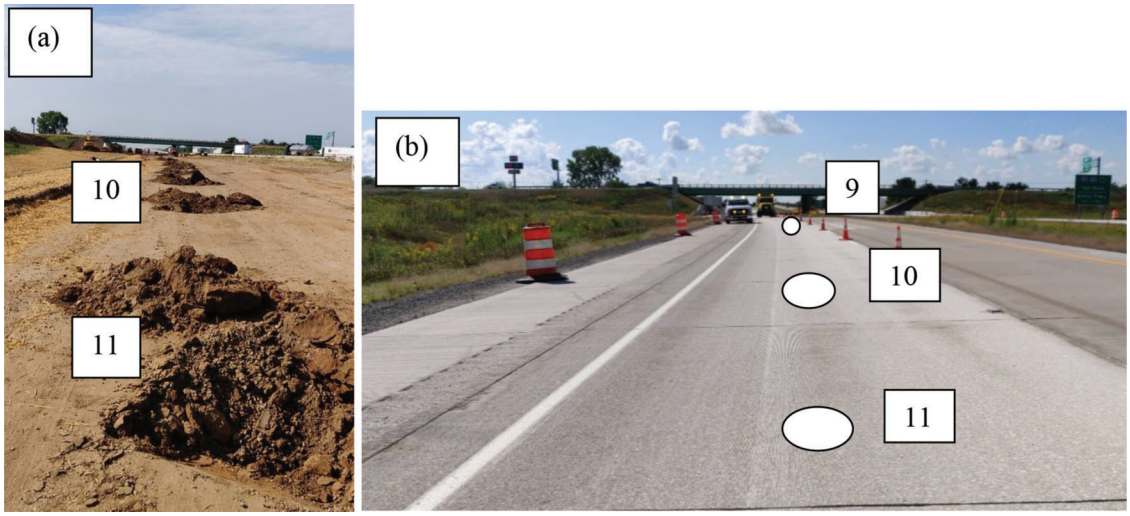

Figure 4.8 Photographs at Site 3, US-31 NB: (a) subgrade sample collection (b) locations marked for FWD and GPR tests.

TABLE 4.7
US-31 Pavement Design Cross-Section as Provided by INDOT

Layer	Design Thickness (in.)	Northbound GPR Measured Thickness (in.)	Southbound GPR Measured Thickness (in.)
QC/QA PCCP	10.0	11.3	10.7
Subbase for PCCP (3 in. of Compacted Aggregate No. 8, over 6 in. of Compacted Aggregate No. 53) on Geotextile for Pavement, Type 1B	9.0	8.8	5.2 + 5.4
Subgrade Treatment, Type 1B (cement option only)	14.0	ND	ND

Note: ND = Not Detected.

TABLE 4.8
Cases for MODTAG and ELMOD Analysis for Site 3: US-31 NB

	MODTAG and ELMOD			MODTAG		
Layer	Seed Moduli S1 (ksi)[1]	Design D	GPR GPR	Seed Moduli S2 (ksi)[1]	Design_S2 D_S2	GPR_S2 GPR_S2
PCCP	2,000	10.0	11.3	4,500	10.0	11.3
SB	40	9.0	8.8	50	9.0	8.8
TSG	100	14.0	14.0	100	14.0	14.0
UBSG	10	–	–	5	–	–
Hard Bottom	500	Ignored		500	Ignored	

Note: All thicknesses in inches.
[1]1 ksi = 1,000 psi.

composed of default values used in MODTAG (Table 4.8). The MODTAG default seed moduli values (S2) were associated with high RMS error values. The SB and TSG layers were more sensitive to changes in the seed moduli of the PCCP layer when compared to the PCCP and UBSG (unbound subgrade) layers. Increasing the seed moduli for PCCP layer resulted in a percentage difference of 4% to 60% in the SB layer, and a 10% to 80% difference in the TSG layer, while the % difference for PCCP and UBSG layers was found to be less than 25%. The results of both ELMOD and MODTAG were affected by changes in pavement thickness. The comparison between design and GPR cross-section with ELMOD resulted in a percent difference of up to 60% in the TSG and SB layers.

FWD and GPR tests were also performed on the southbound lane. It was observed that the pavement of US-31 northbound had a single subbase layer (9-in. thick), while the US-31 southbound had two subbase layers, with an average thickness 5.2 and 5.4 in., respectively. These two layers were treated as a single layer (SB = 10.6 in.) in the analysis. It was observed

that MODTAG results were fairly reasonable at all locations for the TSG layer (average 50,000 psi) and had low RMS error values (less than 2.2%) (Figure 4.9). This suggests that the quality of FWD data for the southbound lane was much better than for northbound lane, and also that the results obtained from MODTAG are highly sensitive to the quality of the data. The average moduli for the treated subgrade layer calculated using ELMOD was 94,000 psi. The ELMOD modulus for the subbase was 70% higher, 110% lower for the unbound subgrade layer, and 80% lower for the PCCP, when compared with MODTAG.

The results from ELMOD and MODTAG analysis for the design and GPR cases were compared with laboratory resilient modulus data (Figure 4.10). The FWD moduli of the unbound subgrade layer evaluated using ELMOD ranged from 18,000 to 40,000 psi, while using MODTAG, from 17,000 to 32,000 psi. ELMOD and MODTAG overestimated the modulus values with $E_{ELMOD\_D} = 2.6\ M_{R,UNTREATED}$ and $E_{ELMOD\_GPR} = 2.5\ M_{R,UNTREATED}$; $E_{MODTAG\_D} = 1.9\ M_{R,UNTREATED}$ and $E_{MODTAG\_GPR} = 2.0\ M_{R,UNTREATED}$ (Figure 4.10a). The backcalculated moduli for cement treated subgrade specimens shows that: $E_{ELMOD\_D} = 3.0\ M_{R,TREATED}$ and $E_{ELMOD\_GPR} = 3.4\ M_{R,TREATED}$. MODTAG results were unreasonably high, with most values greater than 500,000 psi (Figure 4.10b). The results from the back-calculation analysis for Site 3 are presented in Appendix F, Table F.3 to F.6.

TABLE 4.9
Comparison Between ELMOD and MODTAG Analysis for Site 3, US-31 NB

	PCCP_GPR	SB_GPR	TSG_GPR	UBSG_GPR
Station	%	%	%	%
0	-14.6	High	90.2	-1.3
10	-62.7	89.1	High	53.1
19	-51.3	58.1	High	17.9
27	-24.2	33.3	High	44.2
37	-40.7	91.5	High	8.4
46	-70.5	74.2	36.2	-37.2
55	-72.2	85.0	-375.7	-20.3
64	-70.6	69.3	-306.0	19.2
74	-40.5	79.4	High	-23.4
83	-54.5	61.7	High	25.9
92	-82.9	91.3	High	45.0

4.2.1.3 Site 5: SR-37. This site was situated in Martinsville, Indiana. The subgrade soil samples were collected in July 2020 from the southbound lane, but the FWD and GPR tests could be only performed on the northbound section. These field tests were completed in September 2021 during the day. The northbound lane was newly constructed and was not open to traffic at the time of the FWD and GPR testing. Figure 4.11 shows photographs taken at the site during subgrade sample collection and FWD and GPR testing. The pavement design cross-section shared by INDOT and estimated using GPR data is tabulated in Table 4.10.

MODTAG and ELMOD Analysis

Table 4.11 tabulates the cases considered for the analysis, while Figure 4.12 shows a comparison of backcalculation results obtained from ELMOD and

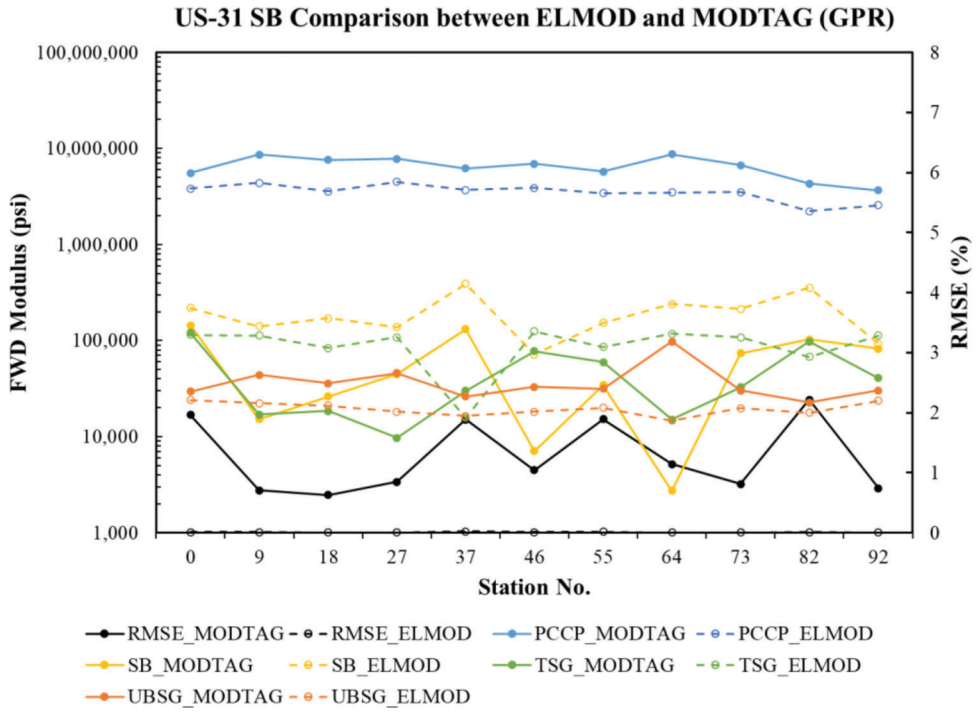

Figure 4.9 Comparison between ELMOD and MODTAG analysis for Site 3, US-31 SB.

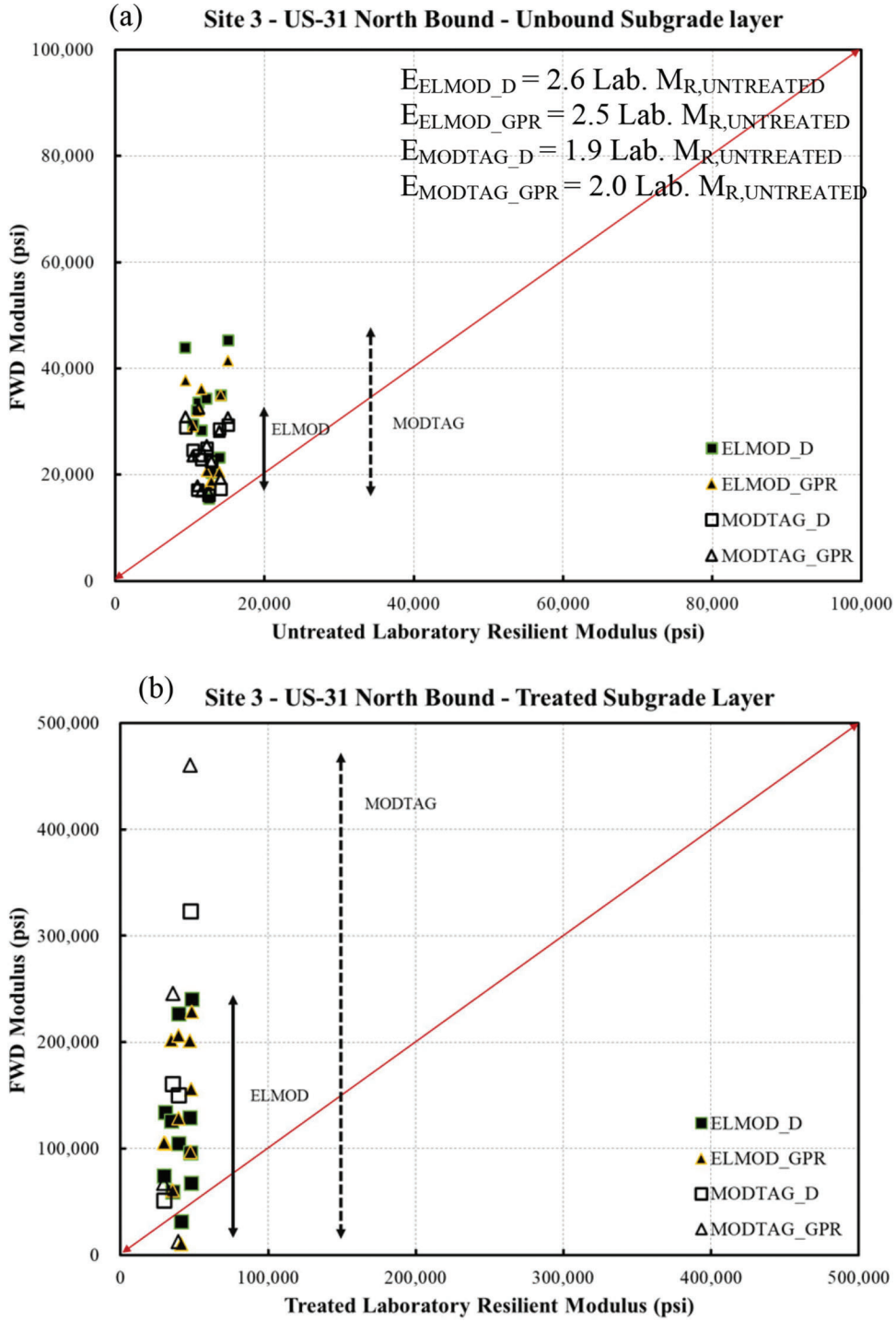

Figure 4.10 Comparison between laboratory M_R and FWD modulus for Site 3, US-31 NB: (a) unbound subgrade layer (UBSG) (b) treated subgrade layer (TSG).

MODTAG. MODTAG was found to overestimate the moduli for the PCCP and the treated subgrade layer, while ELMOD overestimated the modulus of the subbase. The average modulus for the treated subgrade layer was 220,000 psi with ELMOD and 500,000 psi with MODTAG. The RMS error associated with MODTAG was less than 2%, which shows good reliability of the FWD data. The reason for the back-calculated modulus values to be on the high range end could be that the pavement was newly constructed and not exposed to any traffic loading. A comparison of moduli for design and GPR cross section shows a percent difference of up to 45% in the SB (subbase) and TSG (treated subgrade) layers.

Figure 4.11 Photographs at Site 5, SR-37: (a) subgrade sample collection from SR-37 SB (b) locations marked for FWD and GPR tests performed on SR-37 NB.

TABLE 4.10
SR-37 Pavement Design Cross-Section as Provided by INDOT

Layer	Design Thickness (in.)	Northbound GPR Measured Thickness (in.)
QC/QA PCCP	10.0	11.0
Subbase for PCCP (3 in. of Compacted Aggregate No. 8, over 6 in. of Compacted Aggregate No. 53) on Geotextile for Pavement, Type 1B	9.0	8.0
Subgrade Treatment, Type 1B (14-in. cement modification)	14.0	ND

Note: ND = Not Detected.

TABLE 4.11
Cases for MODTAG and ELMOD Analysis for Site 5: SR-37 NB

	MODTAG and ELMOD			MODTAG		
		Design	GPR		Design_S2	GPR_S2
Layer	Seed Moduli (ksi)[1]	D	GPR	Seed Moduli S2 (ksi)[1]	D_S2	GPR_S2
PCCP	2,000	10.0	11.0	4,500	10.0	11.0
SB	40	9.0	8.0	50	9.0	8.8
TSG	100	14.0	14.0	100	14.0	14.0
UBSG	10	–	–	5	–	–
Hard Bottom	500	Ignored		500	Ignored	

Note: All thicknesses in inches.
[1]1 ksi = 1,000 psi.

From the cases analyzed with a rigid pavement, it can be seen that the results obtained from ELMOD are more realistic. These results are also supported with low RMS error values. It was also observed that the effects of pavement thickness variation and seed moduli were more pronounced in MODTAG and less evident in ELMOD. The quality of MODTAG results also relied heavily on the quality of FWD data. Figure 4.13 provides a comparison between the laboratory resilient modulus tests and results obtained with ELMOD using GPR-obtained thickness values. The colored marker points are representative of tests performed at the same location where subgrade soil samples were collected during construction. The backcalculated moduli for both treated subgrade and unbound soil are higher than the results obtained in the laboratory. A summary of these results is provided in Table 4.12. A detailed analysis of all cases considered with rigid pavement is provided in Appendix F.

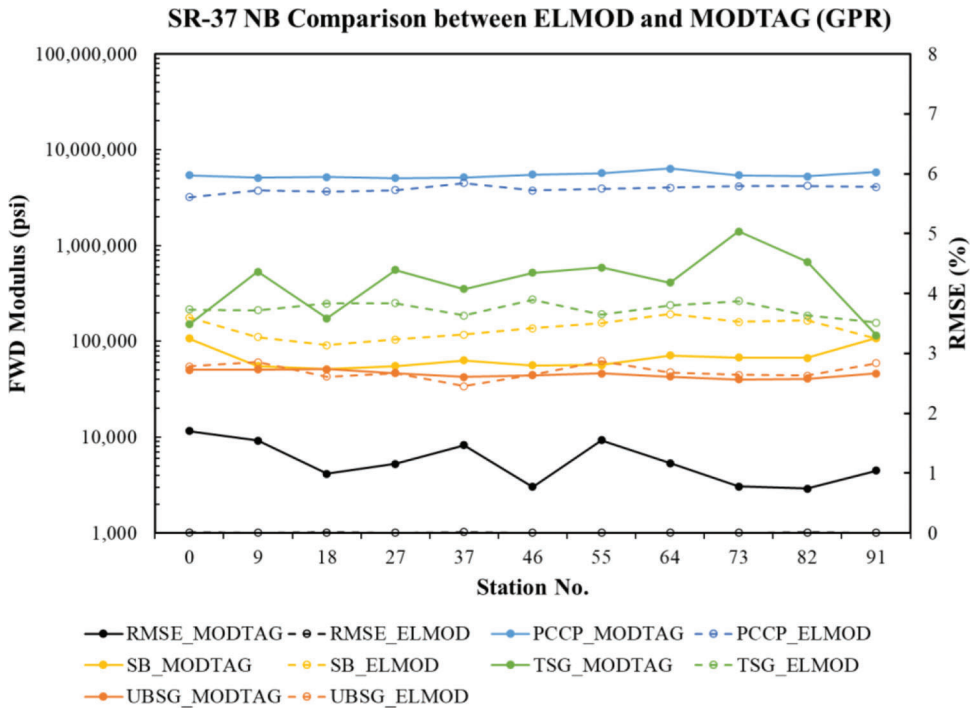

Figure 4.12 Comparison between ELMOD and MODTAG analysis for Site 5, SR-37 NB.

4.2.2 Flexible Pavements

4.2.2.1 Site 2: SR-46. This site was located in Clay County. The subgrade soil samples were collected in October 2019 while the FWD and GPR tests were performed in July 2020 during the day. The site photographs, with locations marked where samples were collected, are shown in Figure 4.14a, while Figure 4.14b shows the marked stations for FWD and GPR tests. Table 4.13 presents the INDOT design cross-section of the site, as well as the layer thicknesses estimated from GPR data. The pavement structure was composed of HMA layers placed over a compacted aggregate subbase layer. The differences of layers thicknesses between design and GPR measurements were small, less than an inch.

MODTAG and ELMOD Analysis

The effect of pavement thickness measurements, hard bottom and seed moduli were evaluated using MODTAG and ELMOD. Table 4.14 shows the different cases completed for the analysis. Two types of pavement structures were considered: a 3-layer system comprising an AC layer, a subbase (SB) and an unbound subgrade layer (UBSG), and a 4-layer system composed of an AC layer, a subbase (SB) and two subgrade layers (SG and UBSG). The subgrade was divided into two layers, layer 1 (SG) with a thickness of 24 in., and layer 2, the unbound subgrade layer (UBSG) which extended to the hard bottom. The average depth to hard bottom was estimated at 277 in. It was observed that considering a hard bottom layer overestimated the backcalculated moduli of the layers. The effect of HB was most pronounced for the subbase moduli, where an increase of 90%–100% was observed when the HB was included in the MODTAG analysis. The ELMOD analysis does not consider a hard bottom layer. Increasing the seed moduli values for the asphalt layer had little to no effect on the MODTAG results (average % error $< 3.5\%$). Details of the analyses and the effect of seed moduli and hard bottom are provided in Appendix G.

The results show that increasing the number of layers, from a 3-layer pavement structure to a 4-layer, reduced the RMS error values by 35%. However, increasing the number of layers resulted in an increase in the subbase (SB) moduli by 120% and a slightly reduction of the moduli of the subgrade layer with MODTAG. With ELMOD, the SB moduli was reduced by 30% and the SG moduli increased by 130%. In addition, the subgrade moduli values for the unbound subgrade layer were compared with the laboratory-M_R data (Figure 4.15). It was observed that the 4-layer system analysis with ELMOD resulted in 1:1 relationship between the backcalculated and laboratory modulus values ($E_{ELMOD\_D4L} = 1.0\ M_{R,UNTREATED}$ for the 4-layer system and $E_{ELMOD} = 1.4\ M_{R,UNTREATED}$ for the 3-layer system). On the other hand, MODTAG results for both the 3- and 4-layer system gave a 2:1 relationship ($E_{MODTAG} = 2.1\ M_{R,UNTREATED}$ and $E_{MODTAG\_D4L} = 2.1\ M_{R,UNTREATED}$). The results obtained from MODTAG and ELMOD backcalculation analysis are tabulated in Appendix G, Table G.1.

Figure 4.16 shows the comparison between the FWD modulus and laboratory resilient modulus (untreated)

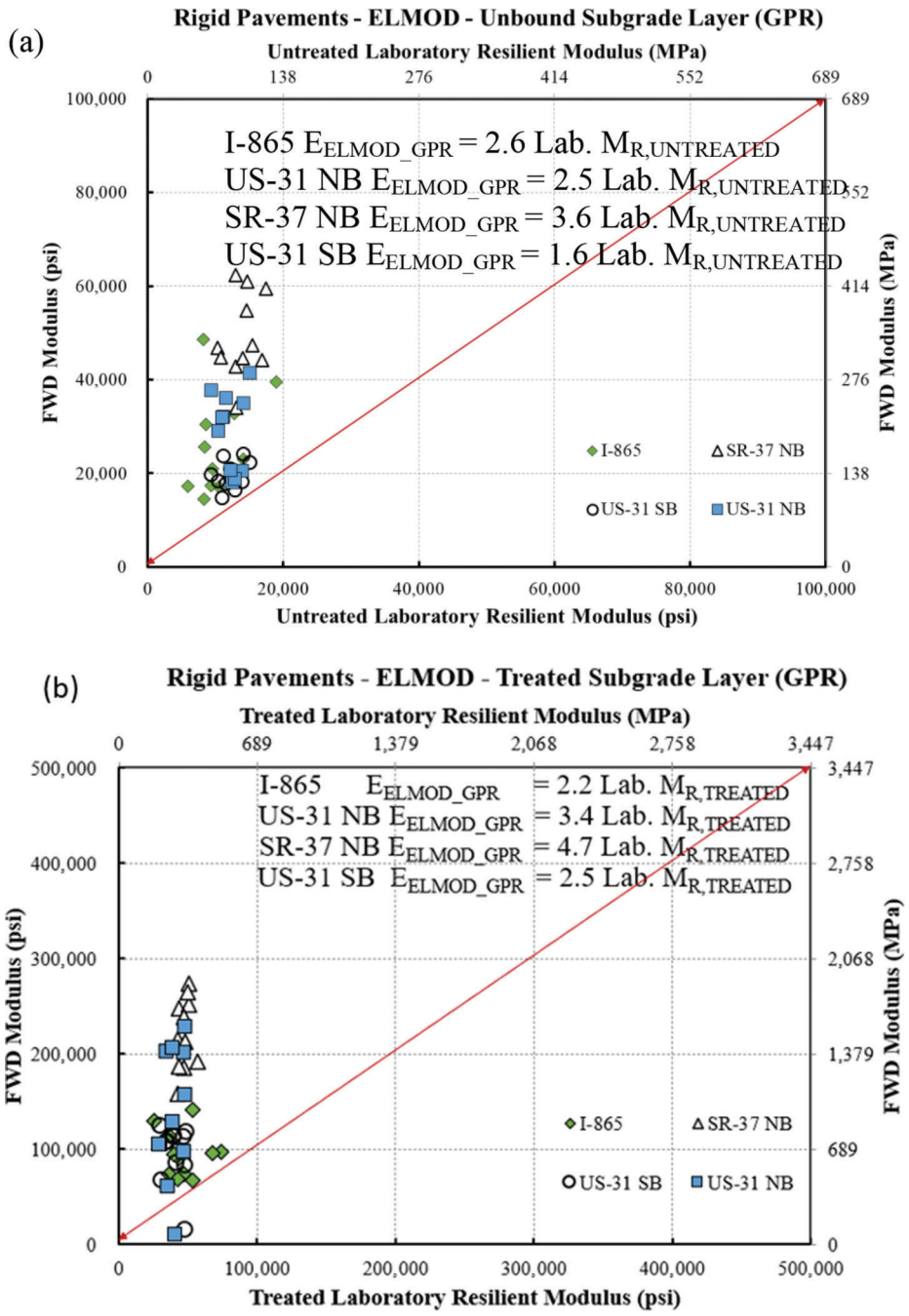

Figure 4.13 Comparison between laboratory M_R and FWD modulus for rigid pavements: (a) unbound subgrade layer (UBSG) (b) treated subgrade layer (TSG).

TABLE 4.12
Comparison Between Laboratory M_R and FWD Modulus for Rigid Pavements

Site	ELMOD–Unbound Subgrade (GPR) E_{ELMOD_GPR} /Lab. $M_{R,UNTREATED}$ Average (Range)	ELMOD–Treated Subgrade Layer (GPR) E_{ELMOD_GPR} /Lab. $M_{R,TREATED}$ Average (Range)
I-865	2.6 (1.6–5.9)	2.2 (1.3–5.1)
US-31 NB	2.5 (1.4–4.0)	3.4 (0.3–5.9)
SR-37 NB	3.6 (2.6–4.8)	4.7 (3.3–5.4)
US-31 SB	1.6 (1.3–2.1)	2.5 (0.3–4.3)

Figure 4.14 Photographs at Site 2, SR-46: (a) subgrade sample collection from SR-37 SB (b) locations marked for FWD and GPR tests performed on SR-37 NB.

TABLE 4.13
SR-46 Pavement Design Cross-Section as Provided by INDOT

Layer	Design Thickness (in.)	GPR Measured Thickness (in.)
QC/QA HMA 3, 64, Surface 9.5 mm	1.5	9.9
HMA 2, 64, Intermediate, 19.0 mm	3.0	
HMA 2, 64, Base, 19.0 mm	6.0	
Special Subgrade Treatment Type 1C (Compacted Aggregate No. 53)	12.0	12.7

TABLE 4.14
Cases for MODTAG and ELMOD Analysis for Site 2: SR-46

Layer	Seed Moduli S1 (ksi)[1]	Seed Moduli S2 (ksi)[1,2]	Design 3Layer D	GPR 3Layer GPR	Design 4Layer D_4L	Design 3Layer D_HB	GPR 3Layer GPR_HB	Design 4Layer D_4L_HB
AC	300	500	10.5	9.9	10.5	10.5	9.9	10.5
SB	40	50	12.0	12.7	12.0	12.0	12.7	12.0
SG	10	5	–	–	24.0	–	–	24.0
UBSG	10	5	–	–	–	–	–	–
Hard Bottom	500	500		Ignored			Considered	

Note: All thicknesses in inches.
[1]1 ksi = 1,000 psi.
[2]Used only for MODTAG analysis.

TABLE 4.15
Cases for MODTAG Analysis for Site 2: SR-46—Based on AC Layer Thickness Variation

		Design			Design–4 Layer		
Layer	Seed Moduli (ksi)[1]	D_AC	D_AC+1	D_AC-1	D4L_AC	D4L_AC+1	D4L_AC-1
AC	300	10.5	11.5	9.5	10.5	11.5	9.5
SB	40	12.0	12.0	12.0	12.0	12.0	12.0
SG	10	–	–	–	24.0	24.0	24.0
UBSG	10	–	–	–	–	–	–
Hard Bottom	500		Ignored			Ignored	

Note: All thicknesses in inches.
[1]1 ksi = 1,000 psi.

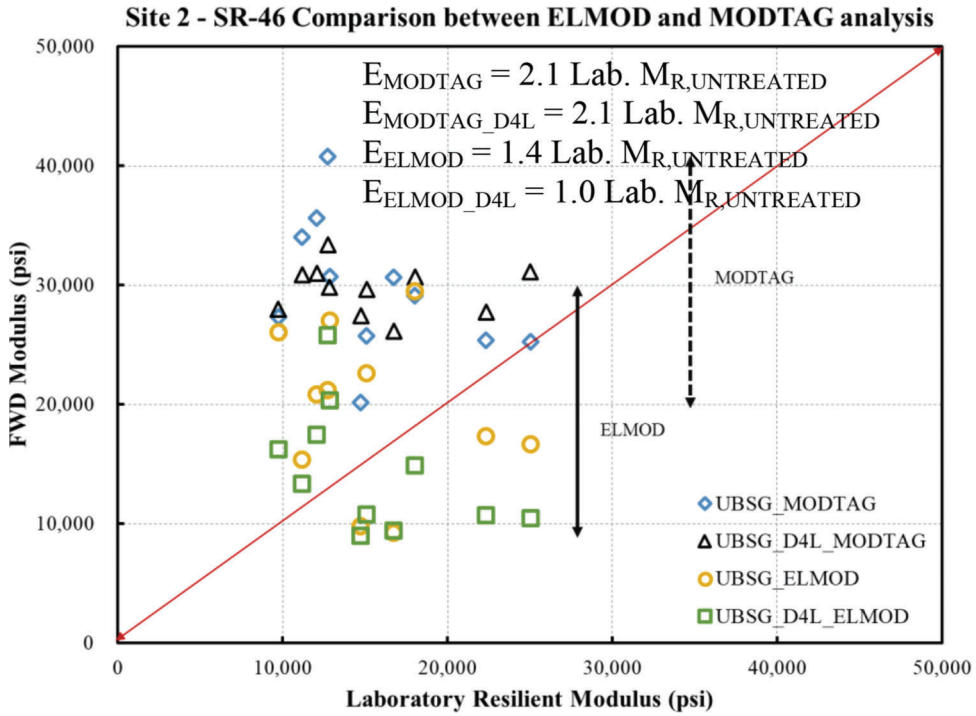

Figure 4.15 Comparison between ELMOD and MODTAG analysis for Site 2, SR-46—design 3-layer and design 4-layer system.

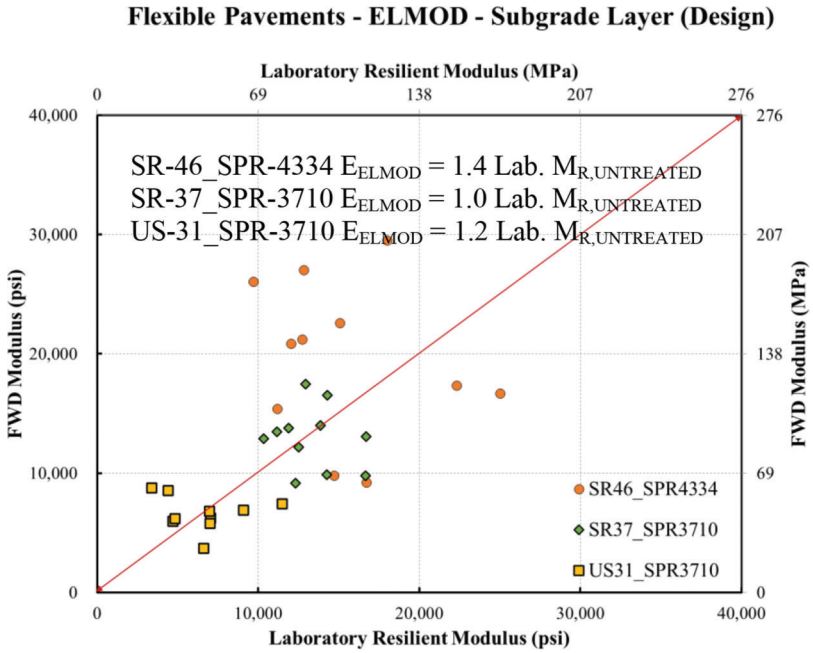

Figure 4.16 Comparison between laboratory M_R and FWD modulus for flexible pavements.

for the SR-46 samples. As one can see, the comparison is quite reasonable, with the FWD moduli giving values similar to those of the laboratory resilient modulus. The figure also includes similar information for US-31 and SR-37 subgrade soils, extracted from a previous JTRP project, SPR-3710 (Park et al., 2018), where a similar task was completed. The new results not only complement the existing data but reinforced the conclusion reached in the previous project that the subgrade resilient modulus can be well estimated from FWD tests. Further, the results suggest that ELMOD is a good tool to assess the stiffness of subgrade soils in flexible pavements.

The results obtained using the design cross-section and using GPR-measured layer thickness did not show differences because the design dimensions and GPR measurements differed by less than one inch. To study the effect of pavement thickness variation on the backcalculated moduli, a number of MODTAG analyses were performed considering ± 1 inch variation in the AC layer (Table 4.15). For a 3-layer system, a 1 inch reduction in asphalt layer caused a 35% reduction in subbase moduli and a 20% increase in modulus of the unbound subgrade layer, while a 1-in. increase resulted in 65% increase of the subbase moduli and a 11% reduction of the modulus of the subgrade layer.

5. SUMMARY, CONCLUSIONS AND RECOMMENDATIONS FOR IMPLEMENTATION

5.1 Summary

The resilient modulus (M_R) is a key factor in the *Mechanistic-Empirical Pavement Design Guide* (MEPDG). It provides the stiffness of the subgrade soil, but its determination requires direct sampling of the soils and specialized equipment. The large size of some new projects and the difficulty to collect soils from pavement rehabilitation projects calls for obtaining resilient modulus values using non-destructive testing methods. This project builds on the recently completed JTRP project SPR-3710 (Park et al., 2018) where significant work was done on establishing correlations between FWD results and laboratory resilient modulus tests. The goal of this project is to improve the reliability and interpretation of FWD tests though the following:

1. performing a comprehensive literature review of available FWD protocols and backcalculation tools,
2. evaluating non-destructive testing methods for pavement thickness determination, and
3. expanding the existing database of high-quality data pairs of FWD and M_R.

With the help of INDOT personnel, six site locations were identified for sample collection and FWD and GPR testing. Five of the sites were road construction projects and one site was a research project. The selected sites included roads with rigid pavement and treated subgrade and flexible pavement with untreated subgrade. At each construction site, a 30-ft representative section was identified, and eleven points placed 30 ft apart were marked for subgrade soil collection in all projects except at the research site (S-BRITE) where, because of its short length, only three points at 15-ft intervals were identified. Thus, 11 samples were collected at each side (except at the S-BRITE site). Laboratory tests were conducted on the soils obtained that included granulometry, Atterberg limits, compaction, and resilient modulus tests. The first site was on I-865 in Marion County, Indiana. The pavement structure was composed of Portland cement concrete pavement (PCCP) over a cement stabilized subgrade layer (6% cement). The untreated subgrade soil was A-4, according to AASHTO, with 53% fines and PI = 8%. The second site was on SR-46 in Clay County, Indiana, and had an asphalt pavement over an untreated subgrade. The soil of the subgrade was A-6 with 47% fines and PI = 11%. Site three was on US-31 near South Bend, Indiana. It was composed of a PCCP pavement over a cement treated subgrade (4% cement). The untreated subgrade soil was A-1 with 16% fines with PI = 6%. The fourth site was a research project located at S-BRITE, in West Lafayette. It was composed of a compacted base over a cement treated subgrade layer (4% cement). The untreated subgrade soil was A-6 with 49% fines and PI of 11%. Site five was on SR-37 in Martinsville, Indiana. The pavement structure had PCCP over a cement treated subgrade (5% cement). The soil was A-2-4 with 26% fines and PI = 8%. The last site, Site 6, was located on I-65 in Tippecanoe County. The pavement was PCCP over a cement treated subgrade (5% cement). The untreated subgrade soil was A-6 with 68% fines and PI = 13%.

Due to challenges faced in scheduling, large demand for FWD and GPR tests during the construction period and traffic control issues, FWD and GPR tests could be performed on only four of the site locations: I-865, SR-46, US-31, and SR-37. The FWD tests were performed on the same locations where soil samples were taken. The GPR tests were performed along the entire 300-ft stretch. In SR-37, due to traffic control issues, access to the lane where soils were collected was not feasible, and the FWD and GPR tests were performed on the opposing lane, at the corresponding locations where the soils were sampled. The FWD test results were analyzed using the codes MODTAG and ELMOD. The results from each code were compared with the laboratory resilient modulus results for both treated and untreated soil specimens to establish correlations between the two tests.

5.2 Conclusions

The following conclusions can be drawn from the laboratory and field tests performed.

1. A review of FWD testing protocol available for FHWA, VirDOT, PennDOT, NJDOT, and WisDOT, etc. shows that most states use a drop sequence comprising of a seating load and repetitive drops for the same load.

Repetitive loading can help improve the accuracy of the results and allow for better interpretation of FWD data.

2. Regression analyses performed to correlate resilient modulus values with soil properties such as OMC, MDD, Atterberg limits and percentage of fines did not yield any statistically significant result for stress-independent models.
3. Regression analyses were also performed for the stress-dependent models:
   Uzan Model

$$log\left(\frac{M_R}{P_a}\right) = logk_1 + k_2 log\frac{\sigma_{bulk}}{P_a} + k_3 log\frac{\sigma_{dev}}{P_a}$$

$$log\left(\frac{M_R}{P_a}\right) = logk_1 + k_2 log\frac{\sigma_{bulk}}{P_a} + k_3 log\frac{\sigma_{dev}}{P_a}$$

   Octahedral Stress Model

$$log\left(\frac{M_R}{P_a}\right) = logk_1 + k_2 log\frac{\sigma_{bulk}}{P_a} + k_3 log\left(\frac{\tau_{oct}}{P_a} + 1\right)$$

   - For untreated specimens, the results showed a weak dependence on deviatoric stress and confining stress.
   - For treated specimens, it was observed that the parameter k_1 increased with treatment, consistent with an increase in M_R with treatment.
   - For both treated and untreated specimens, k_2 values ranged from 0.25 to 0.56, somewhat consistent with the expectation of soil stiffness increasing with the square root of stress confinement.
   - For both treated and untreated specimens, k_3 values were negative, suggesting a decrease of the resilient modulus with an increase in deviatoric/octahedral stress. It was found that k_3 increased with treatment. The regression analyses do not provide reliable predictions at any given site and so their use is not recommended.
4. The GPR test provides accurate estimates of the thickness of the asphalt and concrete layers. It can identify discrepancies between as-built and design pavement thickness. For example, at I-865, a difference of approximately 3.5 inches was observed for the base layer between design and GPR-measured thickness.
   For flexible pavements, GPR provides continuous pavement profile, and is able to distinguish between the HMA and the base course layer.
   For rigid pavements, the presence of dowel bars and tie bars at the joints affects the GPR signals at the joint locations. The GPR was able to identify the top two layers of the pavement: PCCP and the base/subbase layer.
5. The deflection results obtained from FWD tests show that, for the same load, the deflections produced in flexible pavements are 2.5–3 times higher than in rigid pavements. The small deflections in the PCCP pavements, together with the "slab" geometry of the pavement (e.g., the deformations measured with the FWD may contain rigid body motions of the slabs) may have played an important role in the poor results obtained when comparing FWD results with M_R data.
6. MODTAG allows for preliminary analysis of the quality of FWD data. Checks such as SLIC transformation, linearity, cumulative differences of deflection, can be used to determine section homogeneity and identify errors associated with sensor location and spacing. However, MODTAG results for rigid pavements are significantly affected by changes in seed moduli, layer thickness, and quality of FWD data.
7. Based on the analysis performed for both flexible and rigid pavements, it was found that the backcalculated moduli values for the treated subgrade layer are generally higher with MODTAG than with ELMOD.
8. For rigid pavements, results of FWD backcalculation analysis using both ELMOD and MODTAG greatly overestimate the resilient modulus of the soil by a factor of two to three. The large differences observed could be due to the small deflection basin associated with stiff rigid slabs, low load levels at which the tests are performed, or rigid body movements of the slabs. Further research is needed to ascertain the causes for the differences.
9. For flexible pavements, results of the FWD backcalculation analysis suggests that a one-to-one correlation exist between FWD modulus and laboratory resilient modulus values for untreated subgrade soils, using either MOD TAG or ELMOD. That is, $E_{FWD} \sim M_{R,UNTREATED}$.
10. Backcalculation of FWD tests on flexible pavements is very sensitive to the thickness of the asphalt layer. Changes in thickness of ± 1 inch, resulted in 30%–65% changes in the subbase moduli and 10%–20% changes in the subgrade moduli.

5.3 Recommendations for Implementation

Based on the literature reviewed for FWD protocols and the results obtained from the field and laboratory tests, the following recommendations for implementation are made.

1. When good quality FWD data are available, the resilient modulus of untreated subgrade soils under flexible pavements can be estimated from FWD tests using ELMOD or MODTAG. The recommended relation is resilient modulus backcalculated from FWD equal to the resilient modulus obtained in the laboratory.
2. The resilient modulus obtained from FWD data performed on rigid (PCCP) pavements overestimates the resilient modulus obtained in the laboratory. The backcalculated moduli for the subgrade are 1.3 to 6 times higher than the laboratory results. An initial estimate of the resilient modulus of the subgrade on rigid pavements could be obtained by dividing the backcalculated moduli from the FWD by a factor of three. However, this estimate should not be used for design, and only as a reference.
3. It is hypothesized that the errors in the resilient modulus on PCCP pavements are due to a number of factors: magnitude of the load and/or small deflections obtained, position of the sensors relative to pavement joints, and rigid movements of the pavement slabs that mask the "basin" deflection expected for the calculations. Further research is recommended to bring the level of interpretation of FWD test results to that of flexible pavements.
4. It is recommended to run, concurrently with FWD tests, GPR tests to determine the actual thickness of the pavement layers, and more specifically of the asphalt and concrete layers (layers with high stiffness). The study conducted suggests that errors on pavement layer

thickness of $\pm 1''$ result in percent difference in the moduli of the subbase and subgrade layers of about 45%.

5. Most of the DOTs surveyed perform FWD tests using a drop sequence comprising of a seating load and repetitive drops for the same load. Repetitive loading seems to improve the accuracy of the results and allows for better interpretation of FWD data. It would be interesting to setup a test program where FWD tests are conducted at the same location following current INDOT protocol and the "drop sequence" used by other DOTs and compare the results, to see if there is an improvement of performance. This may be particularly interesting in PCCP pavements, where the results are not satisfactory. The current protocol that INDOT uses provides satisfactory results on asphalt pavements.
6. Based on the analysis performed for both flexible and rigid pavements, the software ELMOD is preferred for routine calculations based on its simplicity and accuracy. MODTAG could be used for research or for detailed analysis of results, as it offers tools to analyze the quality of data and include a larger number of pavement layers.
7. It is recommended to continue the collection of data from road construction projects in particular from sites comprising of flexible pavements with treated subgrades which have not been investigated to improve these correlations.

REFERENCES

AASHTO M 145-91. (2012). *Standard specification for classification of soils and soil-aggregate mixtures for highway construction purposes*. American Association of State Highway and Transportation Officials.

AASHTO T 89-10. (2011). *Standard method of test for determining the liquid limit of soils*. American Association of State Highway and Transportation Officials.

AASHTO T 90. (2020). *Standard method of test for determining the plastic limit and plasticity index of soils*. American Association of State Highway and Transportation Officials.

AASHTO T 99. (2019). *Standard method of test for moisture-density relations of soils using a 2.5-kg (5.5-lb) rammer and a 305-mm (12 in.) drop*. American Association of State Highway and Transportation Officials.

AASHTO T 307-99. (2007). *Standard method of test for determining the resilient modulus of soils and aggregate materials*. American Association of State Highway and Transportation Officials.

Abdelnaby, A., Camp, C., Baker, C., & Hosseinpour, F. (2018, May). *Structural evaluation of low volume roads using ground penetrating radar* (GPR) (Report No. RES2016-13). Tennessee Department of Transportation.

Ahmed, M. U., & Tarefder, R. A. (2017). Incorporation of GPR and FWD into pavement Mechanistic-Empirical design. *Construction and Building Materials*, *154*, 1272–1282.

Ahmed, M., Tarefder, R., & Maji, A. (2014, June). Variation of FWD modulus due to incorporation of GPR predicted layer thicknesses. In *Proceedings of the 15th international conference on ground penetrating radar* (pp. 345–350). IEEE.

Alland, K., Bech, N., & Vandenbossche, J. M. (2018, April 16). *Interpreting falling weight deflectometer (FWD) data for asphalt and concrete pavements* (Report No. FHWA-PA-2018-004-PIT WO 6). Pennsylvania Department of Transportation. http://www.dot7.state.pa.us/BPR_PDF_FILES/Documents/Research/Complete%20Projects/Maintenance/Interpreting_Falling_Weight_Deflectometer_(FWD)_Data_(for_Asphalt_and_Concrete_Pavements).pdf

Al-Qadi, I. L., & Lahouar, S. (2005). Measuring layer thicknesses with GPR–Theory to practice. *Construction and Building Materials*, *19*(10), 763–772.

ASTM C 136-14. (2015). *Standard test method for sieve analysis of fine and coarse aggregates*. ASTM International.

ASTM D 4694-09. (2009). *Standard test method for deflections with a falling-weight-type impulse load device*. ASTM International.

ASTM D 4695-03. (2003). *Standard guide for general pavement deflection measurements*. ASTM International.

Badu-Tweneboah, K., Manzione, C. W., Miley, W. G., & Ruth, B. E. (1989). Prediction of flexible pavement layer moduli from Dynaflect and FWD deflections. In A. J. Bush (Ed.), *Nondestructive Testing of Pavements and Back-calculation of Moduli*. ASTM International.

Bryce, J. M., Katicha, S. W., Diefenderfer, B. K., & Flintsch, G. W. (2016). *Analysis of repeated network-level testing by the falling weight deflectometer on I-81 in the Virginia Department of Transportation's Bristol District* (Report No. FHWA/VTRC 17-R6). Virginia Transportation Research Council. https://www.virginiadot.org/vtrc/main/online_reports/pdf/17-r6.pdf

Carmichael III, R. F., & Stuart, E. (1985). Predicting resilient modulus: A study to determine the mechanical properties of subgrade soils (abridgment). *Transportation Research Record*, *1043*, 145–148.

Clark, T., Irwin, L., Borter, R., & Johnson, W. L. (2016). *MODTAG: The FWD analysis program Version 5.0*. Virginia Department of Transportation & Cornell University.

Dai, S., & Yan, Q. (2014). Pavement evaluation using ground penetrating radar. In *Pavement Materials, Structures, and Performance* (pp. 222–230).

Dai, S., & Zollars, J. (2002). Resilient modulus of Minnesota road research project subgrade soil. *Transportation Research Record*, *1786*(1), 20–28.

Daniels, J. J. (2000, November 25). *Ground penetrating radar fundamentals*. Prepared as an appendix to a report for the US EPA, Region V, pp. 1–21.

Drumm, E. C., Boateng-Poku, Y., & Johnson Pierce, T. (1990). Estimation of subgrade resilient modulus from standard tests. *Journal of Geotechnical Engineering*, *116*(5), 774–789.

Dynatest. (2013). *ELMOD 6 quick start manual*. Dynatest International A/S.

FHWA-LTPP Technical Support Services Contractor LAW PCS. (2000, August). *LTPP manual for falling weight deflectometer measurements operational field guidelines* (version 3.1). https://www.fhwa.dot.gov/publications/research/infrastructure/pavements/ltpp/fwdman/fwdman1.pdf

Gucunski, N., Zaghloul, S., & Vitillo, N. (2009). *Development of FWD procedures manual* (Report No. FHWA-NJ-2009-005). New Jersey Department of Transportation. https://www.nj.gov/transportation/business/research/reports/FHWA-NJ-2009-005.pdf

Hering, A., Misiek, R., Gyulai, Á., Ormos, T., Dobróka, M., & Dresen, L. (1995). A joint inversion algorithm to process geoelectric and surface wave seismic data. Part I: Basic ideas. *Geophysical Prospecting*, *43*(2), 135–156.

Hicks, R. G., & Monismith, C. L. (1971). Factors influencing the resilient response of granular materials. *Highway Research Record*, *345*, 15–31.

Horak, E. (1987). The use of surface deflection basin measurements in the mechanistic analysis of flexible pavements. *Sixth International Conference, Structural Design of Asphalt Pavements, Volume I, Proceedings* (pp. 99–1001). University of Michigan, Ann Arbor.

Hossain, M. S. (2009). Estimation of subgrade resilient modulus for Virginia soil. *Transportation Research Record*, *2101*(1), 98–109.

Hossain, M. S., & Kim, W. S. (2015). Estimation of subgrade resilient modulus for fine-grained soil from unconfined compression test. *Transportation Research Record*, *2473*(1), 126–135.

Hu, J., Vennapusa, P. K., White, D. J., & Beresnev, I. (2016). Pavement thickness and stabilised foundation layer assessment using ground-coupled GPR. *Nondestructive Testing and Evaluation*, *31*(3), 267–287.

Ismail, M. A., Samsudin, A. R., Rafek, A. G., & Nayan, K. A. M. (2009). In situ determination of layer thickness and elastic moduli of asphalt pavement systems by spectral analysis of surface waves (SASW) method. In *Recent Advancement in Soil Behavior, in Situ Test Methods, Pile Foundations, and Tunneling: Selected Papers from the 2009 GeoHunan International Conference* (pp. 70–76).

Kim, D., Ji, Y., & Siddiki, N. Z. (2010). *Evaluation of in-situ stiffness of subgrade by resilient and FWD modulus* (Joint Transportation Research Program Publication No. FHWA/IN/JTRP-2010/17). Purdue University: West Lafayette, Indiana. https://doi.org/10.5703/1288284314255

Lee, W., Bohra, N. C., Altschaeffl, A. G., & White, T. D. (1997). Resilient modulus of cohesive soils. *Journal of Geotechnical and Geoenvironmental Engineering*, *123*(2), 131–136.

Ling, C., David, E., & Siddharthan, R. (1991). Comparison of dynamic and static backcalculation moduli for three-layer pavements. *Transportation Research Record*, *1293*, 86–92.

Liu, W., & Scullion, T. (2006). *PAVECHECK: Integrating deflection and ground penetration radar data for pavement evaluation* (TTI Report 4495). Texas Transportation Institute.

Loken, M. (2005). *Current state of the art and practice of using GPR for Minnesota roadway applications* (Commercially unpublished final report for investigation) (771). https://citeseerx.ist.psu.edu/viewdoc/download?doi=10.1.1.562.470&rep=rep1&type=pdf

Mohammad, L. N., Huang, B., Puppala, A. J., & Allen, A. (1999). Regression model for resilient modulus of subgrade soils. *Transportation Research Record*, *1687*(1), 47–54.

Moossazadeh, J., & Witczak, M. W. (1981). Prediction of subgrade moduli for soil that exhibits nonlinear behavior. *Transportation Research Record*, *810*. https://onlinepubs.trb.org/Onlinepubs/trr/1981/810/810-002.pdf

Nazarian, S., & Stokoe II, K. H. (1986). Use of surface waves in pavement evaluation. *Transportation Research Record*, *1070*. https://onlinepubs.trb.org/Onlinepubs/trr/1986/1070/1070-016.pdf

Nazzal, M. D., & Mohammad, L. N. (2010). Estimation of resilient modulus of subgrade soils for design of pavement structures. *Journal of Materials in Civil Engineering*, *22*(7), 726–734.

NCHRP. (2004). *Laboratory determination of resilient modulus for flexible pavement design* (National Cooperative Highway Research Program Research Results Digest 285). The National Academies Press. https://doi.org/10.17226/21960

Newcomb, D. E. (1986). *Development and evaluation of regression method to interpret dynamic pavement deflections*. University of Washington.

Olson, L. D., & Miller, P. (2009). Comparison of surface wave tests for pavement system thicknesses/moduli. In X. Zhang, X. Yu, H. Fu, & J. Zhang (Eds.), *Characterization, Modeling, and Performance of Geomaterials: Selected Papers from the 2009 GeoHunan International Conference* (pp. 174–179).

Park, S. S., Bobet, A., & Nantung, T. (2018). *Correlation between resilient modulus (M_R) of soil, light weight deflectometer (LWD), and falling weight deflectometer (FWD)* (Joint Transportation Research Program Publication No. FHWA/IN/JTRP-2018/08). West Lafayette, IN: Purdue University. https://doi.org/10.5703/1288284316651

Pekcan, O., Tutumluer, E., & Thompson, M. R. (2008, October). Artificial neural network based backcalculation of conventional flexible pavements on lime stabilized soils. In *Proceedings of the 12th International Conference of International Association for Computer Methods and Advances in Geomechanics* (IACMAG) (pp. 1647–1654).

Ping, W. V., Yang, Z., & Gao, Z. (2002). Field and laboratory determination of granular subgrade moduli. *Journal of Performance of Constructed Facilities*, *16*(4), 149–159.

Puppala, A. J., Hoyos, L. R., & Potturi, A. K. (2011). Resilient moduli response of moderately cement-treated reclaimed asphalt pavement aggregates. *Journal of Materials in Civil Engineering*, *23*(7), 990–998.

Rahim, A. M. (2005). Subgrade soil index properties to estimate resilient modulus for pavement design. *International Journal of Pavement Engineering*, *6*(3), 163–169.

Rahim, A., & George, K. P. (2003). Falling weight deflectometer for estimating subgrade elastic moduli. *Journal of Transportation Engineering*, *129*(1), 100–107.

Roesset, J. M., Chang, D. W., Stokoe II, K. H., & Aouad, M. (1990). Modulus and thickness of the pavement surface layer from SASW tests. *Transportation Research Record*, (1260), 53–60.

Rohlf, J. G., & Rogness, R. O. (1985). Multivariate analysis of pavement Dynaflect deflection data. *Transportation Research Record*, *1060*, 16.

Rout, R. K., Ruttanapormakul, P., Valluru, S., & Puppala, A. J. (2012). Resilient moduli behavior of lime-cement treated subgrade soils. In *GeoCongress 2012: State of the Art and Practice in Geotechnical Engineering* (pp. 1428–1437).

Saarenketo, T., & Scullion, T. (2000). Road evaluation with ground penetrating radar. *Journal of Applied Geophysics*, *43*(2–4), 119–138.

Saarenketo, T., Van Deusen, D., & Maijala, P. (2000, April 27). Minnesota GPR Project 1998: testing ground penetrating radar technology on Minnesota roads and highways. In *Eighth International Conference on Ground Penetrating Radar*, *4084*, 396–401. International Society for Optics and Photonics.

Saltan, M., Uz, V. E., & Aktas, B. (2013). Artificial neural networks–based backcalculation of the structural properties of a typical flexible pavement. *Neural Computing and Applications*, *23*(6), 1703–1710.

Schmalzer, P. N. (2006, December). *LTPP manual for falling weight deflectometer measurements, version 4.1* (Publication No. FHWA-HRT-06-132). Federal Highway Administration.

Scullion, T., Lau, C.-L., & Chen, Y. (1994). *Implementation of the Texas ground penetrating radar system* (Interim report–Report No. FHWA/TX-92/1233-1). Texas Transportation Institute.

Sharma, S., & Das, A. (2008). Backcalculation of pavement layer moduli from falling weight deflectometer data using an artificial neural network. *Canadian Journal of Civil Engineering*, *35*(1), 57–66.

Siekmeier, J. A., Young, D., & Beberg, D. (1999). Comparison of the dynamic cone penetrometer with other tests during subgrade and granular base characterization in Minnesota. In *Nondestructive Testing of Pavements and Backcalculation of Moduli: Third Volume*. ASTM International.

Smith, K. D., Bruinsma, J. E., Wade, M. J., Chatti, K., Vandenbossche, J. M., & Yu, H. T. (2017). *Using falling weight deflectometer data with mechanistic-empirical design and analysis, Volume I* (Report No. FHWA-HRT-16-009). Federal Highway Administration.

Socco, L. V., & Strobbia, C. (2004, November). Surface-wave method for near-surface characterization: A tutorial. *Near Surface Geophysics*, *2*(4), 165–185.

Titi, H. H., Tabatabai, H., & Faheem, A. (2018). *Evaluation of the long-term degradation and strength characteristics of in-situ Wisconsin virgin base aggregates under HMA pavements* (Report No. WHRP 0092-15-06). Wisconsin Department of Transportation.

Uzan, J. (1985). Characterization of granular material. *Transportation Research Record*, *1022*(1), 52–59.

Uzarowski, L., Maher, M., & Balasundaram, A. (2005). Practical application of GPR to supplement data from FWD for quick pavement performance prediction. In *The 2005 Annual Conference of the Transportation Association of Canada Calgary, Alberta* (pp. 1–16).

Von Quintus, H. L., & Killingsworth, B. (1998, January 1). *Analysis relating to pavement material characterizations and their effects on pavement performance* (Report No. FHWA-RD-97-085).

Walubita, L. F., Scullion, T., Leidy, J., & Liu, W. (2009). Non-destructive testing technologies: Application of the ground penetrating radar (GPR) to perpetual pavements. *Road Materials and Pavement Design*, *10*(2), 259–286.

Willett, D. A., Mahboub, K. C., & Rister, B. (2006). Accuracy of ground-penetrating radar for pavement-layer thickness analysis. *Journal of Transportation Engineering*, *132*(1), 96–103.

Willet, D. A., & Rister, B. (2002). *Ground penetrating radar: Pavement layer thickness evaluation* (Research Report No. KTC-02-29/FR101-00-1F). University of Kentucky Transportation Center.

Witczak, M. W., & Uzan, J. (1988). *The universal airport pavement design system, Report I of V: Granular material characterization*. University of Maryland, College Park.

Zhou, F. W., & Scullion, T. (2007, May). *Guidelines for evaluation of existing pavements for HMA overlay* (Report No. FHWA/TX-07/0-5123-2). Texas Transportation Institute.

APPENDICES

Appendix A. AASHTO Classification and Compaction Results

Appendix B. Resilient Modulus Test Results

Appendix C. FWD Deflection Data

Appendix D. Uzan Model Parameters

Appendix E. Octahedral Stress Model Parameters

Appendix F. Backcalculation Analysis for Rigid Pavements

Appendix G. Backcalculation Analysis for Flexible Pavements

APPENDIX A. AASHTO CLASSIFICATION AND COMPACTION RESULTS

Table A.1 AASHTO Classification and Compaction Results for I-865 Samples

Sample	LL %	PL %	PI %	% Fines	Classification AASHTO	OMC %	MDD g/cc (lb/ft^3)
1	24.2	12.3	11.9	54.44	A-6	9.5	2.08 (129.9)
2	20.2	12.7	7.4	43.27	A-4	10.5	2.04 (127.4)
3	18.6	12.4	6.3	53.43	A-4	9.3	2.06 (128.6)
4	20.6	12.3	8.6	68.16	A-4	10.2	2.05 (128.0)
5	19.5	12.5	7.0	48.27	A-4	9.2	2.05 (128.0)
6	20.3	9.6	10.7	51.95	A-6	9.7	2.05 (128.0)
7	21.1	11.7	9.3	58.10	A-4	9.2	2.04 (127.4)
8	21.3	12.4	8.9	60.74	A-4	9.8	2.04 (127.4)
9	20.9	12.5	8.4	49.56	A-4	9.6	2.04 (127.4)
10	17.9	12.6	5.3	49.23	A-4	9.2	2.06 (128.6)
11	19.5	14.0	5.5	45.85	A-4	10.4	2.04 (127.4)

Table A.2 AASHTO Classification and Compaction Results for SR-46 Samples

Sample	LL %	PL %	PI %	% Fines	Classification AASHTO	OMC %	MDD g/cc (lb/ft^3)
1	35.6	22.6	13.1	58.8	A-6	15.8	1.77 (110.5)
2	31.4	20.1	11.4	54.1	A-6	15.1	1.74 (108.6)
3	25.4	17.9	7.5	42.2	A-4	13.3	1.85 (115.5)
4	34.3	22.3	12.0	50.5	A-6	15.0	1.72 (107.4)
5	35.0	22.7	12.3	50.8	A-6	14.4	1.80 (112.4)
6	25.4	15.3	10.1	38.3	A-6	9.1	1.98 (123.6)
7	25.8	14.6	11.2	52.6	A-6	11.3	1.94 (121.1)
8	26.3	16.0	10.4	34.2	A-2-4	8.9	1.98 (123.6)
9	26.0	14.5	11.5	49.9	A-6	9.3	1.99 (124.2)
10	23.6	14.8	8.7	36.9	A-4	9.3	1.99 (124.2)
11	27.5	14.7	12.8	54.0	A-6	10.2	2.00 (124.9)

Table A.3 AASHTO Classification and Compaction Results for US-31 Samples

Sample	LL %	PL %	PI %	% Fines	Classification AASHTO	OMC %	MDD g/cc (lb/ft^3)
1	21.4	14.7	6.7	15.4	A-1-b	11.2	1.95 (121.7)
2	18.2	NP	NP	17.7	A-1-b	11.0	1.97 (123.0)
3	18.5	NP	NP	13.6	A-1-b	11.2	1.92 (119.9)
4	NP	NP	NP	12.8	A-2-4	11.0	1.83 (114.2)
5	23.3	NP	NP	19.1	A-1-b	12.0	1.91 (119.2)
6	23.6	17.3	6.3	19.8	A-1-b	12.0	1.88 (117.4)
7	19.1	16.0	3.1	12.4	A-1-a	10.2	1.99 (124.2)
8	19.5	13.1	4.4	13.4	A-1-b	10.8	1.96 (122.4)
9	18.3	14.7	3.6	10.9	A-1-a	12.4	1.93 (120.5)
10	25.9	14.4	11.5	17.4	A-1-b	11.6	1.93 (120.5)
11	23.5	NP	NP	22.0	A-2-4	10.4	1.86 (116.1)
	18~26	13~17	3~11	11~22	A-1	10~12	1.83~1.99 (114~124)

NP = Non-Plastic

Table A.4 AASHTO Classification and Compaction Results for S-BRITE Samples

Sample	LL %	PL %	PI %	% Fines	Classification AASHTO	OMC %	MDD g/cc (lb/ft^3)
1	29.6	17.6	12.0	49.1	A-6	12.4	1.89 (117.9)
2	27.2	16.4	10.8	48.3	A-6	12.3	1.88 (117.7)
3	27.0	15.4	11.6	49.8	A-6	12.8	1.88 (117.4)

Table A.5 AASHTO Classification and Compaction Results for SR-37 Samples

Sample	LL %	PL %	PI %	% Fines	Classification AASHTO	OMC %	MDD g/cc (lb/ft^3)
1	23.2	12.4	10.8	23.0	A-2-4	10.0	2.01 (125.5)
2	21.4	12.6	8.8	21.5	A-2-4	10.0	2.03 (126.7)
3	23.1	13.7	9.4	21.8	A-2-4	9.7	2.03 (126.7)
4	21.0	12.3	8.7	25.9	A-2-4	9.6	2.01 (125.5)
5	21.0	12.5	8.5	26.9	A-2-4	9.6	2.03 (126.7)
6	21.5	12.7	8.8	29.6	A-2-4	10.4	2.00 (124.9)
7	21.7	12.7	9.0	29.1	A-2-4	9.8	2.01 (125.5)
8	20.1	13.8	6.3	23.5	A-2-4	9.8	2.02 (126.1)
9	20.6	12.5	8.1	30.3	A-2-4	9.8	2.03 (126.7)
10	19.9	12.7	7.2	28.8	A-2-4	9.8	2.03 (126.7)
11	20.4	14.7	5.7	29.0	A-2-4	9.6	2.01 (125.5)

Table A.6 AASHTO Classification and Compaction Results for I-65 Samples

Sample	LL %	PL %	PI %	% Fines	Classification AASHTO	OMC %	MDD g/cc (lb/ft^3)
1	21.5	11.4	10.1	51.7	A-4	9.5	2.07 (129.2)
2	28.5	16.0	12.5	67.9	A-6	14.3	1.82 (113.4)
3	25.4	16.3	9.1	53.7	A-4	14.0	1.84 (114.9)
4	30.1	16.8	13.3	80.1	A-6	14.7	1.84 (115.0)
5	31.4	16.6	14.8	65.9	A-6	14.8	1.84 (114.9)
6	32.7	18.8	13.9	69.8	A-6	16.0	1.79 (111.7)
7	24.1	15.1	9.0	46.0	A-4	15.0	1.85 (115.5)
8	36.2	19.7	16.5	78.9	A-6	17.0	1.71 (106.8)
9	31.0	17.9	13.1	73.3	A-6	16.0	1.75 (109.2)
10	35.1	17.7	17.4	75.8	A-6	16.5	1.76 (109.9)
11	35.3	18.7	16.6	80.2	A-6	16.5	1.75 (109.2)

APPENDIX B. RESILIENT MODULUS TEST RESULTS

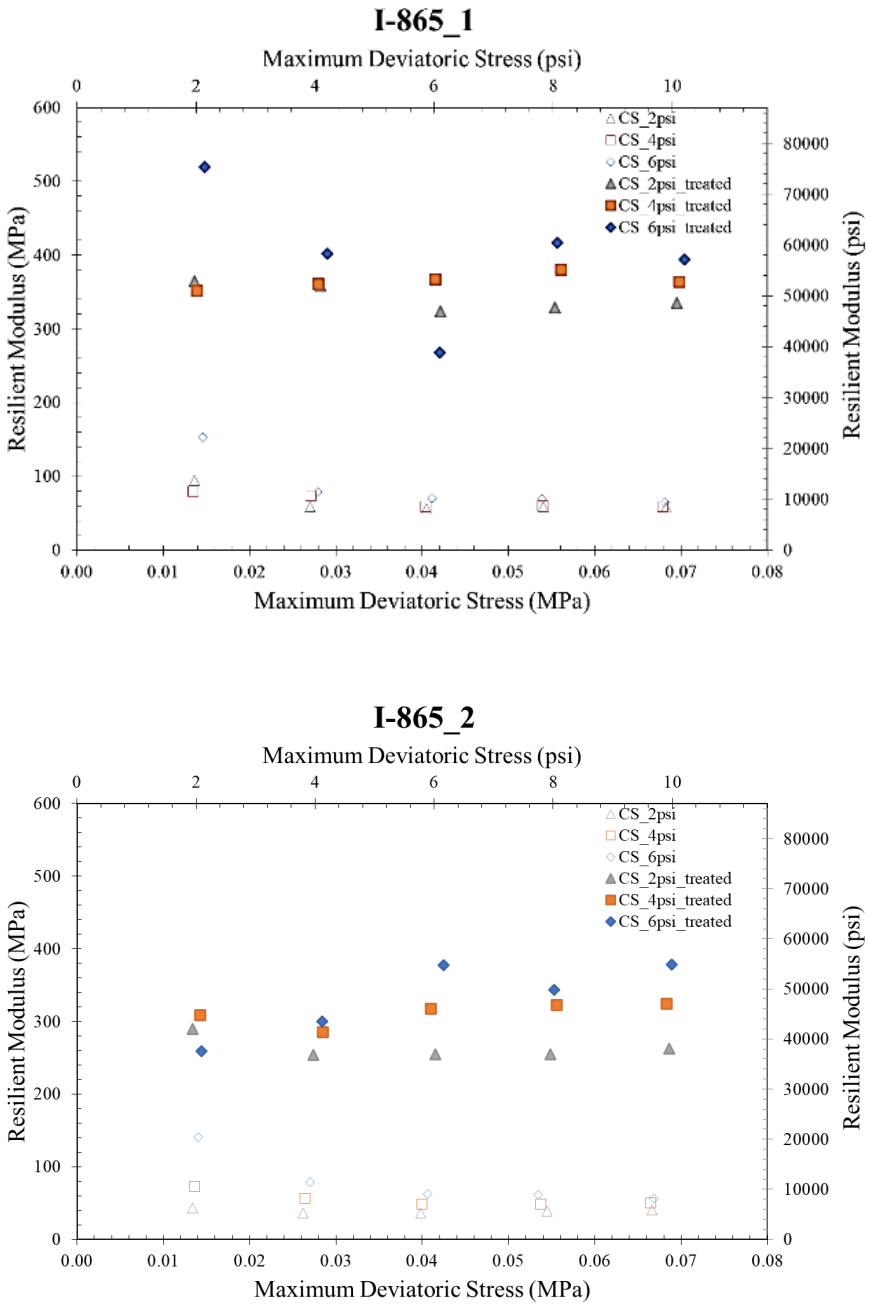

Figure B.1 Resilient modulus test results of I-865 soils.

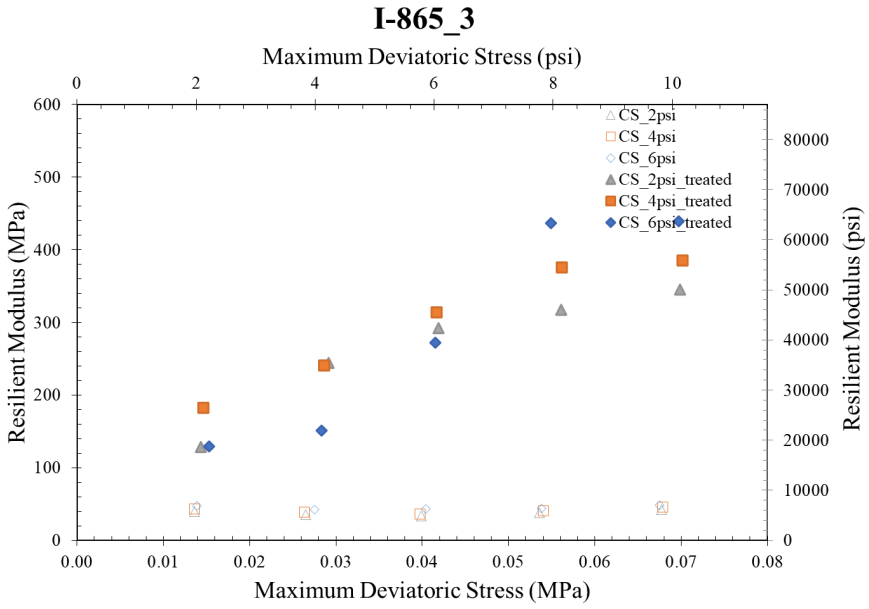

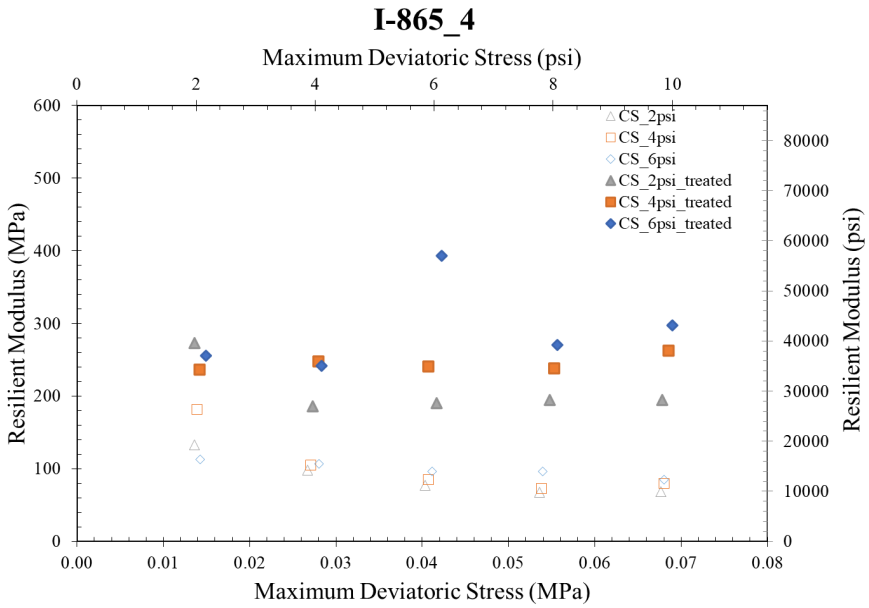

Figure B.1 Resilient modulus test results of I-865 soils (continued).

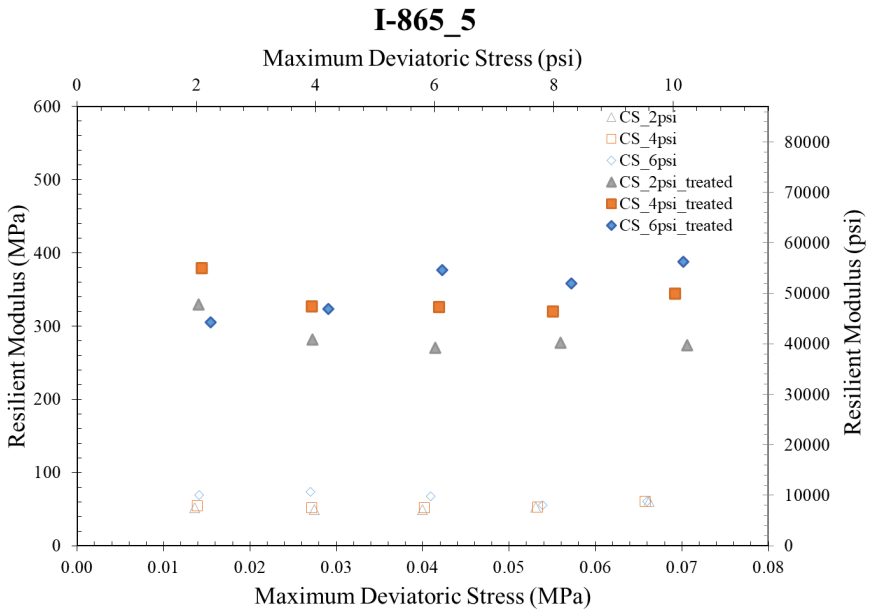

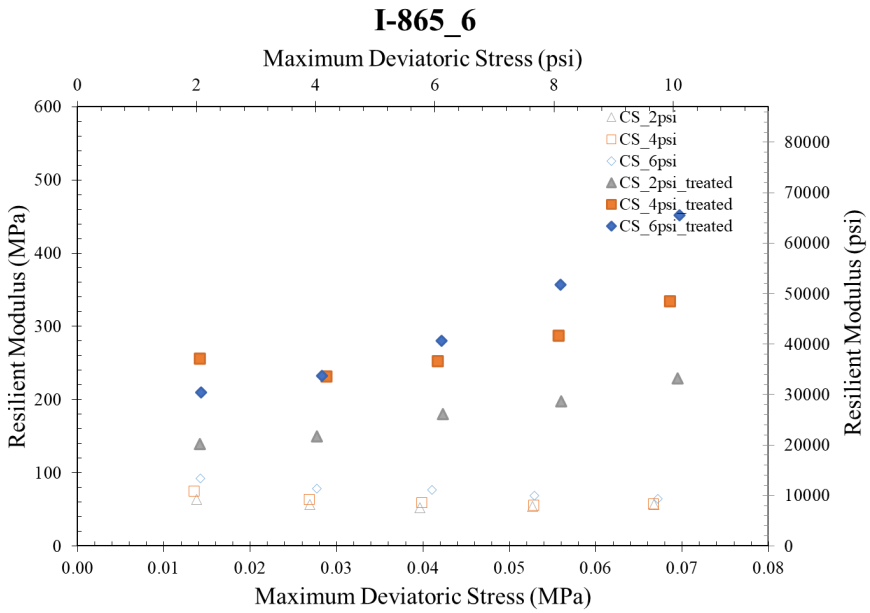

Figure B.1 Resilient modulus test results of I-865 soils (continued).

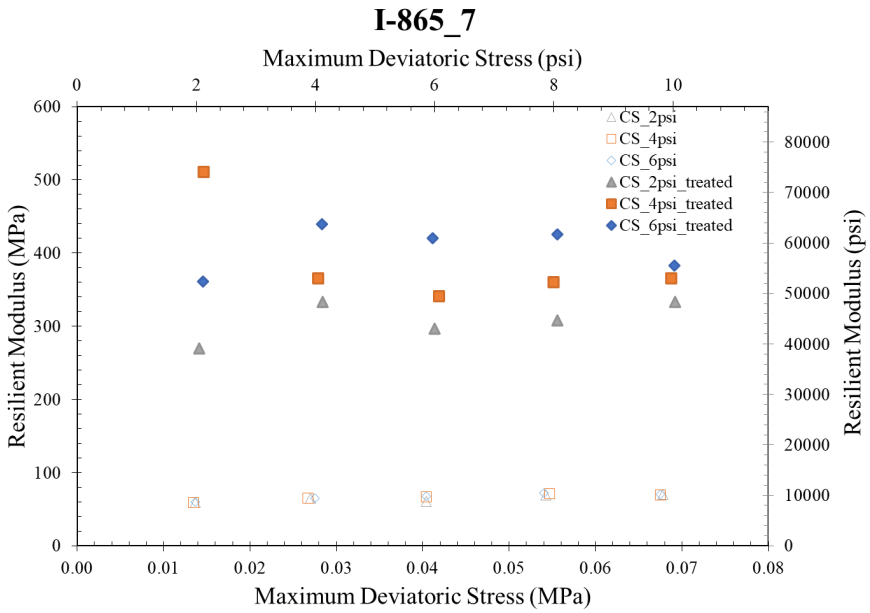

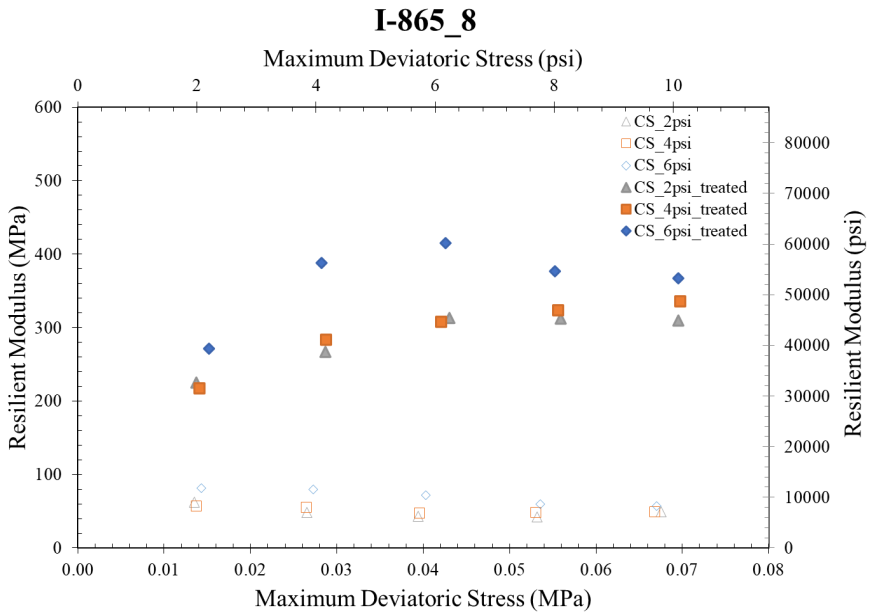

Figure B.1 Resilient modulus test results of I-865 soils (continued).

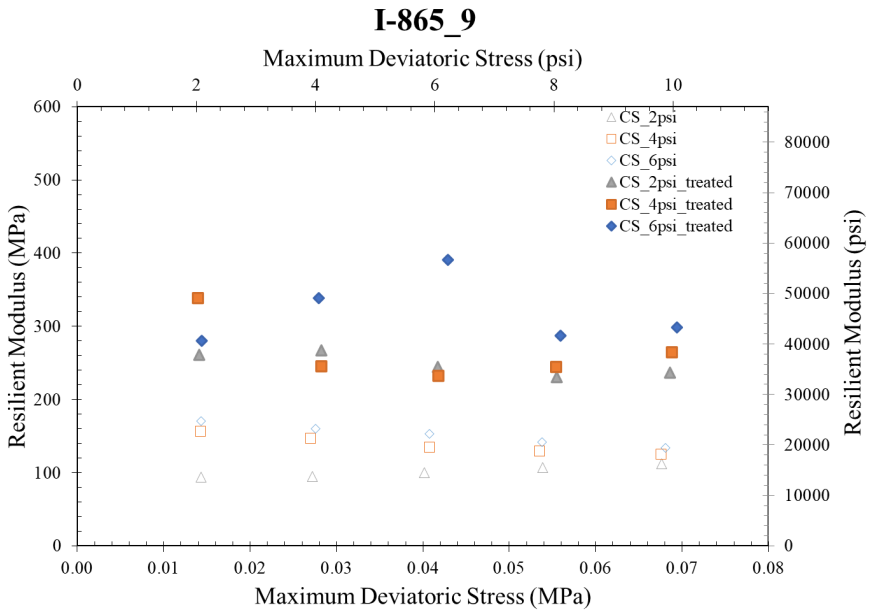

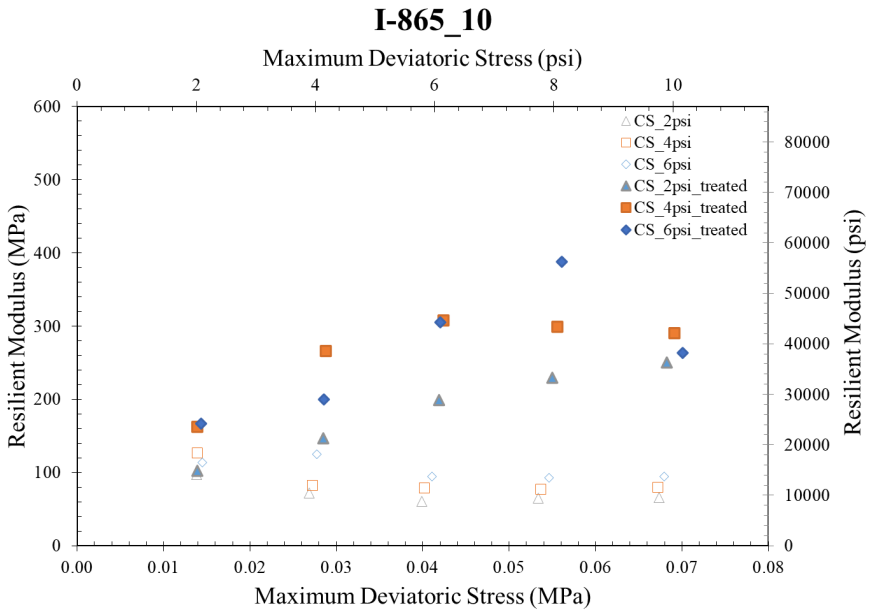

Figure B.1 Resilient modulus test results of I-865 soils (continued).

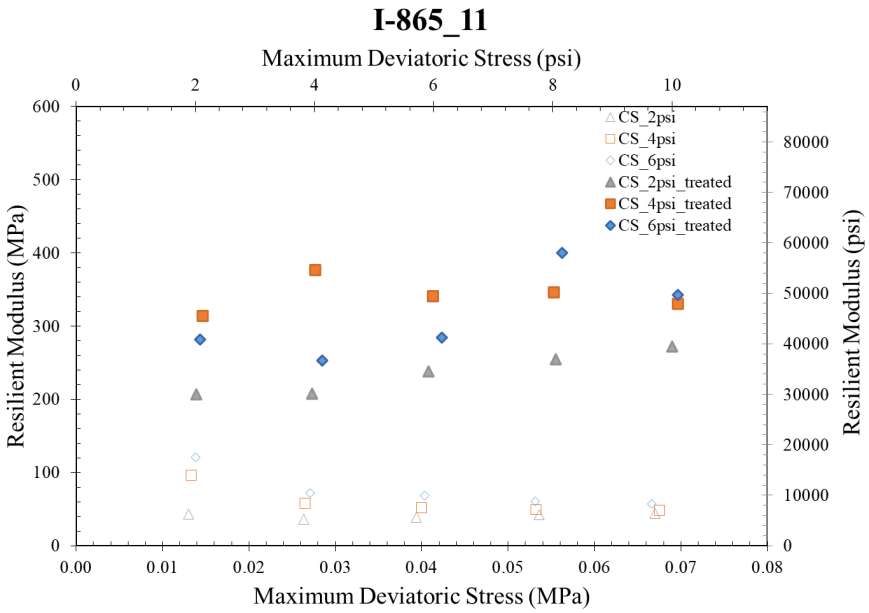

Figure B.1 Resilient modulus test results of I-865 soils (continued).

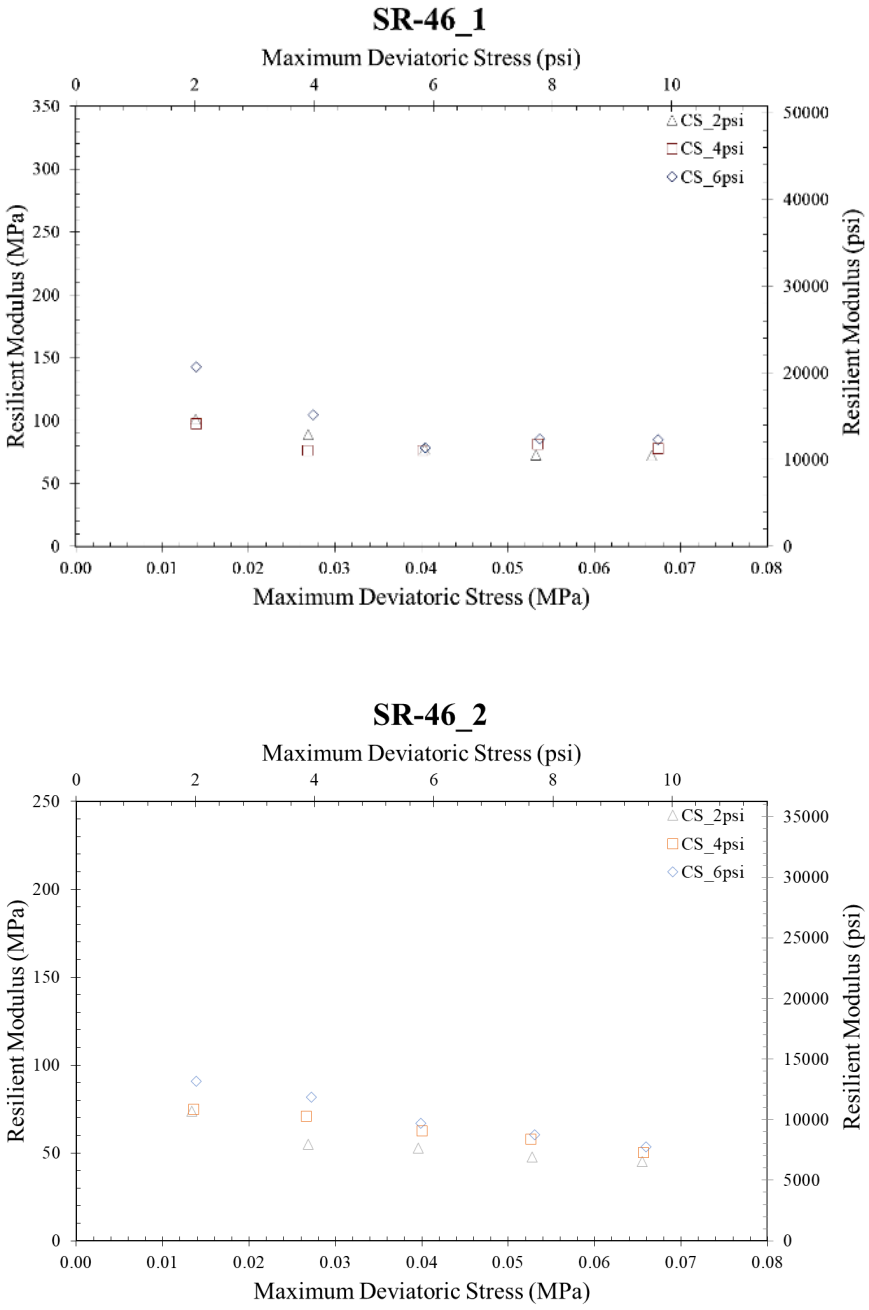

Figure B.2 Resilient modulus test results of SR-46 soils.

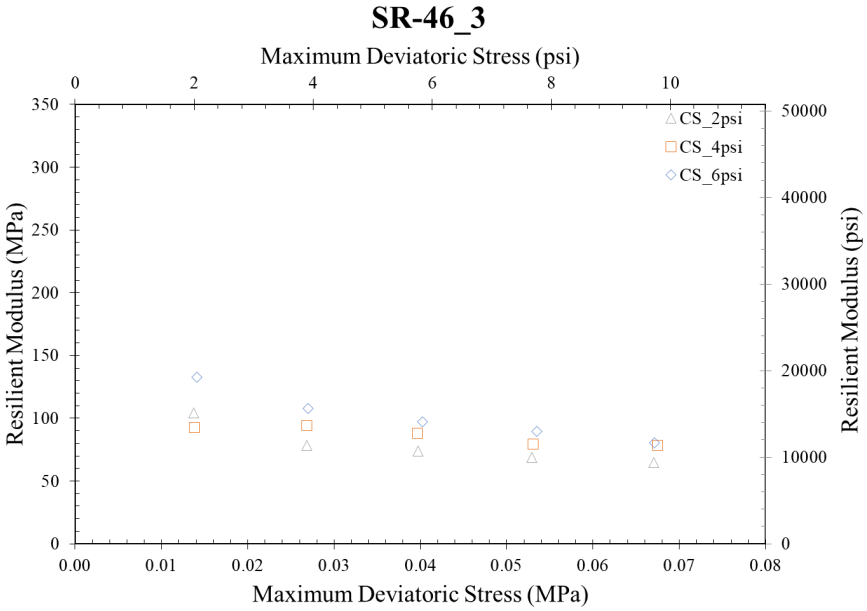

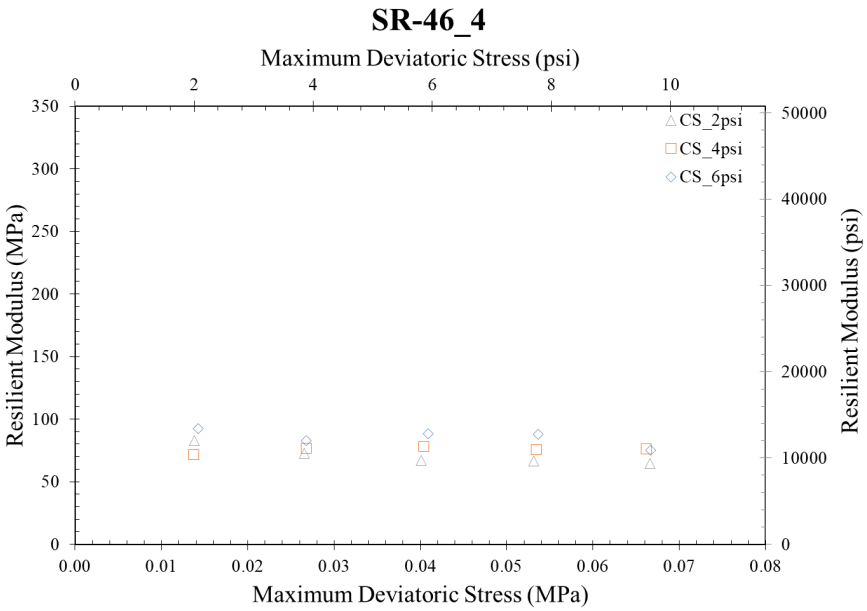

Figure B.2 Resilient modulus test results of SR-46 soils (continued).

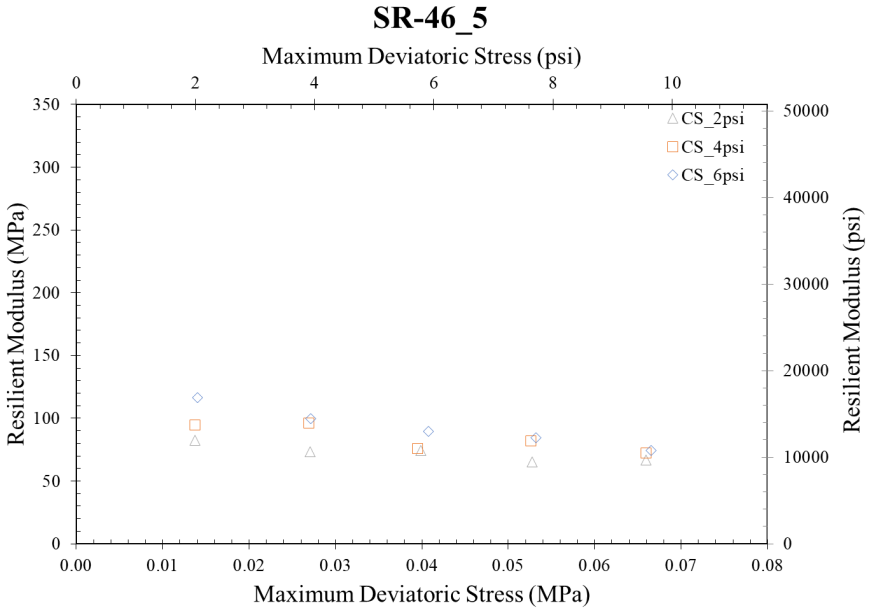

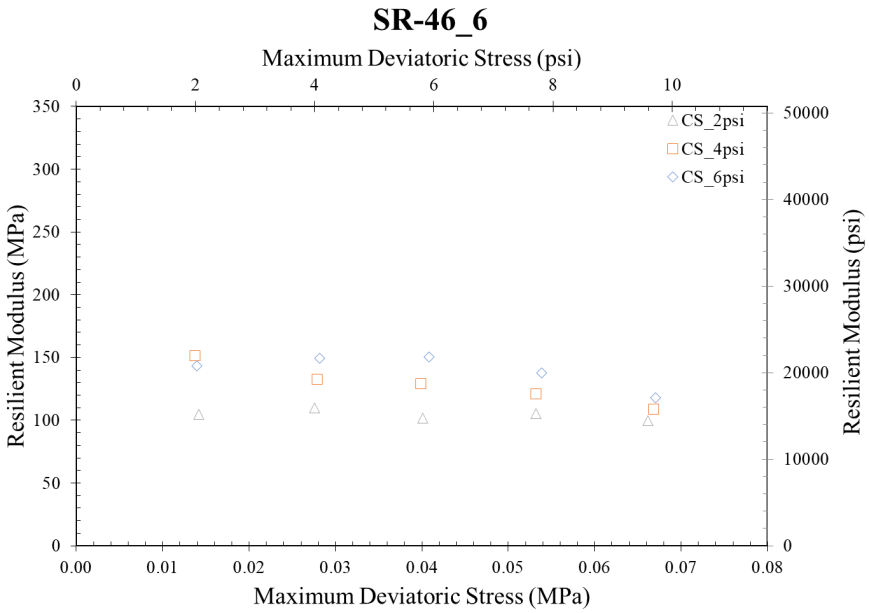

Figure B.2 Resilient modulus test results of SR-46 soils (continued).

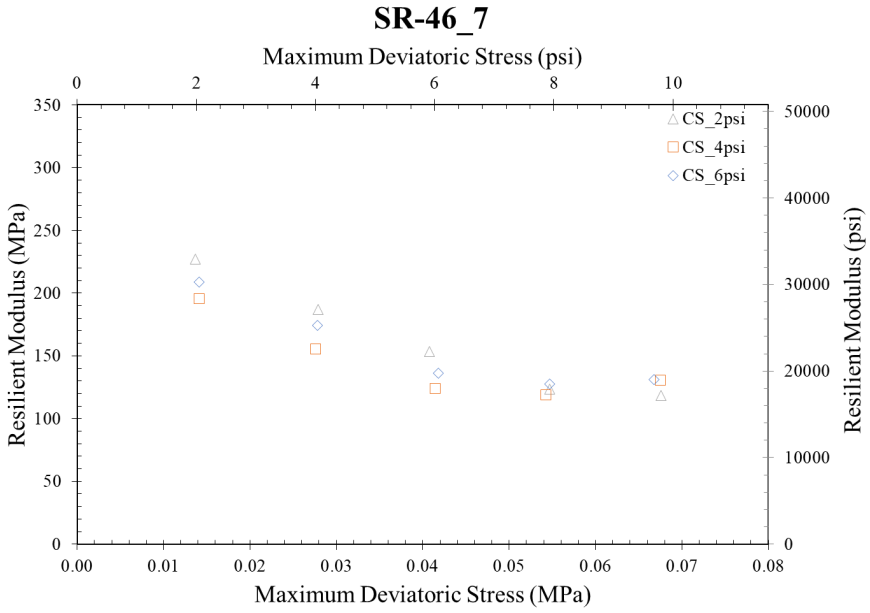

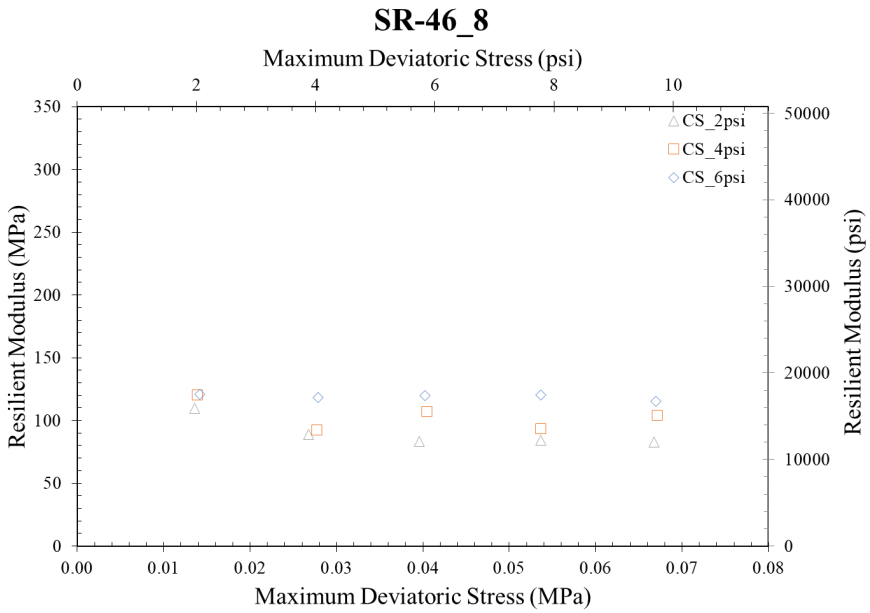

Figure B.2 Resilient modulus test results of SR-46 soils (continued).

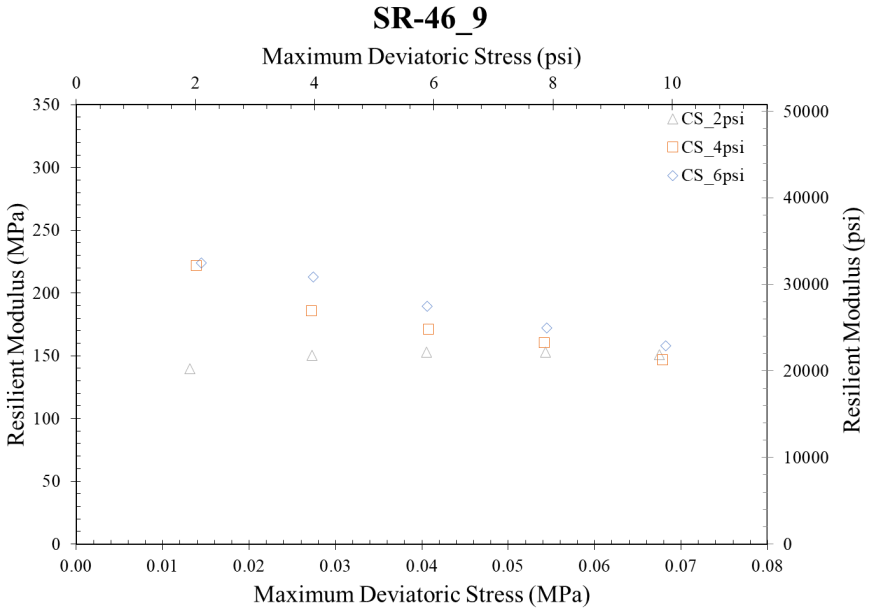

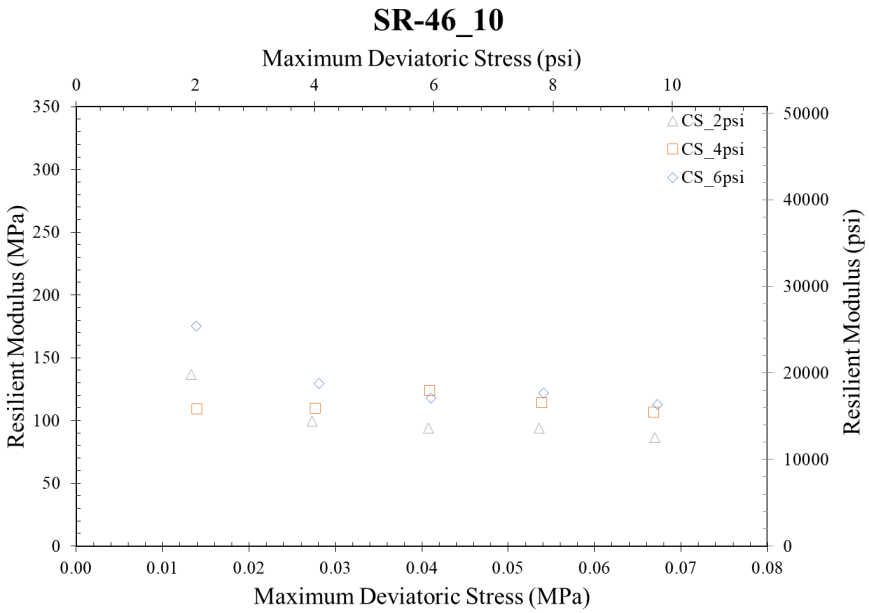

Figure B.2 Resilient modulus test results of SR-46 soils (continued).

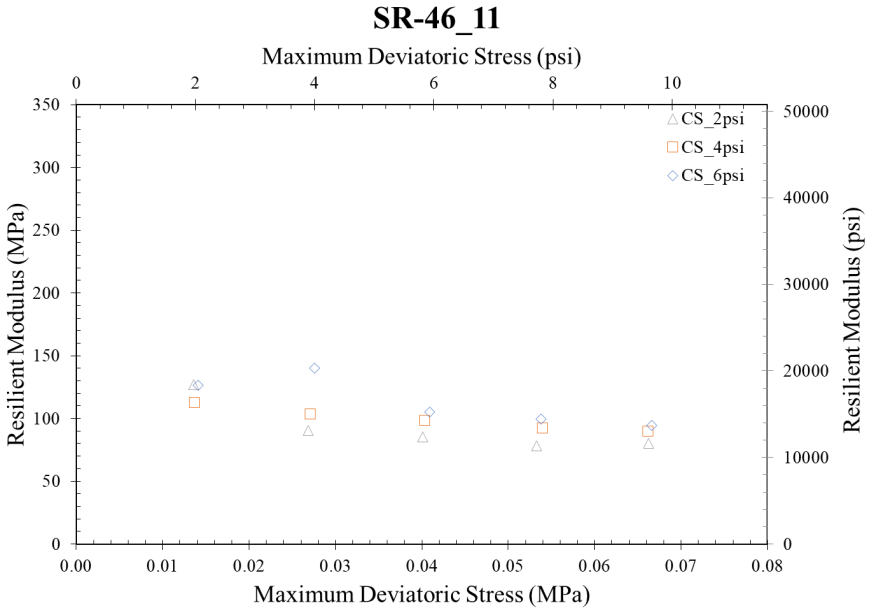

Figure B.2 Resilient modulus test results of SR-46 soils (continued).

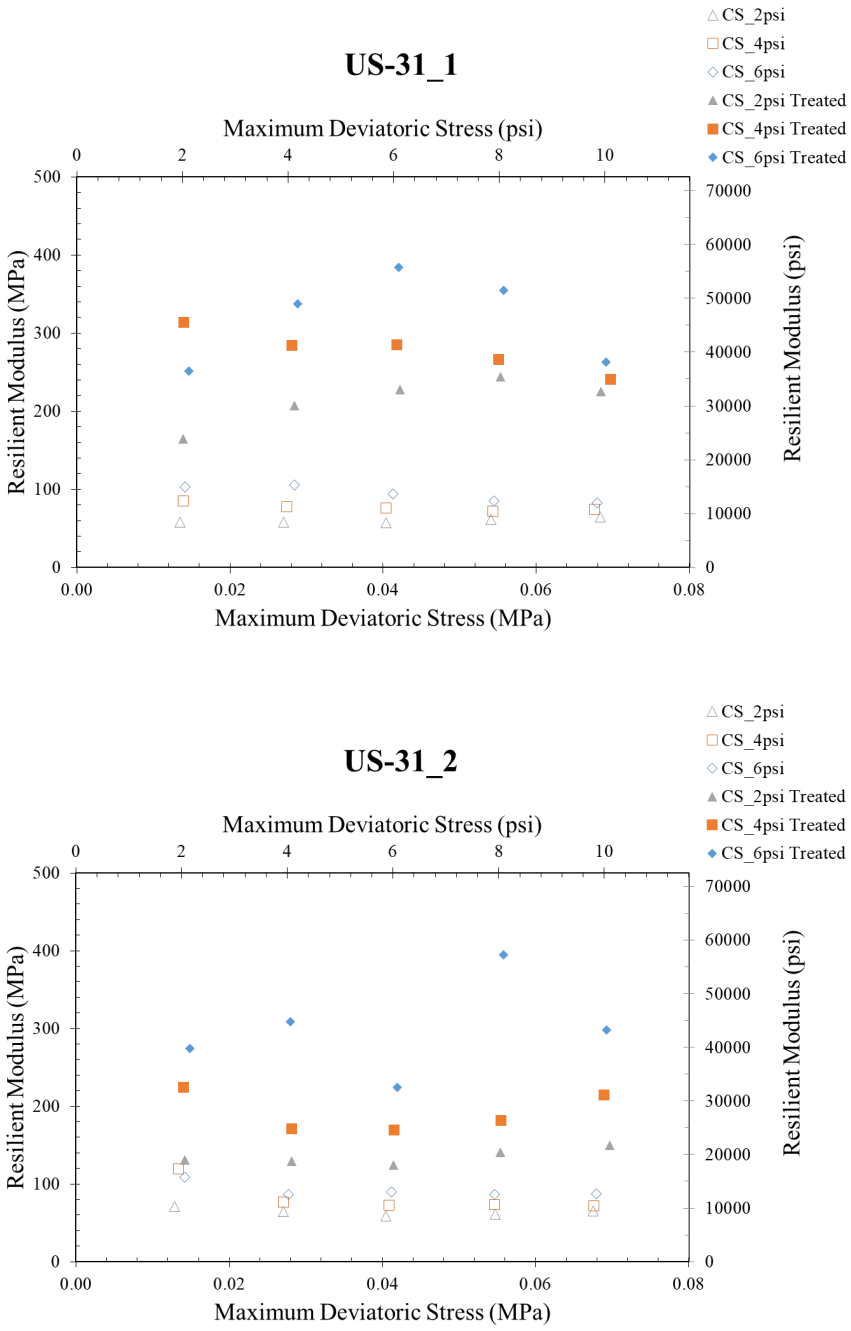

Figure B.3 Resilient modulus test results of US-31 soils.

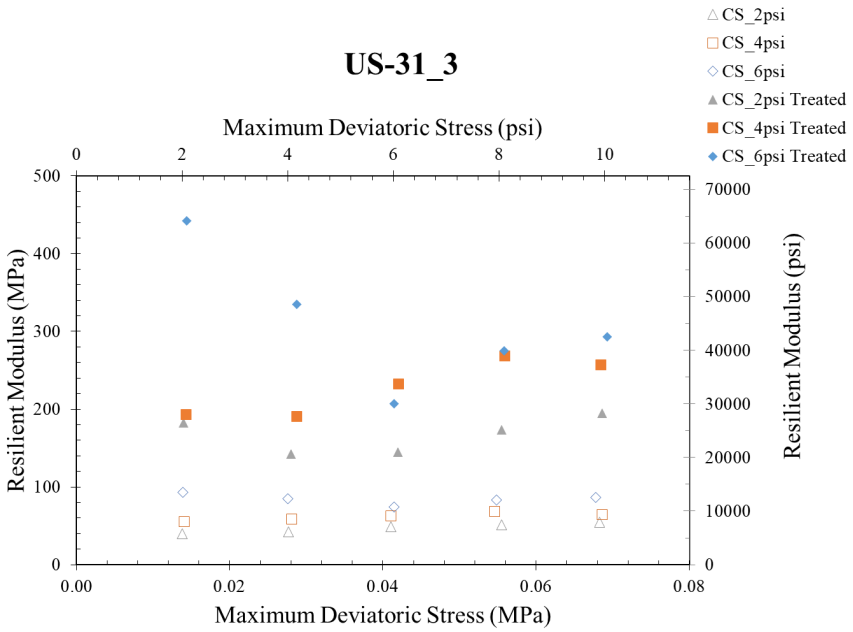

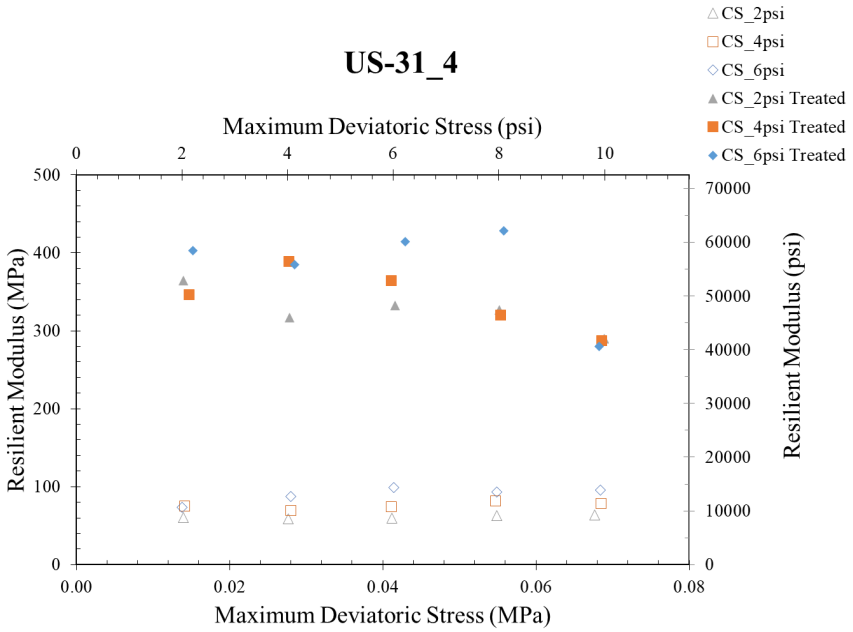

Figure B.3 Resilient modulus test results of US-31 soils (continued).

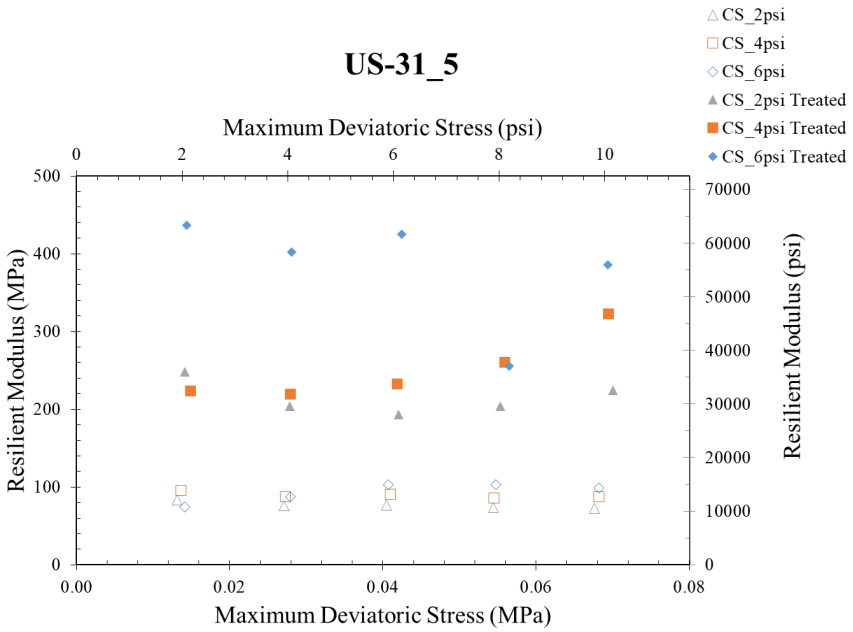

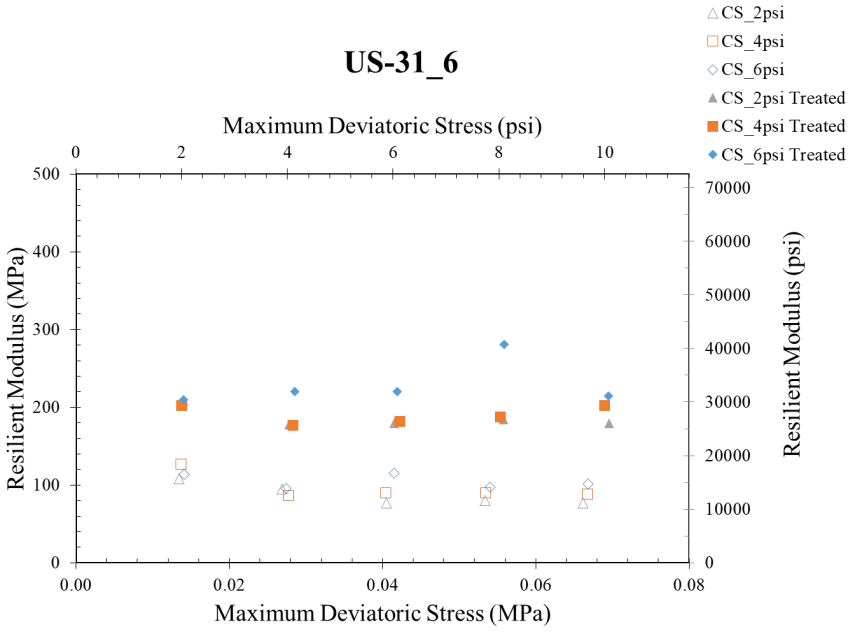

Figure B.3 Resilient modulus test results of US-31 soils (continued).

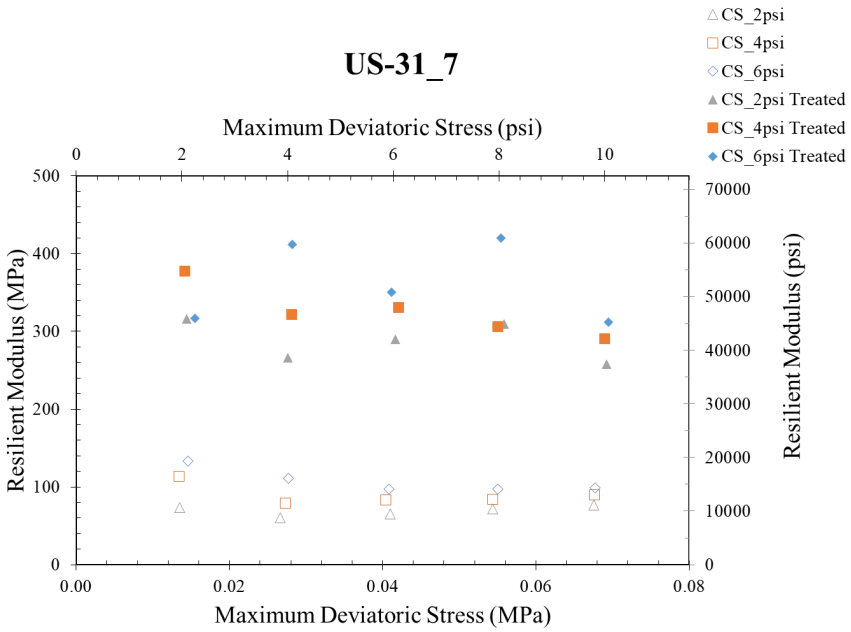

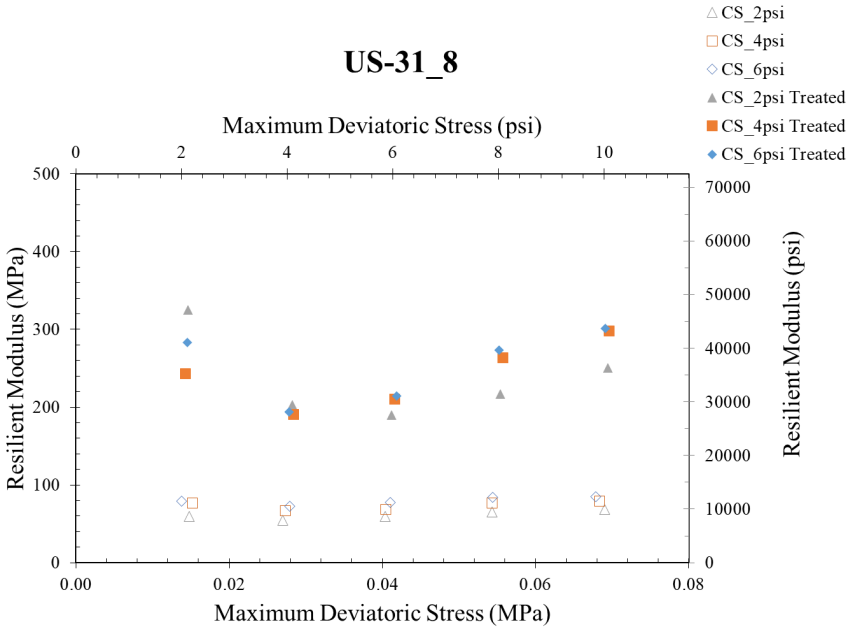

Figure B.3 Resilient modulus test results of US-31 soils (continued).

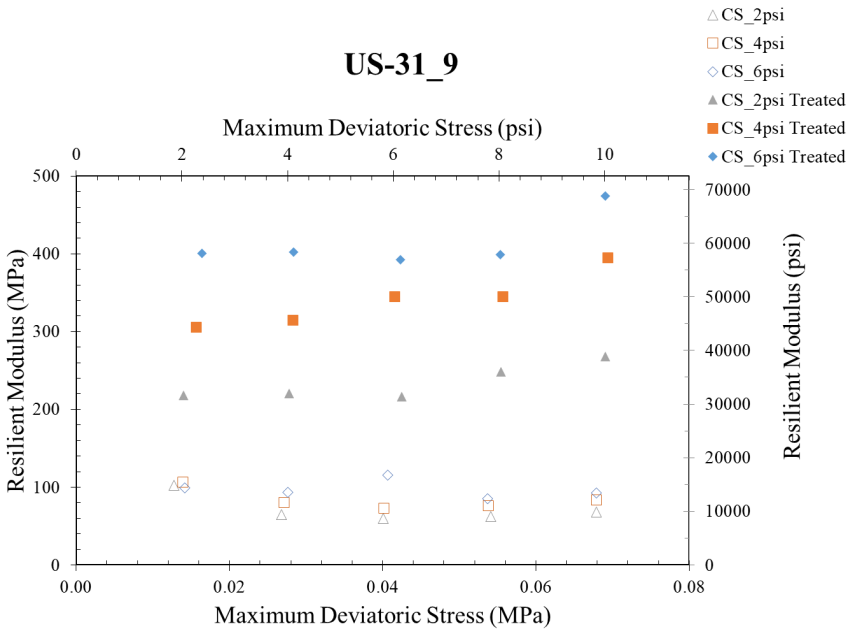

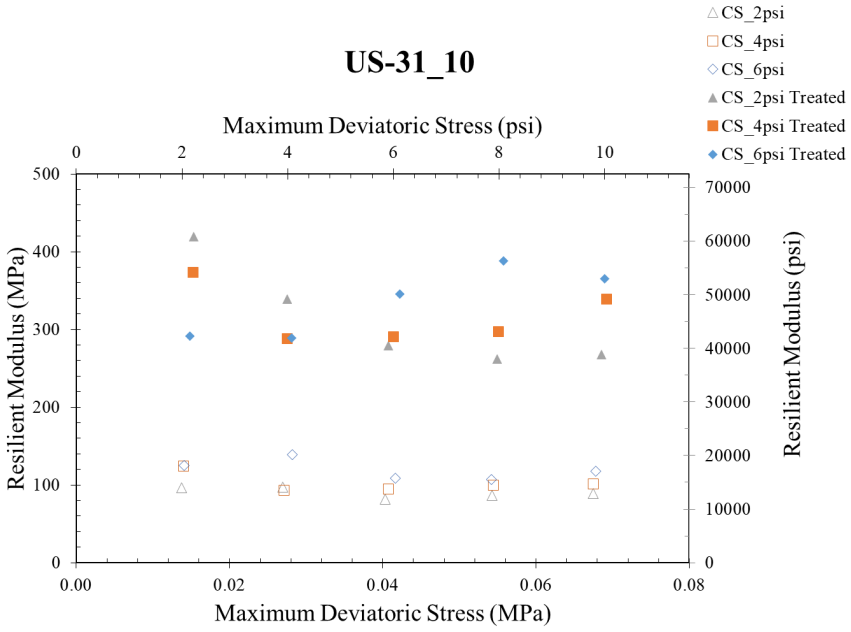

Figure B.3 Resilient modulus test results of US-31 soils (continued).

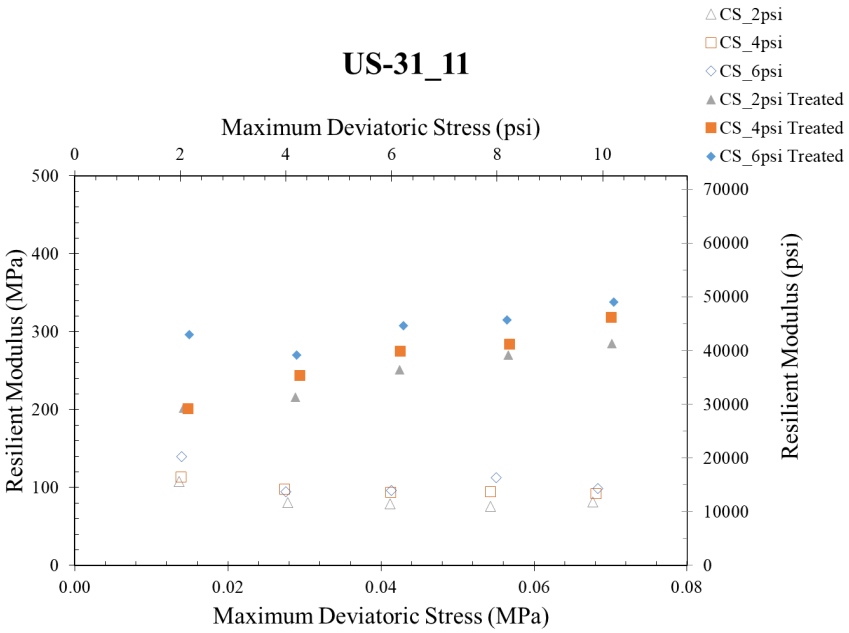

Figure B.3 Resilient modulus test results of US-31 soils (continued).

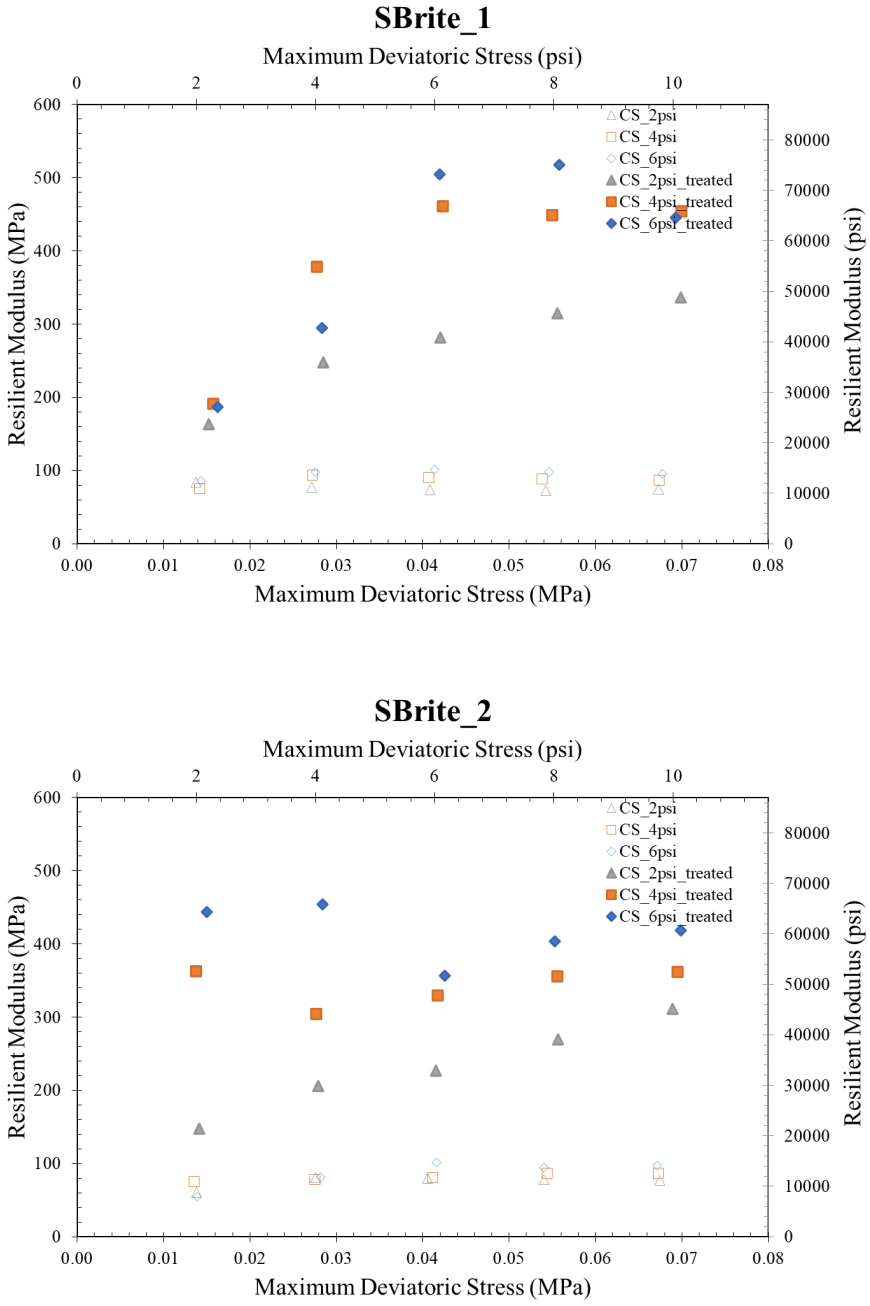

Figure B.4 Resilient modulus test results of S-BRITE soils.

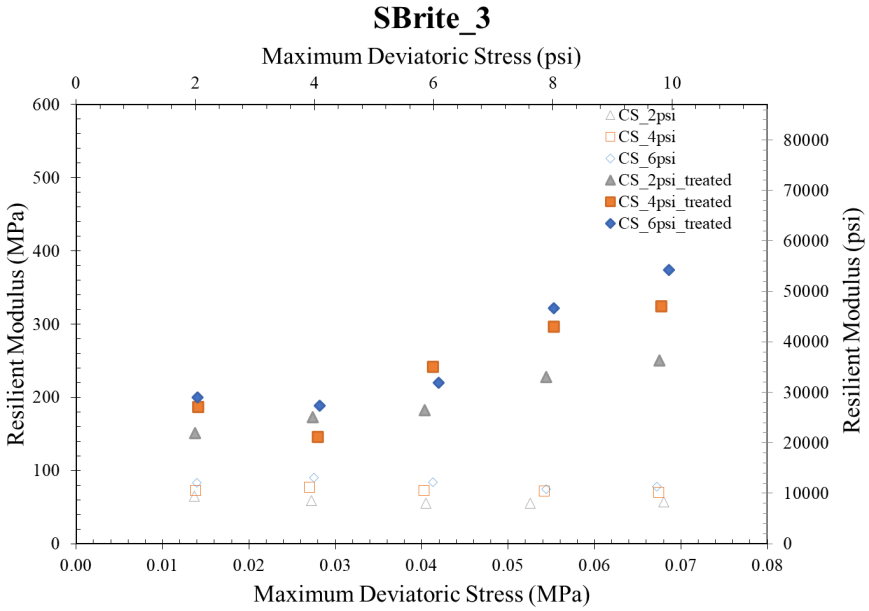

Figure B.4 Resilient modulus test results of S-BRITE soils (continued).

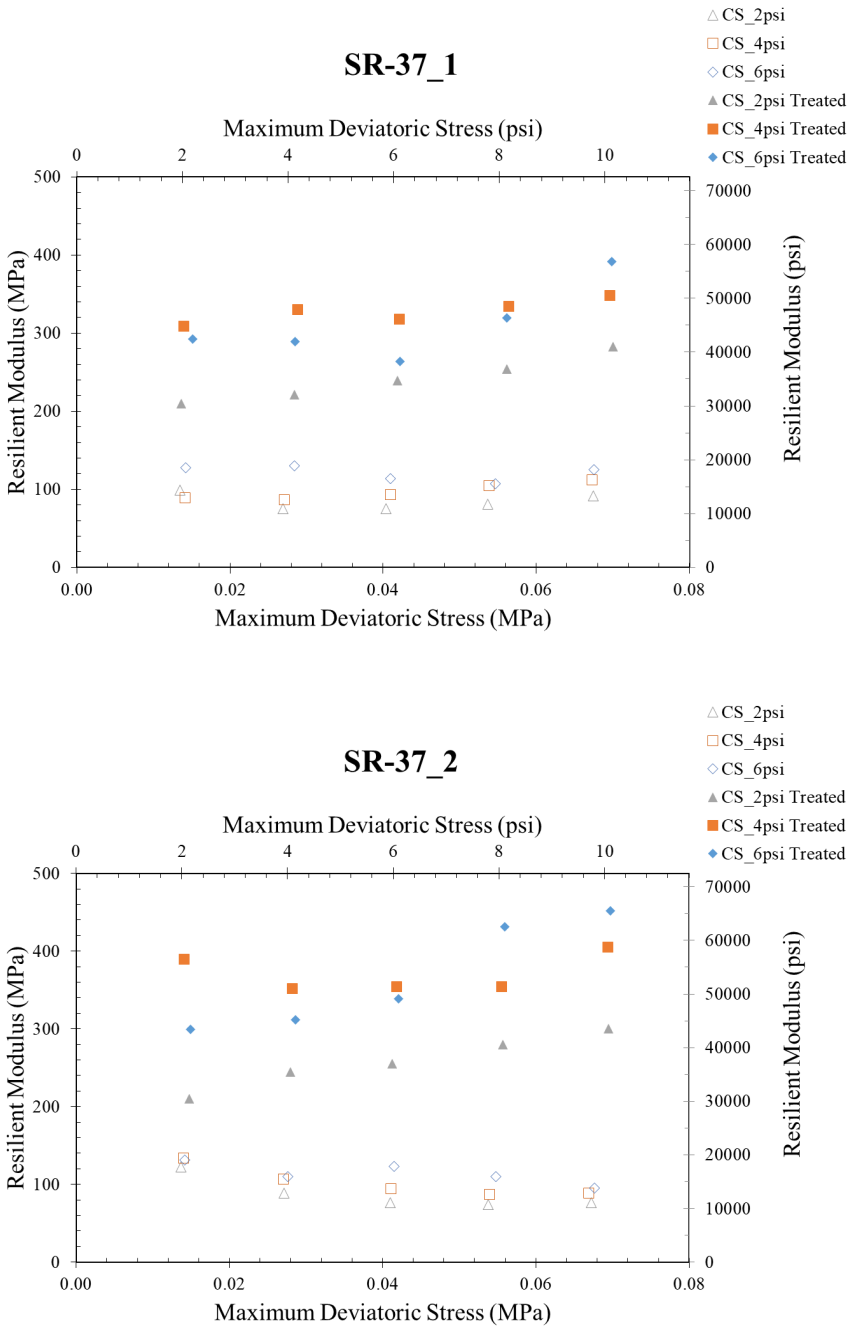

Figure B.5 Resilient modulus test results of SR-37 soils.

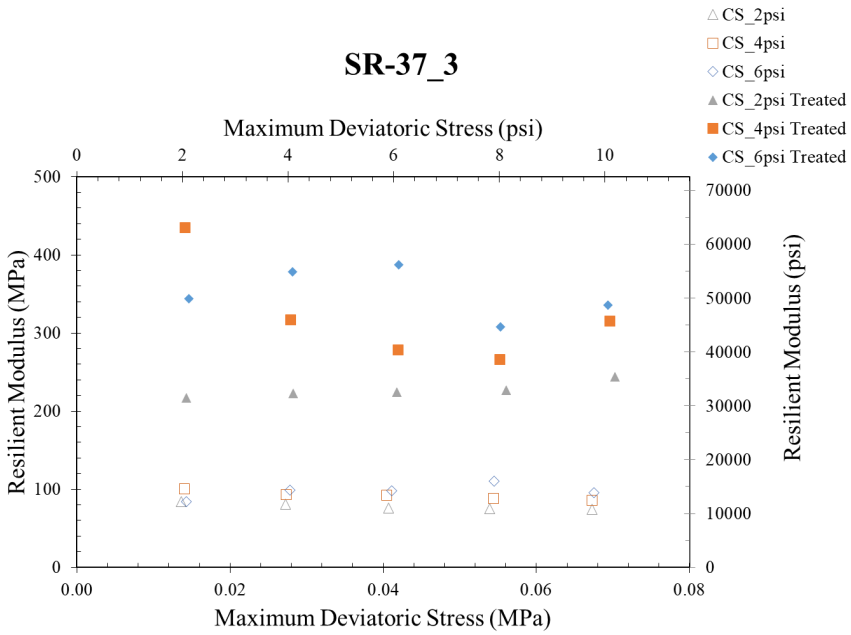

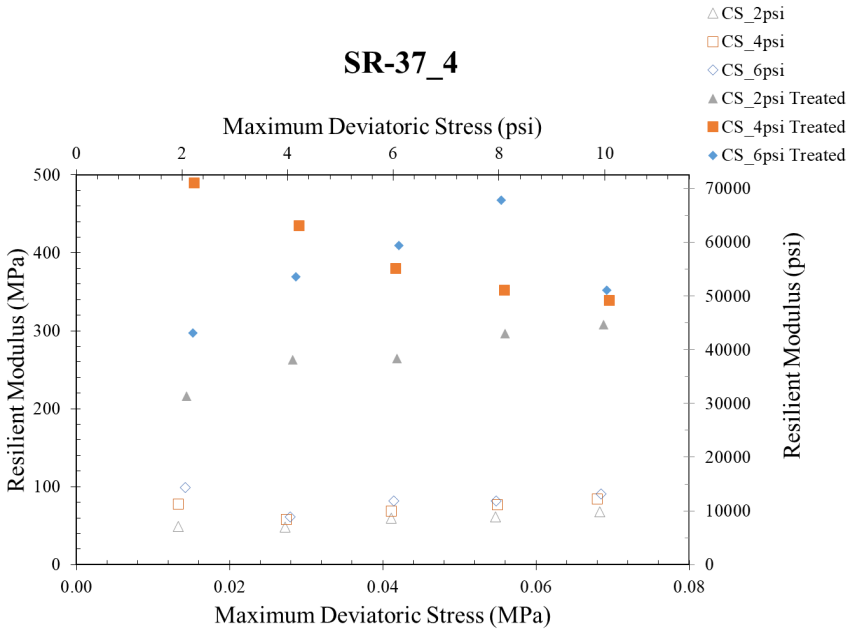

Figure B.5 Resilient modulus test results of SR-37 soils (continued).

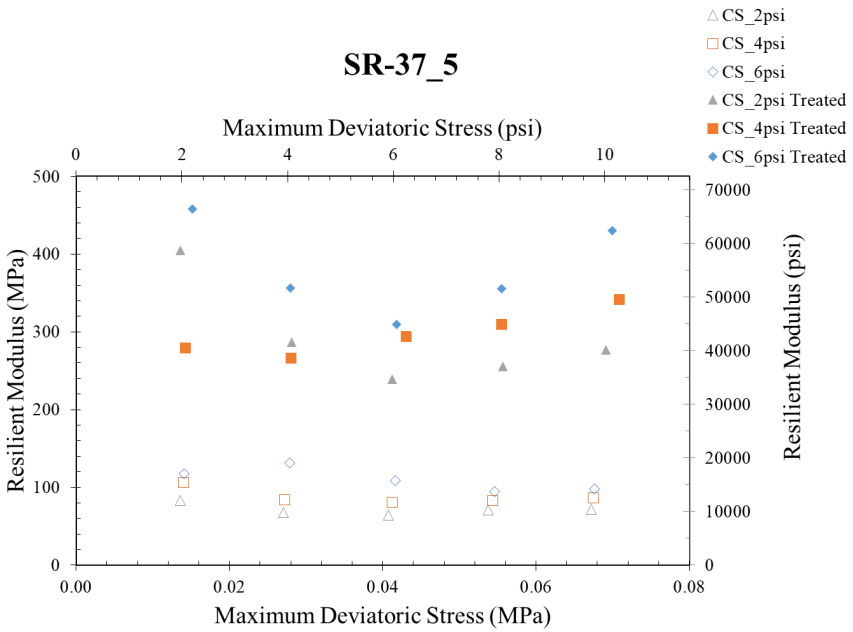

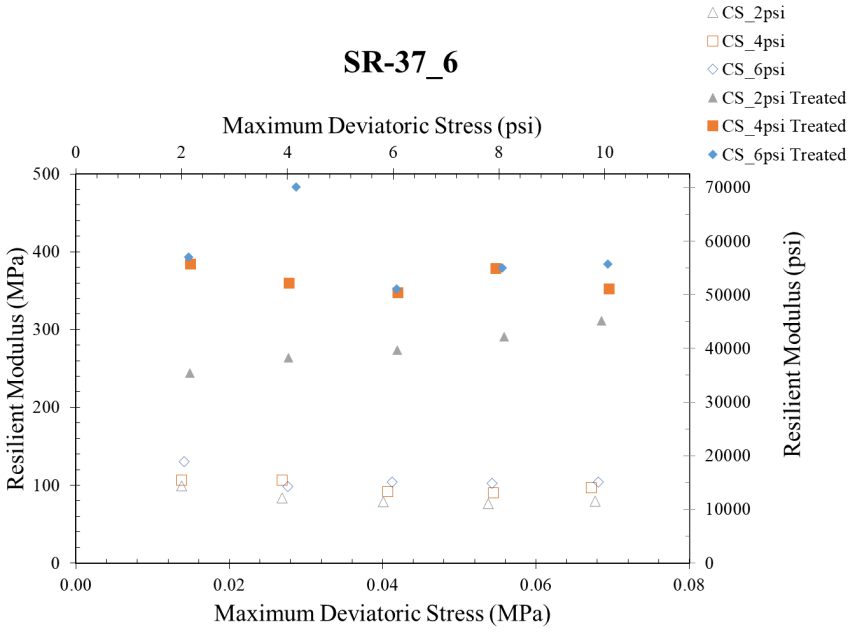

Figure B.5 Resilient modulus test results of SR-37 soils (continued).

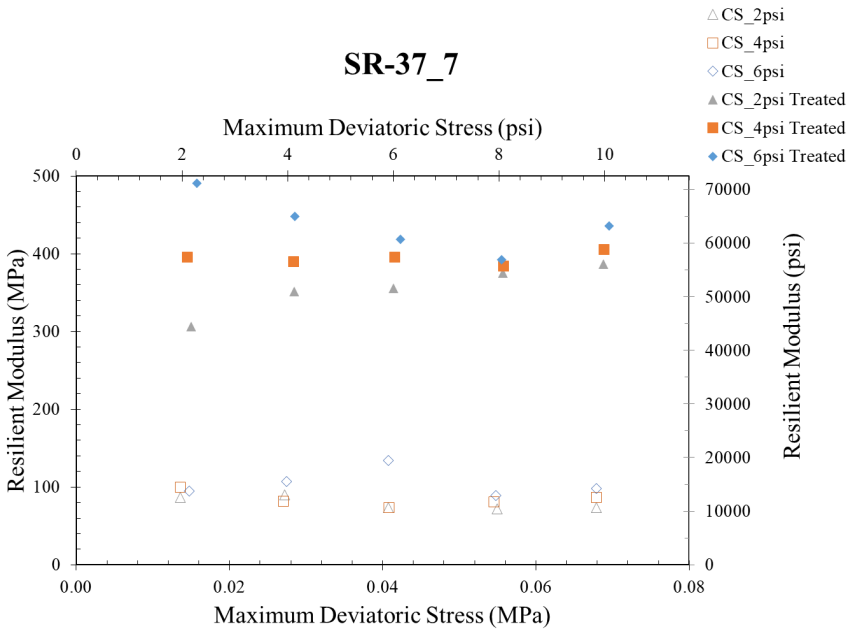

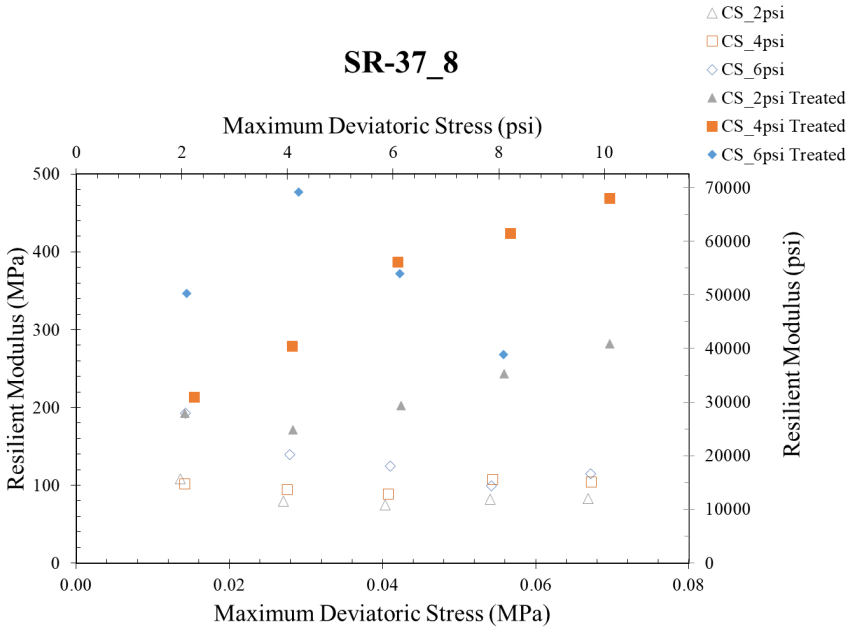

Figure B.5 Resilient modulus test results of SR-37 soils (continued).

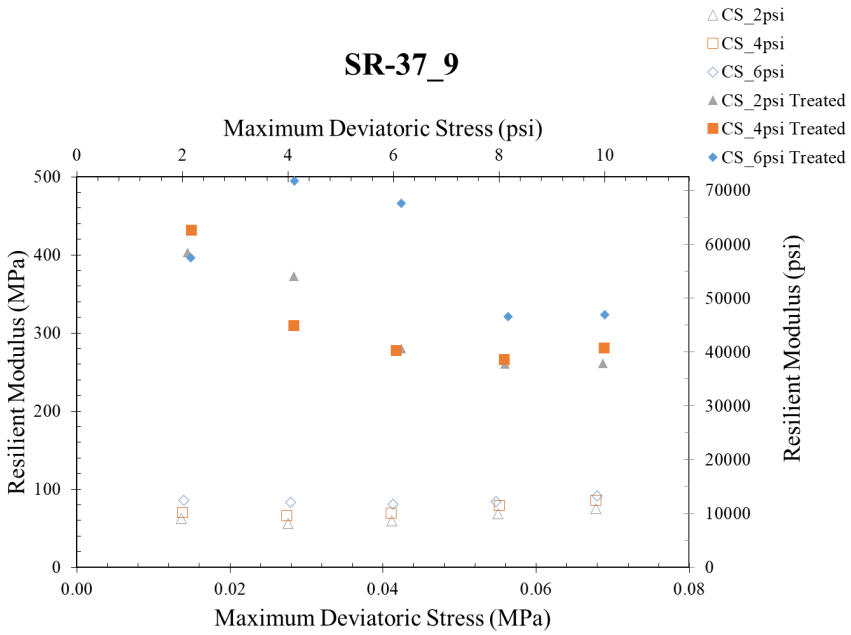

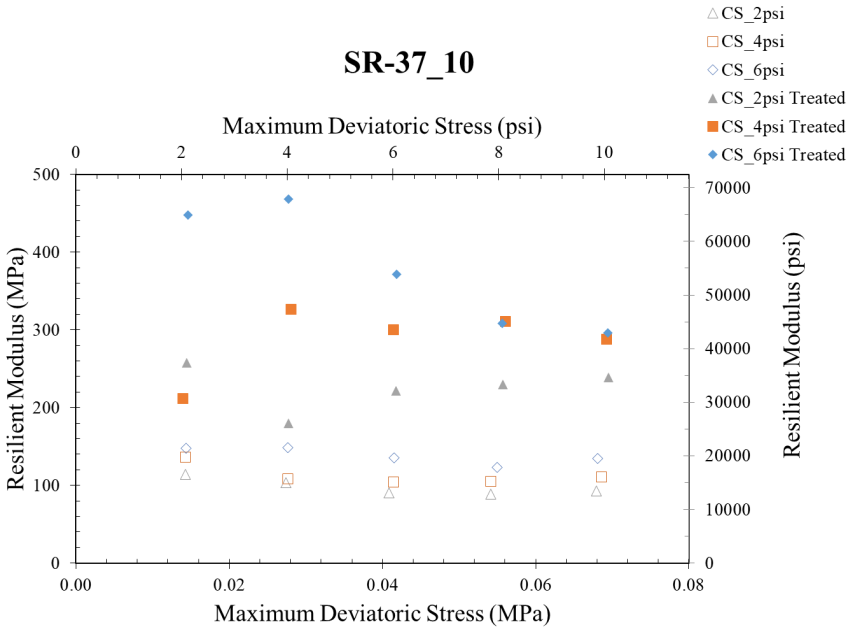

Figure B.5 Resilient modulus test results of SR-37 soils (continued).

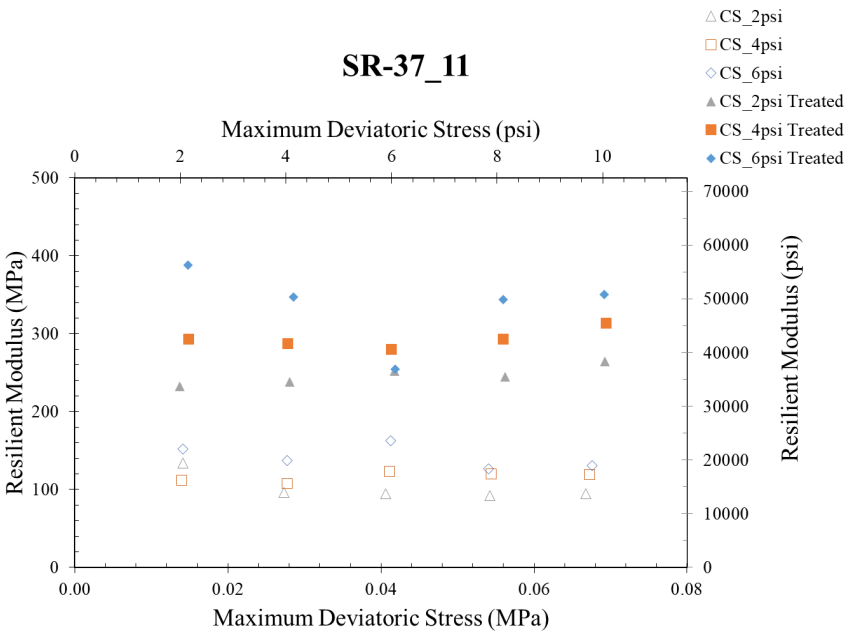

Figure B.5 Resilient modulus test results of SR-37 soils (continued).

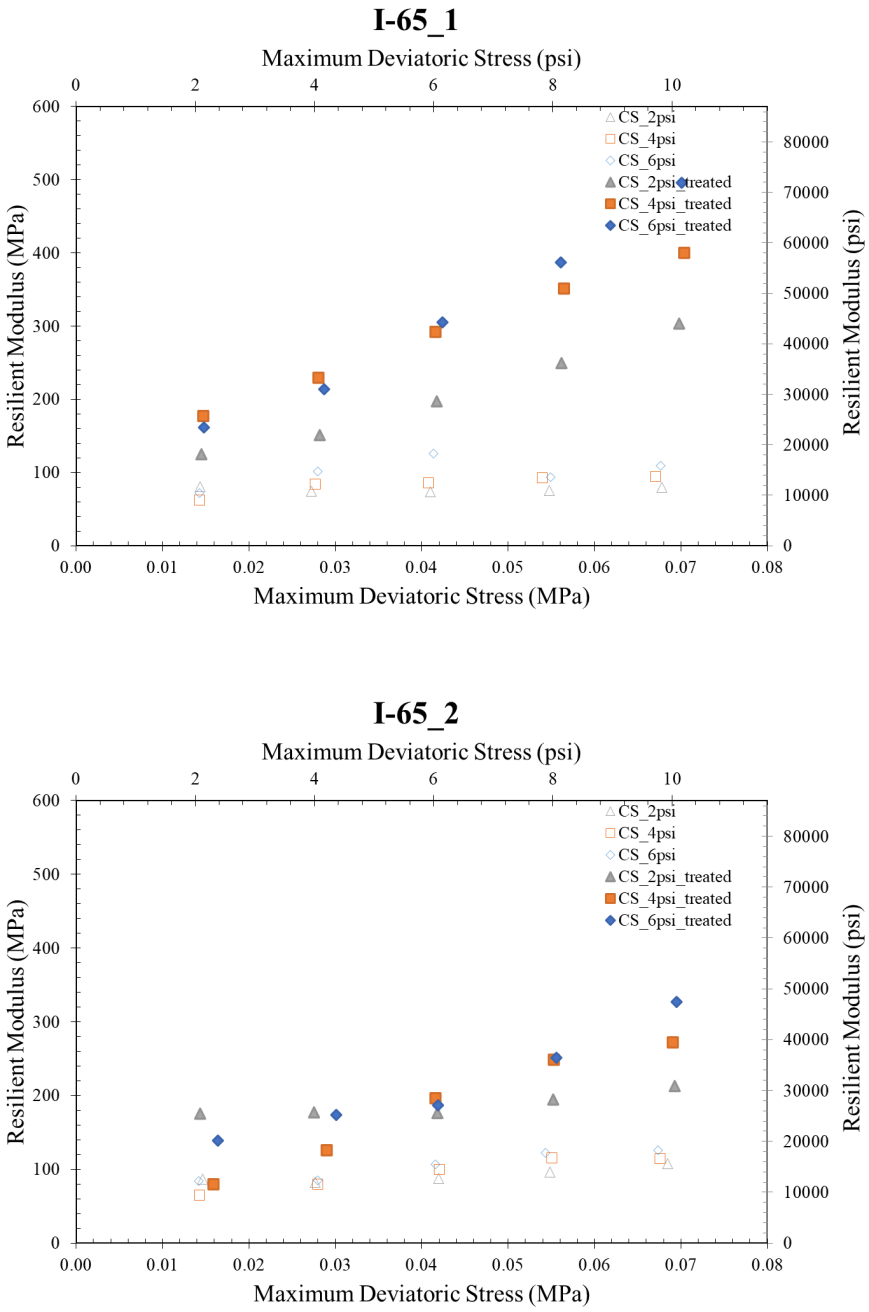

Figure B.6 Resilient modulus test results of I-65 soils.

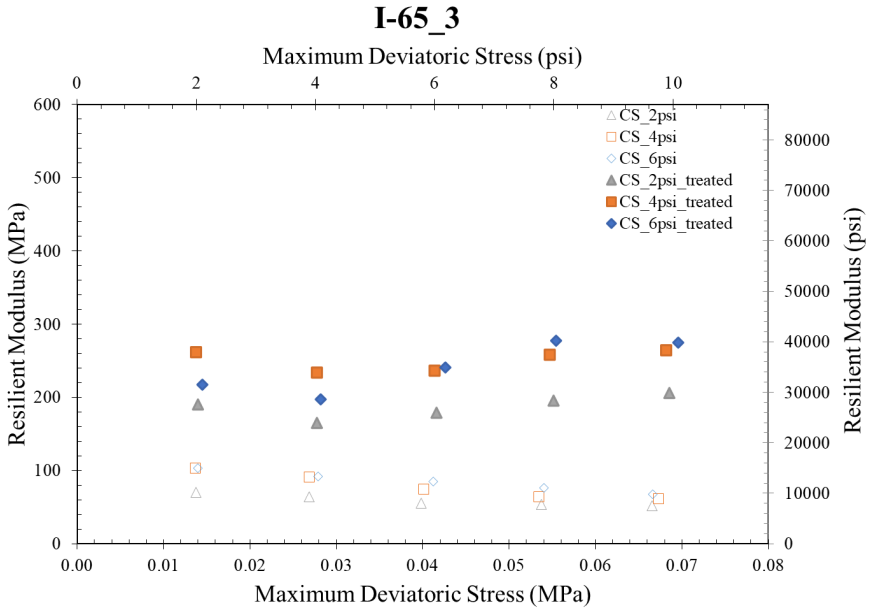

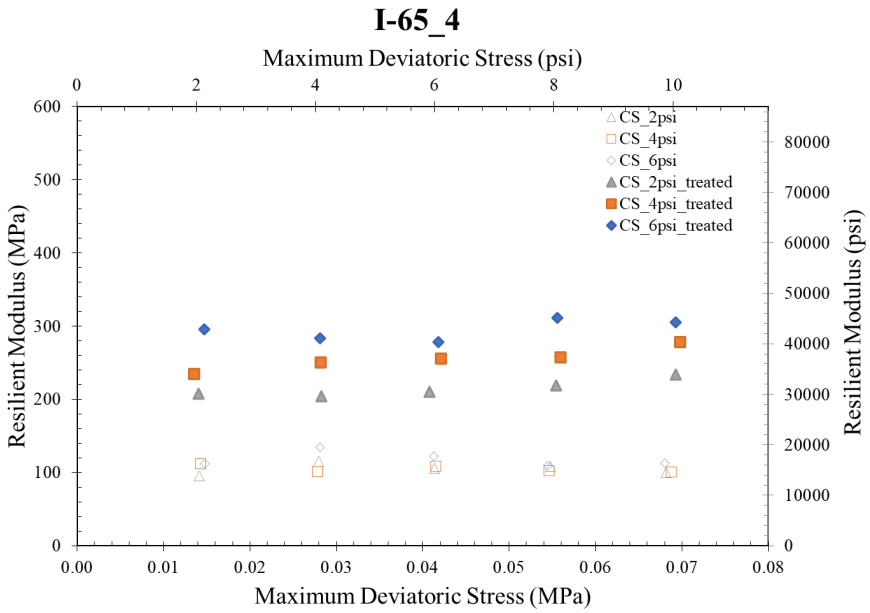

Figure B.6 Resilient modulus test results of I-65 soils (continued).

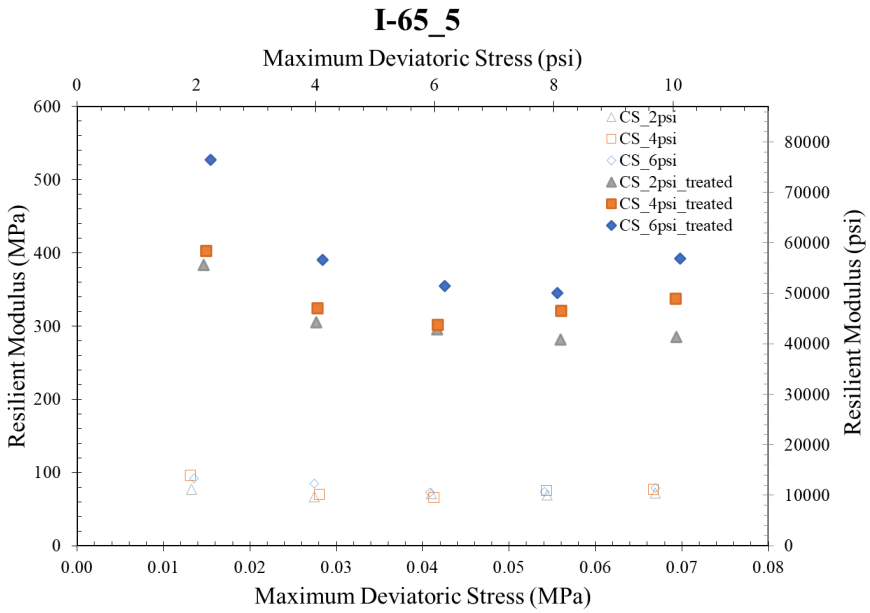

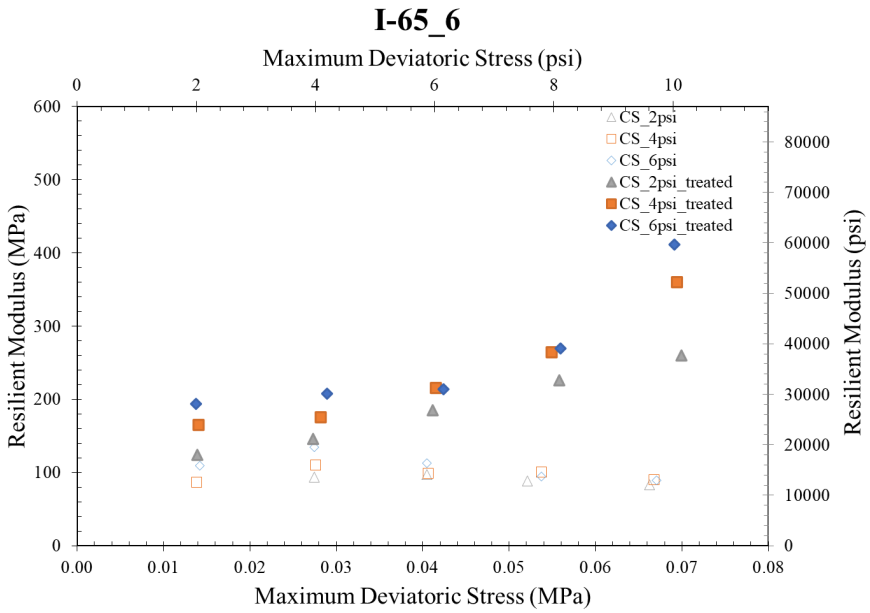

Figure B.6 Resilient modulus test results of I-65 soils (continued).

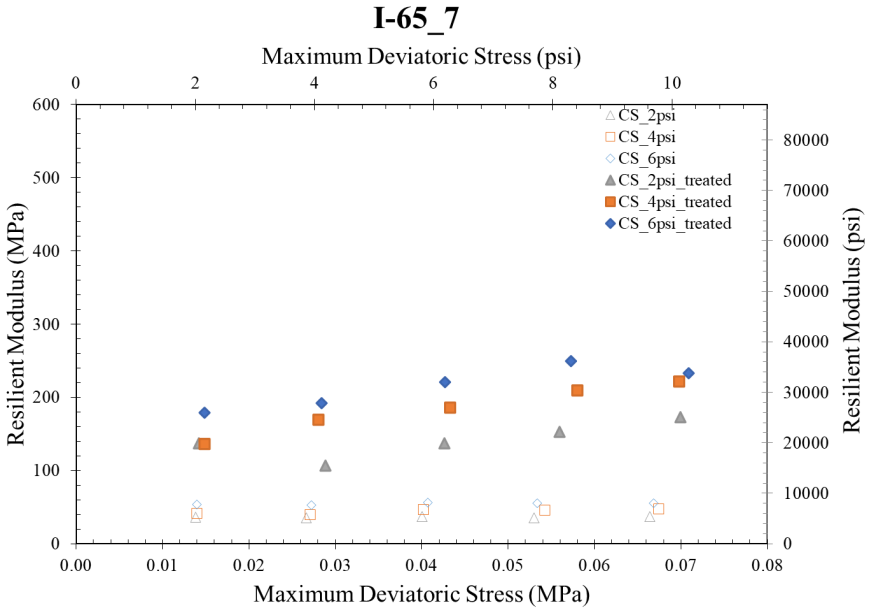

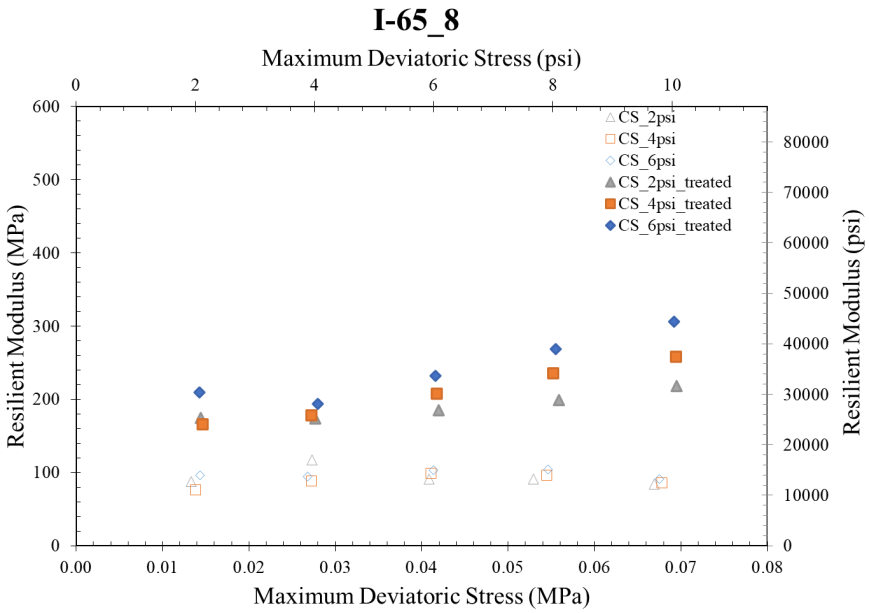

Figure B.6 Resilient modulus test results of I-65 soils (continued).

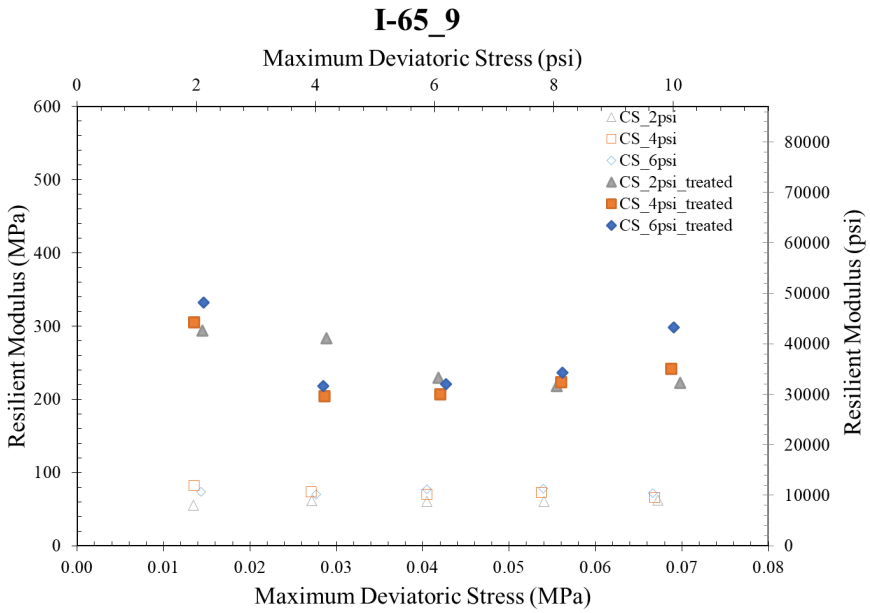

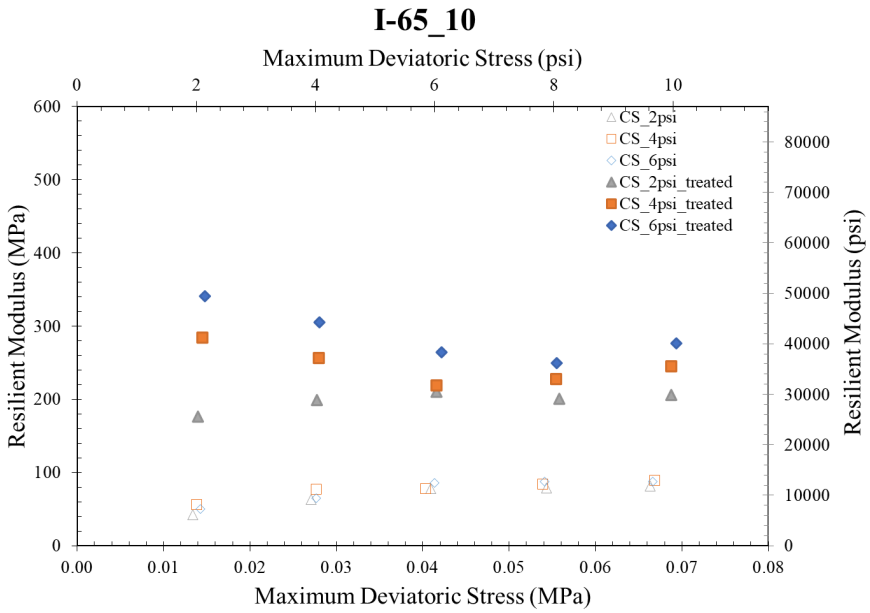

Figure B.6 Resilient modulus test results of I-65 soils (continued).

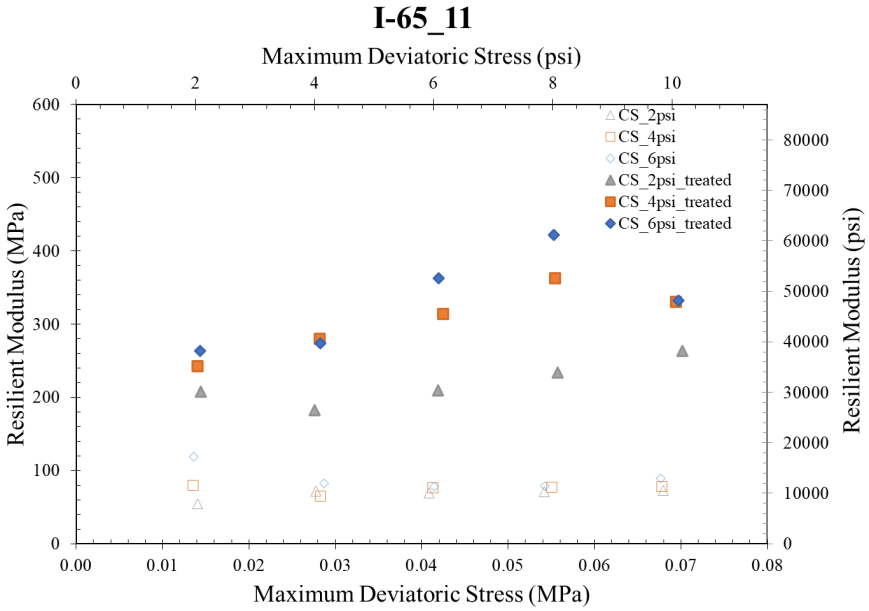

Figure B.6 Resilient modulus test results of I-65 soils (continued).

APPENDIX C. FWD DEFLECTION DATA

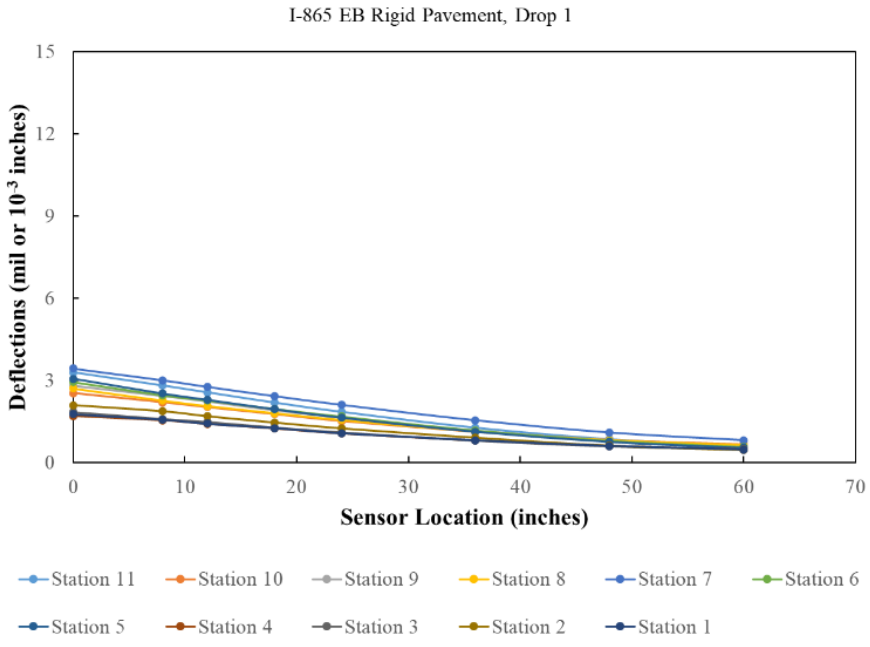

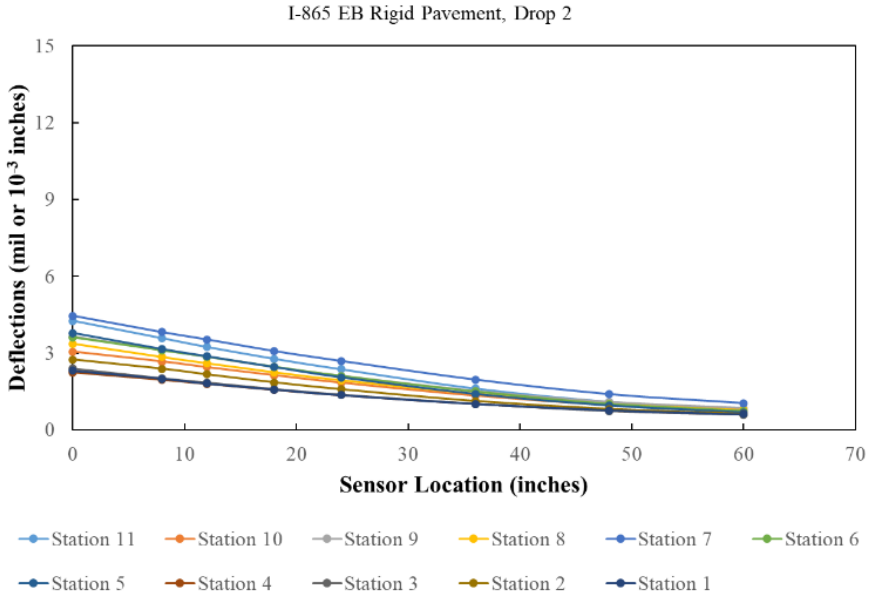

Figure C.1 FWD deflection data for Site 1: I-865 East Bound.

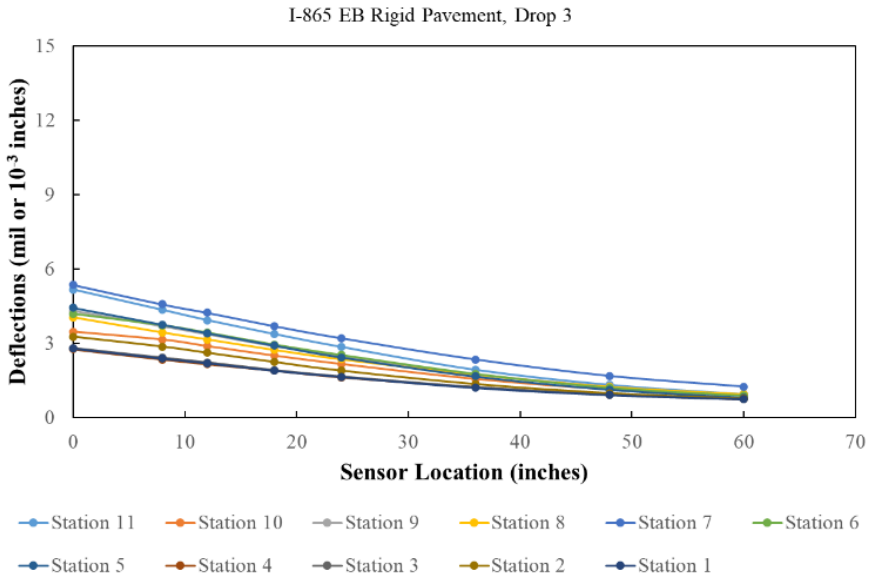

Figure C.1 FWD deflection data for Site 1: I-865 East Bound (continued).

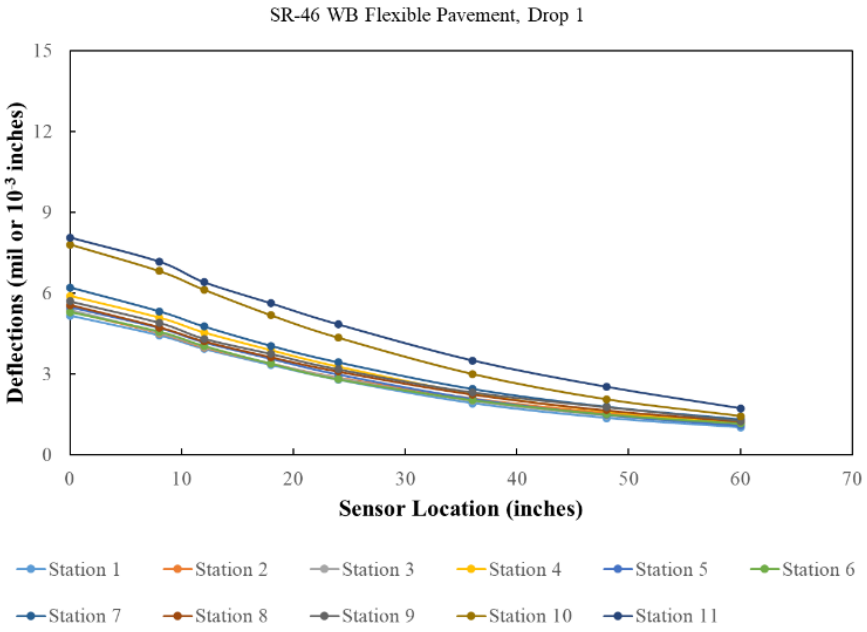

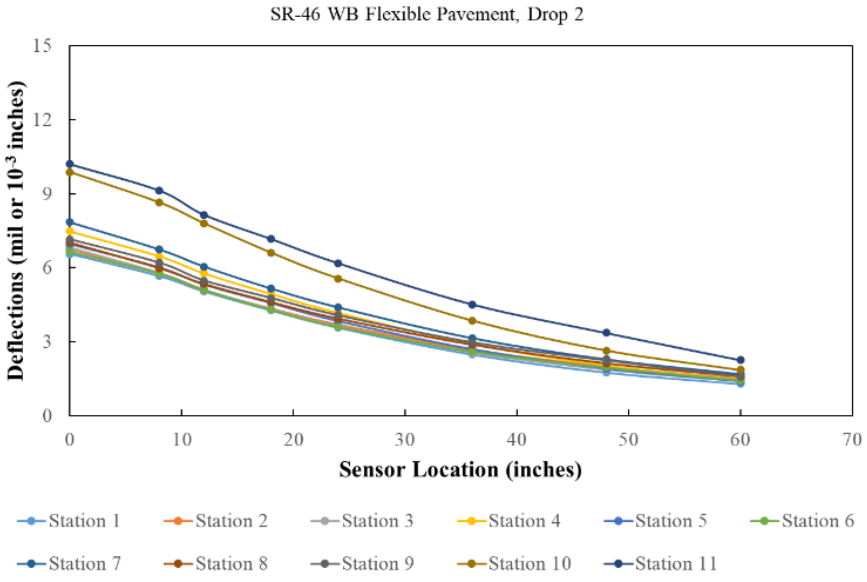

Figure C.2 FWD Deflection data for Site 2: SR-46 West Bound.

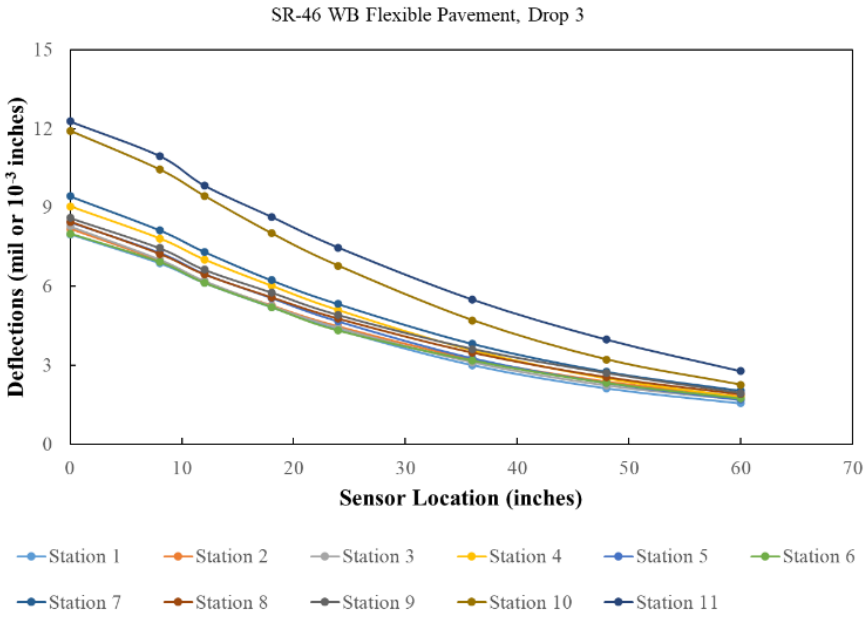

Figure C.2 FWD deflection data for Site 2: SR-46 West Bound (continued).

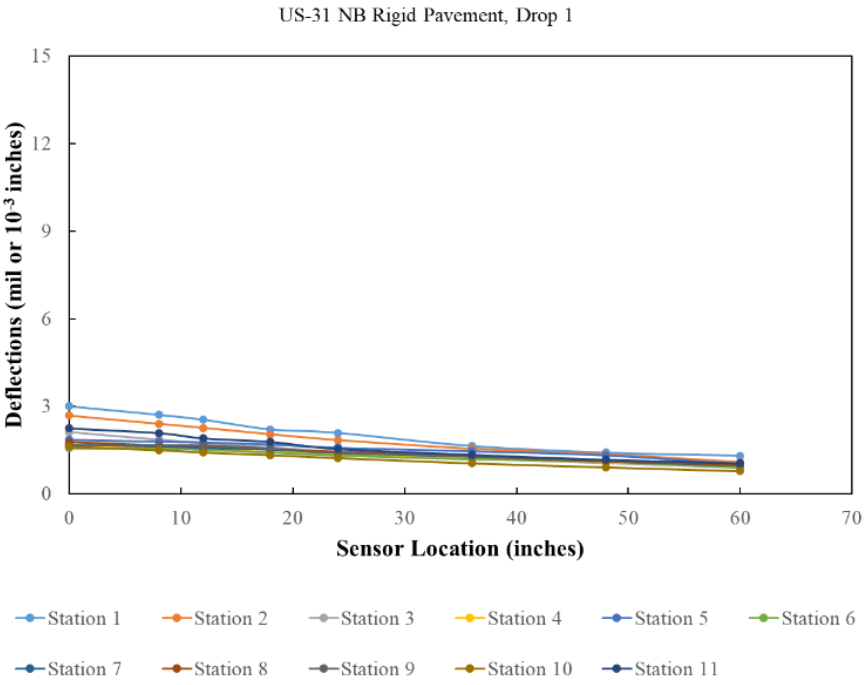

Figure C.3 FWD deflection data for Site 3: US-31 North Bound.

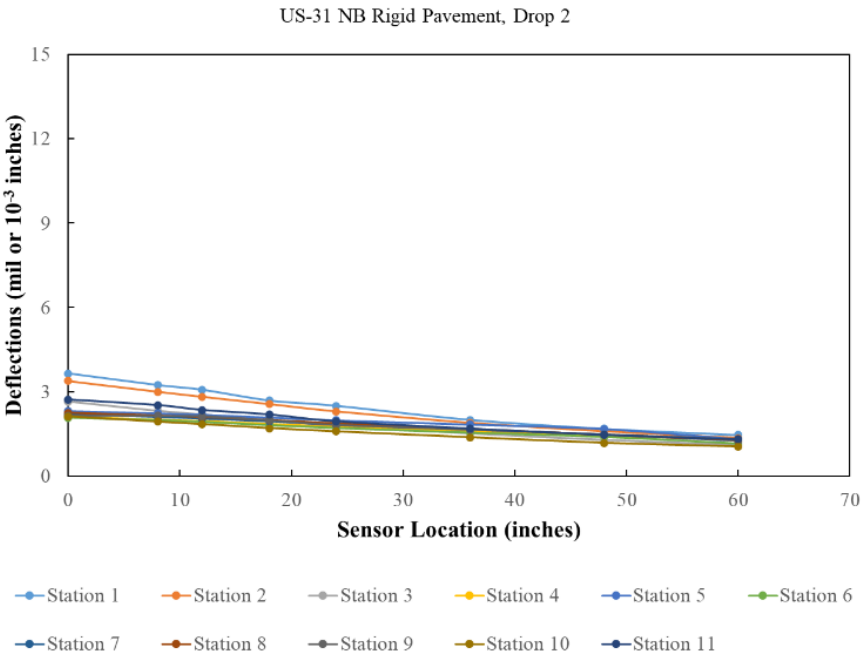

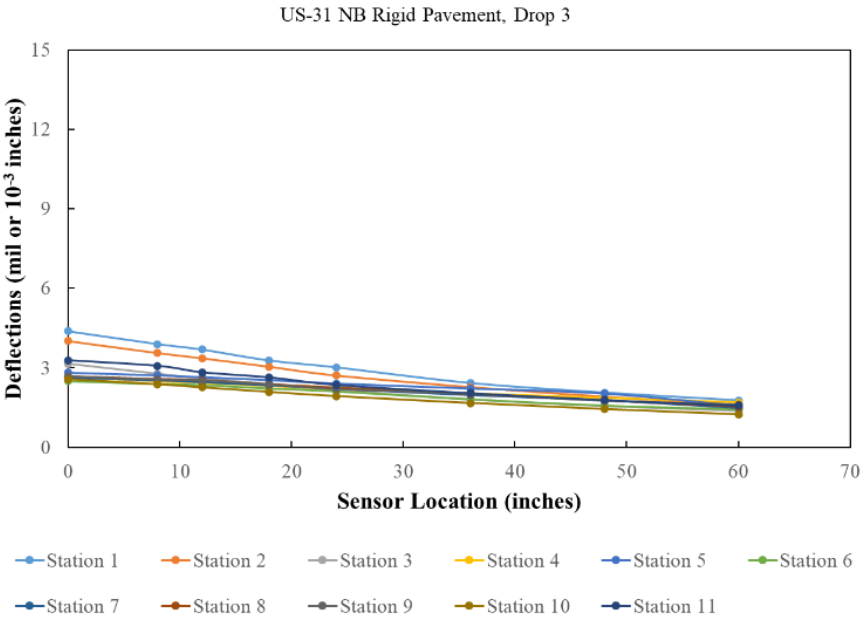

Figure C.3 FWD deflection data for Site 3: US-31 North Bound (continued).

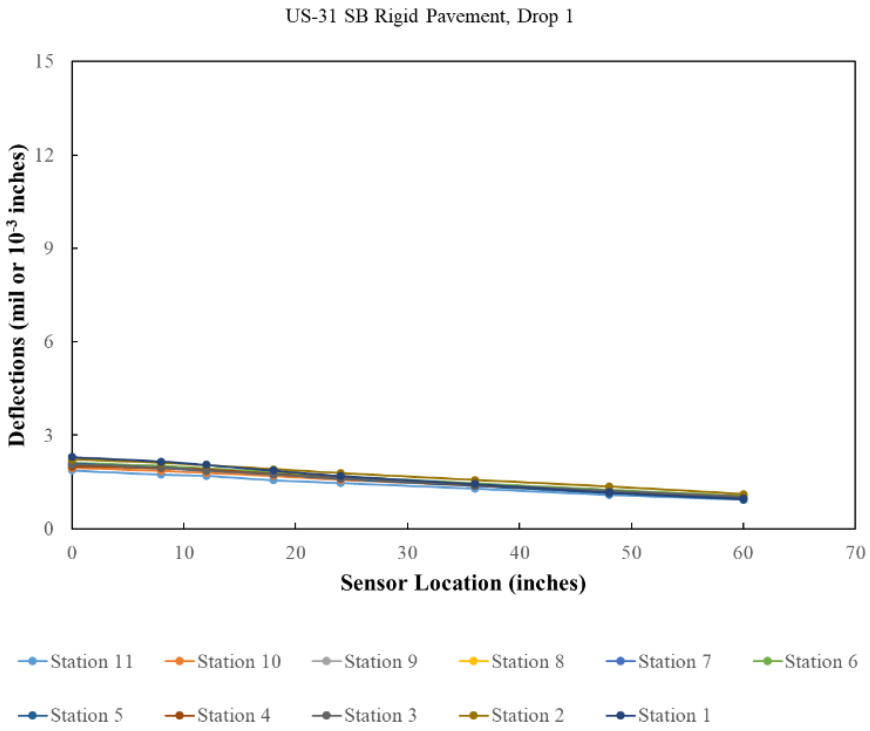

Figure C.4 FWD deflection data for Site 3: US-31 South Bound.

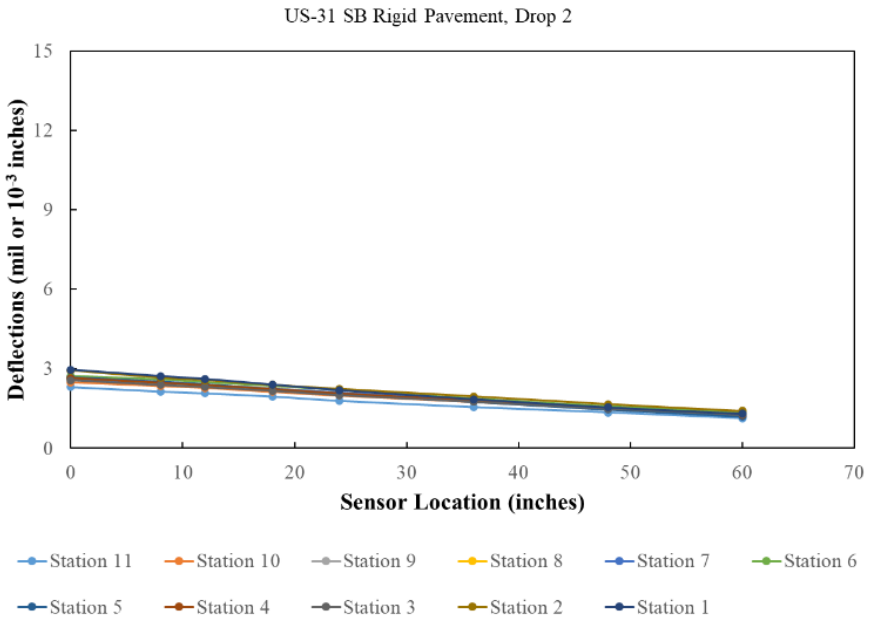

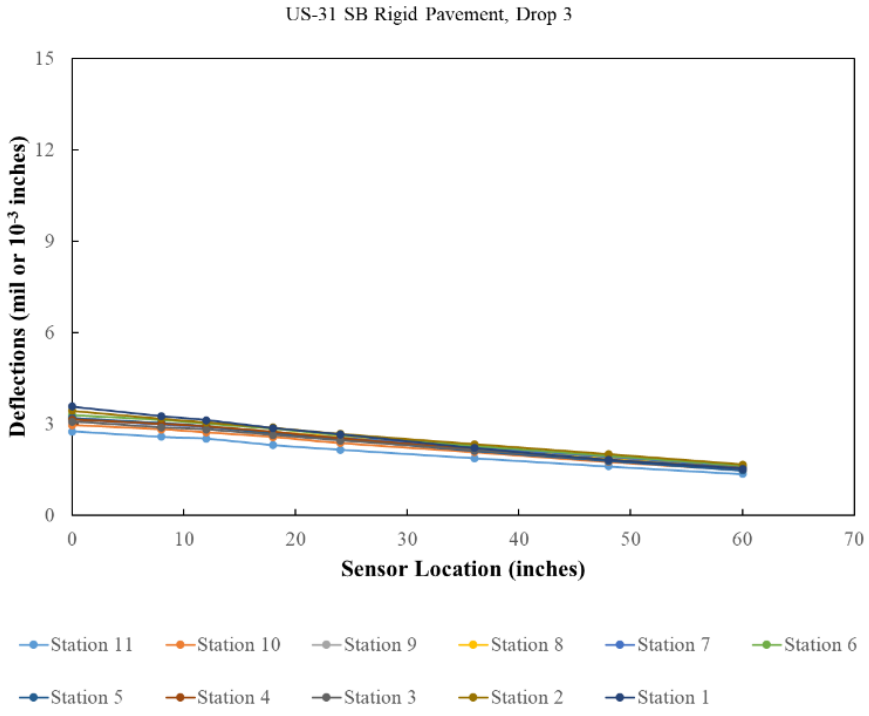

Figure C.4 FWD deflection data for Site 3: US-31 South Bound.

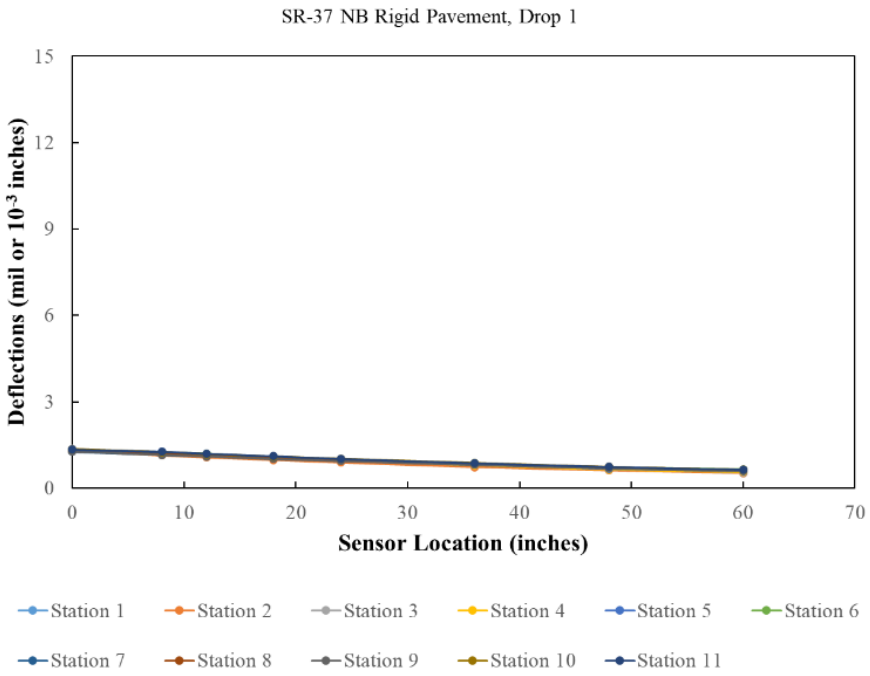

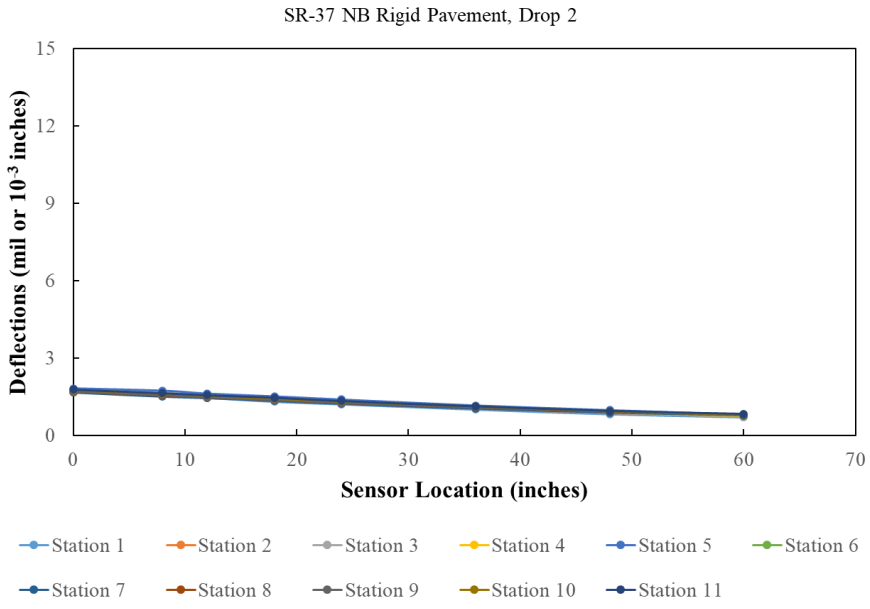

Figure C.5 FWD deflection data for Site 5: SR-37 North Bound.

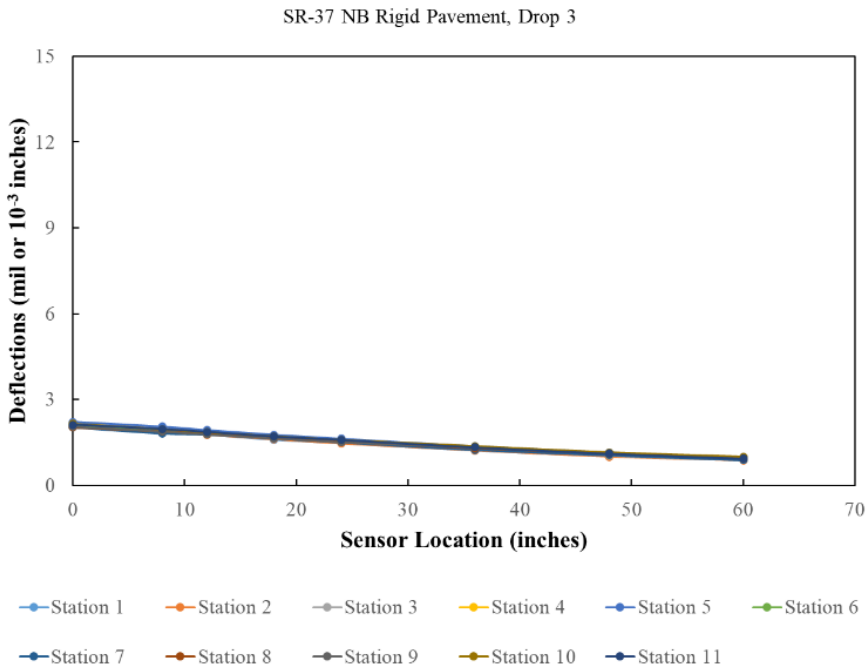

Figure C.5 FWD deflection data for Site 5: SR-37 North Bound (continued).

APPENDIX D. UZAN MODEL PARAMETERS

Uzan Model

$$log\left(\frac{M_R}{P_a}\right) = \log k_1 + k_2\, log\frac{\sigma_{bulk}}{P_a} + \; k_3\, log\frac{\sigma_{dev}}{P_a}$$

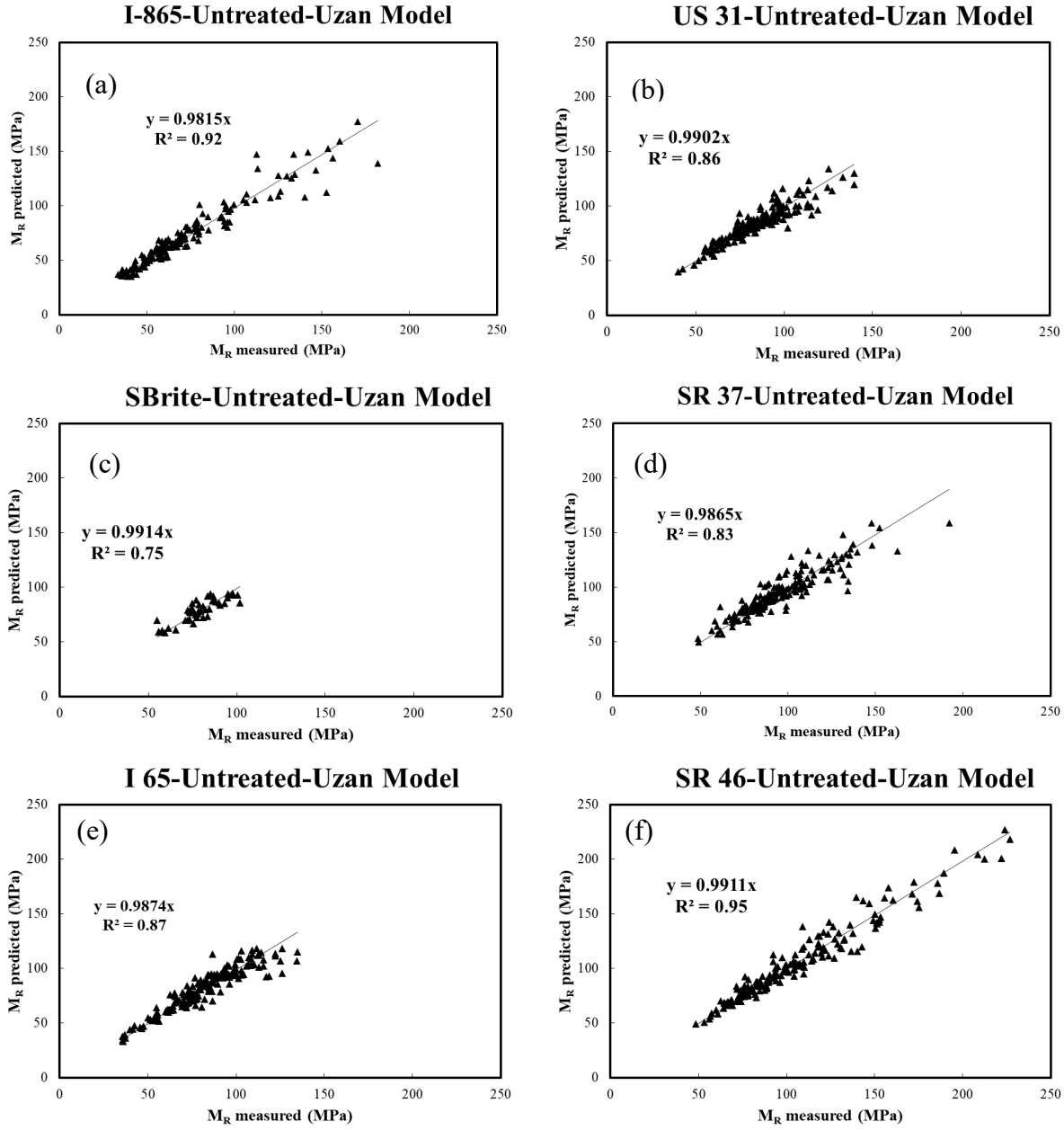

Figure D.1 Regression analysis results for Uzan Model. (a) I-865 untreated; (b) US-31 untreated; (c) S-BRITE Untreated; (d) SR-37 untreated; (e) I-65 untreated; (f) SR-46 untreated.

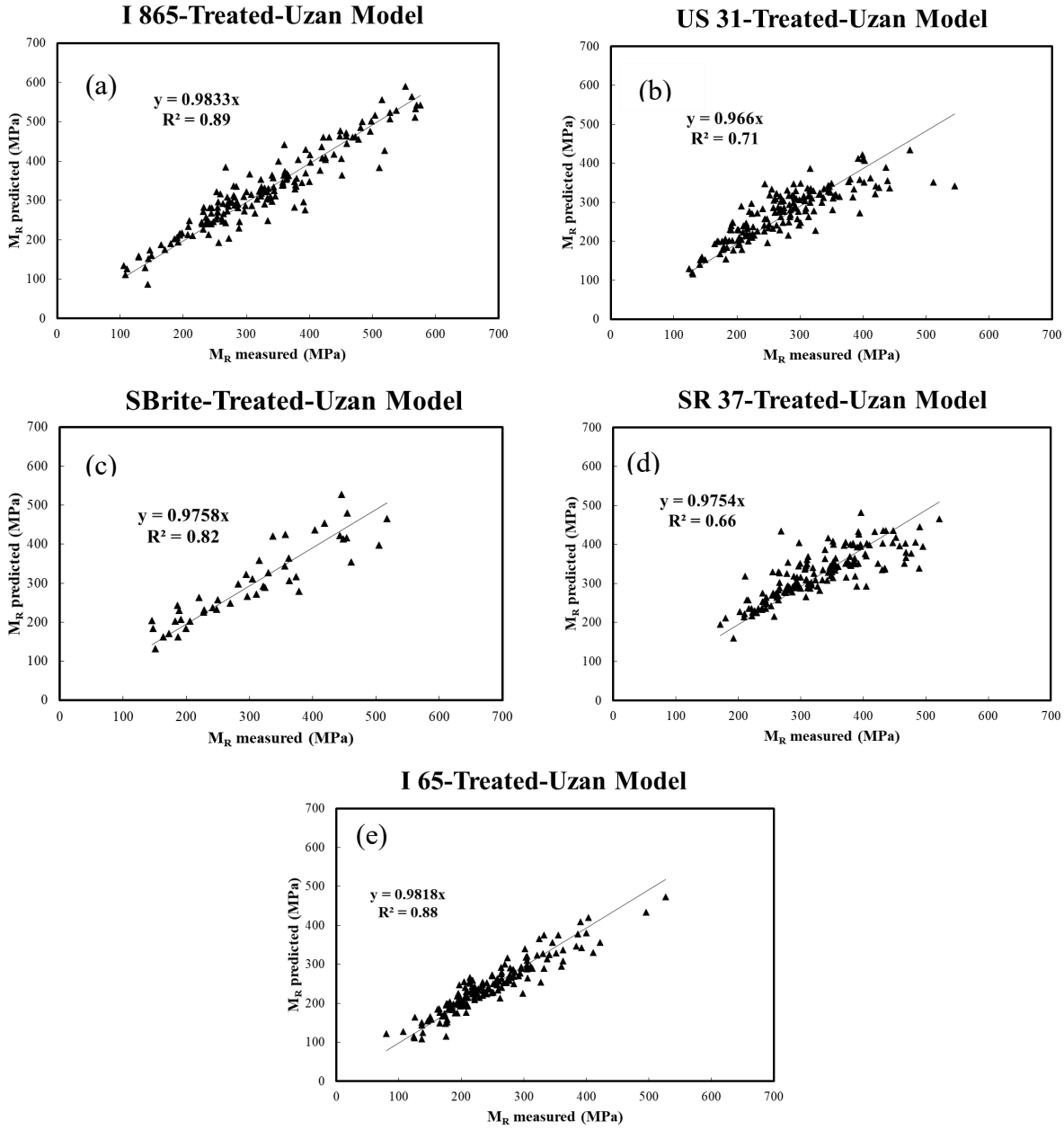

Figure D.2 Regression analysis results for Uzan Model. (a) I-865 treated; (b) US-31 treated; (c) S-BRITE treated; (d) SR-37 treated; (e) I-65 treated.

Table D.1 Results of Regression Analysis of Treated I-865 Soil Specimens

I-865–Treated				
	k_1	k_2	k_3	R^2
Sample 1	3,047.8	0.20	-0.13	0.34
Sample 2	2,811.5	0.27	-0.01	0.51
Sample 3	1,725.8	0.64	0.15	0.76
Sample 4	1,955.3	0.42	-0.14	0.36
Sample 5	2,779.4	0.26	-0.10	0.41
Sample 6	2,332.7	0.72	0.09	0.81
Sample 7	2,910.4	0.40	-0.14	0.49
Sample 8	4,283.7	0.23	-0.12	0.70
Sample 9	2,173.1	0.31	-0.17	0.40
Sample 10	3,669.2	0.23	-0.18	0.73
Sample 11	2,726.0	0.41	0.01	0.46

Table D.2 Results of Regression Analysis of Untreated I-865 Soil Specimens

I-865–Untreated				
	k_1	k_2	k_3	R^2
Sample 1	408.0	0.38	-0.45	0.72
Sample 2	255.3	0.96	-0.57	0.90
Sample 3	361.3	0.26	-0.07	0.57
Sample 4	562.9	0.20	-0.45	0.71
Sample 5	490.7	0.30	-0.09	0.55
Sample 6	442.5	0.40	-0.28	0.91
Sample 7	713.6	0.04	0.10	0.84
Sample 8	367.4	0.47	-0.32	0.74
Sample 9	905.1	0.59	-0.24	0.90
Sample 10	521.7	0.52	-0.40	0.78
Sample 11	272.6	0.87	-0.55	0.92

Table D.3 Results of Regression Analysis of Untreated SR-46 Soil Specimens

SR-46–Untreated				
	k_1	k_2	k_3	R^2
Sample 1	596.6	0.23	-0.31	0.73
Sample 2	397.7	0.41	-0.41	0.92
Sample 3	570.8	0.34	-0.34	0.85
Sample 4	632.6	0.23	-0.14	0.58
Sample 5	564.6	0.34	-0.30	0.90
Sample 6	906.2	0.40	-0.23	0.78
Sample 7	1,051.3	-0.06	-0.34	0.91
Sample 8	773.9	0.37	-0.21	0.72
Sample 9	1,232.3	0.37	-0.25	0.81
Sample 10	800.1	0.34	-0.28	0.68
Sample 11	692.3	0.27	-0.30	0.72

Table D.4 Results of Regression Analysis of Treated US-31 Soil Specimens

US-31–Treated				
	k_1	k_2	k_3	R^2
Sample 1	2,151.1	0.54	-0.11	0.55
Sample 2	1,227.6	1.07	-0.29	0.76
Sample 3	1,455.6	0.86	-0.28	0.70
Sample 4	3,029.6	0.23	-0.03	0.18
Sample 5	1,835.5	0.75	-0.26	0.67
Sample 6	1,757.0	0.25	-0.08	0.36
Sample 7	2,594.5	0.29	-0.16	0.43
Sample 8	2,269.0	0.10	-0.03	0.02
Sample 9	2,429.3	0.80	-0.14	0.94
Sample 10	2,874.0	0.05	-0.08	0.20
Sample 11	2,787.2	0.32	0.10	0.87

Table D.5 Results of Regression Analysis of Untreated US-31 Soil Specimens

US-31–Untreated				
	k_1	k_2	k_3	R^2
Sample 1	524.1	0.63	-0.25	0.94
Sample 2	509.1	0.52	-0.32	0.82
Sample 3	465.8	0.80	-0.16	0.93
Sample 4	636.8	0.50	-0.07	0.83
Sample 5	778.1	0.23	-0.05	0.39
Sample 6	705.0	0.24	-0.24	0.64
Sample 7	573.8	0.64	-0.30	0.91
Sample 8	630.2	0.38	-0.05	0.85
Sample9	561.4	0.43	-0.30	0.57
Sample 10	769.6	0.39	-0.21	0.74
Sample 11	687.2	0.34	-0.26	0.76

Table D.6 Results of Regression Analysis of Treated S-BRITE Soil Specimens

S-BRITE–Treated				
	k_1	k_2	k_3	R^2
Sample 1	4,696.7	0.42	0.44	0.72
Sample 2	2,339.4	0.91	-0.15	0.86
Sample 3	2,760.3	0.36	0.27	0.79

Table D.7 Results of Regression Analysis of Untreated S-BRITE Soil Specimens

S-BRITE–Untreated				
	k_1	k_2	k_3	R^2
Sample 1	763.1	0.27	-0.06	0.57
Sample 2	928.0	0.12	0.17	0.59
Sample 3	532.3	0.45	-0.20	0.84

Table D.8 Results of Regression Analysis of Treated SR-37 Soil Specimens

SR-37–Treated				
	k_1	k_2	k_3	R^2
Sample 1	2,708.5	0.38	0.01	0.60
Sample 2	2,983.2	0.51	0.01	0.65
Sample 3	1,984.9	0.63	-0.28	0.70
Sample 4	2,821.4	0.50	-0.10	0.36
Sample 5	2,468.0	0.35	-0.19	0.35
Sample 6	2,671.4	0.53	-0.15	0.76
Sample 7	3,396.7	0.31	-0.08	0.76
Sample 8	2,671.8	0.84	0.01	0.65
Sample 9	2,220.0	0.28	-0.35	0.53
Sample 10	1,970.3	0.70	-0.25	0.67
Sample 11	2,321.8	0.44	-0.14	0.73

Table D.9 Results of Regression Analysis of Untreated SR-37 Soil Specimens

SR-37–Untreated				
	k_1	k_2	k_3	R^2
Sample 1	785.6	0.49	-0.14	0.71
Sample 2	634.9	0.37	-0.36	0.90
Sample 3	751.8	0.28	-0.11	0.50
Sample 4	581.8	0.55	-0.08	0.66
Sample 5	581.0	0.59	-0.31	0.84
Sample 6	702.6	0.35	-0.23	0.84
Sample 7	684.5	0.34	-0.19	0.40
Sample 8	642.2	0.61	-0.36	0.77
Sample 9	661.0	0.40	-0.04	0.84
Sample 10	799.3	0.46	-0.27	0.85
Sample 11	887.3	0.42	-0.21	0.59

Table D.10 Results of Regression Analysis of Treated I-65 Soil Specimens

I 65–Treated				
	k_1	k_2	k_3	R^2
Sample 1	3,509.4	0.55	0.43	0.94
Sample 2	2,991.2	0.02	0.49	0.68
Sample 3	2,029.4	0.36	-0.03	0.53
Sample 4	2,174.6	0.43	-0.07	0.94
Sample 5	2,398.6	0.36	-0.29	0.80
Sample 6	2,700.1	0.46	0.29	0.81
Sample 7	1,654.1	0.58	0.05	0.90
Sample 8	2,265.7	0.30	0.13	0.81
Sample 9	2,028.0	0.05	-0.17	0.37
Sample 10	1,721.9	0.54	-0.23	0.89
Sample 11	2,626.7	0.55	0.04	0.76

Table D.11 Results of Regression Analysis of Untreated I-65 Soil Specimens

I 65–Untreated				
	k_1	k_2	k_3	R^2
Sample 1	876.7	0.29	0.07	0.51
Sample 2	1,171.7	0.14	0.23	0.79
Sample 3	427.7	0.50	-0.42	0.90
Sample 4	986.3	0.15	-0.06	0.29
Sample 5	612.1	0.19	-0.16	0.64
Sample6	827.4	0.10	-0.15	0.27
Sample 7	360.8	0.53	-0.11	0.92
Sample 8	937.3	0.01	0.02	0.01
Sample 9	579.5	0.31	-0.11	0.67
Sample 10	983.7	0.12	0.33	0.88
Sample 11	617.9	0.41	-0.14	0.57

APPENDIX E. OCTAHEDRAL STRESS MODEL PARAMETERS

Octahedral Stress Model

$$log\left(\frac{M_R}{P_a}\right) = \log k_1 + k_2\, log\frac{\sigma_{bulk}}{P_a} + k_3 \log\left(\frac{\tau_{oct}}{P_a} + 1\right)$$

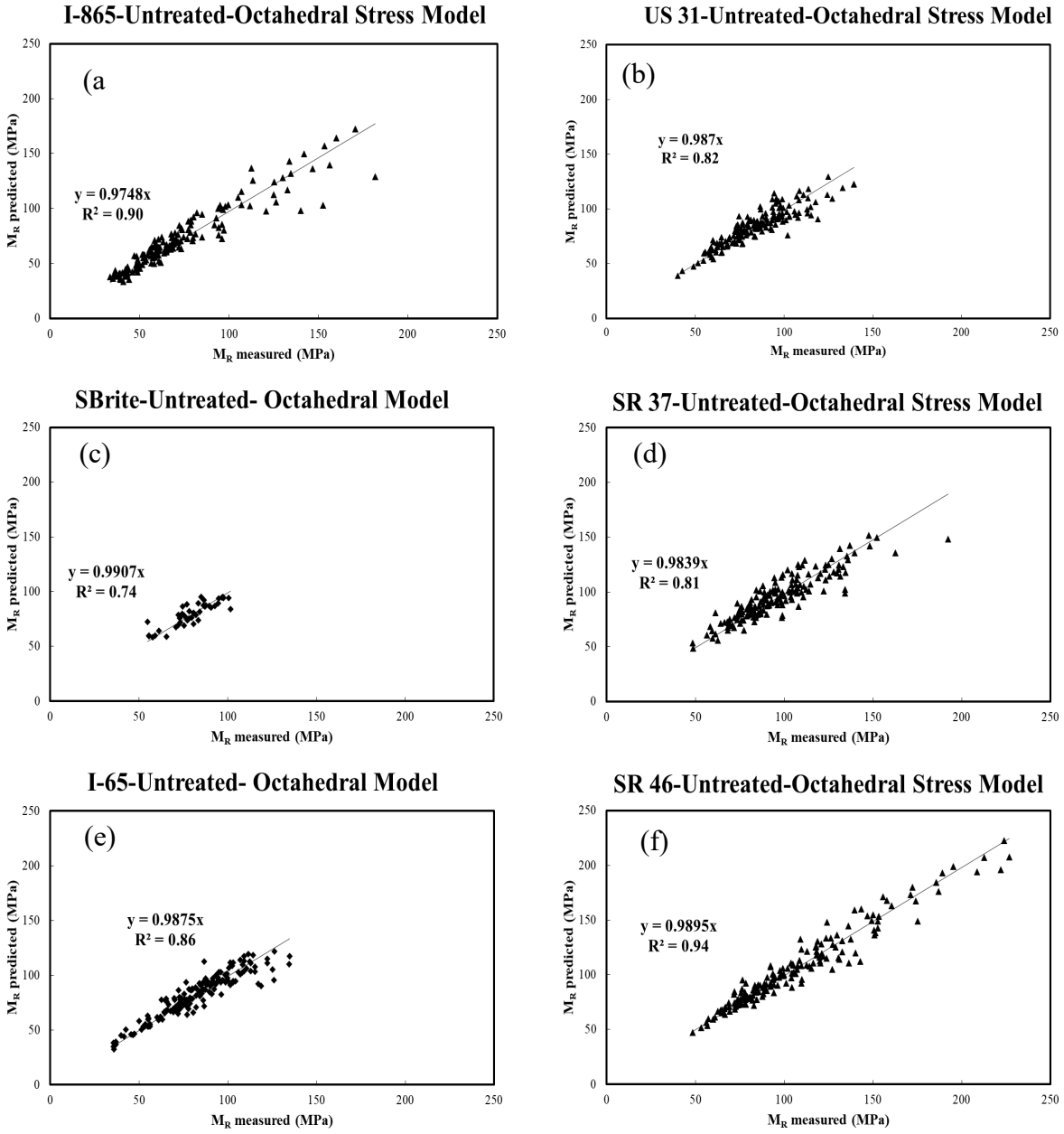

Figure E.1 Regression analysis results for Octahedral Stress Model. (a) I-865 untreated; (b) US-31 untreated; (c) S-BRITE untreated; (d) SR-37 untreated; (e) I-65 untreated; (f) SR-46 untreated.

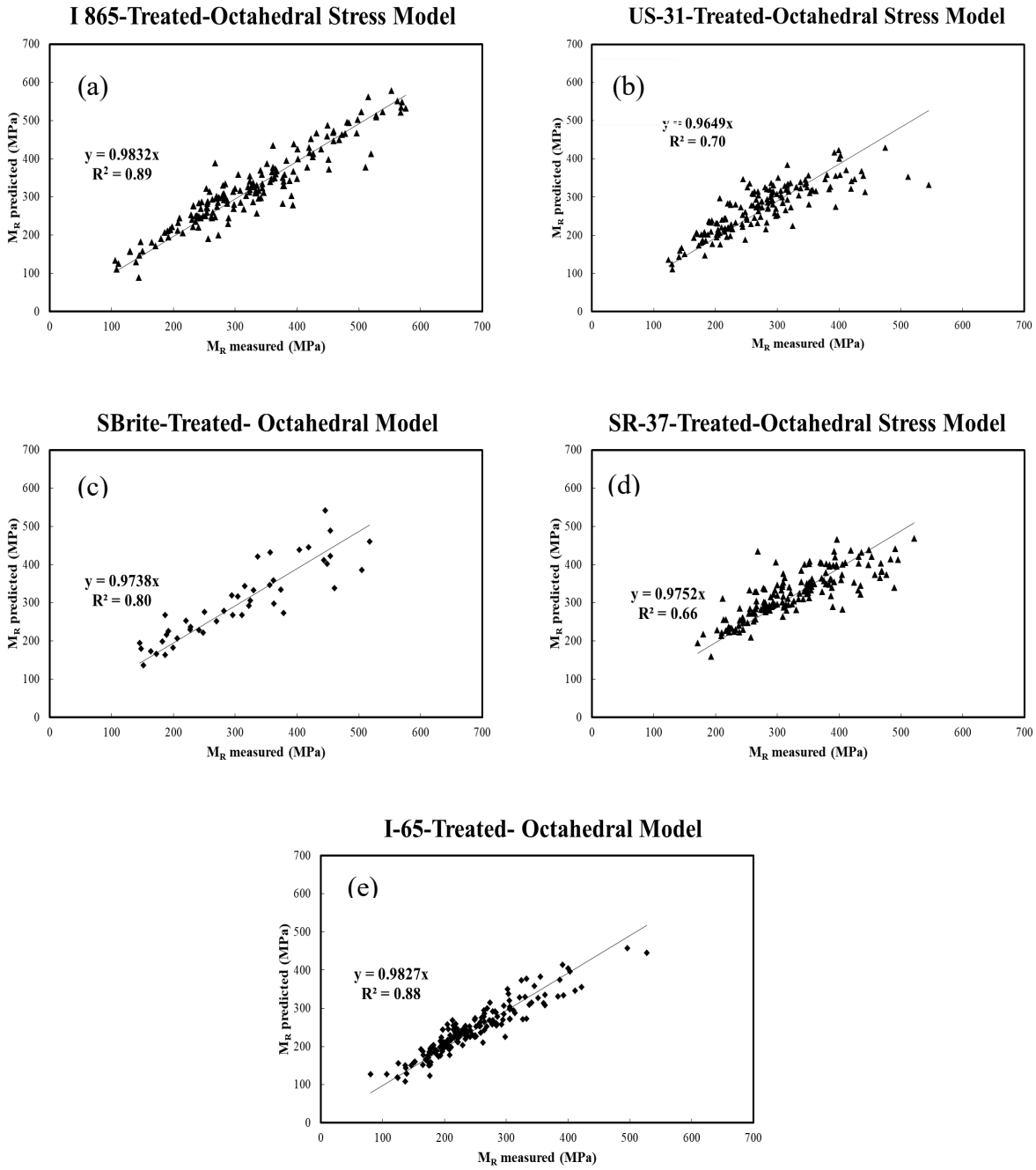

Figure E.2 Regression analysis results for Octahedral Stress Model. (a) I-865 treated; (b) US-31 treated; (c) S-BRITE treated; (d) SR-37 treated; (e) I-65 treated.

Table E.1 Results of Regression Analysis of Treated I-865 Soil Specimens

I-865–Treated				
	k_1	k_2	k_3	R^2
Sample 1	4,059.4	0.19	-0.84	0.27
Sample 2	2,856.3	0.27	-0.03	0.51
Sample 3	1,171.0	0.61	1.35	0.78
Sample 4	2,674.5	0.41	-0.96	0.36
Sample 5	3,409.3	0.25	-0.59	0.38
Sample 6	1,841.3	0.70	0.86	0.83
Sample 7	4,061.0	0.40	-1.07	0.49
Sample 8	5,597.8	0.23	-0.84	0.67
Sample 9	3,213.8	0.31	-1.26	0.42
Sample 10	5,507.8	0.23	-1.28	0.71
Sample 11	2,667.3	0.40	0.08	0.46

Table E.2 Results of Regression Analysis of Untreated I-865 Soil Specimens

I-865–Untreated				
	k_1	k_2	k_3	R^2
Sample 1	1,117.9	0.34	-3.09	0.61
Sample 2	937.0	0.93	-4.08	0.79
Sample 3	409.6	0.24	-0.28	0.50
Sample 4	1,568.8	0.18	-3.20	0.64
Sample 5	601.2	0.29	-0.63	0.53
Sample 6	847.6	0.40	-2.07	0.87
Sample 7	574.3	0.05	0.69	0.80
Sample 8	762.9	0.46	-2.32	0.73
Sample 9	1,585.9	0.59	-1.81	0.91
Sample 10	1,269.1	0.50	-2.76	0.72
Sample 11	946.9	0.84	-3.90	0.80

Table E.3 Results of Regression Analysis of Untreated SR-46 Soil Specimens

SR-46–Untreated				
	k_1	k_2	k_3	R^2
Sample 1	1,185.0	0.22	-2.12	0.62
Sample 2	1,011.7	0.41	-2.99	0.85
Sample 3	1,263.5	0.34	-2.56	0.84
Sample 4	879.3	0.24	-1.08	0.59
Sample 5	1,137.4	0.34	-2.29	0.93
Sample 6	1,559.1	0.41	-1.82	0.86
Sample 7	2,285.2	-0.07	-2.45	0.87
Sample 8	1,240.2	0.36	-1.47	0.66
Sample 9	2,218.6	0.37	-1.92	0.85
Sample 10	1,509.2	0.33	-2.01	0.62
Sample 11	1,399.2	0.27	-2.27	0.73

Table E.4 Results of Regression Analysis of Treated US-31 Soil Specimens

US-31–Treated				
	k_1	k_2	k_3	R^2
Sample 1	2,880.5	0.58	-1.07	0.61
Sample 2	2,322.6	1.05	-1.94	0.74
Sample 3	2,676.8	0.83	-1.80	0.63
Sample 4	3,225.5	0.23	-0.21	0.18
Sample 5	3,229.5	0.73	-1.71	0.64
Sample 6	2,080.4	0.24	-0.51	0.35
Sample 7	3,749.1	0.30	-1.20	0.47
Sample 8	2,226.8	0.04	0.32	0.03
Sample 9	3,269.6	0.78	-0.88	0.93
Sample 10	3,376.1	0.04	-0.43	0.17
Sample 11	2,197.6	0.31	0.77	0.88

Table E.5 Results of Regression Analysis of Untreated US-31 Soil Specimens

US-31–Untreated				
	k_1	k_2	k_3	R^2
Sample 1	943.0	0.63	-1.89	0.95
Sample 2	1,051.8	0.50	-2.23	0.70
Sample 3	669.7	0.80	-1.15	0.92
Sample 4	745.3	0.51	-0.51	0.84
Sample 5	877.2	0.24	-0.40	0.40
Sample 6	1,209.0	0.23	-1.67	0.54
Sample 7	1,104.5	0.61	-1.99	0.80
Sample 8	693.2	0.36	-0.24	0.83
Sample 9	1,075.9	0.40	-1.97	0.49
Sample 10	1,247.8	0.38	-1.51	0.69
Sample 11	1,223.8	0.32	-1.75	0.61

Table E.6 Results of Regression Analysis of Treated S-BRITE Soil Specimens

S-BRITE–Treated				
	k_1	k_2	k_3	R^2
Sample 1	1,870.3	0.47	2.68	0.64
Sample 2	3,275.0	0.91	-1.04	0.85
Sample 3	1,410.4	0.32	2.32	0.85

Table E.7 Results of Regression Analysis of Untreated S-BRITE Soil Specimens

S-BRITE–Untreated				
	k_1	k_2	k_3	R^2
Sample 1	890.9	0.28	-0.52	0.60
Sample 2	642.4	0.14	1.08	0.52
Sample 3	842.6	0.46	-1.52	0.88

Table E.8 Results of Regression Analysis of Treated SR-37 Soil Specimens

SR-37–Treated				
	k_1	k_2	k_3	R^2
Sample 1	2,619.3	0.37	0.17	0.61
Sample 2	2,893.8	0.49	0.15	0.66
Sample 3	3,691.3	0.62	-1.94	0.68
Sample 4	3,614.0	0.51	-0.86	0.38
Sample 5	3,579.7	0.31	-1.01	0.25
Sample 6	3,769.8	0.53	-1.11	0.77
Sample 7	4,103.0	0.31	-0.59	0.75
Sample 8	2,557.6	0.83	0.19	0.65
Sample 9	4,992.9	0.29	-2.60	0.58
Sample 10	3,585.9	0.71	-1.97	0.72
Sample 11	3,098.4	0.43	-0.85	0.68

Table E.9 Results of Regression Analysis of Untreated SR-37 Soil Specimens

SR-37–Untreated				
	k_1	k_2	k_3	R^2
Sample 1	1,065.2	0.47	-0.88	0.67
Sample 2	1,457.7	0.36	-2.63	0.76
Sample 3	974.2	0.28	-0.86	0.53
Sample 4	674.1	0.52	-0.33	0.62
Sample 5	1,170.7	0.58	-2.22	0.84
Sample 6	1,186.8	0.34	-1.62	0.74
Sample 7	1,055.8	0.34	-1.40	0.42
Sample 8	1,426.8	0.58	-2.46	0.68
Sample 9	699.7	0.38	-0.09	0.83
Sample 10	1,471.7	0.45	-1.91	0.81
Sample 11	1,428.5	0.41	-1.51	0.58

Table E.10 Results of Regression Analysis of Treated I-65 Soil Specimens

I 65–Treated				
	k_1	k_2	k_3	R^2
Sample 1	1,295.3	0.54	3.19	0.95
Sample 2	978.0	0.01	3.57	0.71
Sample 3	2,109.8	0.34	-0.03	0.53
Sample 4	2,535.8	0.43	-0.47	0.93
Sample 5	4,498.4	0.33	-1.87	0.64
Sample 6	1,307.4	0.43	2.46	0.89
Sample 7	1,471.9	0.57	0.41	0.90
Sample 8	1,644.3	0.29	1.09	0.85
Sample 9	2,849.3	0.01	-0.92	0.23
Sample 10	2,932.6	0.53	-1.67	0.85
Sample 11	2,398.0	0.55	0.29	0.75

Table E.11 Results of Regression Analysis of Untreated I-65 Soil Specimens

I 65–Untreated				
	k_1	k_2	k_3	R^2
Sample 1	756.9	0.30	0.40	0.50
Sample 2	682.5	0.13	1.77	0.81
Sample 3	1,152.6	0.51	-3.23	0.93
Sample 4	1,163.1	0.16	-0.59	0.37
Sample 5	871.8	0.17	-1.05	0.46
Sample 6	1,214.1	0.12	-1.33	0.36
Sample 7	468.5	0.54	-0.85	0.92
Sample 8	927.5	0.04	-0.07	0.01
Sample 9	746.6	0.31	-0.83	0.67
Sample 10	475.3	0.15	2.24	0.79
Sample 11	832.7	0.39	-0.90	0.50

APPENDIX F. BACKCALCULATION ANALYSIS FOR RIGID PAVEMENTS

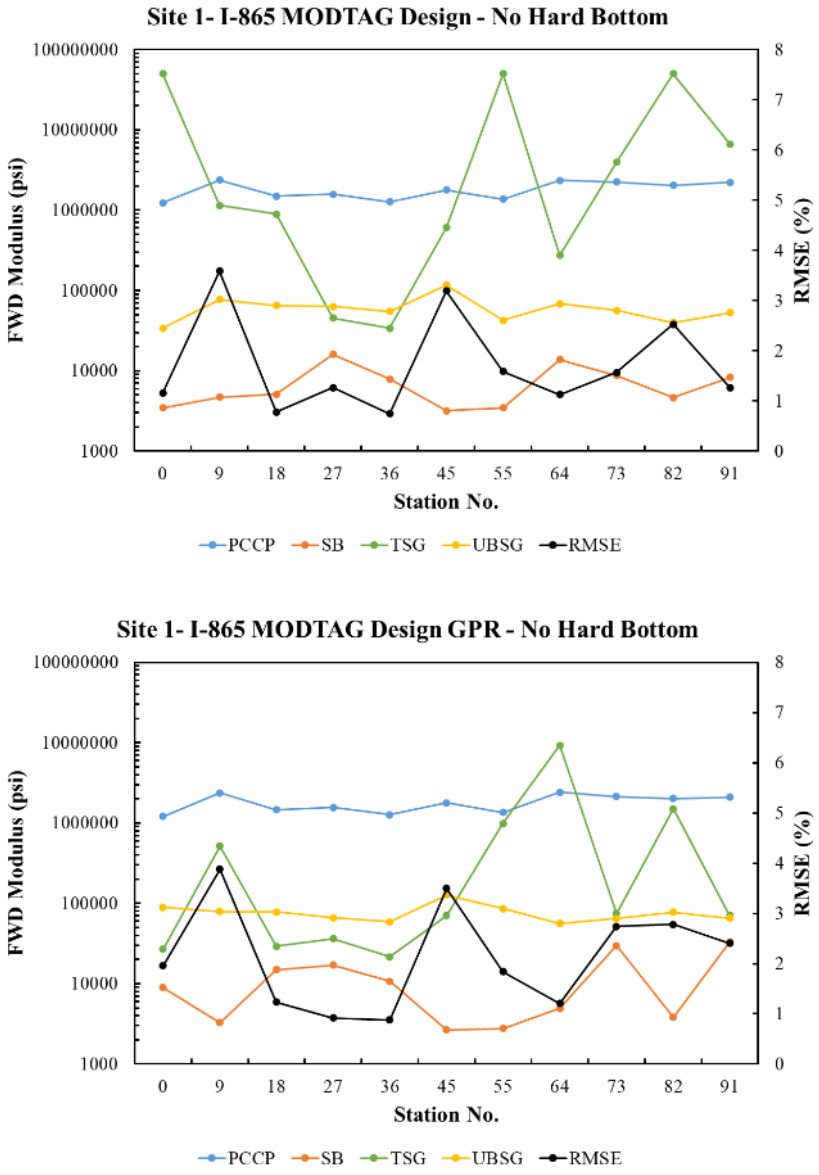

Figure F.1 I-865 Backcalculation analysis—effect of pavement thickness.

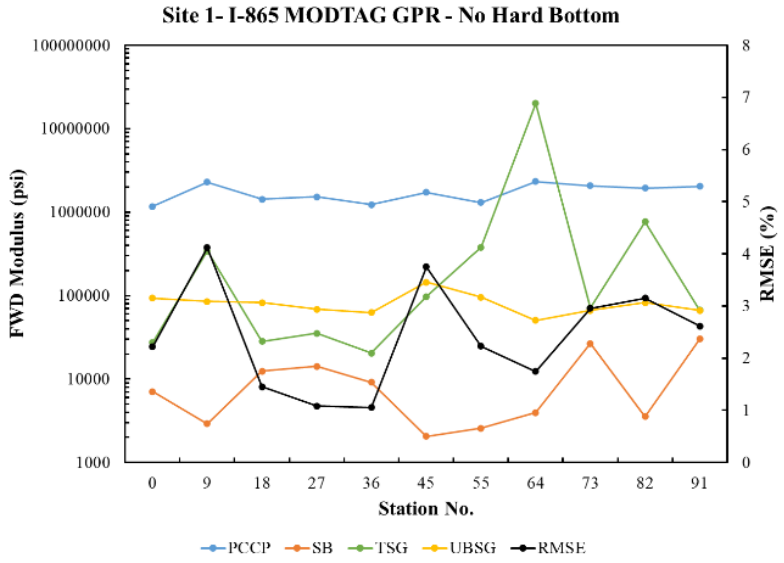

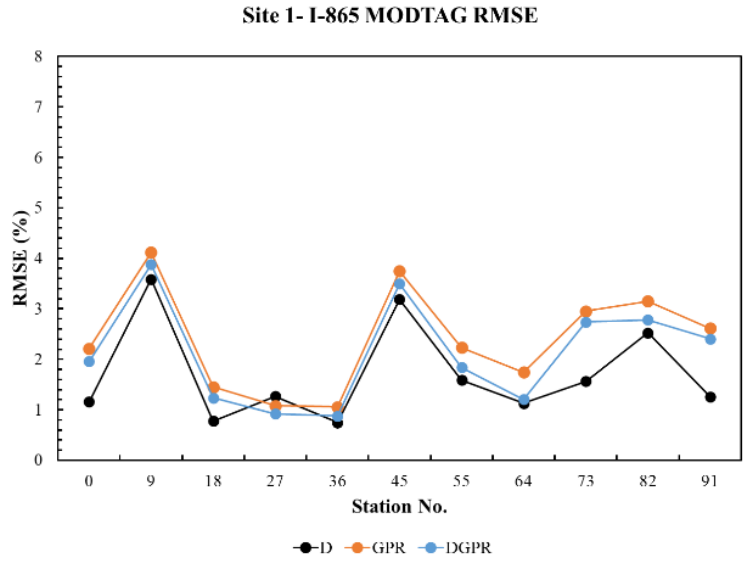

Figure F.1 I-865 Backcalculation analysis—effect of pavement thickness (continued).

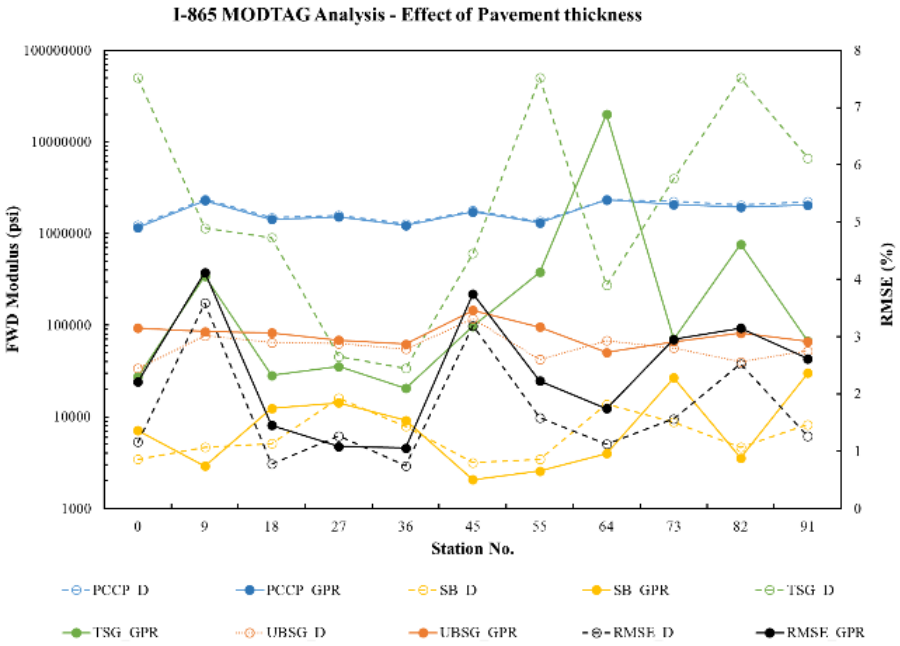

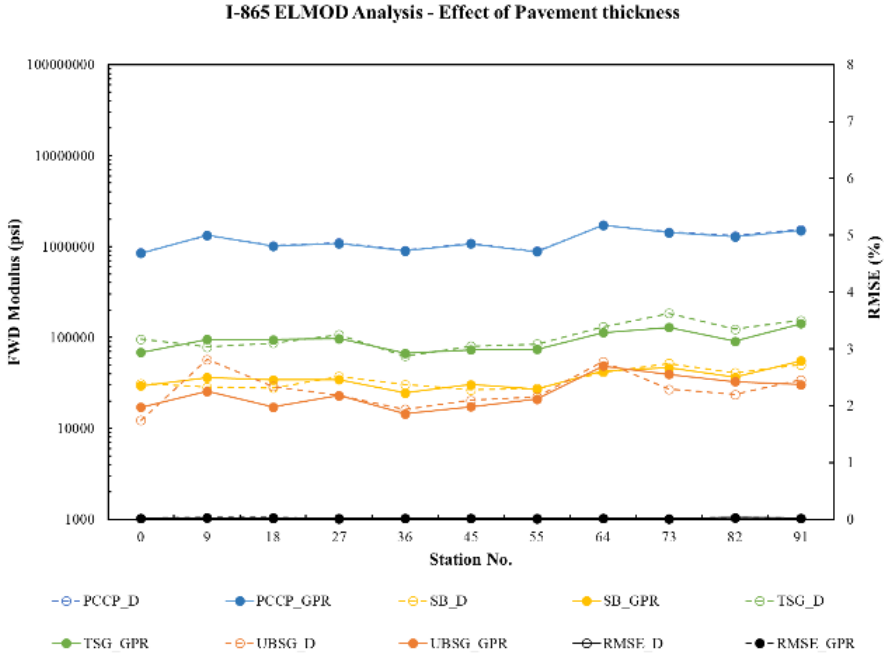

Figure F.1 I-865 Backcalculation analysis—effect of pavement thickness (continued).

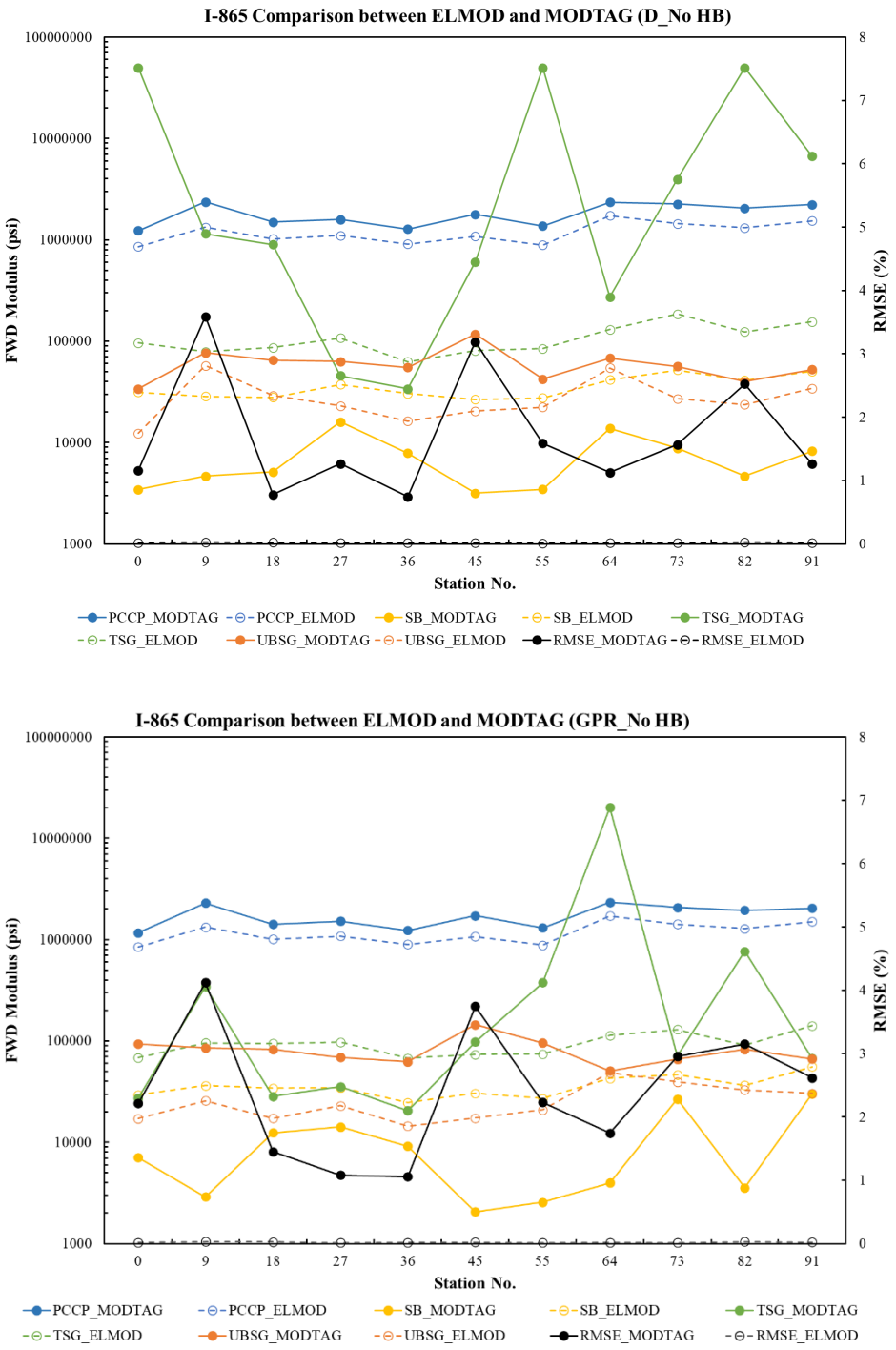

Figure F.2 I-865—comparison between ELMOD and MODTAG.

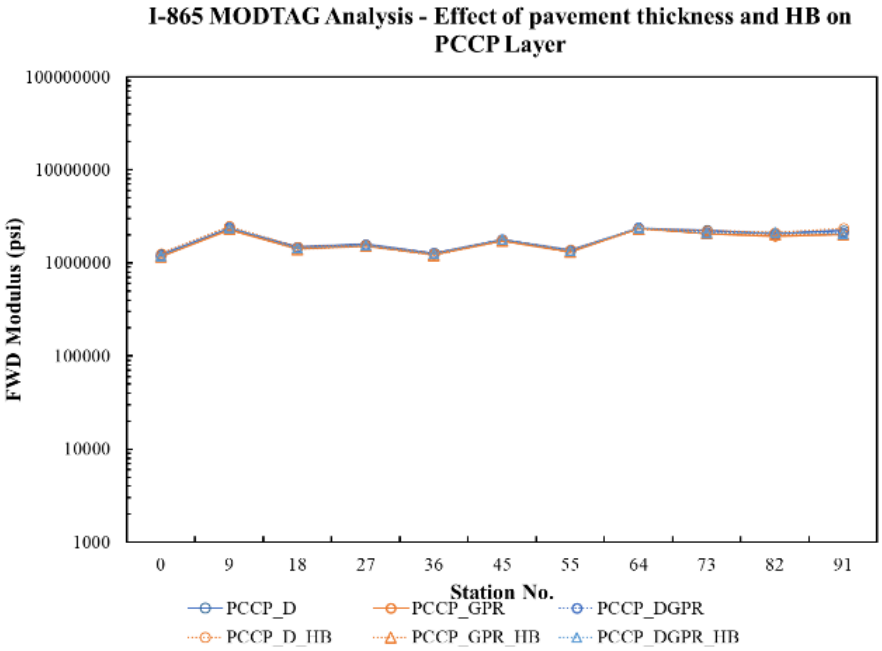

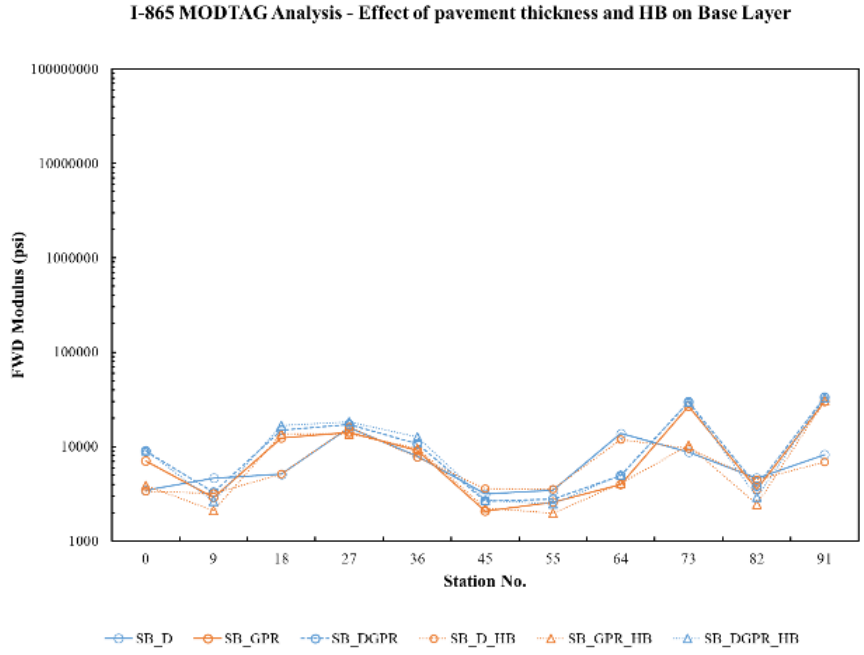

Figure F.2 I-865—comparison between ELMOD and MODTAG (continued).

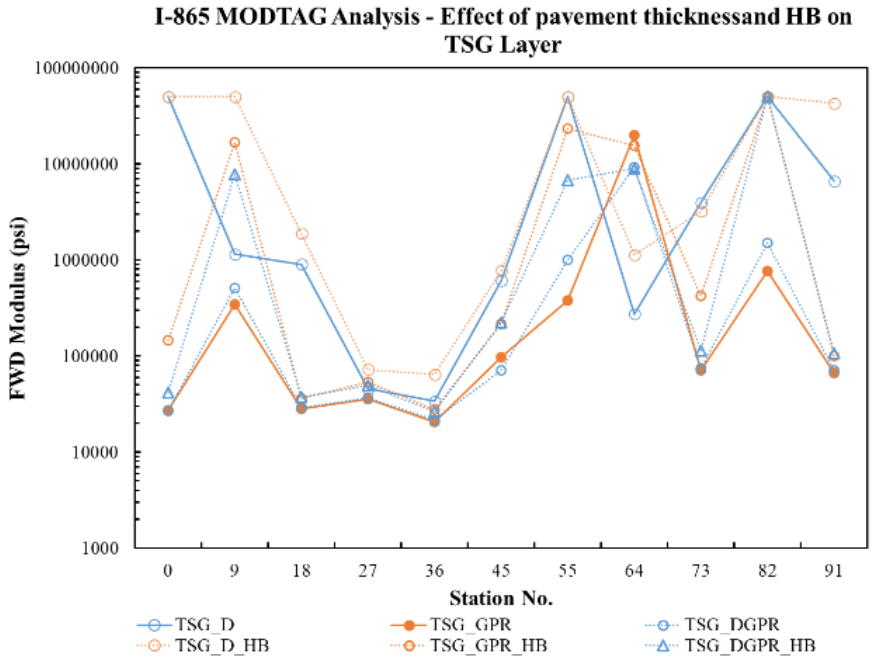

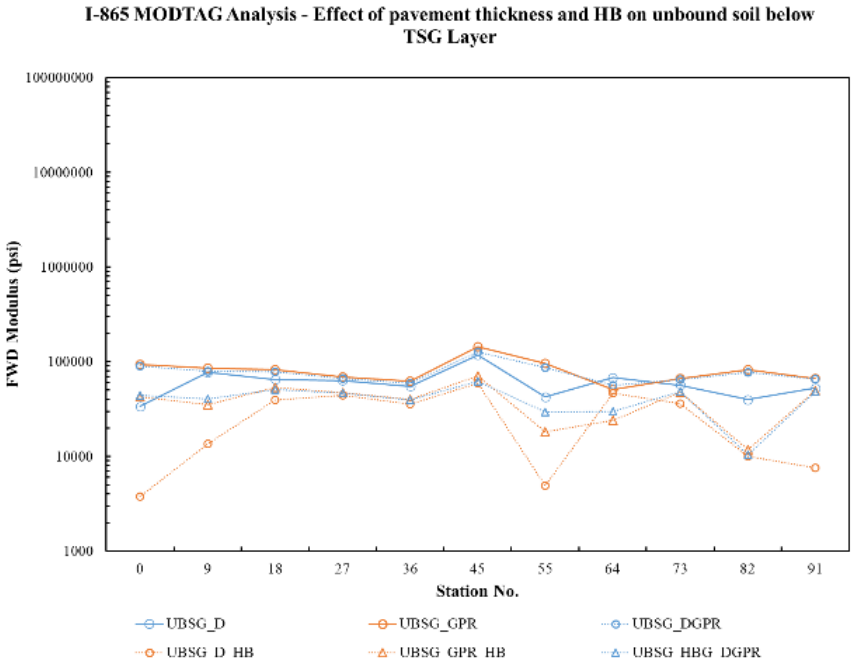

Figure F.2 I-865—comparison between ELMOD and MODTAG (continued).

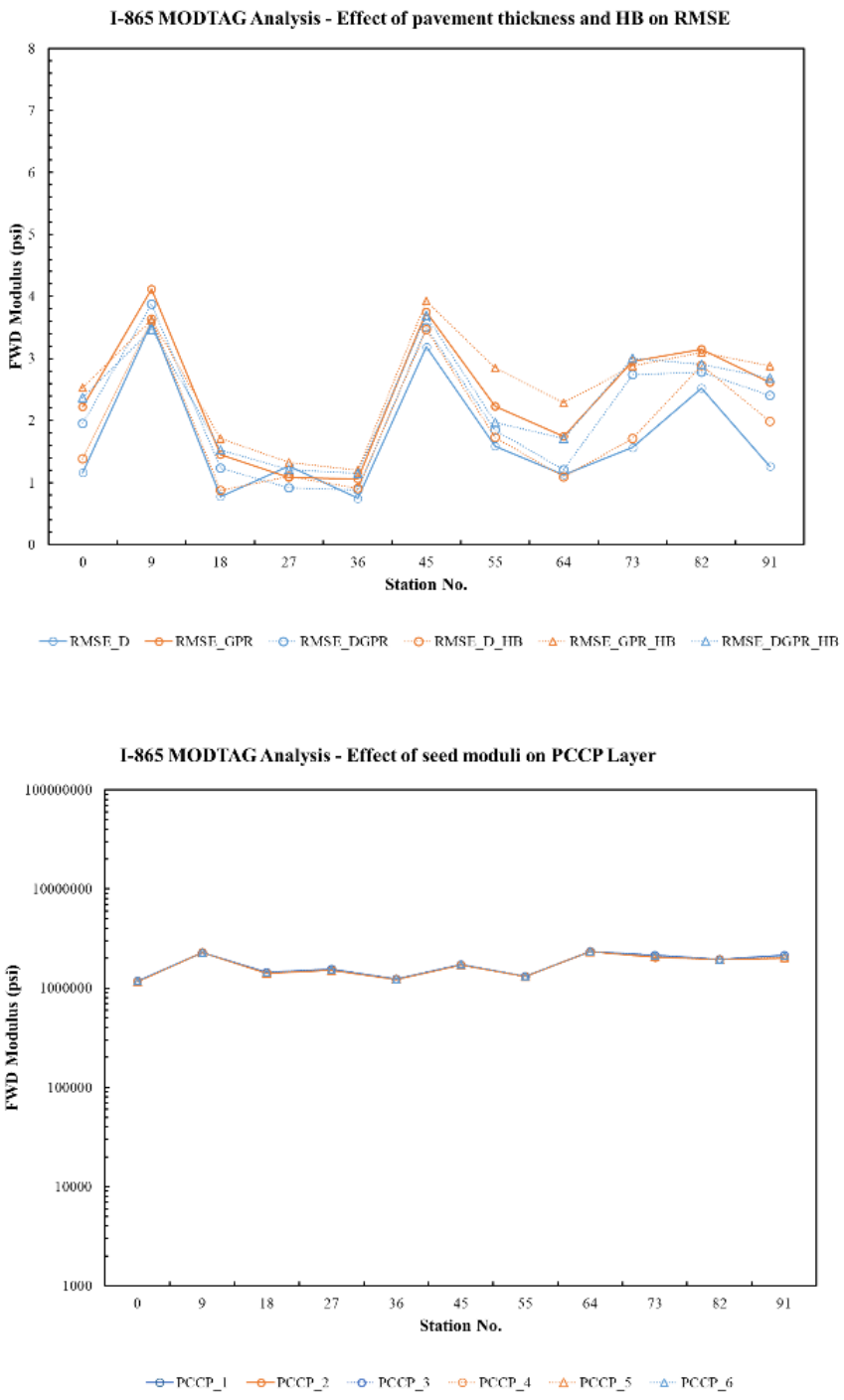

Figure F.3 I-865 MODTAG analysis—effect of pavement thickness and hard bottom.

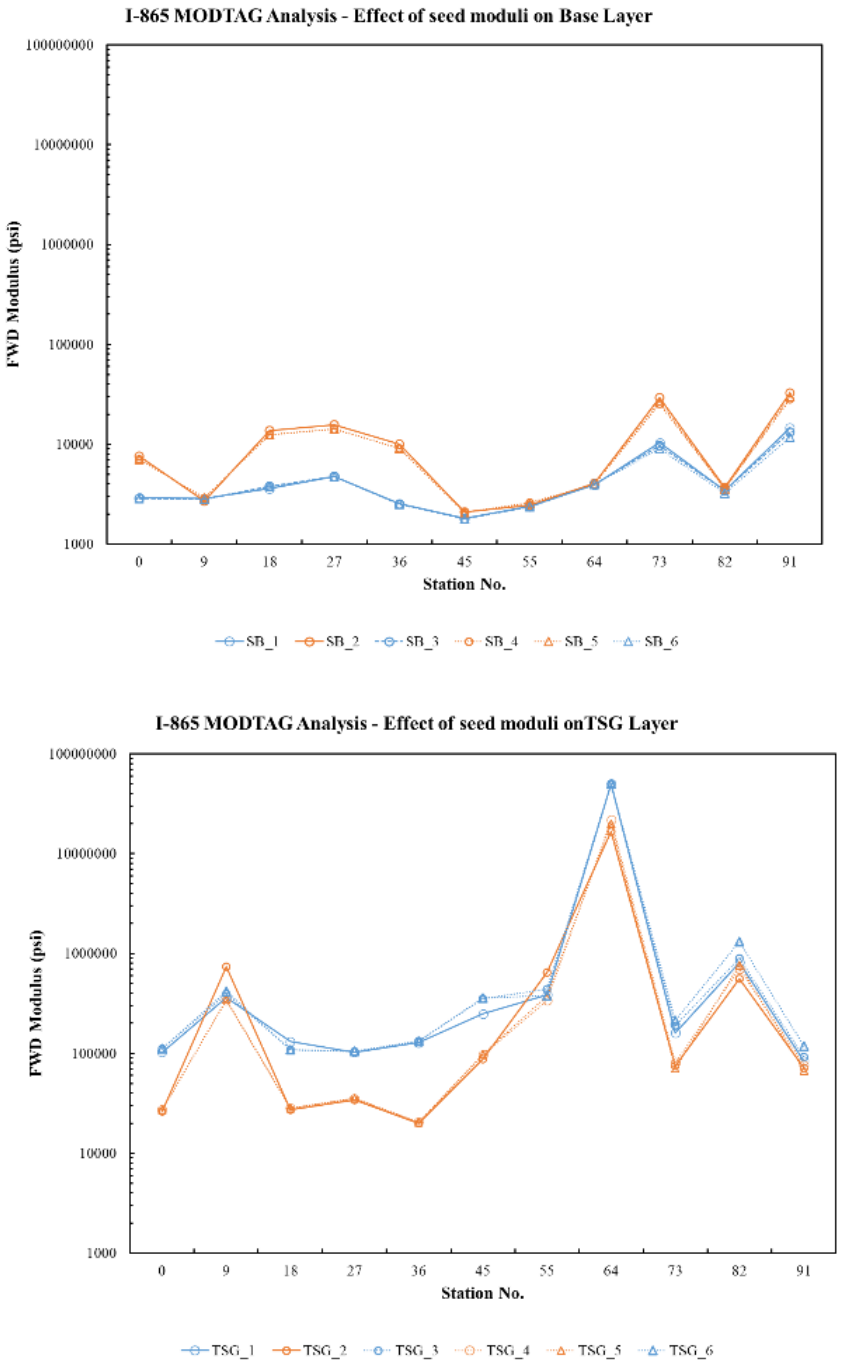

Figure F.3 I-865 MODTAG analysis—effect of pavement thickness and hard bottom (continued).

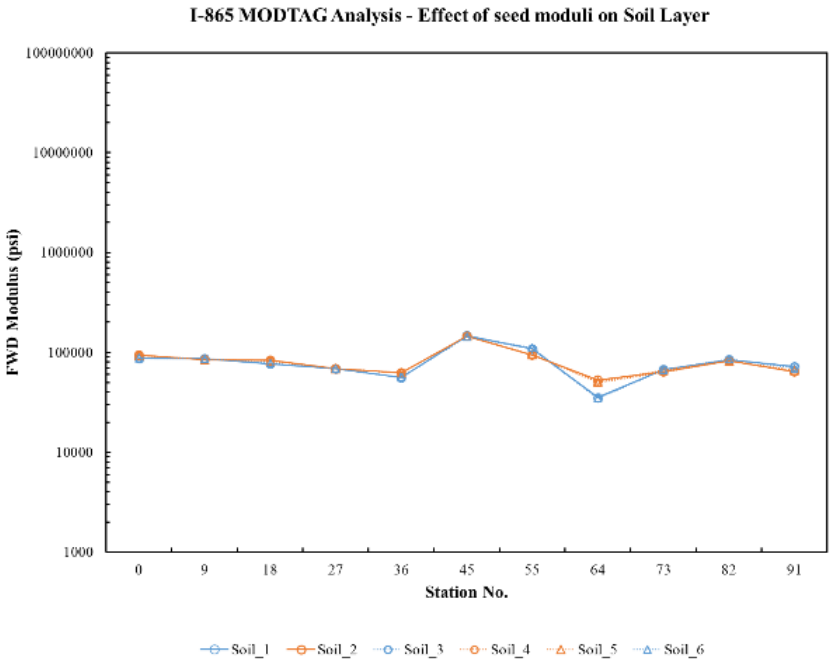

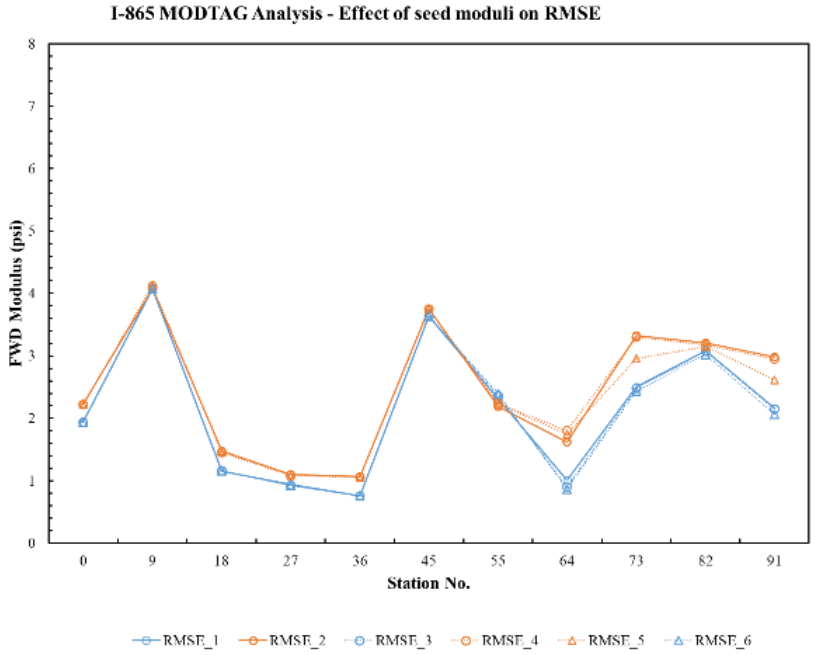

Figure F.4 I-865 MODTAG analysis—effect of seed moduli.

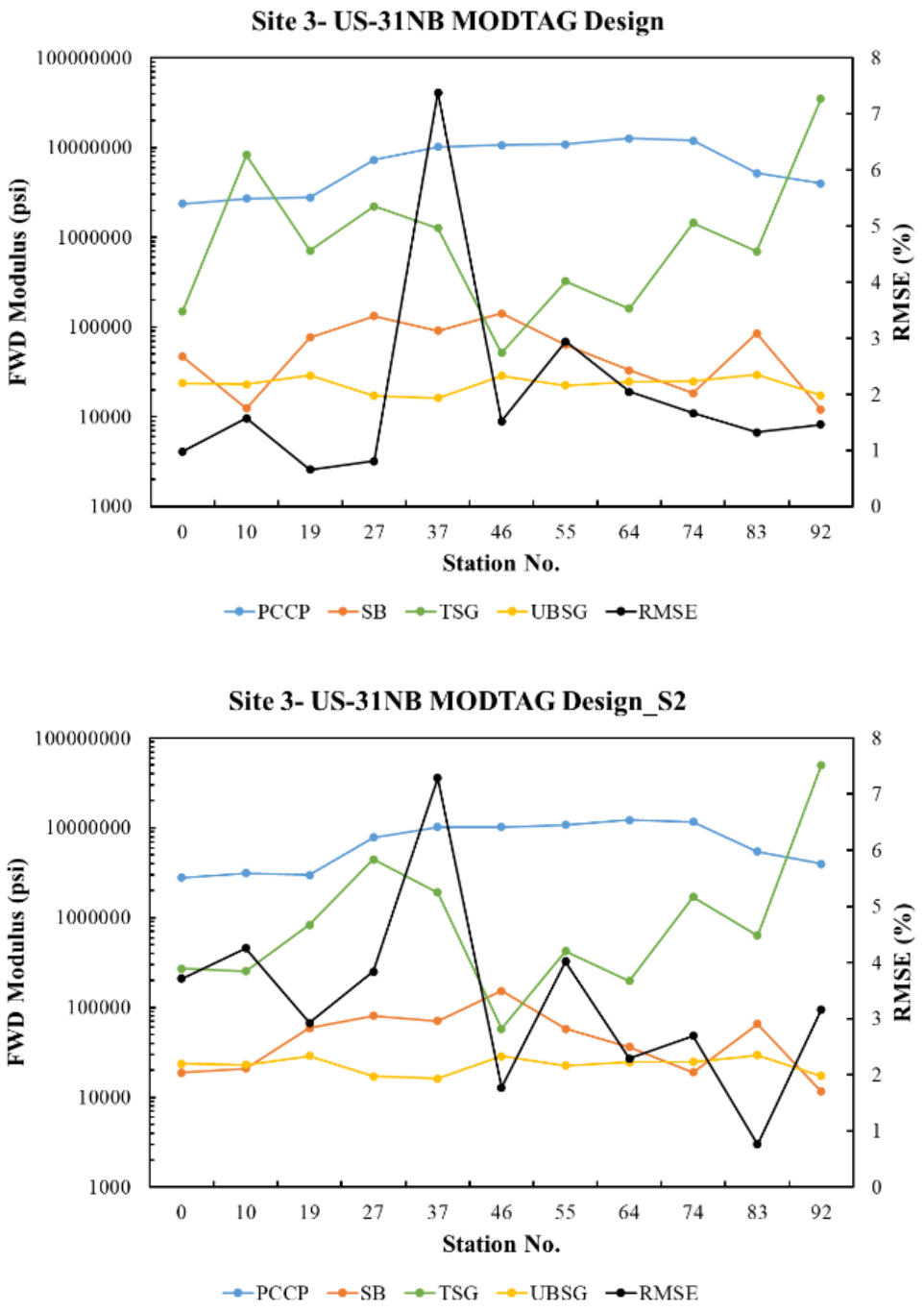

Figure F.5 US-31NB back calculation analysis—effect of pavement thickness.

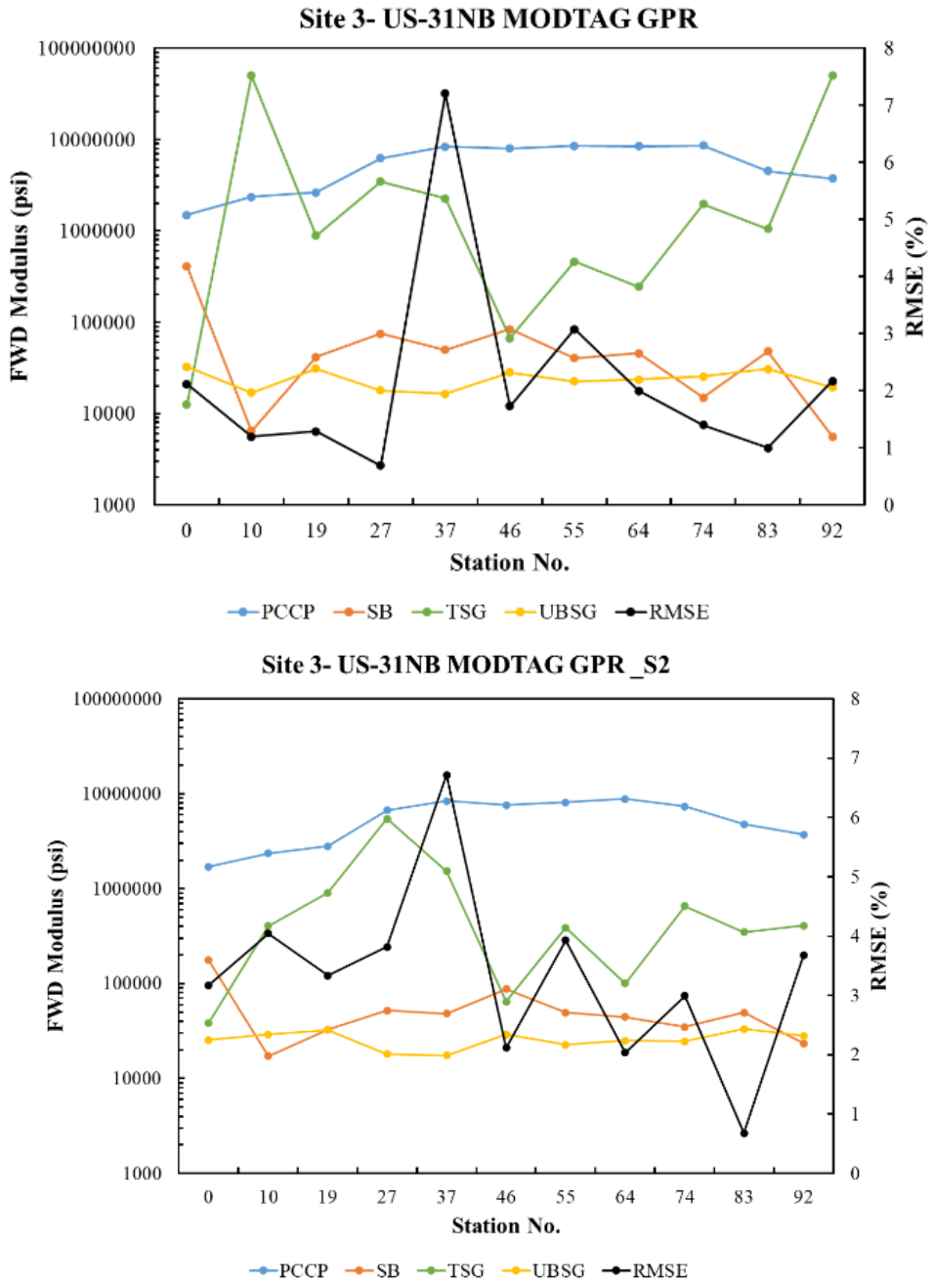

Figure F.5 US-31NB back calculation analysis—effect of pavement thickness (continued).

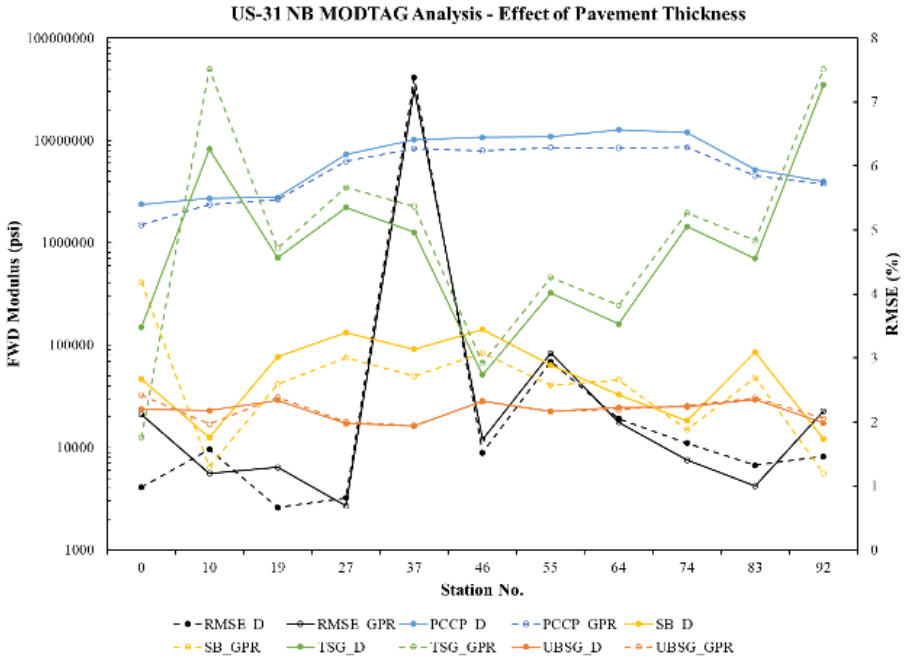

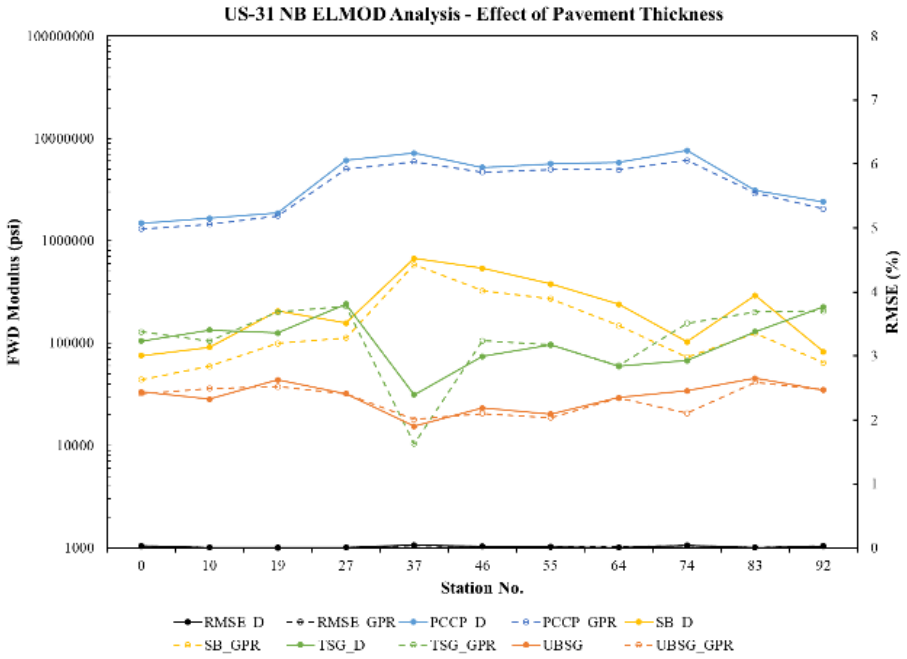

Figure F.5 US-31NB back calculation analysis—effect of pavement thickness (continued).

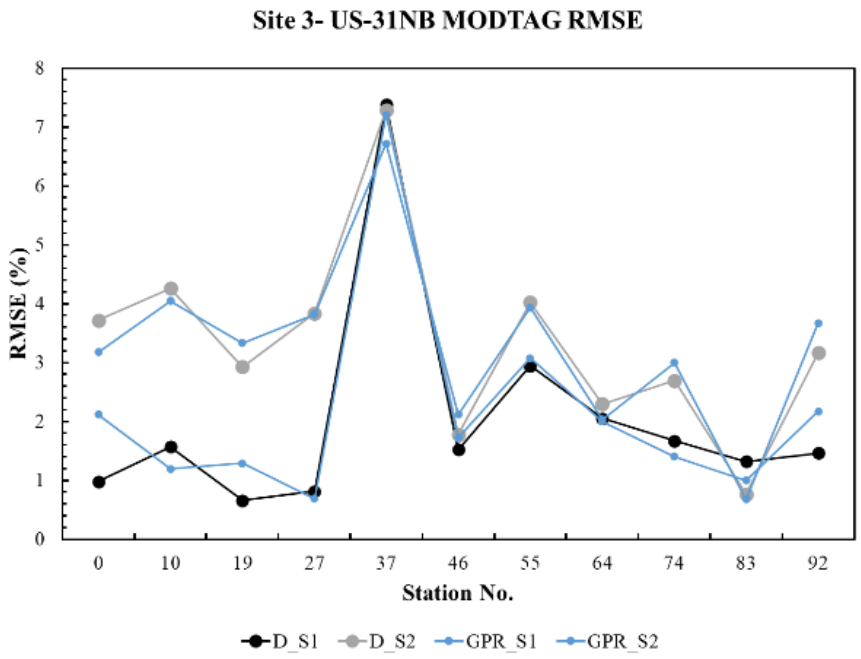

Figure F.5 US-31NB back calculation analysis—effect of pavement thickness (continued).

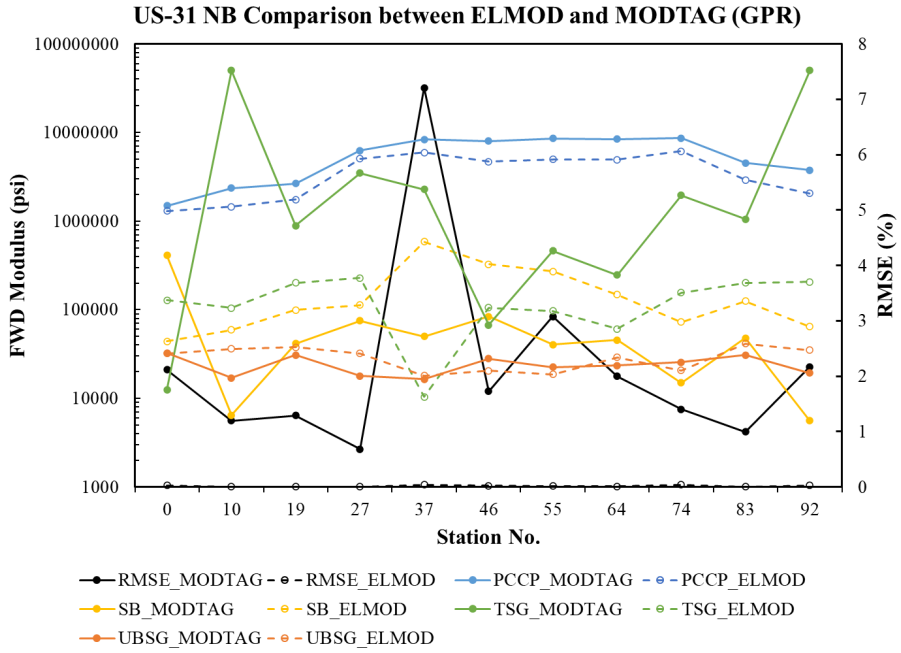

Figure F.6 US-31NB—comparison between ELMOD and MODTAG.

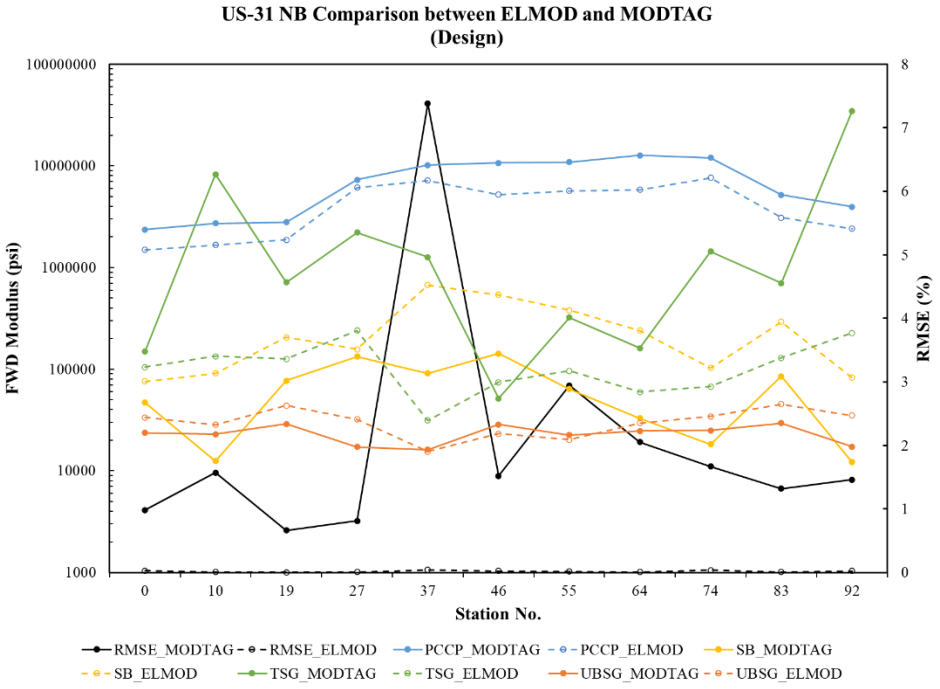

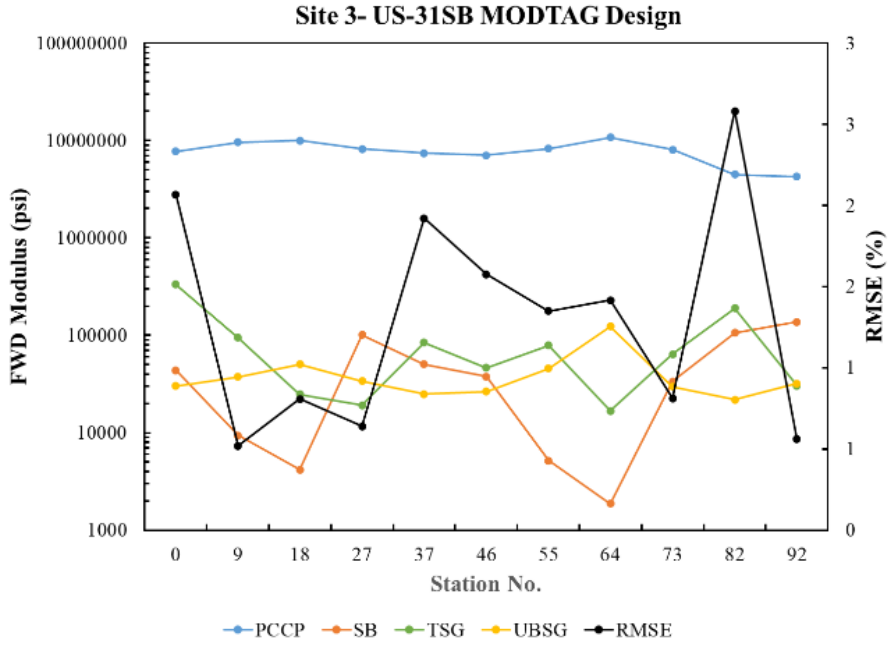

Figure F.6 US-31NB—comparison between ELMOD and MODTAG (continued).

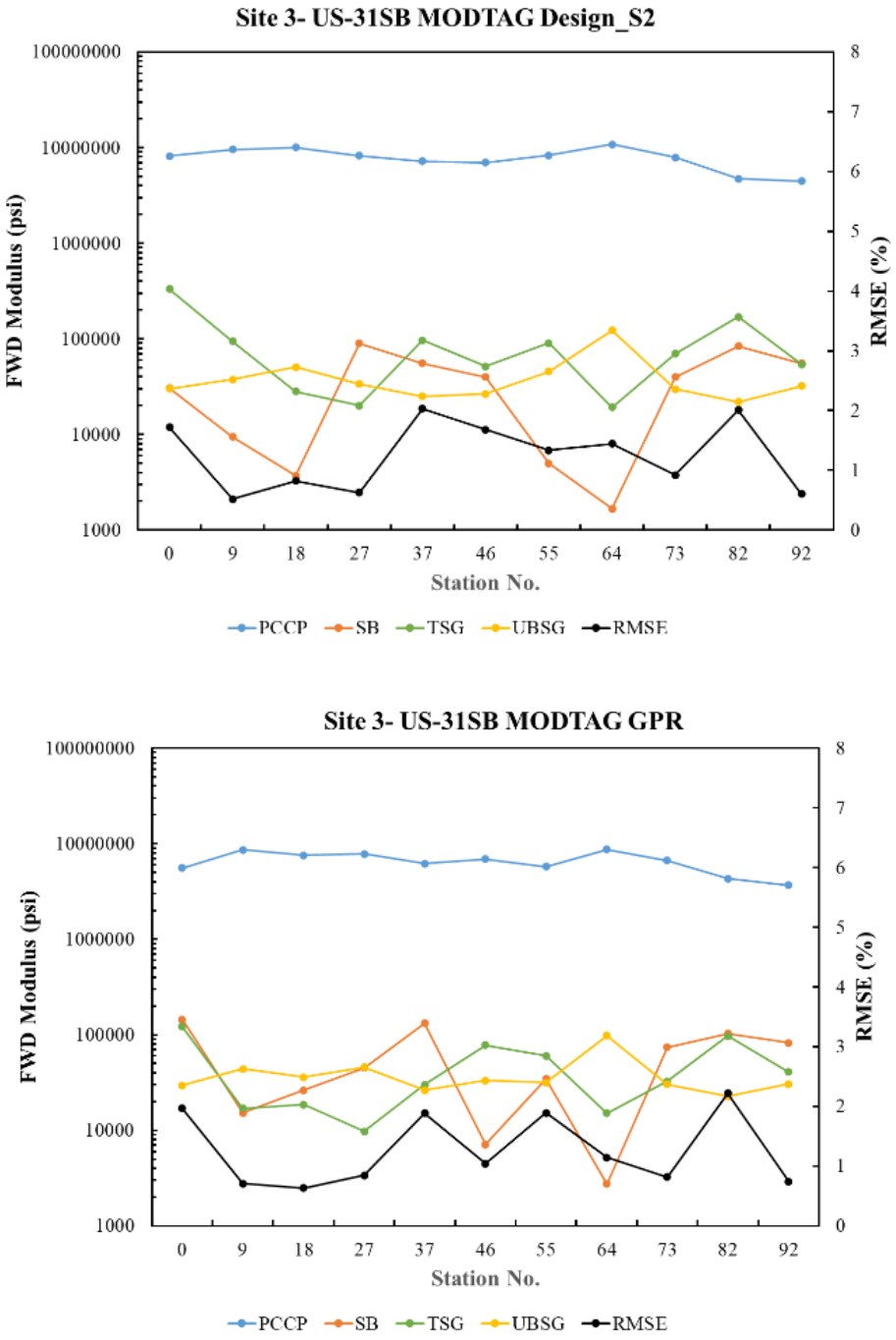

Figure F.7 US-31SB backcalculation analysis—effect of pavement thickness (continued).

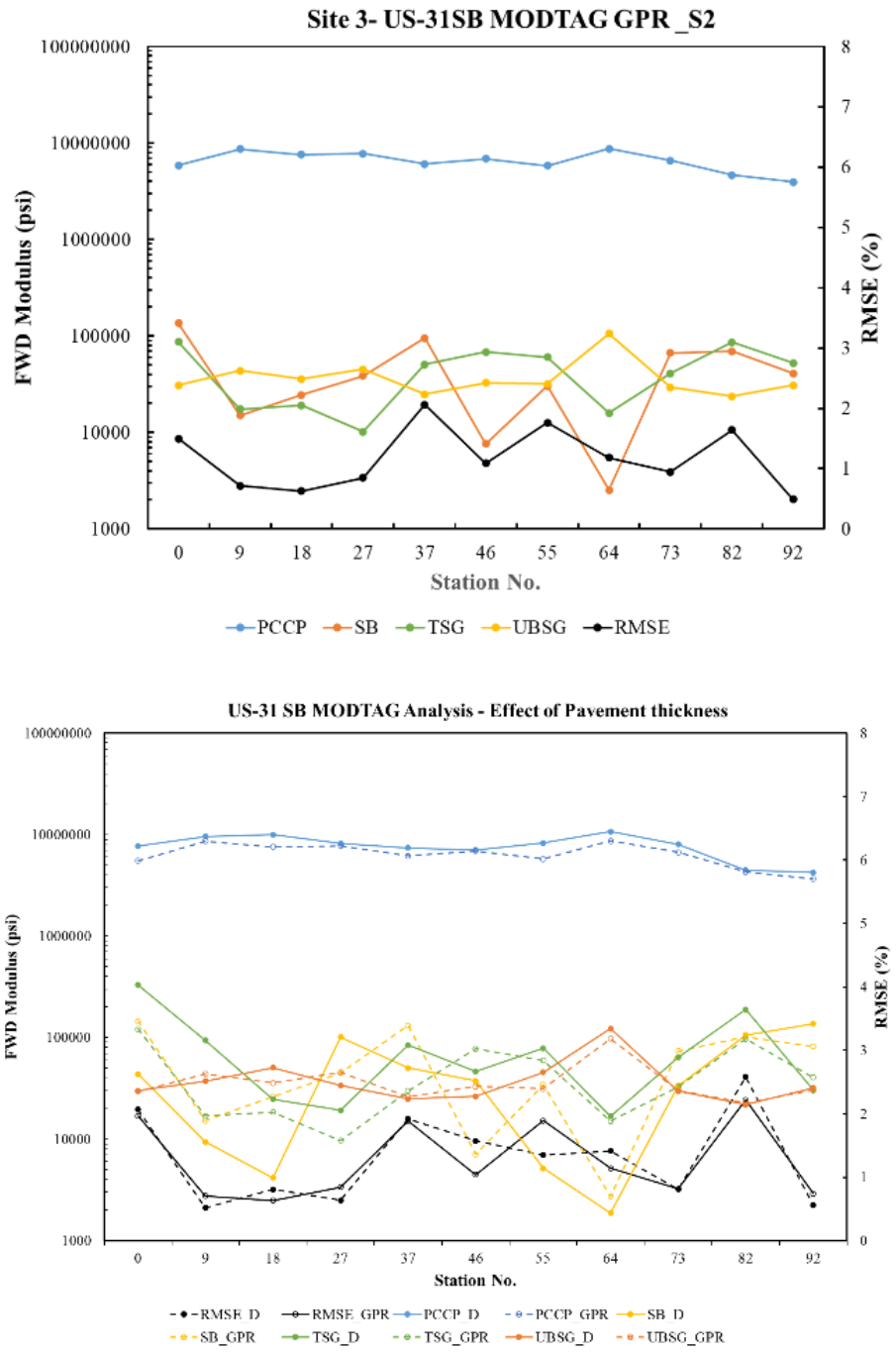

Figure F.7 US-31SB backcalculation analysis—effect of pavement thickness (continued).

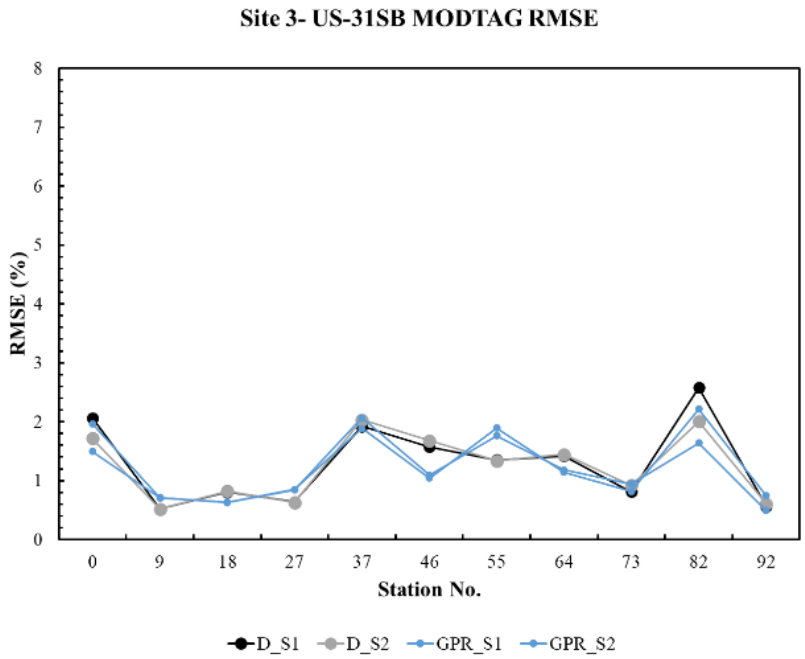

Figure F.7 US-31SB backcalculation analysis—effect of pavement thickness (continued).

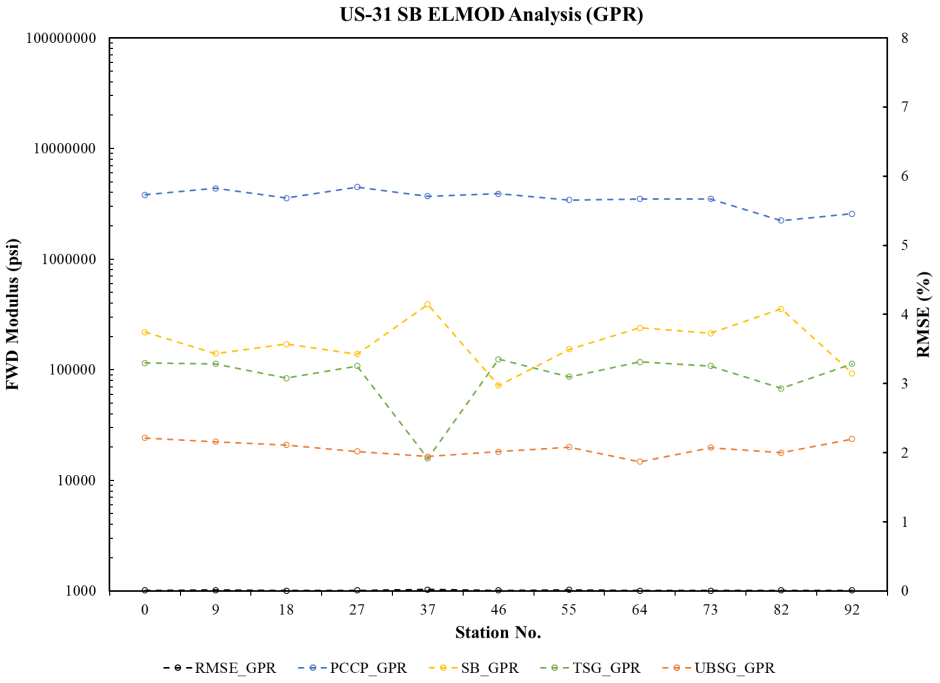

Figure F.8 US-31SB—ELMOD analysis.

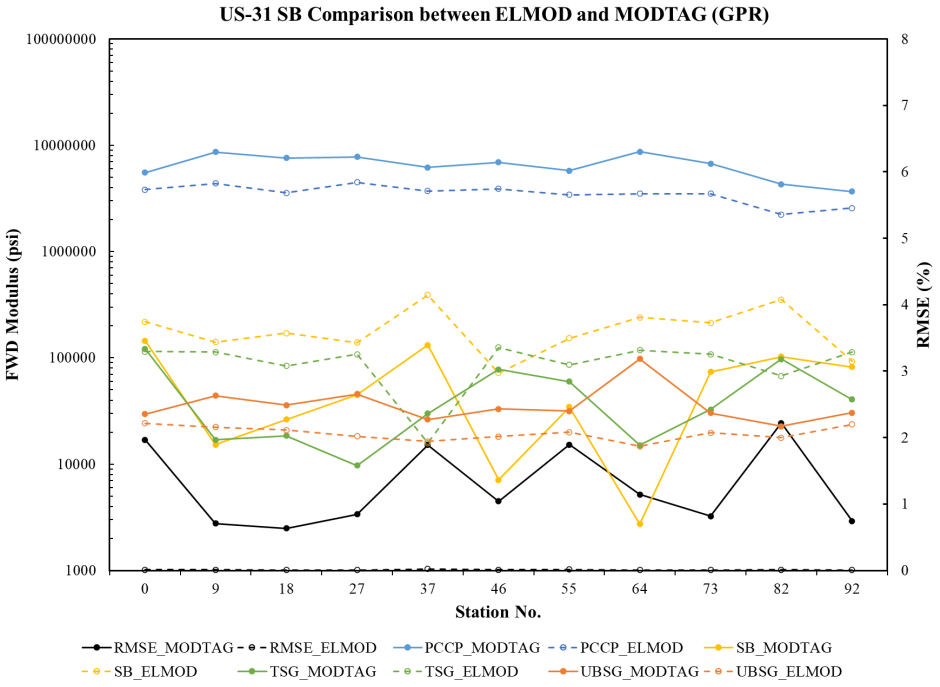

Figure F.9 US-31SB—comparison between ELMOD and MODTAG.

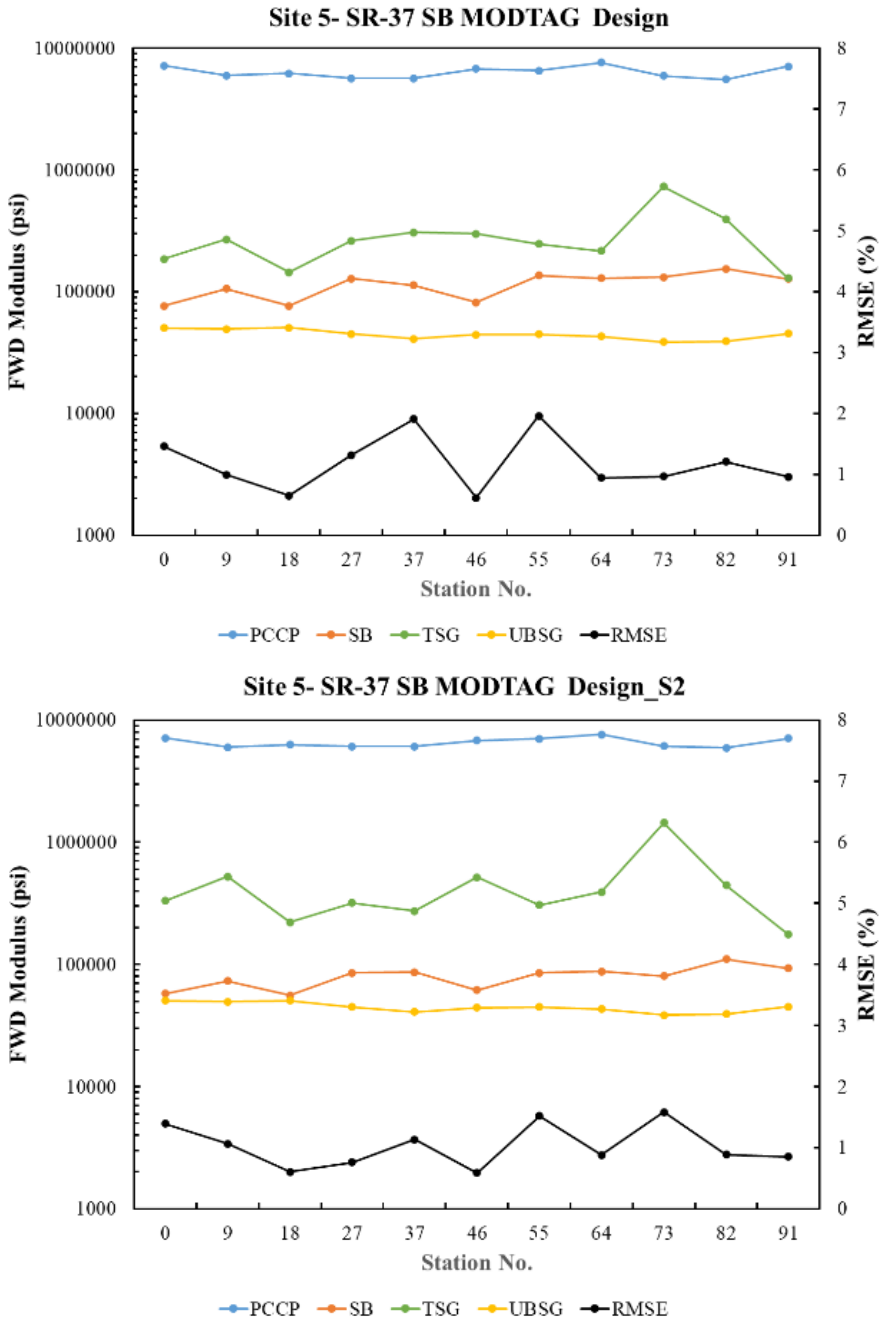

Figure F.10 SR-37NB backcalculation analysis—effect of pavement thickness.

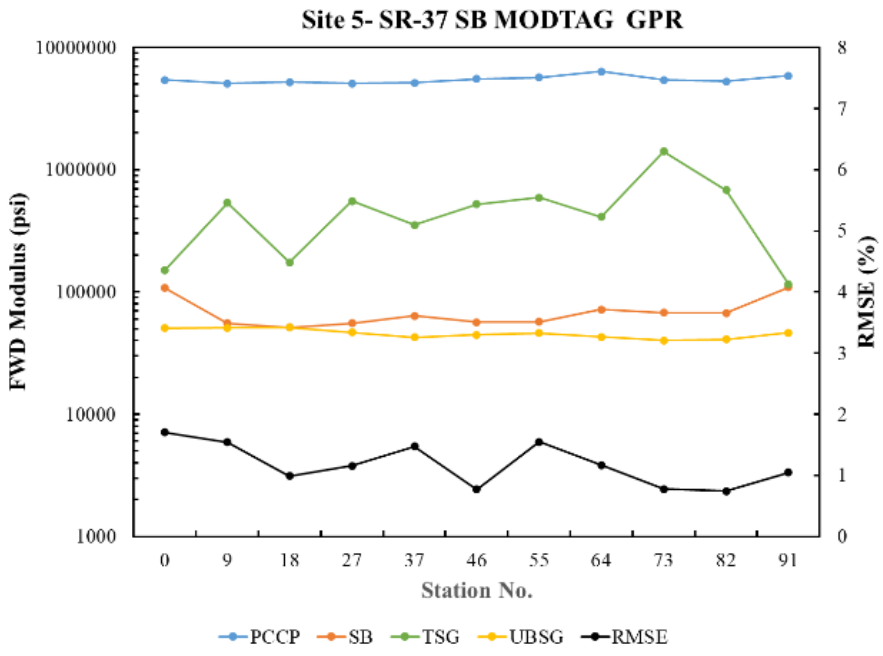

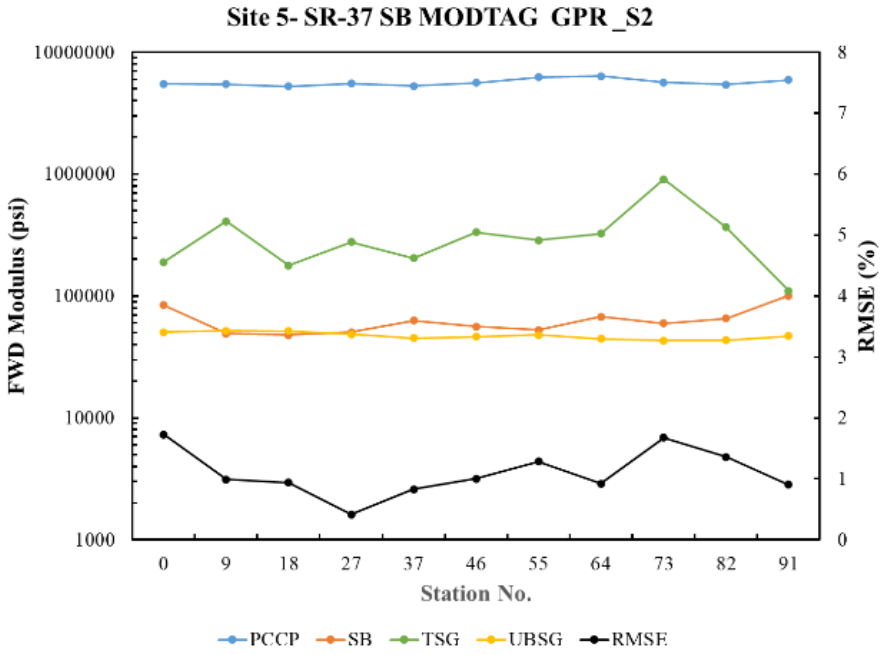

Figure F.10 SR-37NB backcalculation analysis—effect of pavement thickness (continued).

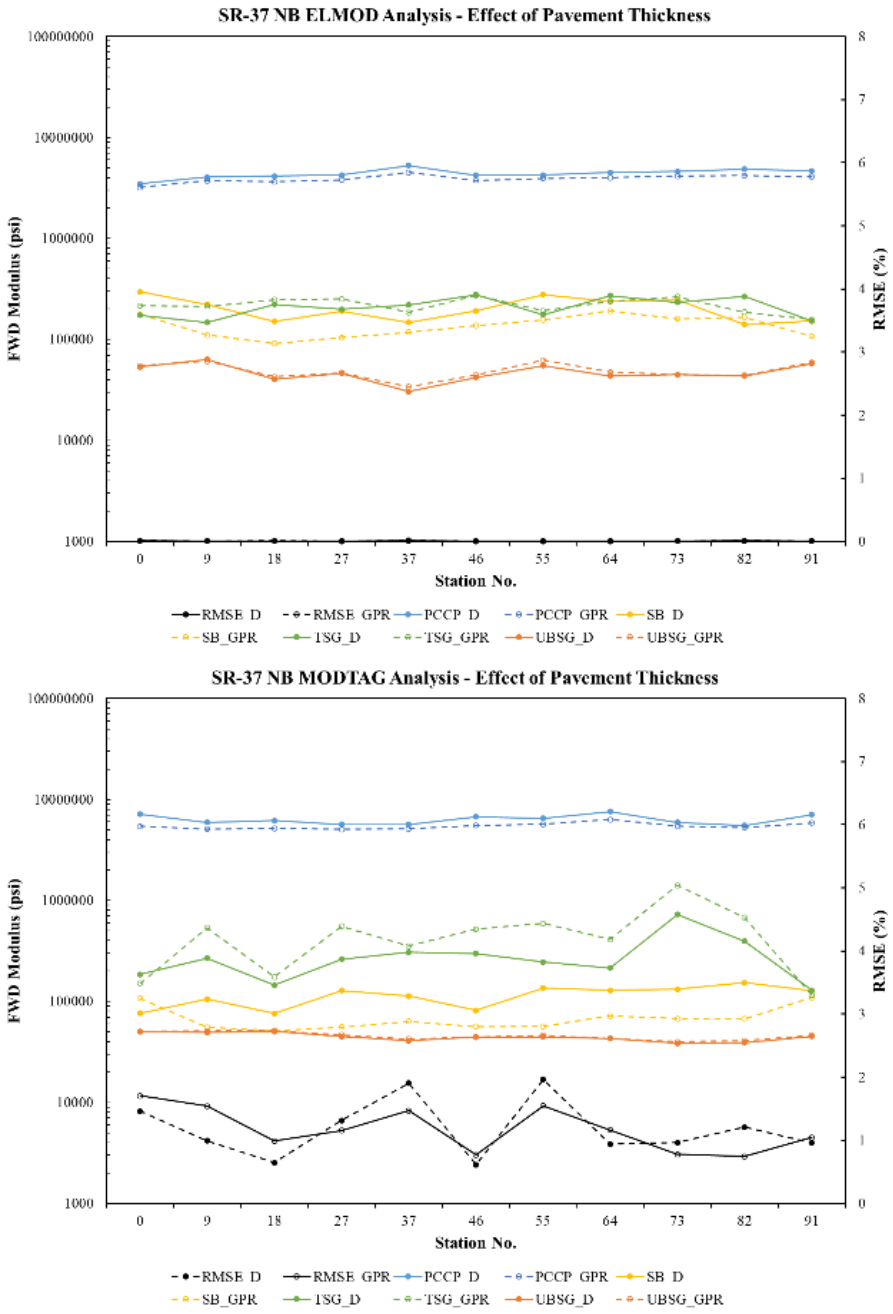

Figure F.10 SR-37NB backcalculation analysis—effect of pavement thickness (continued).

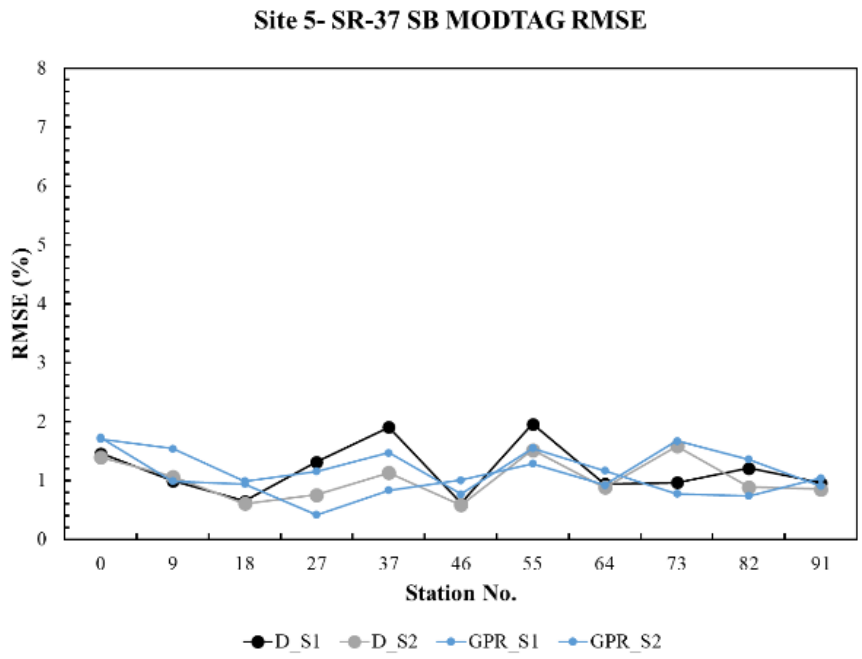

Figure F.10 SR-37NB backcalculation analysis—effect of pavement thickness (continued).

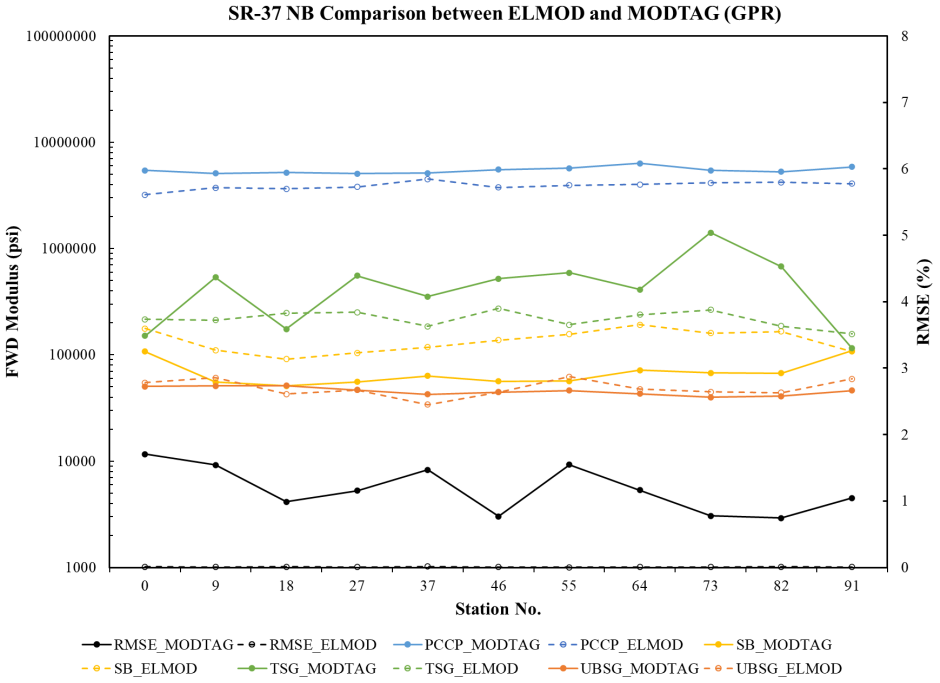

Figure F.11 SR-37NB backcalculation analysis—comparison between ELMOD and MODTAG (continued).

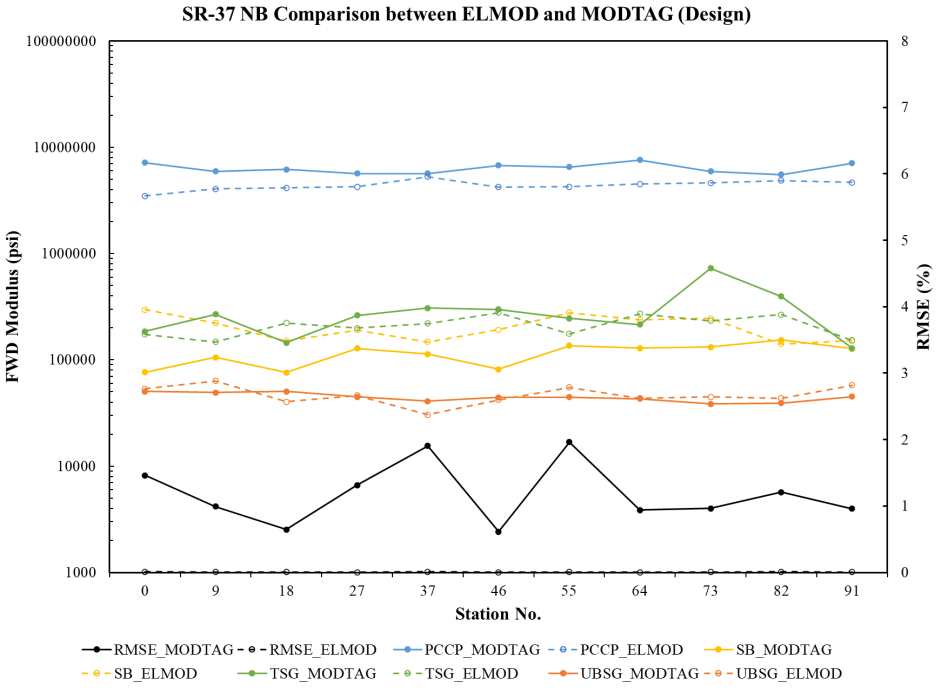

Figure F.11 SR-37NB—comparison between ELMOD and MODTAG (continued).

Table F.1 Results of Backcalculation Analysis Using ELMOD and MODTAG for Site 1: I-865 for Unbound Subgrade (UBSG) Layer

Station	Average Lab. $M_{R,UNTREATED}$	ELMOD_D psi	E_{ELMOD_D} / Lab. $M_{R,UNTREATED}$	ELMOD_GPR psi	E_{ELMOD_GPR} / Lab. $M_{R,UNTREATED}$	MODTAG_D psi	E_{MODTAG_D} / Lab. $M_{R,UNTREATED}$	MODTAG_GPR psi	E_{MODTAG_GPR} / Lab. $M_{R,UNTREATED}$
91	10,560	34,282	3.2	30,485	2.9	52,687	5.0	66,581	6.3
82	8,423	23,645	2.8	32,773	3.9	39,891	4.7	82,311	9.8
73	5,960	27,069	4.5	39,464	6.6	56,383	9.5	66,151	11.1
64	14,175	54,312	3.8	48,670	3.4	67,987	4.8	50,621	3.6
55	8,338	22,349	2.7	20,979	2.5	42,351	5.1	95,473	11.5
45	9,403	20,419	2.2	17,373	1.8	117,572	12.5	144,895	15.4
36	9,572	16,276	1.7	14,503	1.5	54,934	5.7	62,439	6.5
27	8,237	23,005	2.8	23,011	2.8	63,106	7.7	68,628	8.3
18	18,953	29,124	1.5	17,242	0.9	64,904	3.4	82,671	4.4
9	12,809	57,297	4.5	25,666	2.0	77,031	6.0	85,404	6.7
0	8,572	12,319	1.4	17,137	2.0	33,835	3.9	93,098	10.9
		Average	2.8	**Average**	2.8	**Average**	6.2	**Average**	8.6

Table F.2 Results of Backcalculation Analysis Using ELMOD and MODTAG for Site 1: I-865 for Treated Subgrade (TSG) Layer

Station	Average Lab. $M_{R,UNTREATED}$	ELMOD_D psi	E_{ELMOD_D} / Lab. $M_{R,UNTREATED}$	ELMOD_GPR psi	E_{ELMOD_GPR} / Lab. $M_{R,UNTREATED}$	MODTAG_D psi	E_{MODTAG_D} / Lab. $M_{R,UNTREATED}$	MODTAG_GPR psi	E_{MODTAG_GPR} / Lab. $M_{R,UNTREATED}$
91	53,509	155,067	2.9	141,570	2.6	6,653,146		67,160	1.3
82	43,816	123,377	2.8	91,023	2.1	50,000,000		766,428	
73	25,395	185,098	7.3	129,655	5.1	3,960,219		70,737	2.8
64	35,987	130,774	3.6	113,491	3.2	273,168	7.6	20,061,126	
55	47,184	84,553	1.8	74,147	1.6	50,000,000		377,645	
45	36,626	80,627	2.2	73,500	2.0	607,088		97,567	2.7
36	53,296	62,700	1.2	67,458	1.3	33,884	0.6	20,513	0.4
27	73,916	107,518	1.5	97,064	1.3	45,529	0.6	35,434	0.5
18	40,219	86,748	2.2	94,556	2.4	898,220		28,320	0.7
9	67,370	78,842	1.2	95,454	1.4	1,145,396		343,411	
0	43,027	96,127	2.2	68,527	1.6	50,000,000		27,358	0.6
		Average	2.6	**Average**	2.2			**Average**	1.3

Table F.3 Results of Backcalculation Analysis Using ELMOD and MODTAG for Site 3: US-31 North Bound for Unbound Subgrade (UBSG) Layer

Station	Average Lab. $M_{R,UNTREATED}$	ELMOD_D	E_{ELMOD_D} / Lab. $M_{R,UNTREATED}$	ELMOD_GPR	E_{ELMOD_GPR} / Lab. $M_{R,UNTREATED}$	MODTAG_D	E_{MODTAG_D} / Lab. $M_{R,UNTREATED}$	MODTAG_GPR	E_{MODTAG_GPR} / Lab. $M_{R,UNTREATED}$
0	11,168	33,541	3.0	32,115	2.9	23,663	2.1	32,522	6.3
10	11,548	28,330	2.5	36,140	3.1	22,948	2.0	16,945	9.8
19	9,371	43,897	4.7	37,688	4.0	28,880	3.1	30,936	11.1
27	10,960	32,017	2.9	32,017	2.9	17,120	1.6	17,857	3.6
37	12,538	15,435	1.2	18,002	1.4	16,164	1.3	16,494	11.5
46	13,951	23,263	1.7	20,503	1.5	28,617	2.1	28,122	15.4
55	12,898	20,328	1.6	18,741	1.5	22,491	1.7	22,551	6.5
64	10,391	29,432	2.8	29,106	2.8	24,617	2.4	23,507	8.3
74	12,207	34,304	2.8	20,695	1.7	24,966	2.0	25,539	4.4
83	15,108	45,259	3.0	41,450	2.7	29,422	1.9	30,711	6.7
92	14,111	34,954	2.5	35,039	2.5	17,303	1.2	19,284	10.9
		Average	2.6	**Average**	2.5	**Average**	1.9	**Average**	8.6

Table F.4 Results of Backcalculation Analysis using ELMOD and MODTAG for Site 3: US-31 North Bound for Treated Subgrade (TSG) Layer

Station	Average Lab. $M_{R,UNTREATED}$	ELMOD_D	E_{ELMOD_D} / Lab. $M_{R,UNTREATED}$	ELMOD_GPR	E_{ELMOD_GPR} / Lab. $M_{R,UNTREATED}$	MODTAG_D	E_{MODTAG_D} / Lab. $M_{R,UNTREATED}$	MODTAG_GPR	E_{MODTAG_GPR} / Lab. $M_{R,UNTREATED}$
0	39,165	104,858	2.7	128,650	3.3	150,140	3.8	12,557	0.3
10	30,318	134,240	4.4	104,970	3.5	8,258,326		50,000,000	
19	34,148	126,264	3.7	201,751	5.9	713,980		888,445	
27	48,220	240,744	5.0	228,712	4.7	2,212,296		3,476,607	
37	40,974	31,371	0.8	10,395	0.3	1,265,770		2,270,059	
46	29,248	74,250	2.5	105,300	3.6	51,423	1.8	67,141	2.3
55	47,160	96,034	2.0	96,863	2.1	323,015	6.8	460,803	9.8
64	35,355	59,598	1.7	60,539	1.7	160,811	4.5	245,779	7.0
74	47,824	67,427	1.4	156,094	3.3	1,441,450		1,960,995	
83	46,750	129,373	2.8	201,148	4.3	700,456		1,051,807	
92	39,375	226,920	5.8	206,032	5.2	34,775,026		50,000,000	
		Average	3.0	**Average**	3.4				

Table F.5 Results of Back calculation Analysis using ELMOD and MODTAG for Site 3: US-31 South Bound for Unbound Subgrade (UBSG) Layer

Station	Average Lab. $M_{R,UNTREATED}$	ELMOD_D	E_{ELMOD_D} / Lab. $M_{R,UNTREATED}$	ELMOD_GPR	E_{ELMOD_GPR} / Lab. $M_{R,UNTREATED}$	MODTAG_D	E_{MODTAG_D} / Lab. $M_{R,UNTREATED}$
92	11,168	23,643	2.1	32,031	2.9	30,409	2.7
82	11,548	17,774	1.5	21,914	1.9	22,667	2.0
73	9,371	19,749	2.1	29,751	3.2	30,328	3.2
64	10,960	14,715	1.3	123,157		97,854	
55	12,538	19,993	1.6	45,635	3.6	31,476	2.5
46	13,951	18,138	1.3	26,433	1.9	33,072	2.4
37	12,898	16,395	1.3	24,969	1.9	26,322	2.0
27	10,391	18,280	1.8	33,862	3.3	45,727	4.4
18	12,207	20,967	1.7	50,644	4.1	35,858	2.9
9	15,108	22,345	1.5	37,423	2.5	43,958	2.9
0	14,111	24,179	1.7	30,154	2.1	29,630	2.1
		Average	1.6	**Average**	2.7	**Average**	2.7

Table F.6 Results of Backcalculation Analysis Using ELMOD and MODTAG for Site 3: US-31 South Bound for Treated Subgrade (TSG) Layer

Station	Average Lab. $M_{R,UNTREATED}$	ELMOD_D	E_{ELMOD_D} / Lab. $M_{R,UNTREATED}$	ELMOD_GPR	E_{ELMOD_GPR} / Lab. $M_{R,UNTREATED}$	MODTAG_D	E_{MODTAG_D} / Lab. $M_{R,UNTREATED}$
92	39,165	113,311	2.9	30,395	0.8	40,696	1.0
82	30,318	67,750	2.2	190,029	6.3	97,314	3.2
73	34,148	108,281	3.2	63,958	1.9	32,713	1.0
64	48,220	117,960	2.4	16,861	0.3	15,063	0.3
55	40,974	86,186	2.1	78,920	1.9	59,897	1.5
46	29,248	124,811	4.3	46,357	1.6	77,678	2.7
37	47,160	15,825	0.3	84,399	1.8	29,969	0.6
27	35,355	108,279	3.1	19,225	0.5	9,723	0.3
18	47,824	83,916	1.8	24,811	0.5	18,555	0.4
9	46,750	113,009	2.4	94,363	2.0	16,975	0.4
0	39,375	114,939	2.9	332,151	8.4	121,276	3.1
		Average	2.5	**Average**	2.4	**Average**	1.3

Table F.7 Results of Backcalculation Analysis Using ELMOD and MODTAG for Site 5: SR-37 North Bound for Unbound Subgrade (UBSG) Layer

Station	Average Lab. $M_{R,UNTREATED}$	ELMOD_D	E_{ELMOD_D} / Lab. $M_{R,UNTREATED}$	ELMOD_GPR	E_{ELMOD_GPR} / Lab. $M_{R,UNTREATED}$	MODTAG_D	E_{MODTAG_D} / Lab. $M_{R,UNTREATED}$	Station	Average Lab. $M_{R,UNTREATED}$
0	14,617	53,634	3.7	54,860	3.8	50,464	3.5	50,552	3.5
9	14,666	63,326	4.3	61,006	4.2	49,400	3.4	51,029	3.5
18	12,953	40,367	3.1	42,794	3.3	50,574	3.9	51,304	4.0
27	10,313	46,205	4.5	46,827	4.5	44,854	4.3	46,611	4.5
37	13,057	30,497	2.3	34,053	2.6	40,870	3.1	42,636	3.3
46	14,008	42,101	3.0	44,598	3.2	44,259	3.2	44,476	3.2
55	12,995	55,224	4.2	62,410	4.8	44,695	3.4	46,196	3.6
64	15,419	43,675	2.8	47,432	3.1	43,034	2.8	42,947	2.8
73	10,801	44,729	4.1	44,764	4.1	38,590	3.6	39,980	3.7
82	16,852	43,517	2.6	44,135	2.6	39,246	2.3	40,805	2.4
91	17,447	57,778	3.3	59,444	3.4	45,196	2.6	46,272	2.7
		Average	3.5	**Average**	3.6	**Average**	3.3	**Average**	3.4

Table F.8 Results of Back calculation Analysis Using ELMOD and MODTAG for Site 5: SR-37 North Bound for Treated Subgrade (TSG) Layer

Station	Average Lab. $M_{R,UNTREATED}$	ELMOD_D	E_{ELMOD_D} / Lab. $M_{R,UNTREATED}$	ELMOD_GPR	E_{ELMOD_GPR} / Lab. $M_{R,UNTREATED}$	MODTAG_D	E_{MODTAG_D} / Lab. $M_{R,UNTREATED}$	Station	Average Lab. $M_{R,UNTREATED}$
0	42,575	174,150	4.1	215,371	5.1	185,181	4.3	151,105	3.5
9	48,115	147,169	3.1	212,407	4.4	268,186	5.6	534,672	
18	43,485	222,661	5.1	247,666	5.7	144,507	3.3	174,557	4.0
27	50,638	198,705	3.9	251,636	5.0	262,329	5.2	555,582	
37	47,015	219,347	4.7	185,715	4.0	307,020	6.5	353,509	7.5
46	50,251	278,125	5.5	273,601	5.4	298,510	5.9	521,284	
55	57,338	176,361	3.1	191,871	3.3	246,372	4.3	591,460	
64	46,869	271,878	5.8	238,877	5.1	215,287	4.6	410,563	8.8
73	49,748	233,484	4.7	264,865	5.3	728,812		1,409,459	
82	43,073	266,409	6.2	186,745	4.3	395,177	9.2	679,219	
91	42,367	152,930	3.6	157,579	3.7	129,169	3.0	115,569	2.7
		Average	4.5	**Average**	4.7	**Average**	5.2		

APPENDIX G. BACKCALCULATION ANALYSIS FOR FLEXIBLE PAVEMENTS

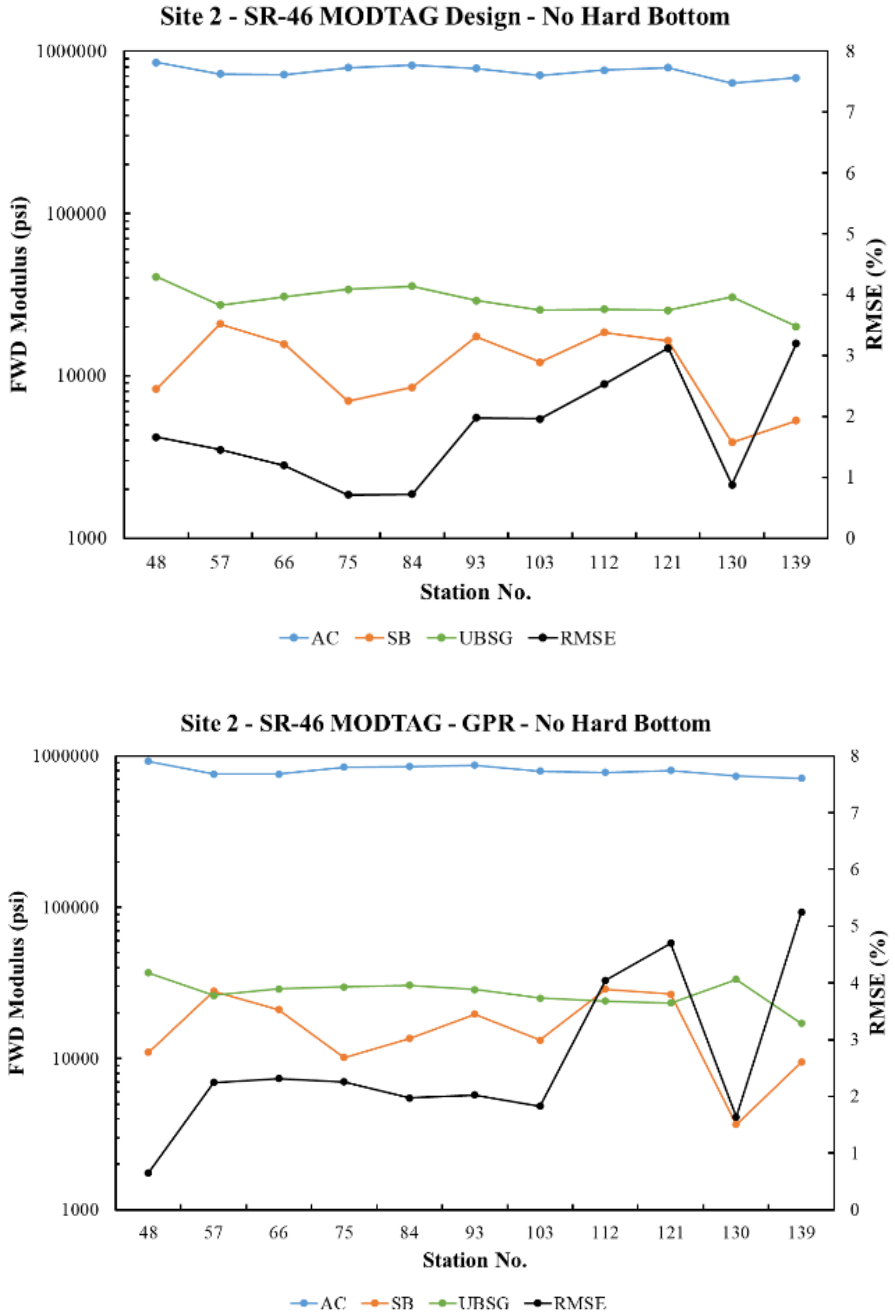

Figure G.1 SR-46 MODTAG analysis—effect of pavement thickness.

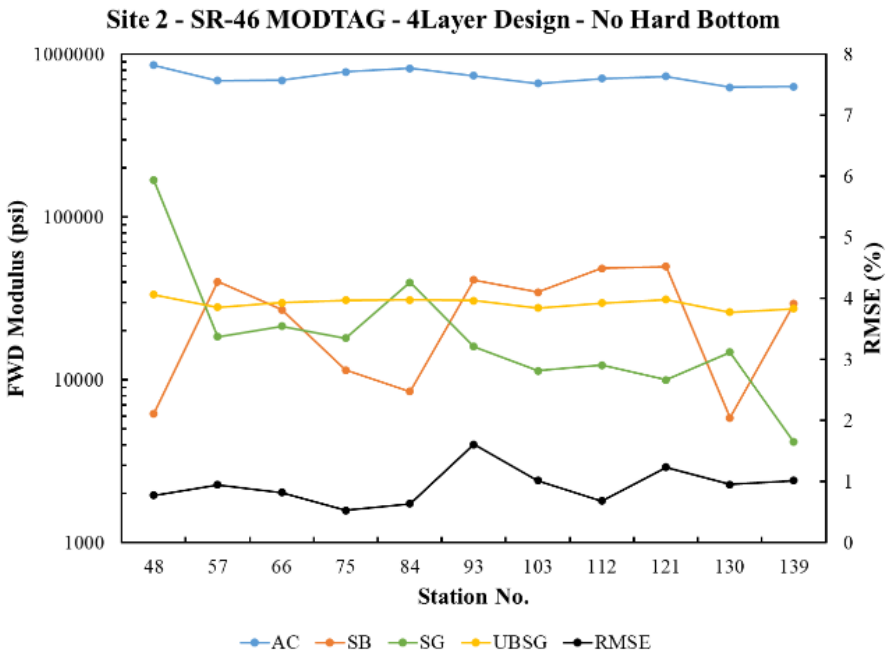

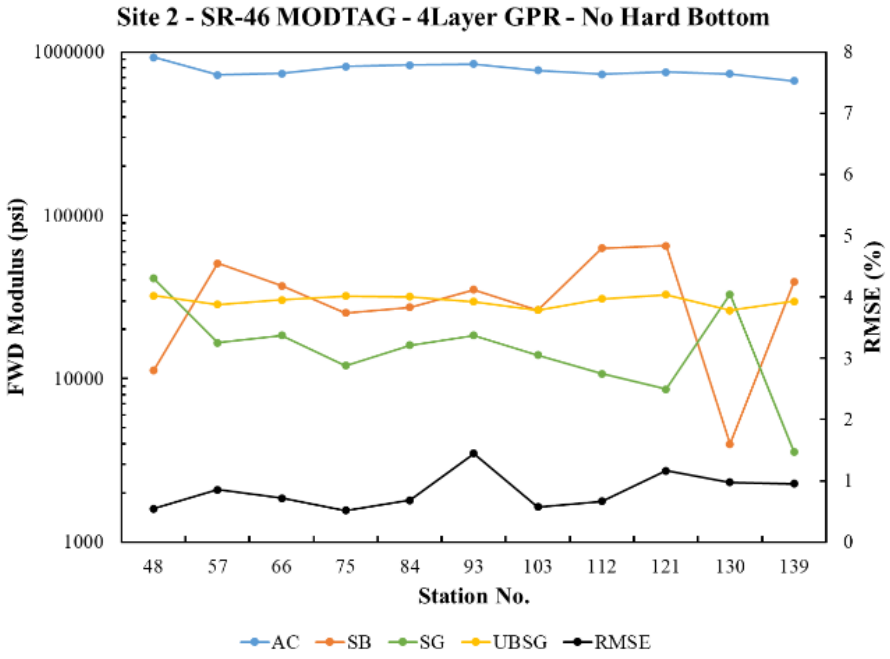

Figure G.1 SR-46 MODTAG analysis—effect of pavement thickness (continued).

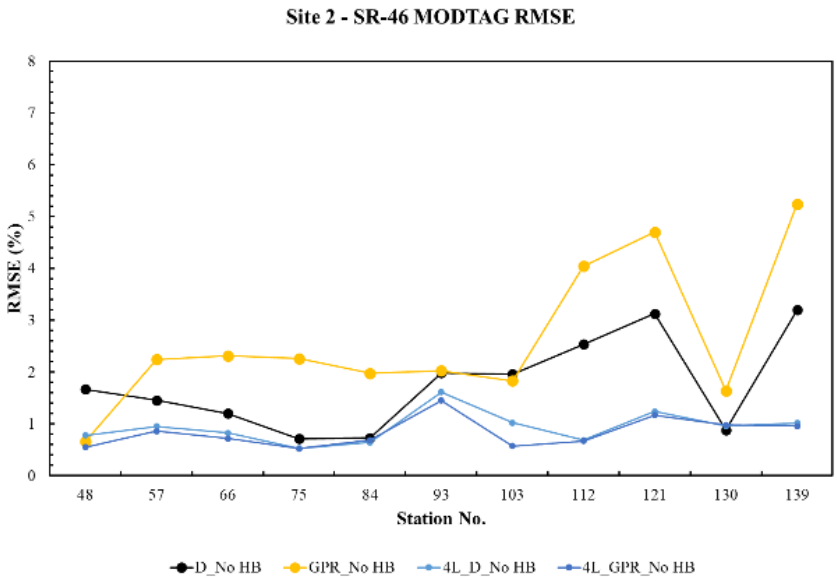

Figure G.1 SR-46 MODTAG analysis—effect of pavement thickness (continued).

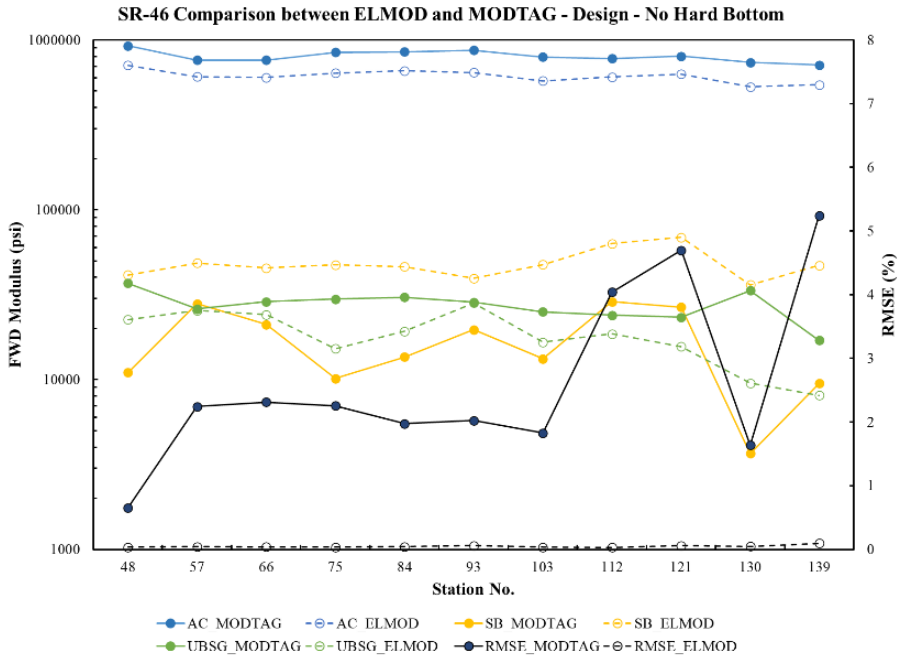

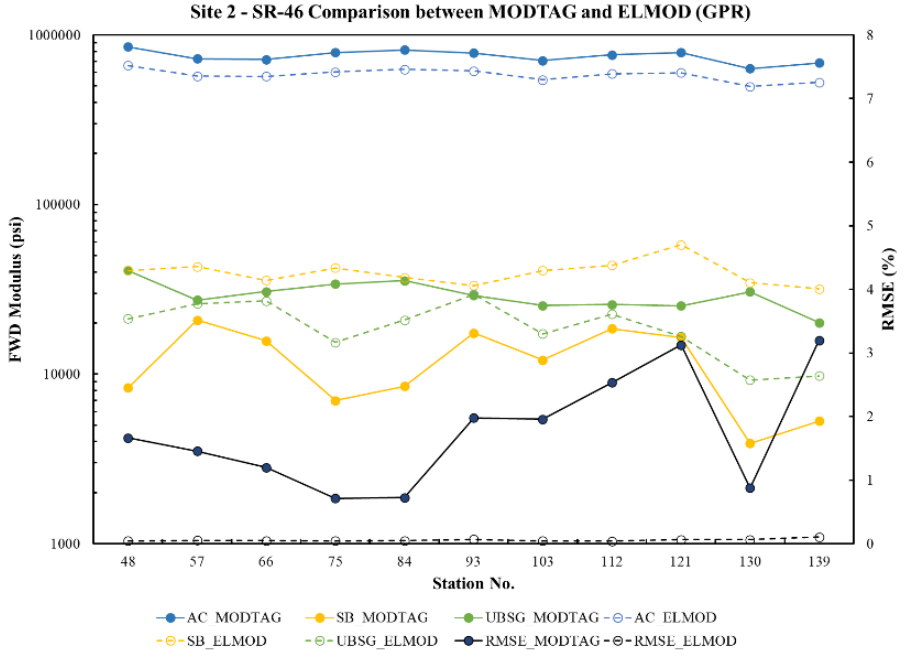

Figure G.2 SR-46–comparison between ELMOD and MODTAG.

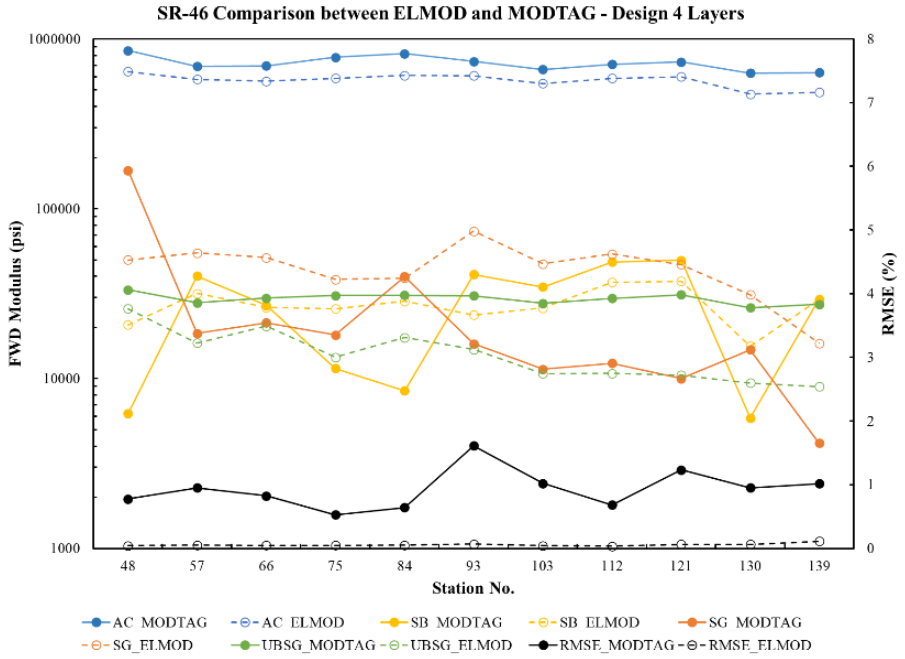

Figure G.2 SR-46–comparison between ELMOD and MODTAG (continued).

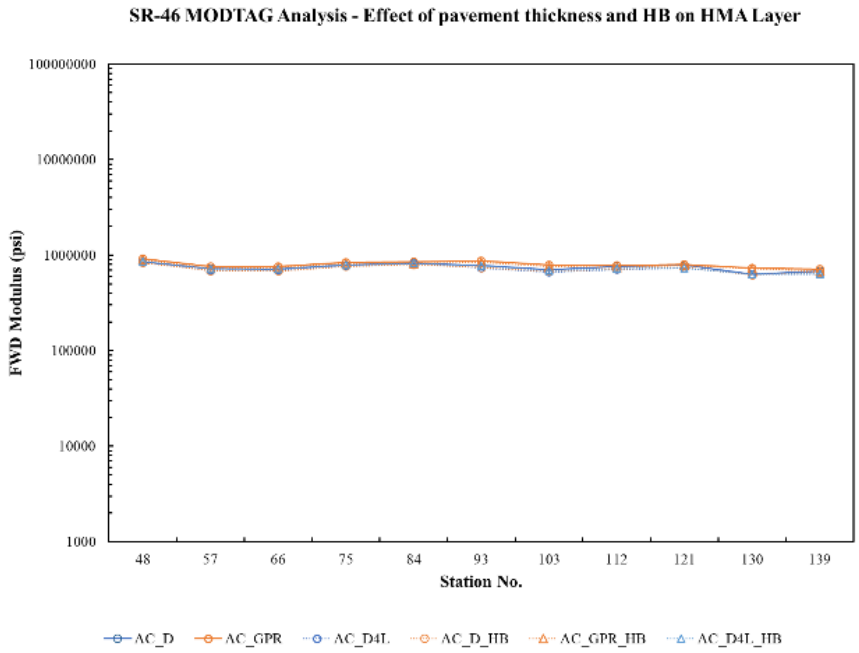

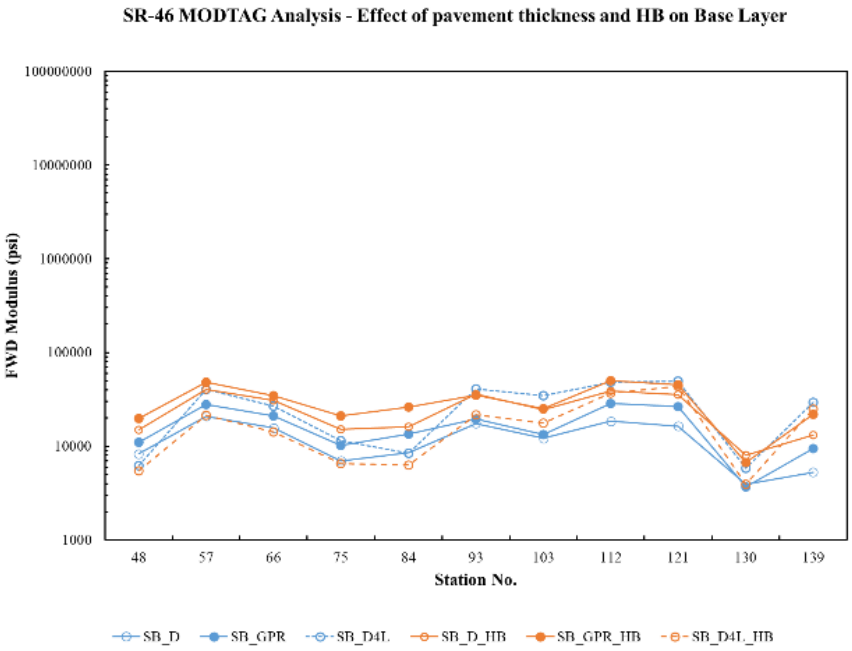

Figure G.3 SR-46 MODTAG analysis—effect of pavement thickness and hard bottom.

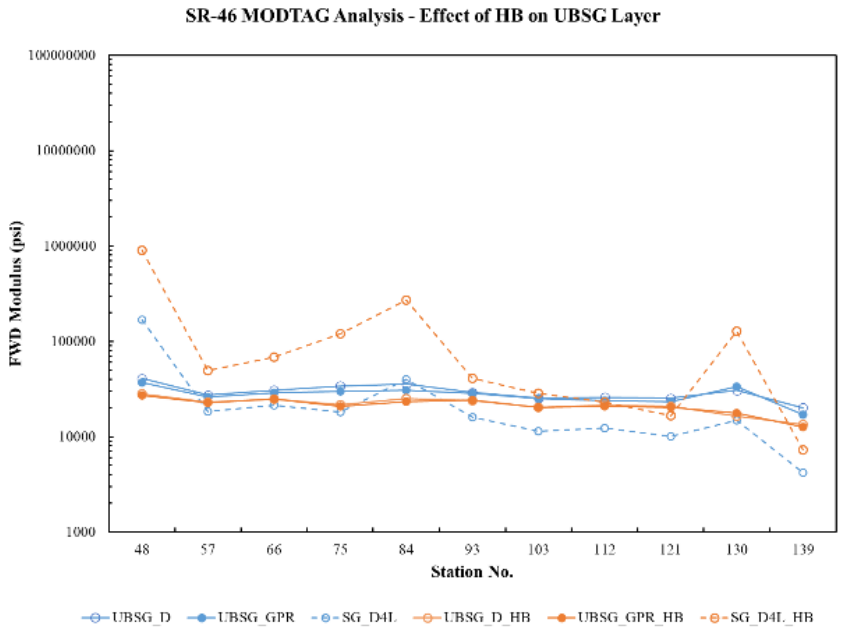

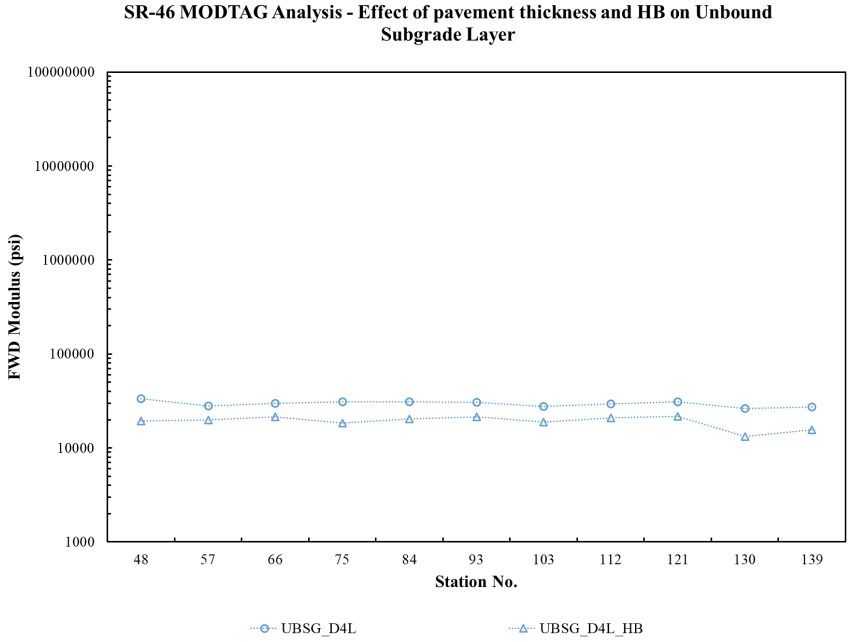

Figure G.3 SR-46 MODTAG analysis—effect of pavement thickness and hard bottom (continued).

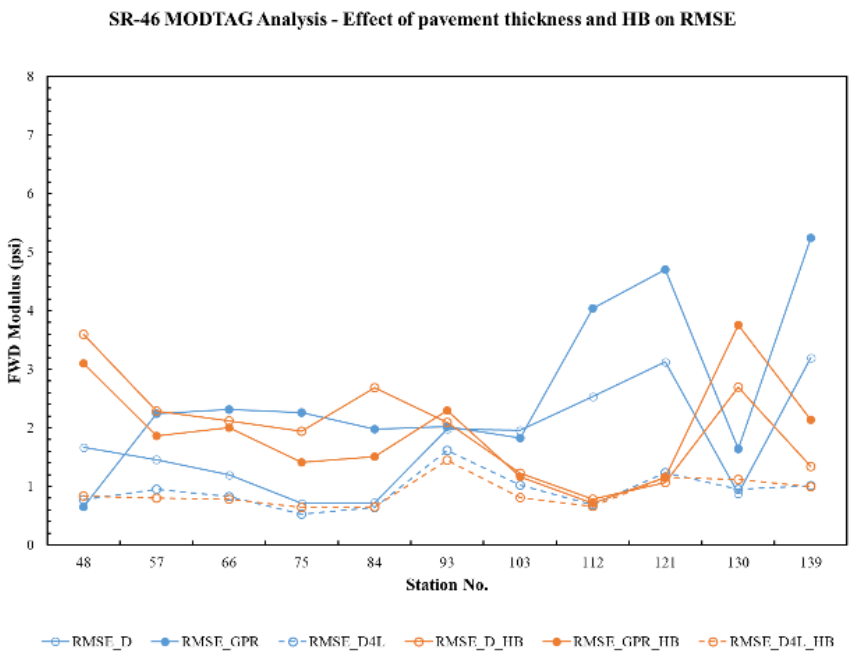

Figure G.3 SR-46 MODTAG analysis—effect of pavement thickness and hard bottom (continued).

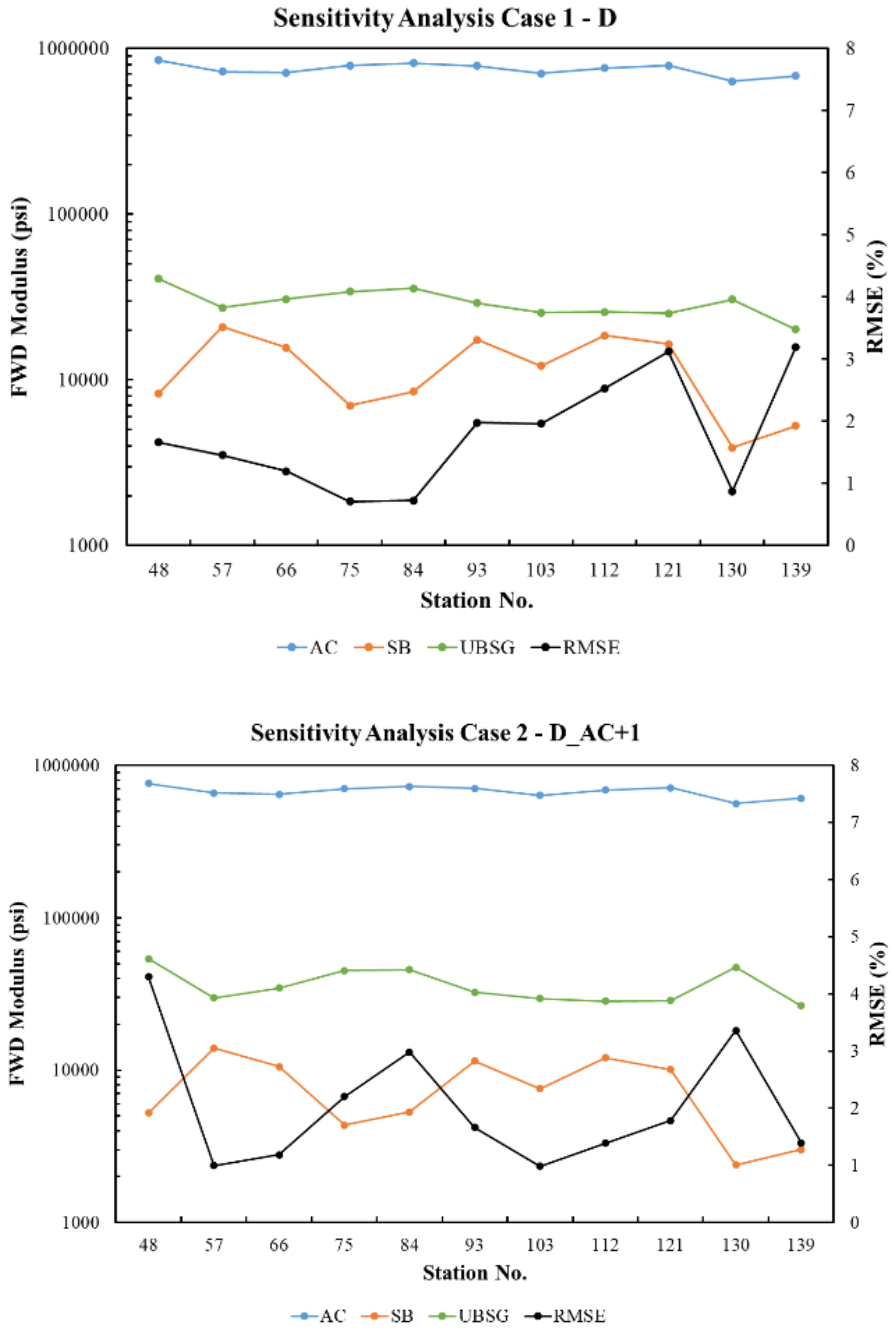

Figure G.4 SR-46 MODTAG analysis—sensitivity analysis-effect of pavement thickness (design 3-layer system).

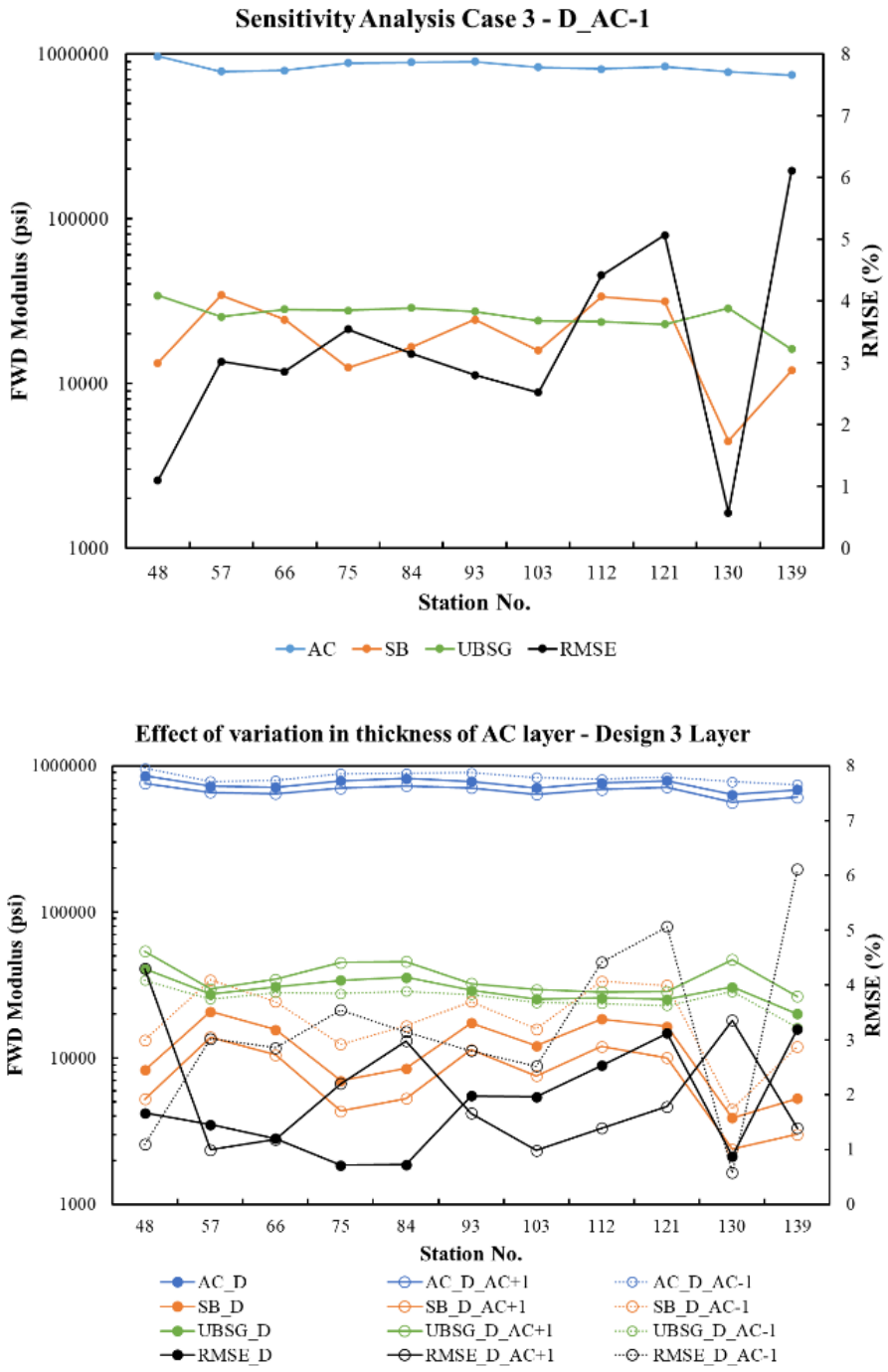

Figure G.4 SR-46 MODTAG analysis—sensitivity analysis-effect of pavement thickness (design 3-layer system).

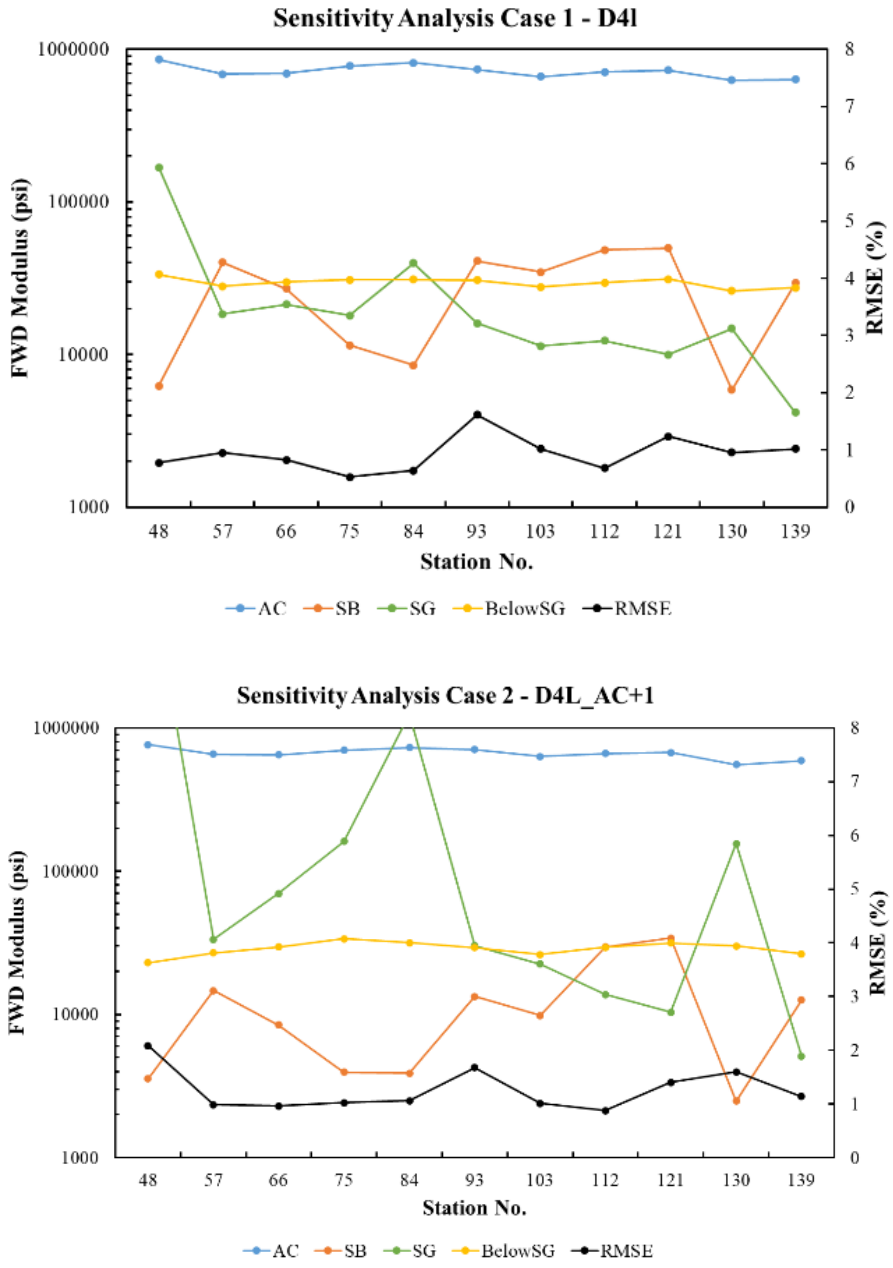

Figure G.5 SR-46 MODTAG analysis—sensitivity analysis-effect of pavement thickness (design 4-layer system).

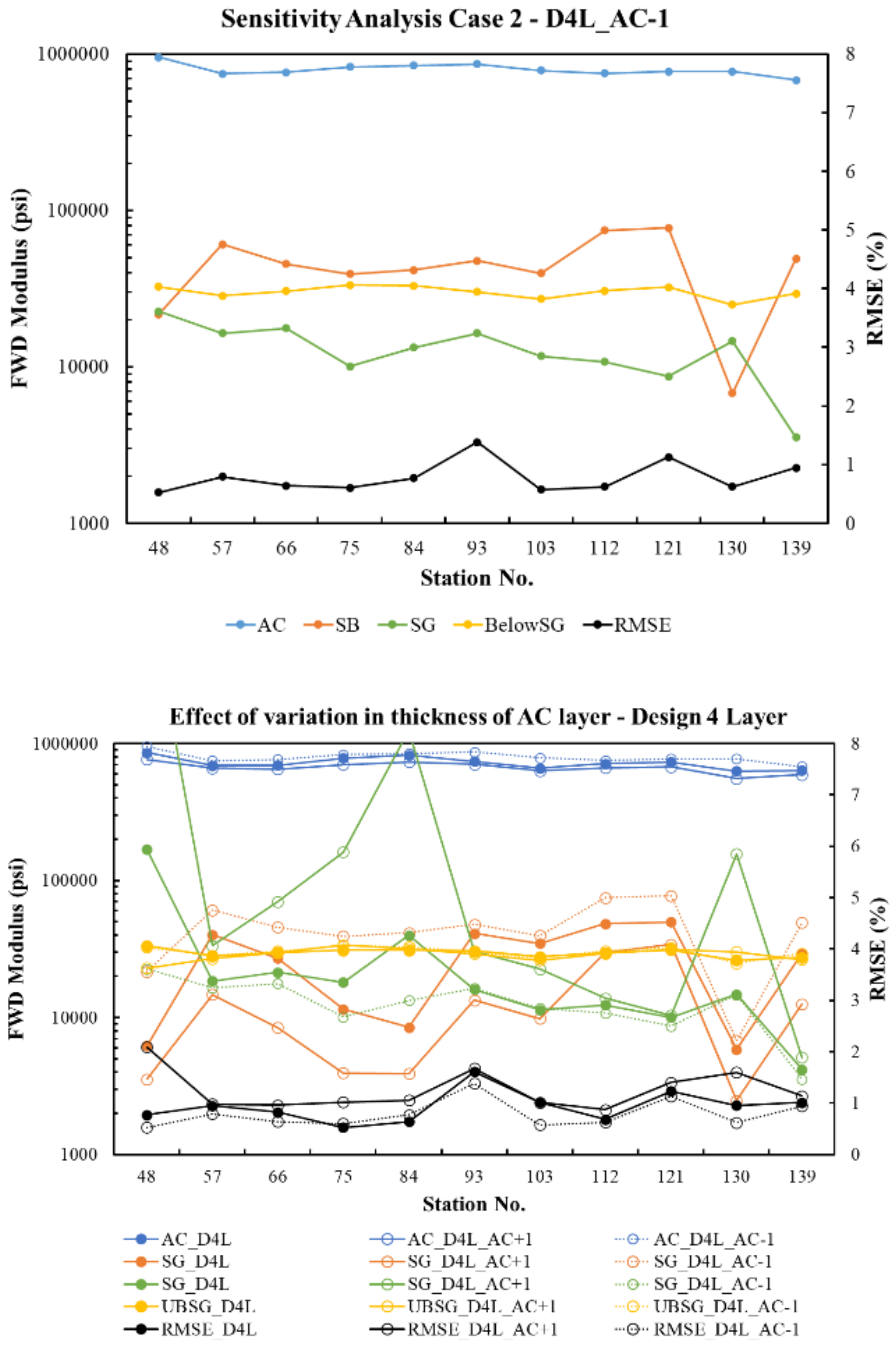

Figure G.5 SR-46 MODTAG analysis—sensitivity analysis-effect of pavement thickness (design 4-layer system).

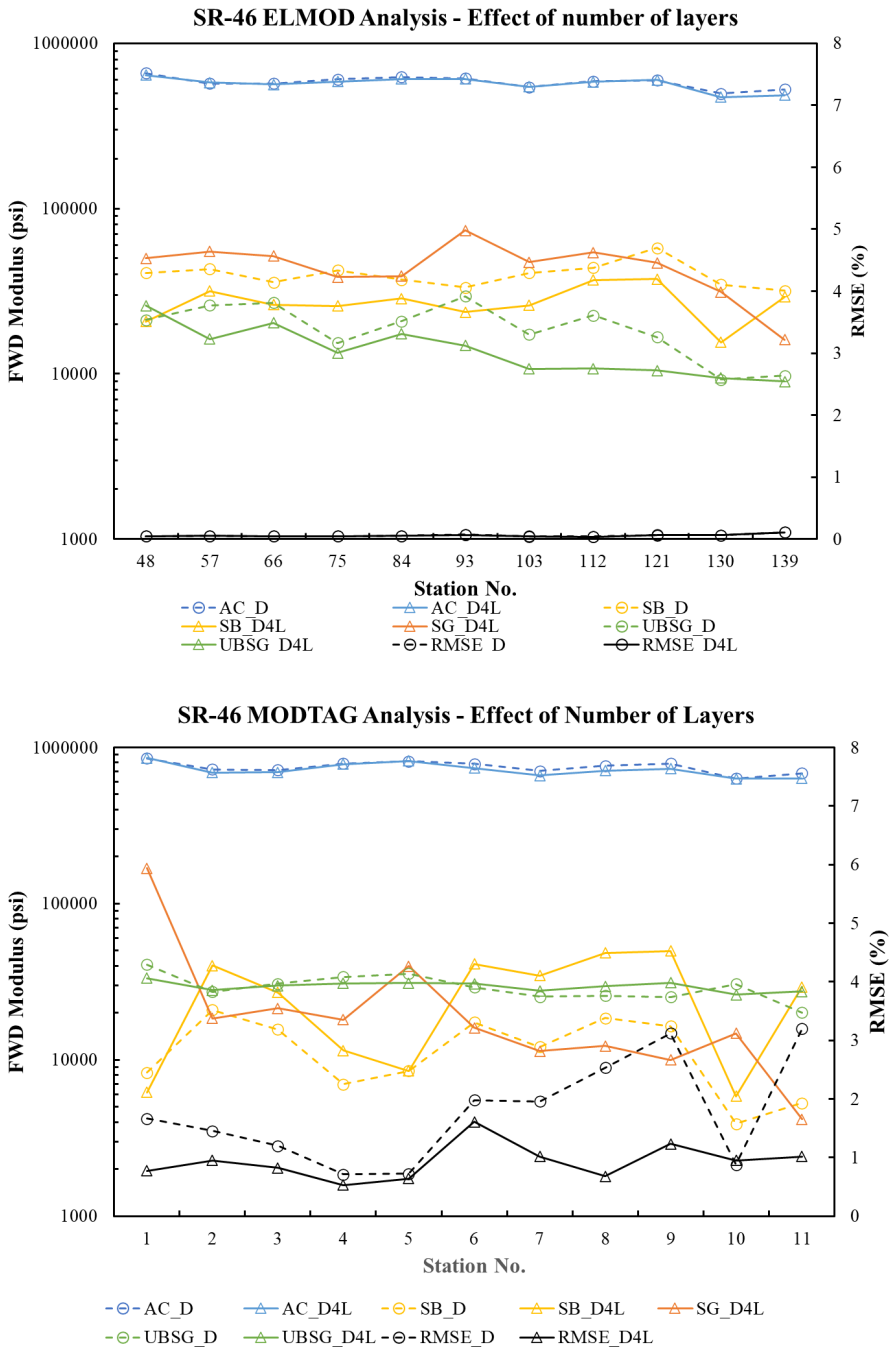

Figure G.6 SR-46 MODTAG analysis—effect of number of layers.

Table G.1 Results of Back Calculation Analysis Using ELMOD and MODTAG for Site 2: SR-46

Station	Average Lab. $M_{R,UNTREATED}$	ELMOD_D	E_{ELMOD_D} / Lab. $M_{R,UNTREATED}$	ELMOD_GPR	E_{ELMOD_GPR} / Lab. $M_{R,UNTREATED}$	MODTAG_D	E_{MODTAG_D} / Lab. $M_{R,UNTREATED}$	Station	Average Lab. $M_{R,UNTREATED}$
48	12,737	21,212	1.7	25,822	2.0	40,771	3.2	33,370	2.6
57	9,729	26,033	2.7	16,230	1.7	27,333	2.8	28,002	2.9
66	12,852	27,001	2.1	20,366	1.6	30,737	2.4	29,824	2.3
75	11,192	15,396	1.4	13,362	1.2	34,047	3.0	30,887	2.8
84	12,070	20,829	1.7	17,450	1.4	35,600	2.9	30,970	2.6
93	18,021	29,494	1.6	14,861	0.8	29,112	1.6	30,702	1.7
103	22,347	17,313	0.8	10,707	0.5	25,401	1.1	27,712	1.2
112	15,097	22,590	1.5	10,752	0.7	25,763	1.7	29,638	2.0
121	25,034	16,676	0.7	10,462	0.4	25,270	1.0	31,135	1.2
130	16,739	9,222	0.6	9,439	0.6	30,618	1.8	26,114	1.6
139	14,735	9,764	0.7	8,970	0.6	20,129	1.4	27,417	1.9
		Average	1.4	**Average**	1.0	**Average**	2.1	**Average**	2.1

About the Joint Transportation Research Program (JTRP)

On March 11, 1937, the Indiana Legislature passed an act which authorized the Indiana State Highway Commission to cooperate with and assist Purdue University in developing the best methods of improving and maintaining the highways of the state and the respective counties thereof. That collaborative effort was called the Joint Highway Research Project (JHRP). In 1997 the collaborative venture was renamed as the Joint Transportation Research Program (JTRP) to reflect the state and national efforts to integrate the management and operation of various transportation modes.

The first studies of JHRP were concerned with Test Road No. 1—evaluation of the weathering characteristics of stabilized materials. After World War II, the JHRP program grew substantially and was regularly producing technical reports. Over 1,600 technical reports are now available, published as part of the JHRP and subsequently JTRP collaborative venture between Purdue University and what is now the Indiana Department of Transportation.

Free online access to all reports is provided through a unique collaboration between JTRP and Purdue Libraries. These are available at http://docs.lib.purdue.edu/jtrp.

Further information about JTRP and its current research program is available at http://www.purdue.edu/jtrp.

About This Report

An open access version of this publication is available online. See the URL in the citation below.

Gupta, K., Park, S. S., Bobet, A., & Nantung, T. (2022). *Improved reliability of FWD test results and correlations with resilient modulus* (Joint Transportation Research Program Publication No. FHWA/IN/JTRP-2022/07). West Lafayette, IN: Purdue University. https://doi.org/10.5703/1288284317370